Prostate Cancer Cells Require a Rab35-Dependent Exosome Sub-Population for Stromal Activation and Tumour Growth

By

Vincent Yeung

A thesis submitted for the degree

DOCTOR OF PHILOSOPHY

Division of Cancer and Genetics

School of Medicine

Cardiff University

2017

Declaration

This work has not been submitted in substance for any other degree or award at this or any other university or place of learning, nor is being submitted concurrently in candidature for any degree or other award.

Signed …… (candidate) Date ……..

STATEMENT 1

This thesis is being submitted in partial fulfilment of the requirements for the degree of PhD.

Signed …… (candidate) Date ……

STATEMENT 2

This thesis is the result of my own independent work/investigation, except where otherwise stated.

Other sources are acknowledged by explicit references. The views expressed are my own.

Signed …… (candidate) Date ……

STATEMENT 3

I hereby give consent for my thesis, if accepted, to be available online in the University's Open Access repository and for inter-library loan, and for the title and summary to be made available to outside organisations.

Signed …… (candidate) Date ……

STATEMENT 4: PREVIOUSLY APPROVED BAR ON ACCESS

I hereby give consent for my thesis, if accepted, to be available online in the University's Open Access repository and for inter-library loans **after expiry of a bar on access previously approved by the Academic Standards & Quality Committee.**

Signed …… (candidate) Date ……

Acknowledgements

First and foremost, I offer my sincerest gratitude to my supervisors Dr Aled Clayton and Dr Jason Webber for their advice, encouragement and guidance they have provided me throughout my time as their student. I have been lucky to have mentors who have invested their time and effort in teaching me during my PhD.

I am also grateful to all those who assisted with the experiments and discussions that have contributed to the work of the thesis, Prof Rachel Errington, Dr Zsuzsanna Tabi, Dr Saly Al-Taei, Dr Lisa Spary, Dr Joanne Welton, Dr Rachel Howard-Jones, Mr Hossein Navabi and Mrs Marie Wiltshire.

A special thank you goes to my friends and colleagues, both past and present, Dr Chi Pooi Lee, Dr Josephine Salimu, Dr Ridwana Chowdhury, Dr Alexandra Shephard, Mr Mark Gurney, Miss Amy Codd and Mr Alexander Cocks. Especially for being the master on BF1. Bankai.

I would like to thank Cardiff University, Division of Cancer and Genetics, and the Life Science Research Network Wales for providing me with funding to support my research. But also for giving me the opportunity to attend conferences nationally and internationally.

A final thank you to Miss Stephanie Yuen for all her support. Also, a thank you to Dr Tony Tong for his help. Finally, I will be forever grateful for the unconditional love and support from my brother Mark, my parents and my aunt Joanne throughout my studies.

Summary

Communication between cancer cells and the microenvironment is a complex yet crucial issue in disease progression. Recent studies highlight an important role for small extracellular vesicles (exosomes) secreted by cancer cells, as modulators of cancer-associated stroma, angiogenesis and metastatic priming. The intrinsic factors regulating exosome biogenesis and secretion in cancer cells are, therefore, highly relevant in studies of cross-communication in the cancer milieu.

We generated prostate cancer cells bearing stable knockdown of putative exosome-regulating factors (CD9, Rab5a, Rab11b, Rab35, VAMP7 and VPS25); and examined the impact on cell health, vesicle secretion and on communication with fibroblastic stromal cells. We highlight that Rab11b or Rab35 regulate phenotypically distinct exosome subpopulations each accounting for only around 20% of the total. Depleting Rab11b or Rab35 leaves a vesicle population insufficient for driving fibroblast to myofibroblast differentiation, leading to diminished angiogenesis and attenuated invasive behaviours in 3D *in vitro* models. Correcting for differences in vesicle quantity revealed that perturbed differentiation due to loss of Rab11b-dependent vesicles, could be restored by normalising quantity. This, however, was not the case for Rab35-dependent vesicles. Co-implantation of tumour cells with stromal fibroblasts in xenografts similarly showed that Rab11b knockdown had little effect on growth rates *in vivo*. In contrast, significant attenuation was evident when using Rab35-knockdown cells.

The study concludes that a Rab35 regulated exosome sub-population is particularly important for communication between cancer and stromal cells; and is required for generating a microenvironment conducive for disease promotion.

Presentations

Yeung V, Webber J, Clayton A. **Exosomes mediates Stromal Cell Influence on Prostate Cancer in 3D Spheroid Models.** Cardiff Institute of Tissue Engineering and Repair (CITER) conference, Carmarthenshire (UK). Poster Presentation. September 2014. **Best Poster Presentation.**

Yeung V**,** Chowdhury R, Gurney M, Welton J, Webber JP, Clayton A. **Prostate Cancer Exosomes as Drivers of Disease Progression.** Division of Cancer and Genetics PhD Seminar Day, Cardiff University (UK). Oral Presentation. October 2014.

Yeung V**,** Chowdhury R, Gurney M, Wiltshire M, Howard-Jones R, Errington R, Welton J, Tabi Z, Mason M, Webber JP, Clayton A. **Prostate Cancer Exosomes as Drivers of Disease Progression.** 1st Drug Discovery Congress, Life Science Research Network Wales (LSRNW), Cardiff (UK). Oral Presentation. November 2014.

Yeung V. **Halting the Royal Mail Delivery System Delivering Cancer to You.** 3 Minute Thesis (3MT®) Competition, Cardiff University (UK). Oral Presentation. May 2015. **3rd Place.**

Yeung V**,** Howard-Jones R, Wiltshire M, Errington R, Brennan P, Mason M, Tabi Z, Webber JP, Clayton A. **Identification of Key Components in Exosome Secretion and Stromal Activation in Cancer.** 30th Annual Post-Graduate Research Day, Cardiff University (UK). Poster Presentation. November 2015.

Yeung V**,** Howard-Jones R, Wiltshire M, Errington R, Brennan P, Mason M, Tabi Z, Webber JP, Clayton A. **Identification of Key Components in Exosome Secretion and Stromal Activation in Cancer.** 2nd Drug Discovery Congress, Life Science Research Network Wales (LSRNW), Cardiff (UK). Poster Presentation. December 2015.

Yeung V**,** Howard-Jones R, Wiltshire M, Errington R, Brennan P, Mason M, Tabi Z, Webber JP, Clayton A. **Identification of Key Components in Exosome Secretion and Stromal Activation in Cancer.** UK extracellular vesicle (UKEV) forum, Cardiff University (UK). Poster Presentation. December 2015.

Yeung V**,** Howard-Jones R, Wiltshire M, Errington R, Brennan P, Mason M, Tabi Z, Webber JP, Clayton A. **Identifying Components that Regulating the Secretion of Stromal-activating Exosomes in Prostate Cancer.** International society for extracellular vesicle (ISEV) 5th annual meeting, Rotterdam (Netherlands). Poster Presentation. May 2016.

Yeung V**,** Howard-Jones R, Wiltshire M, Errington R, Mason M, Tabi Z, Webber JP, Clayton A. **Cancer Exosomes activate Stromal Cells thereby Facilitating Tumour Invasion within 3D culture.** Cardiff Institute of Tissue Engineering and Repair (CITER) Symposium, Cardiff University (UK). Oral Presentation. September 2016.

Yeung V, Webber J, Clayton A. **Prostate Cancer Exosomes as Drivers of Disease Progression: A Novel approach in Targeting Rab11b to Halt Disease Progression.** Inaugural Sêr Cymru Postgraduate Conference, Swansea University (UK). Poster Presentation. September 2016. **Student's Choice award for Poster Presentation.**

Yeung V**,** Howard-Jones R, Wiltshire M, Errington R, Mason M, Tabi Z, Webber JP, Clayton A. Cancer **Exosomes activate Stromal Cells thereby Facilitating Tumour Invasion within 3D co-culture.** 2nd EACR Conference on Goodbye Flat Biology: Models, Mechanisms and Microenvironment, Berlin (Germany). Poster Presentation. October 2016. **High Scoring Abstract.**

Yeung V, Gurney M, Howard-Jones R, Errington R, Tabi Z, Webber JP, Clayton A. **Prostate Cancer Exosomes as Drivers of Disease Progression.** 3rd Drug Discovery Congress, Life Science Research Network Wales (LSRNW), Cardiff (UK). Oral Presentation. November 2016. **Prize for Oral Presentation.**

Yeung V, Gurney M, Tabi Z, Errington R, Webber JP, Clayton A. **Identifying Intrinsic Components that Regulate the Secretion of Stroma-Activating Exosomes in Prostate Cancer.** UK extracellular vesicle (UKEV) forum, Oxford Brookes University (UK). Oral Presentation. December 2016. **Best Oral Presentation.**

2017

Yeung V, Gurney M, Tabi Z, Errington R, Webber JP, Clayton A. **Identifying Intrinsic Components that Regulate the Secretion of Stroma-Activating Exosomes in Prostate Cancer.** 31st Annual Post-Graduate Research Day, Cardiff University (UK). Oral Presentation. January 2017. **Prize for Oral Presentation.**

Yeung V, Gurney M, Tabi Z, Errington R, Webber JP, Clayton A. **Rab GTPases Control Secretion of Stroma-activating Exosome Subpopulations**. 1st Prostate Cancer and Tumour Microenvironment Workshop, Cardiff University (UK). Oral Presentation. February 2017.

Yeung V, Gurney M, Tabi Z, Errington R, Webber JP, Clayton A. **Prostate Cancer Exosomes as Drivers of Disease Progression**. Division of Cancer and Genetics Seminar, Cardiff University (UK). Oral Presentation. March 2017.

Yeung V, Gurney M, Tabi Z, Errington R, Webber JP, Clayton A. **Identifying Intrinsic Components that Regulate the Secretion of Stroma-Activating Exosomes in Prostate Cancer.** International society for extracellular vesicle (ISEV) 5th annual meeting, Toronto (Canada). Poster Presentation. May 2017. **Best Poster Presentation.**

Yeung V, Gurney M, Tabi Z, Errington R, Webber JP, Clayton A. **Prostate cancer cells require a Rab35-dependent exosome sub-population for stromal activation and tumour growth.** Invited speaker for seminar at Harvard University, Boston (USA). Oral Presentation. May 2017.

Yeung V, Gurney M, Tabi Z, Errington R, Webber JP, Clayton A. **Identifying Intrinsic Components that Regulate the Secretion of Stroma-Activating Exosomes in Prostate Cancer.** British Association for Cancer Research (BACR) Tumour Microenvironment Workshop, Nottingham (UK). Poster Presentation. June 2017.

Grants

CITER Travel Grant (£1000) - Travel grant to attend the International Society for Extracellular Vesicle (ISEV) 5th annual meeting (Rotterdam, Netherlands). May 2016.

William Morgan Thomas Fund (£200) – Travel grant to attend the 2nd EACR Conference on Goodbye Flat Biology: Models, Mechanisms and Microenvironment (Berlin, Germany). October 2016.

Tom Owen Fund (£1000) - Travel grant to attend the International Society for Extracellular Vesicle (ISEV) 6th annual meeting (Toronto, Canada). May 2017.

Pilcher Fund (£250) – Travel grant to attend the BACR Tumour Microenvironment; Basic Science to Novel Therapies conference and BACR 3D Models Workshop (Nottingham, UK). June 2017.

Welsh Crucible Grant (£10,000) – Named researcher on the project titled: "Guided by the sun: new cross-disciplinary methods for modelling and analysis of tumour growth". January - September 2017.

Publications

Webber J, **Yeung V**, Clayton A. Extracellular vesicles as modulators of the cancer microenvironment. *Seminars in Cell & Developmental Biology*. 2015. 40:27-34.

Connolly KD, Guschina IA, **Yeung V**, Clayton A, Draman MS, Von Ruhland C, Ludgate M, James PE, Rees DA. Characterisation of adipocyte-derived extracellular vesicles released pre- and post-adipogenesis. *Journal of Extracellular Vesicles*. 2015.

Yeung V, Gurney M, Falcon Perez JM, Tabi Z, Errington R, Webber JP, Clayton A. Prostate cancer cells require a Rab35-dependent exosome sub-population for stromal activation and tumour growth. *Oncogene*. 2017. **Submitted for Review.**

Shephard A, **Yeung V,** Clayton A, Webber JP. Prostate cancer exosomes as modulators of the tumour microenvironment and formation of the pre-metastatic niche. *Journal of Cancer and Metastasis.* 2017. **Submitted for Review.**

Table of Contents

List of Figures and Tables

Abbreviations

3D CRT	Three dimension Conformal Radiotherapy
α-SMA	Alpha-smooth muscle actin
ADAPT	Adaptive dialysis-like affinity technology
ADT	Androgen deprivation therapy
ALIX	Apoptosis-linked gene 2-interacting *Protein* X
AMP	Adenosine monophosphate
ANOVA	Analysis of variance
AP2	Adaptor protein 2
AR	Androgen receptor
ARF6	ADP ribosylation factor 6
ATCC	American Tissue Culture Collection
ATP	Adeonsine triphosphate
BCA	Bicinchoninic acid
BPH	Benign prostate hyperplasia
CD	Cluster of differentiation
CHMP	Charged multivesicular body protein
CM	Conditioned media
CTR	Control
CXCL	Chemokine (C-X-C motif) ligand
D_20	Deuterium oxide
DAPI	4',6-diamidino-2-phenylindole
DES	Diethylstilbestrol
DMEM	Dulbecco's Modified Eagle's Medium
DNA	Deoxyribonucleic acid
dNTP	Deoxynucleotide triphosphate
dsRNA	Double stranded ribonucleic acid
DC	Dendritic cell
DHT	Dihydrotestosterone
DLS	Dynamic light scattering
DRE	Digital rectal examination
DTT	Dithiothreitol
ECM	Extracellular matrix
EEA	Early endosome antigen

EGM	Endothelial cell growth medium
EGF	Epidermal growth factor
EGFR	Epidermal growth factor receptor
ELISA	Enzyme-linked immunosorbent assay
EM	Electron microscopy
ERK	Extracellular signal-regulated kinase
ESCRT	Endosomal sorting complex required for transport
EV	Extracellular vesicle
FBS	Foetal calf serum
FGF	Fibroblast growth factor
FSH	Follicle stimulating hormone
GAP	GTPase activating proteins
GAPDH	Glyceraldehyde 3-phosphate dehydrogenase
GBO	Greiner Bio-One
G-CSF	Granulocyte-colony stimulating factor
GEF	Guanine nucleotide exchange factors
GFP	Green fluorescent protein
GTPase	Guanosine triphosphatases
HA	Hyaluronic acid
HBSS	Hank's balanced salt solution
HEPES	4-(2-hydroxyethyl)-1-piperazineethanesulfonic acid
HER2	Human epidermal growth factor receptor 2
HCL	Hydrochloric acid
HGF	Hepatocyte growth factor
HRP	Horseradish peroxidase
HRS	Hepatocyte growth factor regulated kinase substrate
HSP	Heat shock protein
HUVEC	Human umbilical vein endothelial cell
IGF	Insulin-like growth factor
IHC	Immunohistochemistry
IL	Interleukin
ILV	Intraluminal vesicle
IMRT	Intensity Modulated Radiotherapy
ISEV	International Society of Extracellular Vesicles

IST	Increased sodium tolerance protein
LBPA	Lysobisphosphatidic acid
LAMP	Lysosomal-associated membrane protein
LDS	Lithium dodecyl sulphate
LH	Luteinising hormone
LHRH	Luteinising hormone releasing-hormone
LIF	Leuakemia inhibitory factor
LOD	Limit of detection
miRNA	Microribonucleic acid
mRNA	Messenger ribonucleic acid
MAPK	Mitogen-activated protein kinase
MFI	Median fluorescent intensity
MHC	Major histocompatibility complex
MMP	Matrix metalloproteinase
MOI	Multiplicity of infection
MOP	3-Morpholinopropane-1-sulfonic acid
MSC	Mesenchymal stem cell
MTT	3-(4,5-Dimethylthiazol-2-yl)-2,5-diphenyltetrazolium bromide
MV	Microvesicle
MVE	Multivesicular endosome
nSMase	Neutral sphingomyelinase
NaOH	Sodium hydroxide
NK	Natural killer
NM	Non-mammalian
NTA	Nanoparticle Tracking Analysis
PBS	Phosphate buffered saline
PCR	Polymerase chain reaction
PLD2	Phospholipase D2
PDGF	Platelet derived growth factor
PE	Phosphatidylethanolamine
PET	Polyethylene terephthalate
PGF	Placental growth factor
PI3K	Phosphatidylinositol-4,5-bisphosphate 3-kinase
PI3P	Phosphattidylinositol-3-phosphate

PIN	Prostatic intraepithelial neoplasia
PKA	Protein kinase A
PLP	Proteolipid protein
PMEL	Premelanosomal protein
PMSF	Phenylmethane sulfonyl fluoride
Poly-HEMA	Polyhydroxyethylmethacrylate
PSA	Prostate specific antigen
PVDF	Polyvinylidene fluoride
qDot	Quantum dot
qPCR	Quantitative polymerase chain reaction
RFP	Red fluorescent protein
Ri	Refractive index
RIPA	Radioimmunoprecipitation assay
RISC	Ribonucleic acid inducing silencing complex
RNA	Ribonucleic acid
RNAi	Ribonucleic acid interference
RPMI	Roswell Park Memorial Institute
RQ	Relative quantification
RT	Room temperature
SDF	Stromal cell-derived factor
SDS	Sodium dodecyl sulphate
SEM	Standard error of mean
shRNA	Small hairpin ribonucleic acid
siRNA	Short-interfering ribonucleic acid
SNAP	Soluble N-ethylmaleimide-sensitive fusion attachment protein
SNARE	SNAP receptor
STAM	Signal transducing adaptor molecule
STAT	Signal transducer and activator of transcription
TEI	Total exosome isolation reagent
TGF-β	Transforming growth factor-β
TIMP	Tissue inhibitor of metalloproteinase
TRAIL	TNF-related apoptosis-inducing ligand
TRF	Time resolved fluorescence
TRUS	Trans-rectal ultrasound

TSG	Tumour susceptibility gene
TWEAK	TNF-related weak inducer of apoptosis
UKCCCR	United Kingdom Co-ordinating Committee on Cancer Research
UBD	Ubiquitin binding domains
uPA	Urokinase-type plasminogen activator
VAMP	Vesicle-associated membrane protein
VASP	Vasodilator-stimulated phosphoprotein
VEGF	Vascular endothelial growth factor
VPS	Vacuolar protein sorting
vWF	von Willebrand Factor
V/V	Volume per volume
WST	Water soluble tetrazolium
W/V	Weight per volume

CHAPTER 1:

INTRODUCTION

1.1 Prostate Cancer

1.1.1 Aetiology and Risk Factor

Prostate cancer is the most common cancer to affect men in the UK, where more than 46,700 cases are diagnosed each year (CRUK, 2015). The risk factors for developing prostate cancer are complex and remain incompletely understood (Karan et al., 2008). The risk of developing prostate cancer increases exponentially over the age of 50 years (Farmer, 2008). Similarly, a positive family history of prostate cancer can result in an increased risk of prostate cancer diagnosis (Madersbacher et al., 2011), accounting for 5 - 10% of all prostate cancer cases. Other cohort-based and meta-analysis based studies have revealed patients who have 2 or more relatives with prostate cancer, have a greater than 3-fold risk of developing prostate cancer, compared to men with no family history (Carter et al., 1992, Kicinski et al., 2011). The basis for this risk remains unclear, but possible reasons have included recessive or X-linked inheritance.

Furthermore, there is a link between ethnicity and prostate cancer incidence. In a population-based study of men with newly diagnosed prostate cancer, it was shown that African-Americans and Hispanics were more likely to present with clinically aggressive advanced-stage prostate cancer, than non-Hispanic Caucasian men (Hoffman et al., 2001). They reported a 3-fold relative risk for prostate cancer in African-Americans, compared with Caucasian men. A comprehensive cohort study on ethnicity and prostate cancer in the UK, found similar findings with the highest incidence rate for prostate cancer in Caribbean men, followed by Caucasian and Asian men (Ben-Shlomo et al., 2008). In contrast, the lowest risk was found among native Asian men (Chinegwundoh et al., 2006). Although the lack of systemic prostate cancer screening in Asian countries may explain part of that difference (Bunker et al., 2002), this alone cannot fully explain the lower incidence in Asian migrants in the UK and US (Odedina et al., 2009). These differences may arise due to a combination of inherited genes and environmental factors. As one environmental factor example, soy food consumption is typically common in Asian populations and is associated with a 25 - 30% reduced risk of prostate cancer (Kurahashi et al., 2007). Taken together, along with major risk factors such as age and family history, a combination of ethnicity and environmental factors, such as diet, may contribute to prostate cancer development.

1.1.2 Diagnosis and Treatment

Diagnosis

Currently, prostate cancer frequently has no clinical symptoms that distinguishes itself from similar problems to the prostate, such as benign prostate hyperplasia (BPH) and prostatitis. It remains difficult to rely on symptoms to discriminate between these diseases (Young et al., 2015). Patients that are suspected of prostate cancer will undergo diagnosis procedures, which may include digital rectal examination (DRE) and examining levels of prostate specific antigen (PSA).

One of the current methods for prostate cancer detection is analysing abnormally high levels of PSA in serum. PSA is a protein secreted by prostate epithelial cells (Webber et al., 1995), which increases with age (Catalona et al., 1991). Typically, men under the age of 60 have a PSA level of 3ng/ml, which increases to 4ng/ml by the age of 60 and further increases to >5ng/ml in men over the age of 70 (Punglia et al., 2003). Elevated PSA levels are also seen in BPH or prostatitis (Cannon and Getzenberg, 2008), hence PSA has poor specificity for prostate cancer. Though, elevated PSA levels (>10ng/ml), are likely to be caused by prostate cancer and occasionally BPH (Punglia et al., 2003). The variability of PSA testing within an individual can often complicate detection. PSA testing can be misleading, as a study revealed 60% of men with abnormally high levels of PSA do not have prostate cancer, compared to 15% of men who has prostate cancer have normal PSA levels (Thompson et al., 2004). Despite these issues, the PSA test is a commonly used approach for aiding diagnosis, but there remains controversy for solely relying on PSA, as other prostate related problems, such as BPH, prostatitis or infections of the prostate (Selley et al., 1997, Cannon and Getzenberg, 2008, Serretta et al., 2008) may be present and cannot be discriminated.

DRE is often used in combination together with PSA testing to screen for prostate cancer, involving the back surface of the prostate being felt for any hard, lumpy or abnormal areas which may indicate prostate cancer. It appears that DRE has a high specificity for prostate cancer, as false negative results are rare (Hoogendam et al., 1999); and including DRE with PSA testing give a significantly higher predictive accuracy, compared to DRE alone for prostate cancer diagnosis (Bretton et al., 1994, Chu et al., 2011). DRE has a limited positive-predictive value in men with a low PSA value and should not necessarily be recommended as a sole screening tool; as it remains insensitive and may miss the early disease stage. Furthermore, patients often undergo trans-rectal ultrasound (TRUS) and then a needle biopsy for a further definitive diagnosis (Lopes et al., 2015). This procedure involves inserting a needle with an ultrasound probe through the rectum, that guides the needle to the

prostate for tissue sample collection (Harvey et al., 2012). Samples can be histologically examined and if positive, the cancer is staged using the Gleason Scoring System. This separates the cancer diagnosis into five different histological grades (Grade 1 tissues are well differentiated and carry the best prognosis; Grade 5 tissues are poorly differentiated and have a poor prognosis). Tissue samples obtained from two different sites with the graded tissue score are added together to give a Gleason score between 2 - 10. A higher score indicates an aggressive cancerous tissue, that has poor prognosis compared to a lower Gleason score (Humphrey, 2004, Chen and Zhou, 2016). There still remains difficulty in precisely locating the tumour, as needle biopsy may be extracted from a non-cancerous region of a cancer-positive prostate resulting in false negatives (Quon et al., 2015). Nonetheless, false negatives should not completely rule out prostate cancer. Using TRUS as a primary screening test is not recommended as it has low sensitivity. Prostatic biopsy is considered when results from PSA or DRE indicates possible prostate cancer. Overall, a combination of PSA testing, DRE and TRUS would give a clearer indication of prostate cancer, compared to performing these tests alone.

Treatment

Men with localised disease can have very different prognosis and face a wide variety of treatment options to minimise intervention-related complications. Prostate cancer treatment is based on risk assessments that often combine patient age, clinical tumour stage, serum PSA, Gleason score and number of positive prostate biopsies. Many low-score (Gleason score of 6 or less) localised (small and organ confined) prostate cancers are typically treated with radical prostatectomy (removal of prostate), external-beam radiotherapy, or brachytherapy (Kupelian et al., 2004), whereas metastatic prostate cancer require different treatments. Radical prostatectomy is normally performed in men with good health and localised prostate cancer (Pierorazio et al., 2010), as surgical risks such as blood loss or infections can arise post-operation that may be detrimental to men with poor health (Gao et al., 2014). After surgery, impotency is one problem that can occur and the patient's quality of life should be considered. Radical prostatectomy may, therefore, only cater to a subset of prostate cancer patients. Low PSA levels can be measured to ensure surgical removal was successful. However, if PSA levels start to rise again, other forms of treatment may be required, such as radiotherapy or hormone therapy.

Radiotherapy is the best alternative for men who do not meet the surgical criteria. Radiation is administered to treat localised prostate cancer, but may be suitable for advanced prostate cancer. External beam radiotherapy is used to treat patients, which involves exposure of high

energy X-rays to target the prostate (Zelefsky et al., 2002), to damage tumour cells and attenuate tumour growth. There are different types of external beam radiotherapy, such as 3D Conformal Radiotherapy (3D CRT), that utilises imaging software to shape the radiation beam closely around the prostate (Fiveash et al., 2000). This minimises damage to the surrounding tissues. An improved approach to 3D CRT, is to use Intensity Modulated Radiotherapy (IMRT), where the radiation beam matches the shape, size and position of the prostate in greater detail (Teh et al., 2001). But importantly, it gives precise controlled doses of radiation beams to cancer cells, whilst minimising damage to outer regions of the prostate compared to 3D CRT. Similarly, brachytherapy (Nickers et al., 1997), involves implanting a small radioactive source at the tumour or metastatic sites. These radioactive sources include small metal implants (radioactive gold or iodine) or radioactive seeds, administered at high doses to kills tumour cells (Langley and Laing, 2004). The side effects that arise with radiotherapy treatment, include bowel, erection and urinary problems (Zelefsky et al., 2002, Gill et al., 2011). In patients with advanced prostate cancer, radiation is applied for palliative purposes to either shrink or slow tumour growth, or to control symptoms such as severe bone pain.

Testosterone is an androgen hormone with multiple functions, playing a role for the development and function of the male reproductive system. Testosterone is converted into dihydrotestosterone (DHT) in the testis, binding with the androgen receptor (AR) that is expressed in most prostate cancer cells (Wu et al., 2013). In aggressive prostate cancer, testosterone activates androgen-responsive genes, playing roles in cell proliferation to accelerate tumour growth (Xiao et al., 2003). Therefore, androgen deprivation by medical or surgical castration (orchiectomy), to remove the testicles could supress testosterone. Orchiectomy was a common method used for reducing testosterone levels (by 60%), whilst the remaining 40% is considered to be produced by the adrenal glands (Labrie et al., 1997). This procedure is irreversible and often associated with significant psychological impact. Alternatively, androgen deprivation therapy (ADT) using anti-androgen agents was developed to maintain low testosterone levels. Diethylstilbestrol (DES) was initially used to treat prostate cancer (Malkowicz, 2001). This mechanism inhibits luteinising hormone releasing-hormone (LHRH) release from the hypothalamus with a subsequent suppression of luteinising hormone (LH) and thus, testosterone suppression. Side effects included significant cardiovascular and thromboembolic toxicity (Malkowicz, 2001). Otherwise, introducing LHRH agonists, such as leuprolide and goserelin, provided an effective treatment for advanced prostate cancer. After an initial surge of LH/follicle stimulating hormone (FSH),

a constant exposure to LHRH agonists results in receptor downregulation in the pituitary gland (Kovacs and Schally, 2001). This cascade decreases testosterone production, as inhibition of LH and FSH is observed. Treatment demonstrated a 90% decline in testosterone, whilst 10% remains. This is due to the peripheral conversion of circulating adrenal steroids into testosterone. ADT in combination with surgery was shown to prolong survival, compared to patients with surgery and no hormone therapy, over 5 years of assessment in randomised trials (Schmitt et al., 2001, Demir et al., 2014). Adverse side effects can arise from ADT, such as metabolic and cardiovascular events (Saylor and Smith, 2009), cognitive function (Mohile et al., 2010) and urinary function (Axcrona et al., 2012). ADT is effective in tumour regression, yet some prostate cancers are androgen independent. Such cancers cannot be treated with ADT and are difficult to treat (Isaacs and Coffey, 1981, Hotte and Saad, 2010).

Androgens have been pivotal in the pathogenesis of prostate cancer and ADT treatment gives a good response to prostate cancer, which leads to remission for 18 – 24 months. After this time, patients receiving ADT often experience a rise in PSA levels, signifying resistance to ADT (Eisenberger et al., 1998), leading to recurrence and alternative forms of treatments. This led the generation of several cytotoxic chemotherapeutic drugs to be used in advanced prostate cancer (Scher et al., 2008). 5-fluorouracil and cyclophosphamide was initially utilised to palliate some advanced prostate cancer patients in earlier clinical trials. Though, mitoxantrone was the first chemotherapeutic drug approved by the FDA to show a significant palliative response in combination with prednisone (Tannock et al., 1996). Docetaxel was the first drug that showed an overall survival benefit in prostate cancer patients, leading to reduced tumour size and slowing tumour progression (Serpa Neto et al., 2011, Miyake et al., 2012). It was clear that docetaxel was the standard of care in advanced prostate cancer patients in combination with prednisone, as multiple small phase 2 trials could not improve the current standard of care. Other treatments include using cabazitaxel in combination with prednisone to show an overall survival benefit to metastatic patients compared to chemotherapy alone (de Bono et al., 2010). Administering these chemotherapeutic drug treatments are not the primary form of treatment for patients with early stage prostate cancer. It is offered to patients with advanced or metastatic prostate cancer, who are not responding to ADT (Stein et al., 2012, Recine and Sternberg, 2015). More often, a combinational treatment of ADT, radiotherapy and chemotherapy is given that can prolong the remission duration for many months, but many side effects are present from this. Toxicity with the docetaxel or cabazitaxel treatment always resulted in side effects that were

exclusively haematologic, such as neutropenia, anaemia or thrombocytopenia (Tannock et al., 1996, de Bono et al., 2010). Therefore, recommended patients considered for chemotherapy must be otherwise in good health. Despite the medical advances in diagnosis and treatment, patients with metastatic prostate cancer remain incurable. Therefore, it remains pivotal to understand the molecular mechanisms involved in tumour growth and metastasis that may allow us to identify new targets to halt or slow down disease progression.

1.2 Cancer-Associated Stroma

1.2.1 The Reactive Stroma

The prostate gland is composed of two distinctive compartments: epithelial (including secretory exocrine glands) and the surrounding connective tissue stroma. The stroma of the prostate is heterogeneous and is composed of smooth muscle cells, fibroblasts, endothelial cells, mesenchymal stem cells (MSCs) and various immune cells. The smooth muscle cells are the major stromal cell type in the normal prostate (Grossfeld et al., 1998). The mutual interaction between epithelia and stroma via androgen receptors, is vital for prostate development and differentiation (Hayward et al., 1997). After peak reproductive age, the histological architecture of the prostate begins to undergo age-related changes. Although key mechanisms are not fully understood, these changes might be attributed to altered androgen action and a persistent effect on the prostate gland.

The normal stromal compartment has an intrinsic flexibility to respond quickly to developing situations, such as wound healing and disrupted homeostasis. Stromal compartments within the microenvironment adjacent the epithelium act co-ordinately when the epithelium sustains damage. The genotypic or phenotypic alterations that occur during this damage response have been referred to as the “reactive stroma”. This altered stroma is like that found in a generic wound healing scenario and includes matrix remodelling and altered expression of repair-associated growth factors and cytokines (Gabbiani, 2003, Desmoulière et al., 2005). As an example, the interstitial smooth muscle cells are displaced by α-smooth muscle actin and vimentin positive myofibroblasts (Tuxhorn et al., 2002b), as shown in Figure 1.1. These changes within the tissue architecture indicates an expanding interstitium, accompanied largest by alpha-smooth muscle actin (α-SMA) positive cells. This leads to tissue remodelling and gradual collapse and it is the tissue with greatest stromal changes that we believe to be proactively involved in this progressive aggressive disease state.

These similar observations are often described in prostatic intraepithelial neoplasia (PIN), where the histological changes are reminiscent of cancer, evidence by loss of cellular polarity, increased proliferative potential and genetic instability (Ayala and Ro, 2007, Bettendorf et al., 2008). With increasing levels of PIN, nuclear aberration and basal cell disruption are observed. This aligns with an increased frequency and incidence that is found in men with prostate cancer than without, consequently, PIN is often considered a precursor for prostate cancer (Sakr, 1999). Though, these changes in the reactive stroma are suggested to be key in the initiation of other prostatic diseases, such as BPH. In prostate cancer, these

interactions are proposed to play a role in the development prostate cancer and metastasis (Tuxhorn et al., 2002a, Cano et al., 2007). These types of reactions are well-documented for breast and colorectal cancer (Orimo et al., 2005, Bendardaf et al., 2007). Therefore, these stromal changes are not secondary to tumour development, but remain an important early event during carcinogenesis and go hand in hand with the development of the disease.

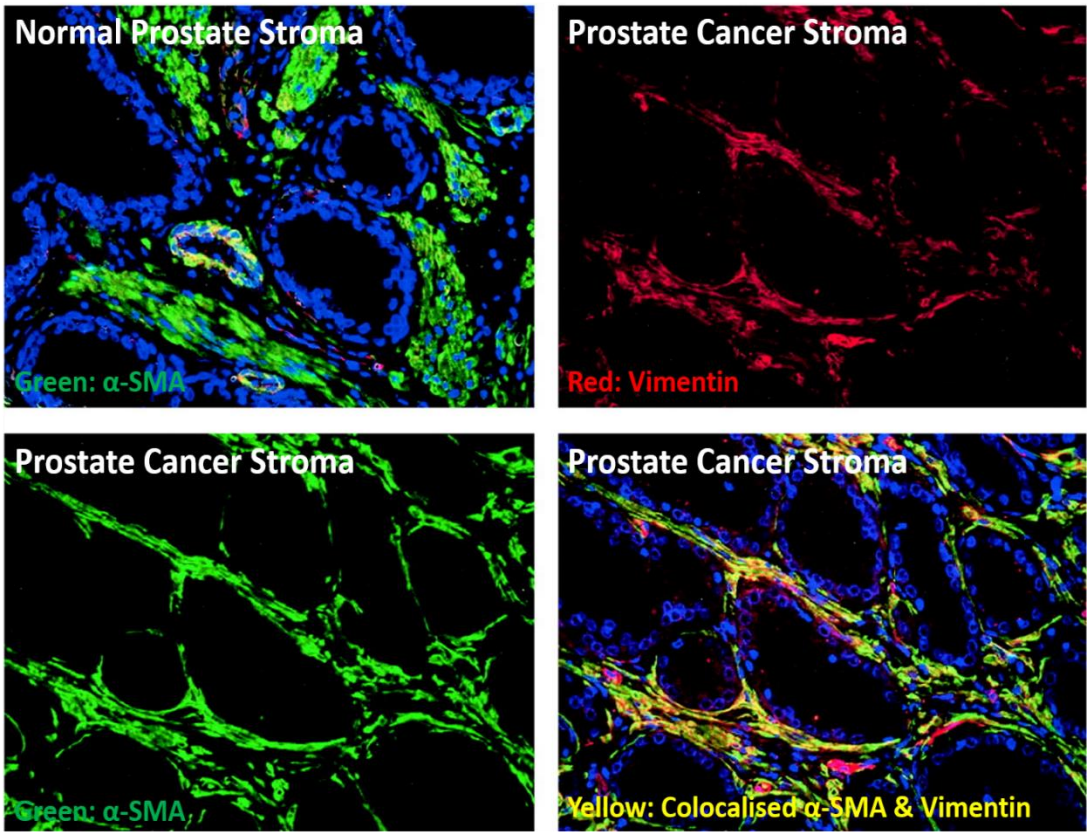

Figure 1.1: Myofibroblasts replace smooth muscle cells in diseased prostate stroma. Normal and cancerous prostate samples were obtained from radical prostatectomy specimens and analysed by immunohistochemistry with α-SMA (green), vimentin (red) and DAPI (blue). Co-localisation was only observed in the blood vessel walls. Enhanced expression of both α-SMA and vimentin double positive cells with the interstitium, indicative of a myofibroblastic phenotype in the prostate cancer. *Source: (Tuxhorn et al., 2002b).*

1.2.2 Tumour-Associated Myofibroblasts

The origins of myofibroblasts with cancerous prostate tissues have been suggested to derive from either fibroblasts (Desmoulière et al., 1993), smooth muscle cells (Xie et al., 2011), pericytes (Hosaka et al., 2016), epithelial cells (Radisky et al., 2007), endothelial cells (Zeisberg et al., 2007), adipose tissue-derived cells (Desai et al., 2014) and MSCs (Mishra et al., 2008), or perhaps all cells above. During tissue repair, fibroblasts undergo a phenotype change from their normal quiescent state, to a proliferative and contractile phenotype termed myofibroblasts. In normal conditions, fibroblasts exhibit homeostatic function, in maintaining an appropriate matrix and tissue structure. First, fibroblasts can differentiate into proto-myofibroblasts, which are characterised by the formation of β- and γ- cytoplasmic actins (Vyalov et al., 1993). The stimuli to trigger this phenotypic transition remains poorly understood, however, mechanical tension has been shown to generate proto-myofibroblasts from fibroblasts (Tomasek et al., 2002), characterised by the formation of stress fibres. These proto-myofibroblasts can generate mechanical tension in the extracellular matrix (ECM), which activates transforming growth factor-β1 (TGF-β1) (Wipff et al., 2007). TGF-β1 can cause differentiation of proto-myofibroblasts into myofibroblasts, characterised by the expression of α-SMA (Darby et al., 1990), ultimately providing contractile capacity akin to a muscle cell.

These differentiated myofibroblasts are morphologically and functionally distinct from their resting and quiescent counterparts (Hinz et al., 2001). These features are shown by a higher organisation of α-SMA stress fibres, connected to the extracellular fibronectin fibrils via focal adhesion complexes (Clark, 1990, Hinz et al., 2001), as shown in Figure 1.2. This connection allows the myofibroblasts to possess a mechanotransduction system, where these actin fibres can generate contractile force to be transmitted to the surrounding ECM (Chrzanowska-Wodnicka and Burridge, 1996). Once induced, myofibroblasts deposit increasing amounts of stiff fibrillar ECM composed of collagen and fibronectin splice variants. This enables the contraction of ECM, activating TGF-β, triggering downstream Smad2/3 phosphorylation, as shown in Figure 1.3. This allows the secretion of other soluble factors released by myofibroblasts allowing further differentiation and growth, thus allowing this positive feedback and remodelling mechanism to occur. Once the original structure of the ECM is repaired at the injury site, the myofibroblasts may undergo apoptosis (Darby et al., 2014); when the wound is eventually fully restored. Though in cancer, restoration does not occur and a persistent 'tissue-repair' state exists in a chronic fashion exacerbating the disease (Schafer and Werner, 2008, Ohlund et al., 2014).

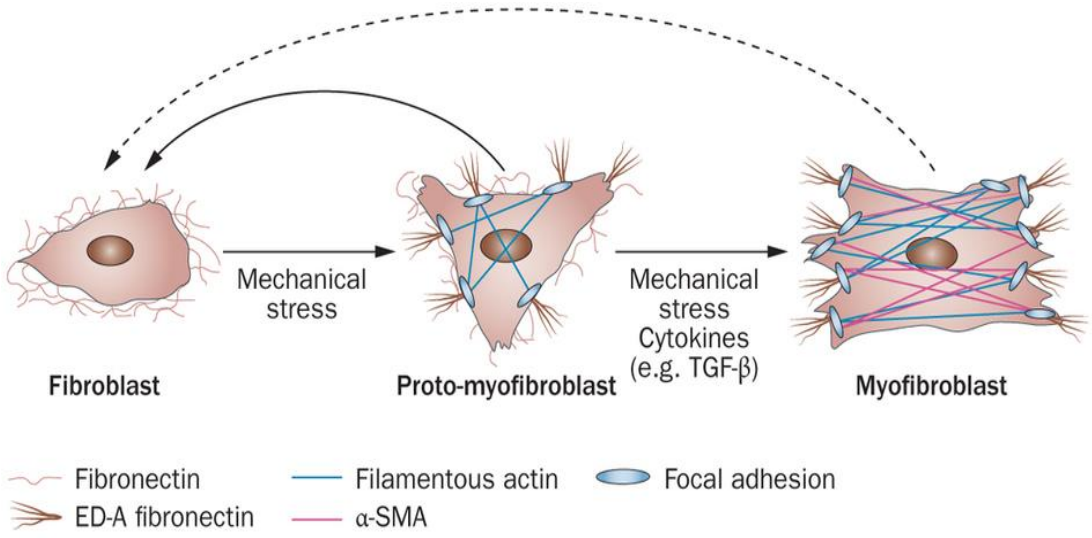

Figure 1.2: Fibroblast differentiation into myofibroblasts during wound healing. The interstitial fibroblasts are characterised by the production of fibronectin and the absences of filamentous actin, α-SMA and ED-A fibronectin. Under mechanical stress, fibroblast can differentiate into proto-myofibroblast, which form actin-containing stress fibres that connects to focal adhesion complexes. Under the control of TGF-β1 and other regulating factors, proto-myofibroblasts can increase the expression of α-SMA and ED-A fibronectin, along with mechanical stress, to differentiate into myofibroblasts and a contractile phenotype. Once wound healing is completed, myofibroblasts may undergo apoptosis, but this remodulation is slow or does not happen in cancer. *Source: (Falke et al., 2015).*

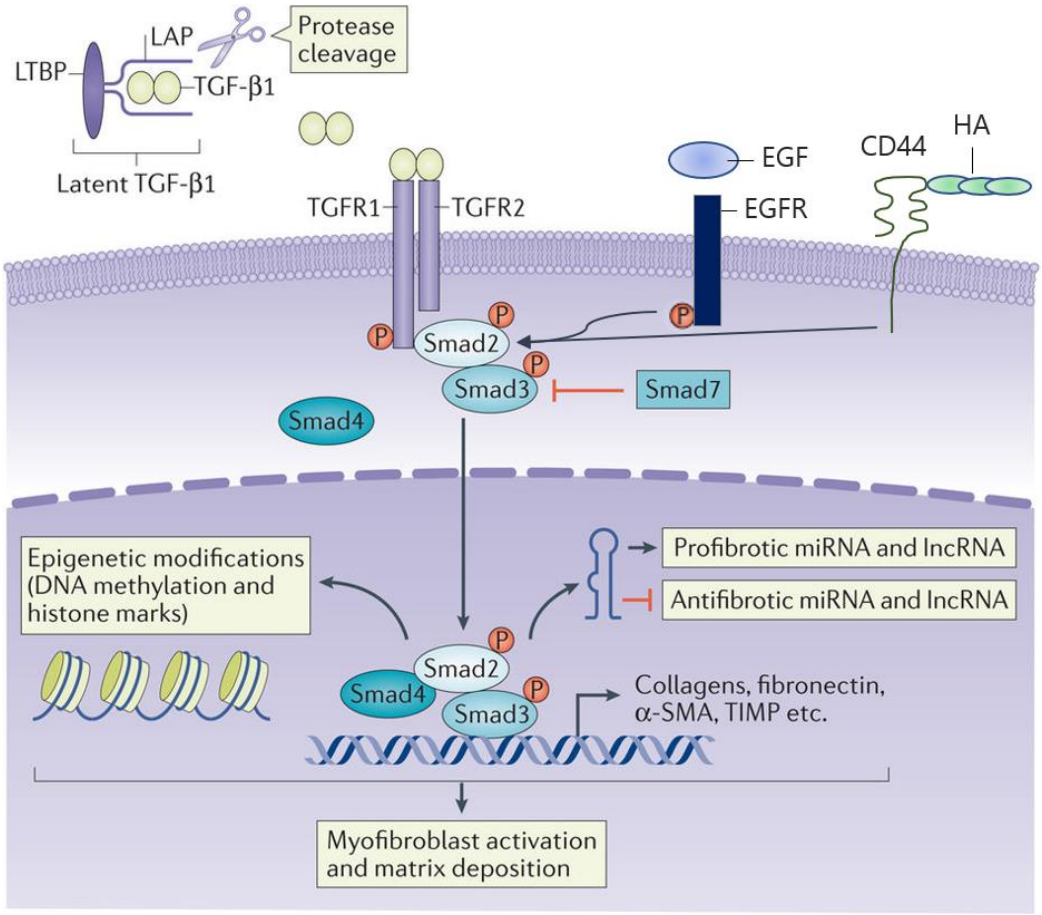

Figure 1.3: TGF-β/Smad and other signalling pathways involved in myofibroblast activation. Once TGF-β1 is released from the latency associated peptide (LAP)-latent TGF-β binding protein (LTBP) complex, the active homodimer form of TGF-β1 binds to TGF-β receptor 2 (TGFR2), which recruits and activates TGFR1. The activate TGFR1 phosphorylates Smad2 and Smad3, which complex with Smad4 and translocate with the nucleus. In addition, other pathways such as EGF/EGFR and CD44/HA interaction can contribute to Smad phosphorylation. This promotes the transcription of α-SMA, collagen type I, fibronectin which induces fibroblast activation and matrix deposition. *Source: (Meng et al., 2016)*

1.2.3 Tumour-Associated Myofibroblasts Promote Cancer Progression

During tumourigenesis, differentiation of fibroblasts to myofibroblasts has been studied since the 1970s (Ryan et al., 1973, Ryan et al., 1974). Such activated "fibroblasts" often termed tumour-associated myofibroblasts, have been assessed for their role in stromal-epithelial interactions regarding tumour progression. In one elegant example, fibroblastic stromal cells isolated from BPH or prostate cancer are added to immune-deficient mice co-implanted with epithelial cells as xenografts (Olumi et al., 1999). It was demonstrated that tumour-associated myofibroblasts could make a non-tumourigenic prostate epithelial cell line tumourigenic, whereas normal tissue fibroblasts were not able to elicit tumourigenesis, as shown in Figure 1.4. We can observe that the prostate cancer tissue with myofibroblasts exhibits greater number of blood vessels, appearing to play a role in promoting angiogenesis, compared to the tissue containing normal fibroblasts. Similarly, myofibroblasts isolated from patients with aggressive breast cancer enhanced the growth rate of breast carcinomas *in vivo*, then that of normal mammary fibroblasts taken from the same patients (Orimo et al., 2005). Tumour-associated myofibroblasts enhanced the aggressive phenotype of breast cancer cells (Yu et al., 2014). There is a consensus that tumour development is not solely determined by malignant cancer cells; and that tumour-associated myofibroblast have a major influence on dictating tumour progression and outcome.

As tumour-associated myofibroblasts play significant roles in the tumour stroma and during tumour progression, they are viewed as good predictors for cancer prognosis in various cancers. In one study, isolated stroma from prostate cancer patients after radical prostatectomy, showed significant differences between the myofibroblast phenotype and progression free-survival. Patients with identical Gleason score, but changes in increased stroma intensity by immunohistochemical (IHC) staining, could identify patients with greater risk of prostate cancer relapse (Tomas et al., 2010). It was also shown in metastatic breast cancer samples to be abundant in α-SMA positive myofibroblasts, compared to non-invasive breast cancer patient samples (Yamashita et al., 2012). In multiple studies, the identification of stromal markers, often myofibroblasts, associate robustly with disease relapse across various cancer types (Moorman et al., 2012, Huang et al., 2014, Calon et al., 2015, Luksic et al., 2015), highlighting the role of tumour stroma in treatment response. Also, the tumour-associated myofibroblasts can promote tumour-supporting functions, by stimulating cancer cell proliferation and progression through the secretion of various cytokines, chemokines or ECM. For example, hepatocyte growth factor (HGF) or vascular endothelial growth factor (VEGF) can enhance tumour progression, by promoting tumour invasion and angiogenesis.

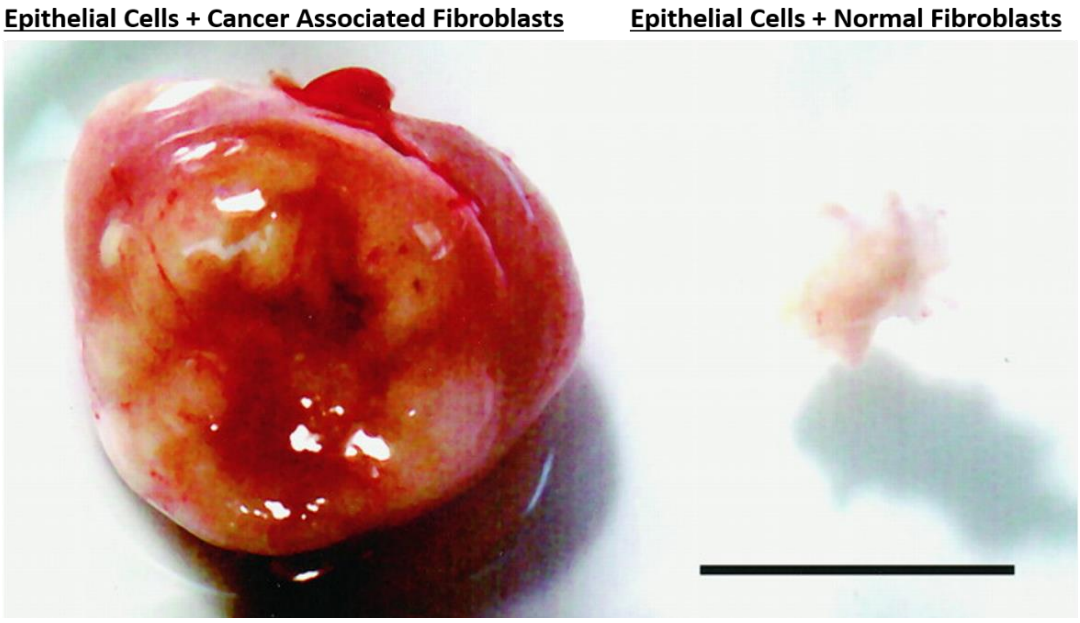

Figure 1.4: Tumour-associated myofibroblast promotes tumour growth. Image of prostate cancer-derived myofibroblast grown with prostate epithelial cells (Left Side), compared to normal fibroblasts with prostate epithelial cells (Right Side). Tissue recombinants were harvested after 85 days of growth in nude mice. The tissue containing tumour-associated myofibroblasts weighed 1250mg, with dramatically stimulated growth and altered histology of the epithelial population and clear macroscopic involvement of angiogenic support. In contrast, the normal fibroblasts weighed 10mg under identical conditions halting endothelial vascularisation. Scale bar: 1cm. *Source: (Olumi et al., 1999).*

Angiogenesis

Angiogenesis, or the formation of new blood vessels from the pre-existing vasculature, is a vital component in numerous physiological and pathological responses. In normal physiological responses, a variety of angiogenic signals induces endothelial cells to detach their junctional adhesion from their neighbouring cells, sprout near gradients of pro-angiogenic factors, proliferate to form provisional tubes, recruit perivascular cells to provide stability and maturation, re-organise with vascular smooth muscle cells and pericytes to form a functional blood vessel network (Carmeliet and Jain, 2000). Monolayer of endothelial cells often form capillaries, creating a semi-permeable barrier between the surrounding tissue and blood, allowing nutrient and waste product exchange to and from surrounding cells (McDonald and Baluk, 2002, Nagy et al., 2010).

In cancer, multiple sources of pro-angiogenic factors contribute to vascular remodelling, that aids tumour growth and progression (Adams and Alitalo, 2007). Once a tumour lesion grows beyond the capacity for nutrient, waste and O_2 to diffuse passively, it experiences hypoxia or nutrient deprivation. Thus, angiogenesis is initiated and tumour cells exploit this process for tumour growth. The secretion of growth factors activates normal surrounding quiescent cells, to initiate a cascade of events that become quickly dysregulated. This involves an 'angiogenic' switch, that is regulated between anti- and pro-angiogenic cytokines and examples of pro-angiogenic growth factors include: fibroblast growth factor (FGF), platelet derived growth factor (PDGF), HGF and VEGF (Ferrara, 1993, Boccaccio et al., 1998, Dunn et al., 2000). VEGF stimulates the migration, sprouting and proliferation of endothelial cells. However, this may initially provide the tumour with more nutrients and oxygen, the ultimate response is poor, as the continuously remodelled tumour vasculature is leaky, causing irregular blood flow (Hoeben et al., 2004). Tumour tissues often exhibit abnormally high blood vessel densities, in comparison to normal tissues (Olumi et al., 1999). These differences in blood vessels were documented to increase during early tumour formation, indicating their role in tumour growth (Kamoun et al., 2010).

Tumour-associated myofibroblasts have been documented to secrete these pro-angiogenic growth factors, such as HGF and VEGF, that can promote angiogenesis at primary tumour sites (Xin et al., 2001, Zhang et al., 2003). In a tumour:fibroblast xenograft model, tumour-associated myofibroblasts extracted from invasive breast carcinomas, promoted tumour growth of breast carcinoma cells significantly more than those with normal mammary fibroblasts (Orimo et al., 2005). They promoted tumour growth by secreting stromal cell-derived factor 1 (SDF-1), promoting angiogenesis by mobilising endothelial cells into

carcinomas; and gives rise to highly vascularised tumours. In an oesophageal carcinoma model, the presence of tumour-associated myofibroblasts was essential for efficient human microvascular endothelial cell network formation; selective VEGF inhibition blocked the formation of a vascular network in this model (Noma et al., 2008). Furthermore, co-culturing diseased stromal cells from prostate cancer with endothelial cells, promoted vessel-like structure formation *in vitro* (Webber et al., 2015). The diseased stromal cells were IHC stained to be α-SMA positive, indicating a myofibroblastic-like phenotype. These studies give evidence that myofibroblasts are important components of the tumour microenvironment that may enhance endothelial vessel formation.

Tumour Invasion and Metastasis

Tumour cells can migrate and invade, escaping from the primary tumour site to a new secondary distant site to form a new secondary tumour. It has been reported that myofibroblasts are present at the invasive leading edge of primary tumours, such as colorectal cancer *in vivo* (Illemann et al., 2004); and proposed to play a role in supporting tumour invasion. In one study, tumour-associated myofibroblasts are commonly found in the stroma of oral squamous cell carcinomas and are often concentrated at the leading edge of the tumour (Lewis et al., 2004). Furthermore, cell conditioned media (CM) obtained from tumour-associated myofibroblasts derived from colorectal cancer, were found to promote invasion of colorectal cells in a collagen gel matrix (Cat et al., 2006). In contrast, cell CM from normal fibroblasts derived from healthy patients, failed to support tumour cell invasion, compared to tumour-associated myofibroblasts. In contrast to fibroblasts, myofibroblasts secrete elevated levels of HGF and VEGF resulting in a significant increase in the invasive capacity of tumour cells through collagen/matrigel matrices (Lewis et al., 2004, Cat et al., 2006). Blocking the HGF and VEGF levels, decreased the invasive capacity of tumour cell invasion (De Wever et al., 2004). Other growth factors, such as epidermal growth factor (EGF), FGF, HGF, insulin-like growth factor (IGF), PDGF and VEGF, are secreted at elevated levels in tumour-associated myofibroblasts, compared to normal fibroblasts (Dunn et al., 2000, Orimo et al., 2005, Weigel et al., 2014, Webber et al., 2015).

Other soluble factors such as matrix metalloproteinases (MMPs) may be involved in enhancing tumour cell's invasive capacity. MMPs are matrix degrading enzymes that breakdown the components of the basement membrane and ECM, such as collagen, elastin, fibronectin and laminin (Sang, 1998, Lu et al., 2011). Expression of MMP-1 is detected in areas of ECM remodelling and has been described in a wide variety of advanced cancer (Bendardaf et al., 2007, Pulukuri and Rao, 2008). Similarly, cell CM from tumour-associated

myofibroblasts derived from aggressive breast cancer cells contained elevated levels of MMP-1, compared to normal mammary fibroblasts (Boire et al., 2005). Furthermore, elevated levels of MMP-13 have been associated with decreased overall survival and lymph node metastasis in breast cancer (Shah et al., 2012), bone metastasis in renal cell carcinoma (Kominsky et al., 2008); and invasive capacity in lung cancer (Hsu et al., 2006) and colorectal cancer (Leeman et al., 2002). Also, administration of a selective MMP-13 inhibitor in mice significantly inhibited primary tumour growth and breast cancer-associated bone remodelling in xenografts (Shah et al., 2012). Inhibition of MMP-1 activity demonstrated a reduction in the motility of both breast and prostate cancer cells in a Boyden transwell invasion chamber (Boire et al., 2005, Giannoni et al., 2010). In the same prostate cancer model, spontaneous metastasis was not observed when administering prostate cancer cells alone or with fibroblasts from healthy stroma into mice (Giannoni et al., 2010). Yet, the ability for prostate cancer cells to metastasise to the lung was obvious, when co-cultured with tumour-associated myofibroblasts *in vivo*.

In prostate and other carcinomas, the interstitial stroma contains an abnormally high amount of tumour-associated myofibroblasts, capable of supporting tumour growth, partly through encouraging angiogenesis, invasion and metastasis. An assortment of factors has been proposed to be involved in triggering fibroblast differentiation. Though, it has been shown that tumour-derived, nanometre sized extracellular vesicles (EVs) can trigger fibroblast differentiation. More specifically, tumour-derived exosomes can generate this response to produce distinct tumour-associated myofibroblasts, supporting angiogenesis and tumour growth.

1.3 Exosome Biology

1.3.1 Different Types of Extracellular Vesicles (EVs)

Cells can secrete different types of membrane-bound vesicles, collectively termed as EVs; and these have been given many names throughout the literature: membrane vesicles, membrane particles, nanoparticles, ectosomes, microvesicles (MVs) and exosomes. We may categorise secreted EVs in terms of their intracellular origin or based on their size (Théry et al., 2009). More commonly characterised vesicles such as exosomes, are formed in endosomal compartments and released upon fusion with the plasma membrane. Other vesicles, however, may be released directly from the plasma membrane by budding and shedding. These include microvesicles or membrane particles (Heijnen et al., 1999). Dying cells can release vesicles, referred to as apoptotic bodies, which are distinct from exosomes (Théry et al., 2001).

Currently there is no consensus in the field as to a proper nomenclature and the precise definition of each type of EVs, because different research groups utilise different methods to isolate, purify and characterise EVs. More recently, one of the position statements published by the International Society of Extracellular Vesicles (ISEV) created minimal experimental requirements for defining EV characterisation and function (Lotvall et al., 2014). To define EVs, researchers firstly must report several proteins or lipids expected to be present in the EVs of interest, including quantitation of contaminants not necessarily expected present on EVs. Furthermore, characterisation of single vesicles within a mixture should be performed, such as low magnification images showing a broad description of the state and morphology of the entire isolated EV population and high magnification to define structural depth of individual vesicles; as well as size distribution measurements providing diameters of many EVs to give an indication of heterogeneity of the EV preparation studied. Some of these requirements may allow us to distinguish vesicles secreted by the plasma membrane from those derived from endocytic compartments, such as exosomes.

1.3.2 Exosome Characterisation

One of the first studies to observe the presence of EVs was by electron microscopy (EM), demonstrating these EVs were involved in calcifying matrix within newly formed bone (Anderson and Reynolds, 1973). Following studies described exosomes during the maturation of red blood cells, as reticulocyte purge cellular mass and the transferrin receptor (Harding et al., 1983, Pan et al., 1985). In the first instance, utilising either gold particles or anti-transferrin antibodies, an EM approach was used to monitor the process of the

endocytosed receptor during trafficking in the cell and following release. The transferrin receptor was detected in early endosomes, before being trafficked to multi-vesicular endosomes (MVEs). Many of the gold particles were located on smaller nanometre sized 'bodies' (around 50nm in diameter), which were released upon MVE fusion with the plasma membrane. Following on, one study demonstrated that secreted vesicles could be isolated and analysed by ultracentrifugation at 100,000 *x g*, normally present on the plasma membrane (Johnstone et al., 1987). The term 'exosome' was first reported used to categorise secreted EVs of heterogeneous sizes, including one population with diameters between 500 and 1000 nm; and a smaller population of around 40nm (Trams et al., 1981).

Later, this nomenclature was adopted for vesicles, as their secretion and presence inside multivesicular endocytic compartments was reported in reticulocytes (Harding et al., 1983, Pan et al., 1985). Exosome are formed by budding of the limiting membrane of 'sorting' vacuolar endosomes towards the lumen of these compartments, thus forming intraluminal vesicles (ILVs), the endosomes are referred as MVEs. The fusion of MVEs with the plasma membrane enables the release of ILVs into the extracellular space and these secreted ILVs are referred to as exosomes. Due to their endosomal origin, exosomes possess several hallmarks of ILVs of the MVEs, such as their size, which ranges from 30 to 150 nm in diameter, reflecting exosome heterogeneity (Colombo et al., 2013).

Molecular Composition of Exosomes

Since their initial description of exosomes, many efforts have been made to further characterise the protein composition of exosomes. Many studies of EVs biochemical composition involved analysis of bulk populations obtained by ultracentrifugation, that often provides a heterogeneous EV population. The development of proteomic analysis soon allowed identification of non-determined proteins in isolated EVs. Mass spectrometry was used for peptide mapping on exosomes derived from dendritic cell (DC) mouse cultures (Théry et al., 1999) and similarly, on exosomes isolated from various cell types (Théry et al., 2001, Lamparski et al., 2002). By characterising exosomes from numerous studies, these results were assembled in a database called ExoCarta (Mathivanan and Simpson, 2009), which was refined into a more comprehensive database called Vesiclepedia (Kalra et al., 2012) and EVpedia (Kim et al., 2015), that incorporates data from other EV types and additional data on lipids and nucleic acid.

Initial proteomic studies showed exosomes contain a specific subset of cellular proteins, some found in all cell types, whereas others are specific to the cell type. These include

proteins from the plasma membrane, endosomes or cytosol, although proteins from the endoplasmic reticulum, mitochondria or nucleus are often absent. For example, the apoptosis-linked gene 2-interacting protein (ALIX) and tumour susceptibility gene 101 (TSG101) are known components of the endosomal complex required for transport machinery (ESCRT) (Morita et al., 2007). The function of the ESCRT complex is involved in forming MVEs, loading and sorting of cargo proteins into ILVs, working at the MVE membrane and recognising ubiquitinylated proteins that are incorporated into the vesicles. Tetraspanins such as cluster of differentiation (CD)9, CD63, CD81 or CD82, are often enriched on the exosome's surface. CD9 was first identified in DC-derived exosomes (Théry et al., 1999); and several studies describe CD63 and CD81 as frequently identified proteins and are considered classical "markers". CD9 is often found enriched in exosomes derived from prostate cancer cell lines (DU145) (Liu et al., 2014, Webber et al., 2014). Also, exosomes express major histocompatibility molecules class I (MHC-I) and II (MHC-II), playing roles in immune-regulation by presenting antigenic peptides (Lamparski et al., 2002). Other common exosomal-associated proteins include heat shock protein 70 (HSP-70) and 90 (HSP-90), which assists in protein folding and trafficking, acting as chaperones (Clayton and Tabi, 2005, Mayer and Bukau, 2005), accelerating peptide loading onto MHC-I and -II and playing roles in the cellular response to environmental stresses (Cho et al., 2005). Also, a subset of the endosomal/lysosomal proteins are found in exosomes, such as the lysosomal associated membrane protein 1 (LAMP1) and 2 (LAMP2). Some examples show exosomes from tumour cells contain LAMP1 (Wolfers et al., 2001) and LAMP2 is detected from DC-derived exosomes (Escola et al., 1998). Moreover, the presence of proteins, such as calnexin or GP96, derived from the endoplasmic reticulum are mostly absent in exosomes (Wolfers et al., 2001, Cho et al., 2005). This highlights some proteins present on the exosome's surface or inside the lumen that differs between cell types, representing a specific subcellular compartment and not an array of random cell fragments.

Fewer studies have analysed the lipid composition of exosomes, but it differs from the plasma membrane. The exosomal membrane does not have an asymmetrical distribution of the lipid phosphatidylethanolamine (PE), compared to asymmetrical distribution in the inner leaflet of the plasma membrane. This may be due to a lack of flippase in exosomes, which actively maintains phospholipid asymmetry in the plasma membrane and possible MVEs (Laulagnier et al., 2004). It was reported exosomes are enriched in ceramide, which was linked to vesicle biogenesis and release from oligodendrocytes (Trajkovic et al., 2008). Cargo was shown to be segregated into distinct subdomains on the endosomal membrane and that

the transfer of exosome-associated domains into the lumen did not depend on the ESCRT machinery, but required ceramide; therefore, an ESCRT-independent mechanism. Also, nucleic acids are often confined within exosomes and reports highlighted that messenger ribonucleic acid (mRNA) or micro ribonucleic acid (miRNA) can be present in exosomes from biological fluids (Valadi et al., 2007, Kosaka et al., 2010). This suggests the expression patterns of these nucleic acids may act as markers for the diagnosis and prognosis of different pathologies. Other reports have revealed possible functions for secreted EVs carrying nucleic acid in tumour cell migration and growth (Skog et al., 2008, Zhang et al., 2010). These studies highlight the complexity behind the molecular composition of exosomes, as there remains no universal marker as shown in Figure 1.5. The use of compiling multiple studies into a main database, such as Vesiclepedia, will contribute to the harmonisation of the nomenclature of different EVs.

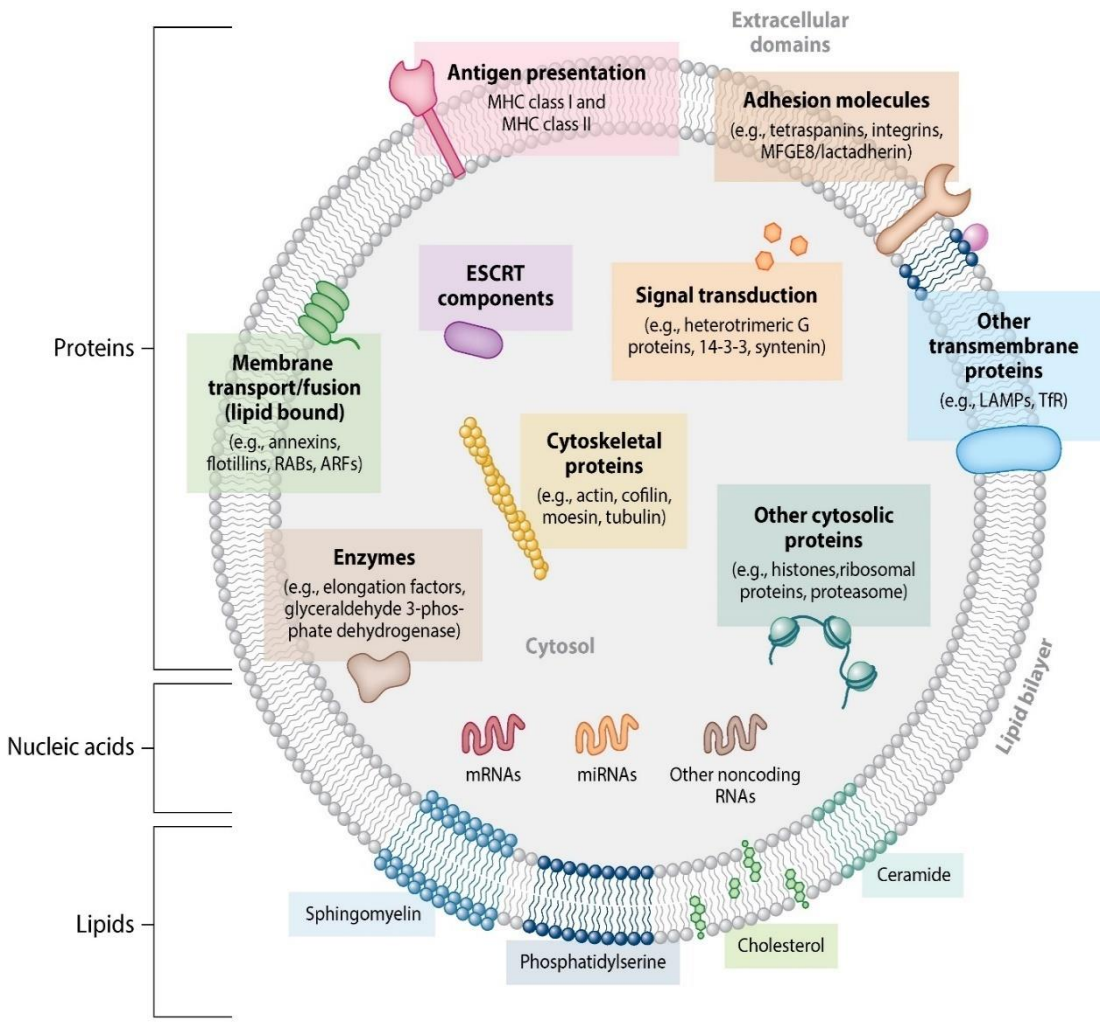

Figure 1.5: Molecular composition often found on exosomes. Schematic representation of the composition and membrane orientation of exosomes, encompassing families of proteins, lipids and nucleic acid. Commonly found are tetraspanins include CD9, CD63 and CD81; and many others such as MHC-I, heat shock proteins (HSP70 and HSP90), LAMP proteins (LAMP1 and LAMP2), ESCRT components (ALIX and TSG101), Rab proteins (Rab5a, Rab11b, Rab27a, Rab35), growth factors, cytokines, mRNA/miRNA and lipids. *Adapted from source: (Colombo et al., 2014).*

1.3.3 Methods for Exosome Isolation and Purification

Exosome Isolation and Purification

The general protocol used in earlier studies to isolate and purify exosomes (Johnstone et al., 1987, Raposo et al., 1996) is based on ultracentrifugation. It involves numerous successive steps (Théry et al., 2006), where a centrifugation spin at 400 x *g* is aimed at removing cell pellets. The remaining supernatant is centrifuged again at 400 x *g* and subsequently at 2000 x *g*, to remove dead cells and larger cellular debris. A subsequent ultracentrifugation step at 10,000 x *g* is used to pellet other types of EVs, such as microvesicles, which are larger in size and sediment easier. Alternatively, some variations are implemented in practice, for example serial filtration through 0.22µm filters will eliminate contaminating vesicles or debris, prior to exosome pelleting. The final ultracentrifugation step at 100,000 – 200,000 x *g* is used to pellet the exosomes as shown in Figure 1.6. It is important to take into consideration that this only enables an enrichment of exosomes and not a proper purification, since other EVs of similar size, as well as protein aggregates, are likely to sediment at the same speed. Ultracentrifugation remains commonly used to isolate or enrich a certain EV type and variations of this protocol can considerable vary from one laboratory to another. Different protocols have been developed to purify the exosomes, which will be discussed in the following paragraphs.

Other protocols have been developed using antibody-coated magnetic beads (Clayton et al., 2001) or latex beads (Lamparski et al., 2002, Caby et al., 2005). These rely on the expression of specific surface proteins, which are used to capture exosomes on beads, which can be analysed by flow cytometry. However, this protocol is limited, requiring their further use in additional experiments, as it remains difficult in extracting exosomes from beads requiring extra steps for functional studies and remains predominantly used to identify molecular signature markers.

Another method to purify exosomes from other contaminants can be performed by using a continuous sucrose density gradient (Raposo et al., 1996, Escola et al., 1998). Exosomes have a biochemical property allowing floatation at a density of 1.1 – 1.2g/ml, compared to vesicles from the golgi apparatus floating at 1.05 – 1.1g/ml (Théry et al., 2006) and the density of protein aggregates at 1.22g/ml (Quillin and Matthews, 2000). The differing density of the potential contaminants (protein aggregates) of exosomes make the sucrose gradient an approach to purify exosomes from crude vesicle concentrates. The exosomes will be obtained in different fractions of the sucrose gradient and the remaining fractions can either be pooled together for analysis or examined independently. An alternative to sucrose density

gradients is to involve ultracentrifugation of the cell CM in sucrose deuterium oxide (D_2O) cushions. This protocol was commonly used to isolate clinical grade exosomes (Lamparski et al., 2002); and is more reproducible as a daily preparative method, compared to gradients.

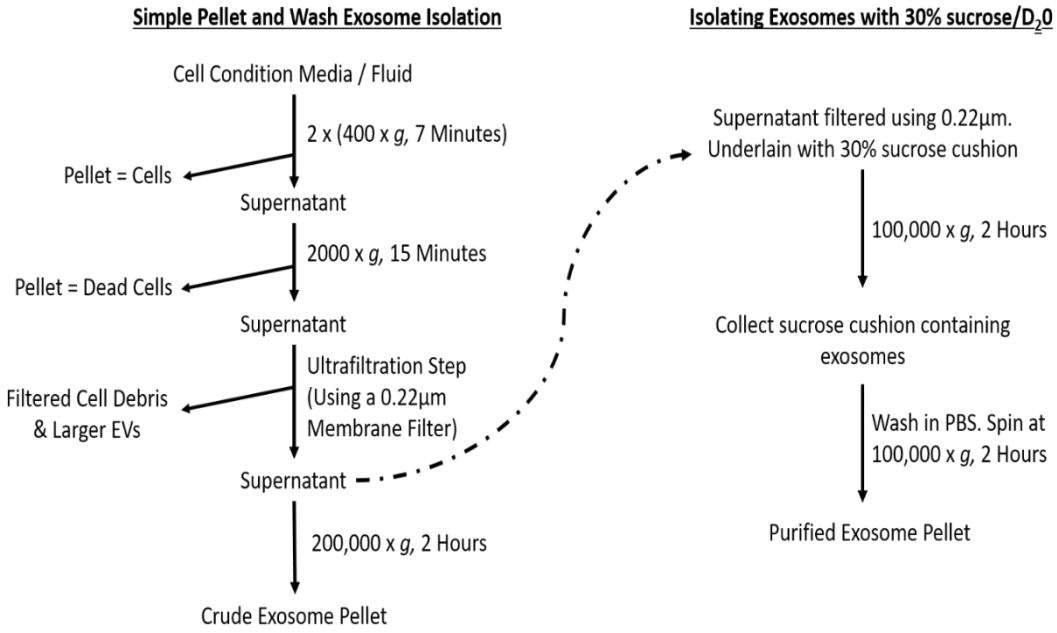

Figure 1.6: Flowchart for isolating and purifying exosomes based on ultracentrifugation and 30% sucrose/D_2O cushion method. Flow chart showing the steps involved for removal of viable cells, dead cells, cellular debris and larger EVs, to obtain a crude exosome pellet. Alternatively, the filtered supernatant is ultracentrifuged with a sucrose cushion to present exosomes from pelleting. The cushion is washed thereafter to obtain a purified exosome pellet. *Adapted from source: (Lamparski et al., 2002, Théry et al., 2006).*

More recently, commercially available methods to promote quick and simple exosome purification protocols, such as Total Exosome Isolation Reagent (TEI), ExoQuick™ or ExoSpin™, have been released (Sunkara et al., 2016). These easy-to-use precipitation solutions have many disadvantages present with these kits. They do not specifically enrich exosomes, but also co-precipitate non-exosomal impurities, showing background contamination in cryo-EM images (Van Deun et al., 2014). There have been suggestions that using density gradient-based isolation method, such as iodixanol (OptiPrep™) can be applied to obtain a purer exosome preparation compared to sucrose-based gradients. A study has encouraged the use of an iodixanol-based gradient, which improves the separation of exosomes from viruses and small apoptotic bodies (Cantin et al., 2008). Though, using the OptiPrep™ gradient is a complex and time-consuming process.

As there are multiple protocols used to isolate exosomes, each technique must be validated for any given cell type or biological fluids as a source of exosomes, to confirm the identify for the given purified exosome. This often requires a combination of multiple assays, which are described in further detail below.

Exosome Detection

As exosomes are small nanometre sized EVs, cryo-EM allows the direct visualisation of the morphology and size of exosomes. Pelleted vesicles, resuspended in a small volume of buffer are normally adsorbed onto glow-discharged holey carbon grids. Exosome samples are vitrified in liquid ethane, to prevent the formation of crystal structures and preserve the native vesicle structure (Conde-Vancells et al., 2008). Furthermore, the presence of selected proteins on the surface of exosomes can be detected by immuno-EM (Théry et al., 2006). Using specific antibodies, gold particles can identify a few proteins in the same sample simultaneously, whilst determining the purity of the exosome preparation to assess if the debris/contaminants are present (Bobrie et al., 2012). Though, it would remain difficult to separate these exosomes for functional based experiments.

Classical biochemistry methods, such as Western blotting, can provide information on the enrichment of proteins present on exosomes. The protein content can be compared between cell lysates and the exosomal pellet. A different pattern often reveals a good purity, since it rules out the presence of cell compartments not usually represented in exosomes, such as the endoplasmic reticulum. Western blotting is routinely used to investigate the presence of specific exosomal-associated proteins and compared to cell lysates (Raposo et al., 1996, Théry et al., 1999). As some examples, exosomes are enriched in ALIX or TSG101

(dependent on the cell type), but does not contain proteins from cell compartments, such as calnexin or GP96 (endoplasmic reticulum marker).

Similarly, another technique that allows the quantitative analysis of protein content is flow cytometry. There are limitations, as a typical flow cytometer detection limit is 500nm and as exosomes are between 30 – 150nm, they would appear as background noise. Beads have been coated with antibodies against proteins, typically found on the exosome's surface that will increase the chances of investigating exosomes exclusively. Alternatively, a microplate immuno-phenotyping assay can also provide a quantitative analysis, as exosomes are bound onto enzyme-linked immunosorbent assay (ELISA) strip plates. Primary antibodies can be used to target proteins of interest typically found on the surface of exosomes; and time-resolved fluorescent can be determined by using a microplate reader. Though, a bulk assay like an ELISA plate would have difficulty in distinguishing sub-population of vesicles, which flow cytometry might be able to accomplish.

Another technique used to give an indication of how heterogeneous the exosome sample is using Nanoparticle Tracking Analysis (NTA) (Nanosight™). NTA is used to measure size distribution and concentration of nanoparticles (Dragovic et al., 2011). Quantification of nanoparticles by NTA are predominantly based on two principles: the movement of particles in suspension under Brownian motion and their movement, which will scatter light that can be individually tracked by the NTA software. This software will calculate the exosome's diameter by using the Stokes Einstein equation. One main advantage of using NTA compared to other technologies, such as resistive pulse sensing or dynamic light scattering (DLS), is the speed and simplicity of analysing many particles simultaneously; and the suitability of the method for particles of heterogeneous sizes. Though, multiple parameters, such as the sample dilution, camera shutter speed and gain, length and number of videos, and detection threshold, must be set by the user to acquire reproducible results. One downfall for NTA, is it does not discriminate the morphology of different EVs (cannot distinguish an exosome and microvesicle of similar sizes) and the results are less accurate when samples are polydispersed; however, this approach is better than using DLS.

There is no consensus on a 'gold standard' method to isolate and/or purify; and subsequently characterise exosomes. There are multiple techniques that can provide different information, in terms of morphology, size and molecular composition about the isolated exosome preparation. It is, therefore, important to use these techniques in an informed fashion and stipulate clearly the method used to characterise the isolated EVs in question.

1.3.4 The Functions of Exosomes in Cancer

Since the 1980s, numerous diverse functions have been attributed to exosomes. Exosomes are known to exhibit functions like their parent cell. For example, initial studies described the release of the transferrin receptor during reticulocyte maturation. It was suggested that these membranous structures (exosomes) were used by cells to remove obsolete molecules (Harding et al., 1983, Pan et al., 1985), a process key for differentiation into erythrocytes. However, this role as cellular waste may not have done the EV field much favour as for a long time, the fate of EVs was amounted with waste and nothing more. Though, seminal work from the Institut Curie groups, identified cell-activating roles for exosomes. Exosomes from antigen presenting cells such as B cells, are enriched in MHC-II and have shown to be functional in antigen presentation, leading to T cell stimulation (Raposo et al., 1996). It was shown that exosomes secreted from DCs bear antigen and MHC-peptide complexes, participating in immune responses (Théry et al., 1999). Other studies have also highlighted that exosomes secreted by intestinal epithelial cells are involved in humoral responses and transfer antigenic information from the apical domain to the immune cells in the gut (Van Niel et al., 2003). Additional reports support the concept that exosomes from one cell may fulfil a function on the recipient cell. The findings that exosomes carry protein, lipid and nucleic acids such as mRNA and miRNA, that are functional in recipient cells (Valadi et al., 2007), strengthens this notion. In cancer, these discoveries suggest exosomes may play roles in cell-to-cell communication and contribute through varied mechanisms for the pathological processes of cancer.

Exosomes and the Immune Response

Many studies have investigated the function of exosomes derived from tumour cells. It has been reported exosomes can carry tumour antigens to induce an efficient anti-tumour response. Melanoma-derived exosomes has been reported to be presented to antigen presenting DCs for cross presentation to cytotoxic T lymphocytes (CD8+ T Cells) via MHC-I molecules (André et al., 2002). These activated T cells can trigger an anti-tumour response that suppresses tumour growth *in vivo* (Wolfers et al., 2001). Although the potential here for immune responses against murine viruses contaminating the EV preparations is high and may explain the specific potent immune response generated by exosomes in mice. Additional studies demonstrated HSP70-enriched exosomes from pancreas and colorectal cancer can stimulate natural killer (NK) cell activity, resulting in NK-mediated apoptosis of tumour cells (Gastpar et al., 2005, Lv et al., 2012). The data suggests that tumour-derived exosomes can inhibit tumour progression by promoting these immunological responses.

On the other hand, tumour exosomes have been described to exert immunosuppressive functions, such as tumour cells escaping from CD8+ T-cells. Some studies have reported that melanoma and prostate cancer cell-derived exosomes express CD95L (Fas-Ligand), inducing apoptosis of Fas positive CD8+ T cells in a dose-dependent manner (Andreola et al., 2002, Abusamra et al., 2005). This apoptotic effect was abrogated by blocking FasL on the tumour exosomes. Also, in another study, tumour-derived exosomes can inhibit myeloid differentiation into DCs and trigger differentiation of myeloid cells into immunosuppressive cells (Yu et al., 2007, Xiang et al., 2009). It was demonstrated the cytotoxic function of NK cells was impaired following tumour exosome treatment (Clayton et al., 2007). But, $CD4^{+}CD25^{+}$ Treg cells remained interleukin (IL)-2 responsive through induction of Foxp3 expression and their inhibitory function was enhanced by tumour exosomes, showing this appears to be contributed by TGF-β-associated exosomes. In one study, a $CD8^{+}$ T cell line pre-incubated with tumour exosomes bearing NKG2D ligands had significantly decreased the $CD8^{+}$ T cell capacity to kill target cells (Clayton and Tabi, 2005). NKG2D is an activating receptor for NK or $CD8^{+}$ T cells, whose aberrant loss in cancer appears key for immune evasion. The follow-up study demonstrated that TGF-β positive exosomes appear to have a role in downregulating NKG2D expression by NK and $CD8^{+}$ T cells, impairing effector immune function (Clayton et al., 2008). Furthermore, it was reported that cancer exosomes expressing CD39 and CD73 can suppress T cells through adenosine production (Clayton et al., 2011). These exosomes are capable of dephosphorylating exogenous adenosine triphosphate (ATP) and 5'AMP to form adenosine, which are due to the functional CD39 and CD73 by exosomes. The mechanisms behind these actions remain poorly understood, however, these are some examples how cancer-derived exosomes may direct escape from immune surveillance.

From numerous studies, tumour exosomes may play different contrasting roles in cancer. Exosomes may exert an anti-tumour response, as well as triggering an immunosuppressive function. These differences in the role of tumour exosomes may possess different phenotypes from different cancer types and thus, the differences in function is observed.

Exosomes and Drug Resistance

Cancer exosomes may have other functions that involve the support for drug resistance. One study demonstrated that ovarian cancer cells resistant to the chemotherapeutic drug, cisplatin, were secreting elevated levels of exosomes, compared to cells sensitive to chemotherapy (Safaei et al., 2005). It is proposed that once the chemotherapeutic drugs reach cancer cells, the secreted exosomes can expel these drugs away from the cancer cells.

Similarly, manipulated breast cancer cell lines that became insensitive to chemotherapeutic drugs, such as adriamycin or docetaxel, were found to transfer mRNA/miRNA traits that were linked to drug resistant traits via exosomes (Levchenko et al., 2005, Chen et al., 2014). It was shown that ribonucleic acid (RNA) is retained within the exosome (Valadi et al., 2007), which can give sufficient protection from RNAse degradation, which may transferred to recipient cells. These observations suggest that cells may also acquire drug resistance traits from exosomal RNA. From multiple studies, cancer cells may acquire drug resistant traits from surviving cells treated with chemotherapy. These surviving cells may carry genes resistant to drug treatment, allowing a small proportion of cancer cells to survive, which may ultimately lead to a positive feedback mechanism to occur that may allow cancer to relapse.

Exosomes and the Stromal Response (Angiogenesis)

Studies have demonstrated tumour exosomes can directly support angiogenesis by interacting with endothelial cells. Murine multiple myeloma-derived exosomes carried multiple angiogenesis-related proteins, such as angiogenin, FGF and VEGF, enhancing angiogenesis and directly promoting endothelial cell growth by modulating pathways such as PI3K/Akt and p120/signal transducer and activator of transcription (STAT) 3 pathway (Wang et al., 2016a). Tspan8 was often overexpressed in pancreatic and prostate cancer (Uhlen et al., 2010), correlating with increasing levels of angiogenesis *in vivo*. These Tspan8-positive exosomes promoted endothelial cell branching and elevated pro-angiogenic growth factor levels *in vitro*, thus promoting angiogenesis (Gesierich et al., 2006). Elevated transcription levels of urokinase-type plasminogen activator (uPA), VEGFR and von Willebrand Factor (vWF) was found in endothelial cells, when treated with Tspan8 positive exosomes from rat adenocarcinoma cells. These observations overlapped with enhanced endothelial cell migration, branching and proliferation (Nazarenko et al., 2010). It was reported that the mRNA content of glioblastoma EV demonstrates an enrichment of transcripts related to pro-angiogenic function; and provided evidence that EV delivers mRNA that is subsequently translated into proteins in recipient cells (Skog et al., 2008). Similar observations have shown an enhanced proliferative impact on endothelial cells and enhanced tubule formation shown in 3D *in vitro* culture (Hong et al., 2009). In one study, exosomes from colorectal cancer were found to promote endothelial proliferation and tubule formation *in vitro* (Huang and Feng, 2016); and the transfer of exosomal miRNA (such as miRNA-92a) may play a role in this process (Umezu et al., 2013). Such alterations in miRNA can enhance endothelial cell migration and tube formation. Similarly, this was shown in squamous carcinoma and colorectal cancer cells secreting exosomes enriched in proteins

and cell cycle-related mRNAs, that can facilitate angiogenesis and metastasis (Thompson et al., 2013). Tumour exosomes, therefore, may play roles in supporting angiogenesis *in vitro* and *in vivo*, possibly due to the transfer of genetic information to recipient endothelial cells.

Stromal Myofibroblasts

Stromal myofibroblasts have been known to support tumour growth and progression (Tuxhorn et al., 2002a, Kalluri and Zeisberg, 2006), but the first report of an exosomal role was documented in a prostate cancer model (Webber et al., 2015). Specifically, TGF-β1 positive cancer exosomes from mesothelioma and prostate (DU145 or PC3) cells have been shown to trigger fibroblast differentiation to myofibroblasts, as characterised by α-SMA onset into stress fibres (Webber et al., 2010). Exosomes from breast (MCF-7), prostate (LNCAP) or colorectal (CaCO2) cancer cell lines with low/undetectable levels of TGF-β1 failed to trigger fibroblast differentiation into α-SMA positive myofibroblasts (Webber et al., 2010). Blocking TGF-β1 signalling revealed fibroblast differentiation into myofibroblasts to be reliant on TGF-β1 associated exosomes, that triggered the SMAD-dependent pathway. Similarly, it was shown that TGF-β1 positive exosomes can modulate MSCs, skewing towards an α-SMA positive myofibroblastic cell, but recombinant human TGF-β1 (rhTGF-β1) could not generate the same phenotype (Chowdhury et al., 2015). So, vesicles containing TGF-β1 is a potent stimulus driving myofibroblast onset irrespective of the precursor type.

Phenotypic analysis discovered major differences in myofibroblasts generated from soluble rhTGF-β1 or TGF-β1 positive exosomes. These differences are highlighted by a significant elevation in secreted pro-angiogenic growth factors, such as FGF-2, HGF, uPA and VEGF, in exosomal-induced myofibroblasts and these effects were inhibited by blocking TGF-β1 signalling (Webber et al., 2015). The myofibroblast type was sufficient to support migration of endothelial cells and formation of vessel-like structures. Myofibroblasts generated from rhTGF-β1-treated conditions failed to recapitulate this pro-angiogenic function (Webber et al., 2015). Similarly, exosome-differentiated MSCs supported the proliferation, motility and organisation of endothelial cells and heightened invasive behaviour (Chowdhury et al., 2015). Exosomes as a stimulus, therefore, provided a myofibroblast type that cannot be generated by soluble TGF-β1 stimulation. The exosome generated stroma exhibits a phenotype of functional properties akin to *in vivo* educated prostate cancer stroma; and supports tumour growth in xenograft (Webber et al., 2015).

The need for cancer exosomes to drive stromal differentiation to a disease-associated phenotype has been shown in different ways. Targeting Rab27a, a guanosine

triphosphatases (GTPase) protein involved with trafficking MVEs to the plasma membrane would potentially inhibit exosome secretion from tumour cells. Silencing Rab27a depleted 80% of exosomes from prostate cancer cells, likely to 15 – 20% of TGF-β1 positive exosome (Webber et al., 2015). In functional terms, CM from wild type prostate cancer cell drove stromal fibroblast differentiation to an α-SMA-positive myofibroblast phenotype, supporting vessel-like structure formation. However, CM from DU145 Rab27a^{KD} cells failed to trigger differentiation and an angiogenic effect, with reduced secretion of pro-angiogenic growth factors. Also, these effects were shown *in vivo* in terms of promoting tumour growth, where Rab27a-dependent exosomes and stromal cells communicate, creating a tumour microenvironment for disease progression. Furthermore, xenografts containing DU145 Rab27a^{KD} cells failed to grow big tumours, even in the presence of fibroblasts, suggesting that stromal-assisted growth is lost. It remains unclear, however, what other intrinsic factors regulating exosome biogenesis and secretion in cancer cells that can modulate the cross-communication within the tumour microenvironment.

1.4 Molecular Mechanisms of Biogenesis and Secretion of Exosomes

1.4.1 The Endocytic Pathway

Different Mechanisms for Endocytosis

Endocytosis is a process where the cells uptake macromolecules or particles that cannot penetrate through the plasma membrane by diffusion, or transport through membrane pores. It involves the creation of a newly formed endosome by invagination and subsequent inward pinching of the plasma membrane. This process plays a role in a variety of cellular response, including remodelling of the plasma membrane, nutrient uptake, antigen uptake and presentation; regulation of the cell surface signalling receptors. There are numerous mechanisms for endocytosis (Doherty and McMahon, 2009), which can be categorised into either phagocytosis or pinocytosis. Phagocytosis engulfs large particles (including bacteria and pathogens) to eliminate them, which occurs in specialised cells, such as macrophages. Binding of the particle to cell surface receptors triggers the plasma membrane to remodel (involving actin polymerisation) and leads to pseudopodia formation surrounding the particle. This internalisation in a structure is called a phagosome, which is destined for lysosomal degradation through the action of hydrolytic enzymes.

Pinocytosis can occur in all cell types via several mechanisms: clathrin-dependent endocytosis, caveolae-dependent endocytosis and macropinocytosis and other related mechanisms, as shown in Figure 1.7. Macropinocytosis occurs in a comparable way to phagocytosis, to the extent of actin remodelling at the plasma membrane, which engulfs extracellular fluid and molecules within to form a large endosome. Caveolae contains a cholesterol-binding protein (caveolin) that forms flask-shape invaginations (50nm) at the plasma membrane. Clathrin-dependent endocytosis (receptor-mediated endocytosis) is one of the most characterised mechanisms (Benmerah and Lamaze, 2007). It involves the polymerisation of clathrin lattices through the action of different adaptor complexes to form clathrin-coated pits, to cluster cargo together via cell surface receptors. The release of clathrin-coated vesicles from the plasma membrane is mediated by dynamin and requires GTP hydrolysis by this protein. The formation of newly-formed endosomes from these various mechanisms, leading next to fusion with an intracellular compartment, is known as an early endosome.

Intracellular Compartments of the Endocytic Pathway

The endocytic pathway consists of multiple complex membrane compartments, which leads to the recycling of endocytosed material to the plasma membrane, trafficked for their degradation in the lysosomes or delivery to the trans-Golgi network (Gruenberg, 2001, Stenmark, 2009). These membrane compartments are enriched in specific proteins, such as Rab GTPases (Stenmark, 2009); and they can be identified by endocytic tracers or by ligands of cell surface receptors. Early endosomes serve as a focal point for the endocytic pathway and sorting events are initiated at this compartment to determine the subsequent fate of internalised proteins or lipids. Early endosomes are tubulo-vesicular structures located at the cell's periphery and are identified by proteins, such as early endosome antigen 1 (EEA1), Rab4 or Rab5; and the presence of the transferrin receptor, following internalisation after 5 - 10 minutes (Rybin et al., 1996, Rubino et al., 2000). The mildly acidic conditions within the early endosomes induces ligand uncoupling that will unload cargo destined for either degradation or recycling. The cargo destined for recycling will accumulate in tubular membrane compartments, termed recycling endosomes, which are less acidic than early endosomes (Stenmark, 2009). These are located near the Golgi apparatus within the perinuclear region, identified by Rab4 and Rab11 proteins; and the transferrin receptor is reached after 15 minutes of internalisation.

MVEs or late endosomes are formed during the maturation of the early endosome (Stoorvogel et al., 1991). These are characterised by the presence of ILVs and these ILVs accumulate other cell-surface receptors and molecules destined for lysosomal degradation. As one example, the EGF receptor once internalised, reaches the late endosome compartment after 30 minutes. These late endosome compartments are identified by proteins, such as LAMP1, LAMP2, CD63 or Rab7 (Kobayashi et al., 2000, Savina et al., 2005). Their main function was to fuse with lysosomes to ensure degradation of their content. Lysosomes have a low pH with a feature of an electron dense morphology, which possess markers, such as LAMP1, LAMP2, CD63 and Rab9 (Eskelinen, 2006, Raposo et al., 2007). Many studies have demonstrated that endosomal compartments with MVE hallmarks can be fated for fusion with the plasma membrane, leading to exocytosis of ILVs as exosomes, rather than fated for lysosomal fusion. This has raised questions whether different subpopulations of MVEs can occur simultaneously in cells with some destined for degradation or for exocytosis.

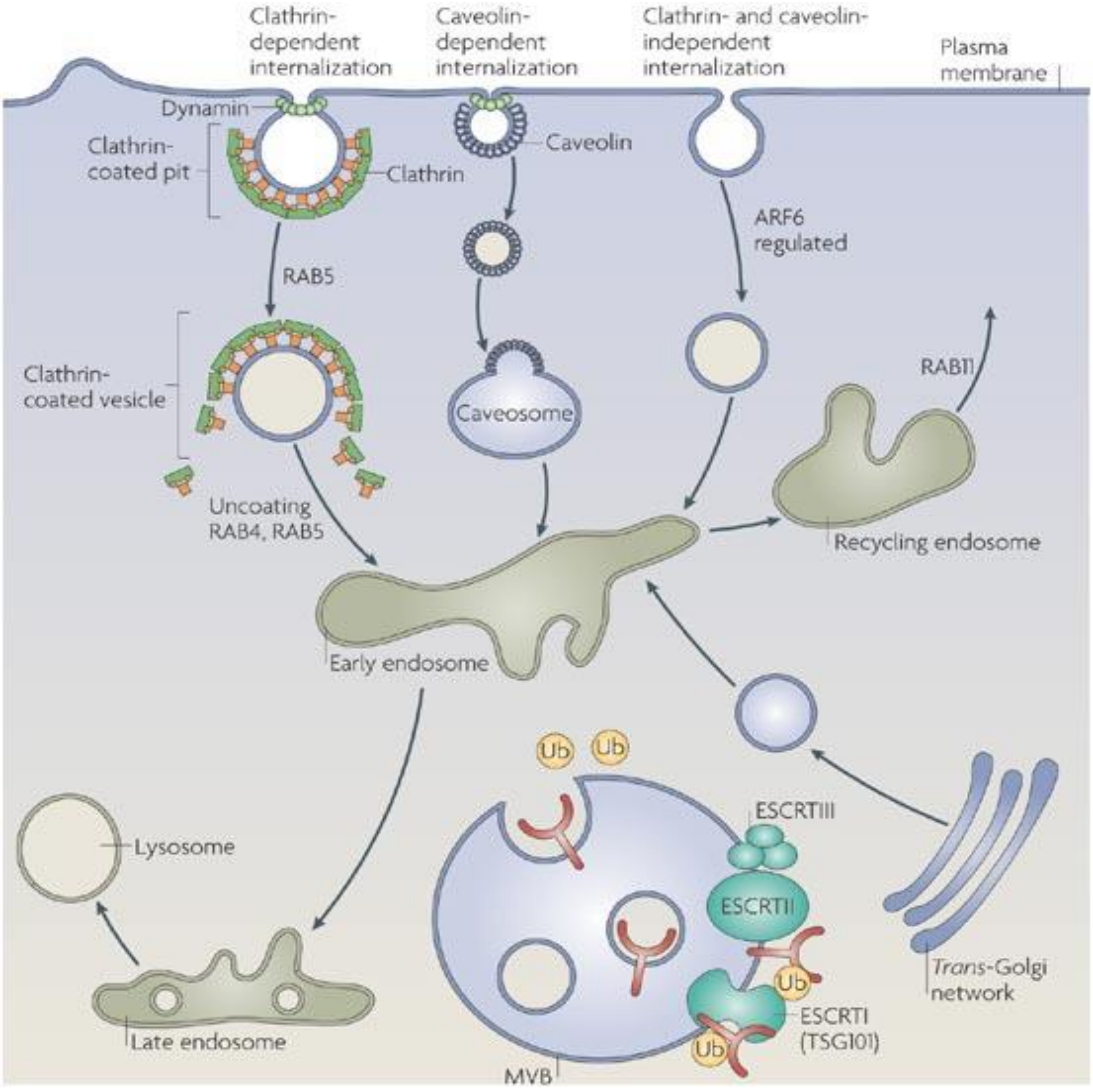

Figure 1.7: Different mechanisms of endocytic pathways. In the classical clathrin-dependent endocytosis, receptors and their bound ligands are organised into specialised domains of the plasma membrane through interactions with adaptor protein complexes during endocytosis. These areas invaginate, leading to scission and are coated with clathrin to form a clathrin-coated pit. Similarly, caveolin-dependent endocytosis and another mechanism that does not require clathrin/caveolin/dynamin can also internalised cargo. These vesicles uncoat and fuse with early endosomes that is direct to late endosomes or lysosomes. *Source: (Gould and Lippincott-Schwartz, 2009).*

MVE Heterogeneity in Cells

The existence of different subpopulations of MVEs in cells were initially observed in the distribution of cholesterol in different endosomal compartments (Möbius et al., 2003); staining cholesterol with perfringolysin O (cholesterol-binding toxin) in an EM technique. MVEs stained positively and negatively for cholesterol in EBV-transformed B cell lines. MVEs which stained positively demonstrated that there were the main lipid compartments which contained most ILVs. This finding agrees with other studies characterising the lipid composition of exosomes, which shows a clear enrichment of exosomes in cholesterol (Laulagnier et al., 2004, Trajkovic et al., 2008), as compared to other cellular membranes. A fusion profile showing the release of cholesterol-enriched EVs was seen within these cells.

Another study also provides evidence of two distinct populations of MVEs (White et al., 2006), after internalisation of EGFR to a subpopulation of MVEs that were positive for CD63. Detailed immuno-EM analysis showed another subpopulation of MVEs that were CD63 and lysobisphosphatidic acid (LBPA) positive, but did not contain any EGFR. It is possible that MVEs containing LBPA were destined for lysosomal degradation, rather that fusion with the plasma membrane. Furthermore, another study revealed the presence of different MVEs by making comparisons between immature DCs and DCs undergoing cognate interactions with T cells (cells loaded with an antigen and incubated with antigen-specific T cells) (Buschow et al., 2009). In immature cells, MHC-II molecules are predominantly sorted into MVEs fated for degradation. Though, in the presence of antigen-specific T cells, DCs secrete exosomes that are enriched in MHC-II and CD9, from newly formed MVEs. This study points to a difference in MHC-II sorting, indicating two distinct MVE pathways: one for lysosomal targeting and the other for exosome secretion. The gives some evidence that different subpopulations of exosomes can exist, although there might be other types of EVs that exists from different MVE, suggesting that different MVE can co-exist in the same cell.

1.4.2 Biogenesis of Exosomes

ESCRT-Dependent Mechanisms

As previously described, exosomes are formed within MVEs during early endosome maturation. Research into the molecular mechanisms that proceeds with ILV formation was first observed in yeast *Saccharomyces cerevisiae*, a model organism for studies involving endocytic trafficking and a pathway of lysosomal degradation (Raymond et al., 1992). Mutations in the vacuolar sorting (VPS) protein showed impaired MVE formation and an accumulation of cargo that was directed for vacuolar degradation (Rieder et al., 1996). Additional studies showed their orthologues in mammalian cells could form ESCRT complexes, which were described as 4 different components: ESCRT-0 (Katzmann et al., 2002), ESCRT-I (Katzmann et al., 2002), ESCRT-II (Babst et al., 2002b) and ESCRT-III (Babst et al., 2002a), as shown in Figure 1.8. These complexes interact with one another and are recruited by the endosomal limiting membrane where they carry out their function. The recruitment of these complexes to the endosome membrane is transient, since the function of VPS4 (ATPase) is to release these complexes once their function is complete (Babst et al., 1998).

ESCRT-0

The ESCRT-0 complex is a heterodimer formed by HRS (HGS, hepatocyte growth factor regulated kinase substrate) and STAM (signal transducing adaptor molecule). This complex is key for selecting ubiquitinylated cargo at the endosomal membrane. Phosphattidylinositol-3-phosphate (PI(3)P) is abundant in endosome membranes which is bound onto by HRS, initiating recruiting of this complex to the endosomal membrane. HRS and STAM contribute to cargo selection by interacting with monoubiquitinated proteins, through their ubiquitin binding domains (UBD) (Urbe et al., 2003). These subunits are proposed to recruit clathrin to form a double-layered coat on the endosomal membrane (Sachse et al., 2002), to accumulate cargo into microdomains that will subsequently bud to form ILVs. HRS recruits ESCRT-I by interaction with the ESCRT-I subunit, TSG101 (Katzmann et al., 2002, Bache et al., 2003).

ESCRT-I

The ESCRT-I complex consists of TSG101, VPS28, one isoform of VPS37 and one of the MVB12 subunits. ESCRT-I can bind ubiquitin through the UBD of TSG101, which increases the efficiency of ubiquitinated cargo sorting (Teo et al., 2004). Furthermore, this complex of ESCRT-0 and ubiquitin has been shown to interact with ALIX and ESCRT-II. TSG101 is key in the ESCRT-dependent pathway and depletion leads to a loss of function of the entire complex (Hanson and Cashikar, 2012).

ESCRT-II

The ESCRT-II complex consists of VPS22, VPS36 and together two subunits of VPS25. In yeast, VPS36 contains a GLUE domain which interacts with PI(3)P, ubiquitin and ESCRT-I; and the two VPS25 subunits are able to bind to the ESCRT-III subunit, VPS20 (Teis et al., 2010). This ESCRT-II complex enables the recruitment of ESCRT-III to endosomal membrane (Babst et al., 2002a). It remains unknown whether inhibition of two ESCRT-II subunits (VPS25) in mammalian cells will stop the recruitment of ESCRT-III.

ESCRT-III

In mammalian cells, the ESCRT-III complex consists of 4 core subunits: charged multivesicular body proteins (CHMPs) 6, CHMP4, CHMP3 and CHMP2; and other associated proteins CHMP1, CHMP5 and IST1. In yeast, the ESCRT-III complex also consist of 4 core subunits: VPS20, VPS32, VPS24 and VPS2; and other associated proteins DID2, VPS60 and IST1 (Increased Sodium Tolerance Protein 1). In yeast, the ESCRT-II protein, VPS25, binds to VPS20 (Teis et al., 2010), initiating ESRCT-III recruitment to the endosome and complex formation. VPS20 recruits VPS32 (CHMP4 in mammalian cells), which polymerises and forms filaments that clusters cargo together (Teis et al., 2008). VPS32 recruits VPS24 and in turn recruits VPS2, which engages with the ATPase VPS4 that uncouples the ESCRT-III complex. Furthermore, VPS32 recruits the accessory protein ALIX, which stabilises VPS32 filaments and recruits DOA4 (deubiquitinating enzyme) required for cargo deubiquitination (Hurley and Odorizzi, 2012). ESCRT-III associated proteins CHMP1, CHMP5 and IST1 have been described as modulators of VPS4 ATPase activity (Nickerson et al., 2010), which can influence the size and rate of ILV formation.

Accessory Proteins

VPS4 is a vital aspect of the ESCRT pathway, since it uncouples the ESCRT-III subunit from the endosomal limiting membrane, recycling these components for additional formation of new MVEs. In mammalian cells, a dominant negative form of the VPS4 protein demonstrates an impaired capacity to hydrolyse ATP, therefore, inhibiting ILV formation and promoting accumulation of ESCRT protein on abnormal endosomes (Sachse et al., 2004). The accessory protein ALIX has been shown to interact with ESCRT-I and ESCRT-III; and proposed to be a key mediator in viral budding (Fisher et al., 2007) and cytokinesis (Carlton et al., 2008). ALIX also appear to play a role in MVE formation. During MVE formation, it has been proposed ALIX binds to CHMP4 and TSG101, as well as other proteins in the formation of multiple ESCRT complexes, but their exact function in the ESCRT pathway for ILV formation is unknown.

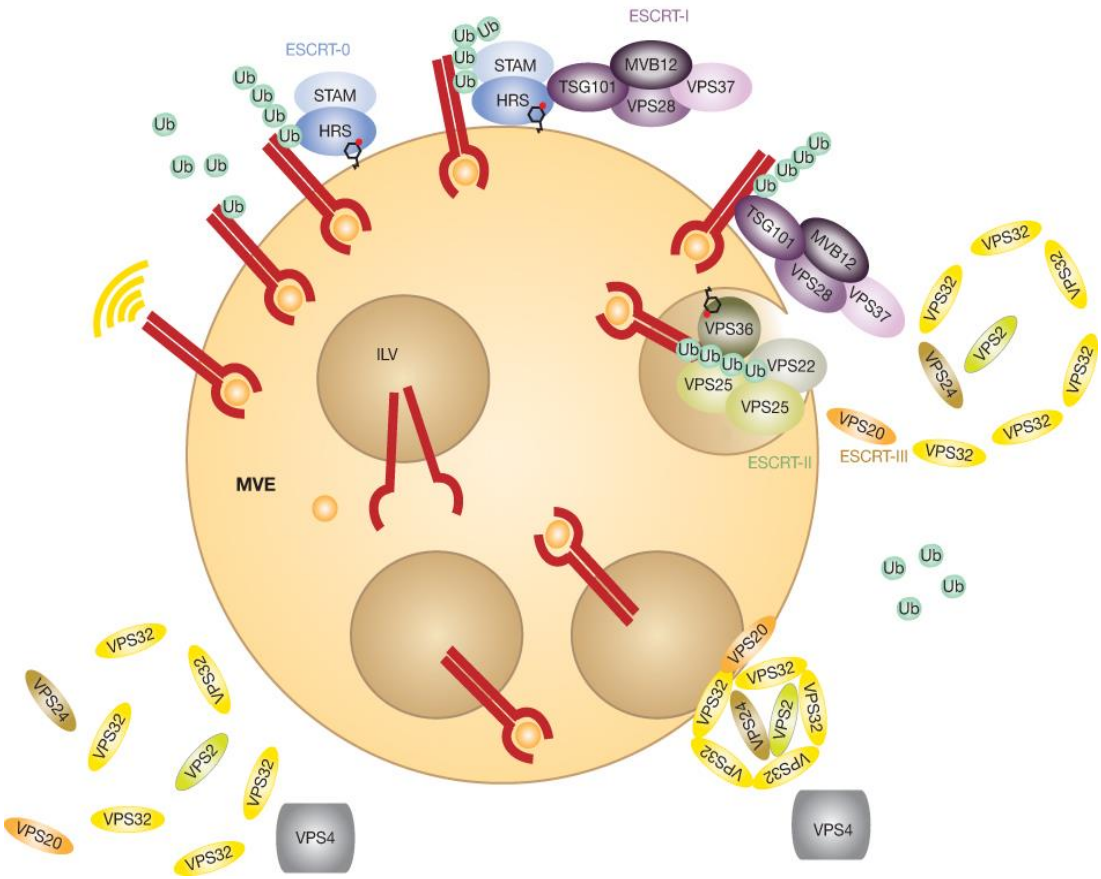

Figure 1.8: The ESCRT-dependent machinery in endosomal sorting and MVE biogenesis. Receptors in the limiting membrane of MVE are ubiquitinated in response to ligand binding. ESCRT-0 recognises the ubiquitin moieties which internalises cargo into specific domains of the limiting membrane. ESCRT-0 recruits ESCRT-I, in conjunction with the transfer of ubiquitinated cargo. Together with ESCRT-II, ESCRT-I mediates invagination of the MVE's limiting membrane. ESCRT-III is recruited by binding onto ESCRT-II and cargo is deubiquitinated. Spiral-shaped ESCRT-III filaments assembles around the neck of the forming vesicle to promote abscission, forming an ILVs. VPS4, recruited by ESCRT-III, mediates the disassembly of ESCRT-III oligomers, so that the subunits are recycled. *Source: (Rusten et al., 2012).*

ESCRTs and Exosomes

The role for ESCRT proteins in exosome biogenesis has been based on accumulating evidence from several cell lines. A study observed on mouse DCs demonstrated that silencing the HRS gene (ESCRT-0 component) attenuates exosome release (Tamai et al., 2010). The authors observed a significant attenuation in exosome release from DCs deficient (siRNA-treated DCs) in HRS, which were stimulated for exosome secretion with a calcium ionophore. This attenuation resulted in defective antigen presentation to cytotoxic T cells and was not due to a compromised lysosomal degradation pathway. Additionally, an RNA interference screen was performed to target 23 individual ESCRT components in HeLa cells (Colombo et al., 2013). Silencing ESCRT-0 (HRS and STAM1) or the ESCRT-I gene (TSG101) reduced the secretion of exosomes (characterised by CD63 and MHC-II expression).

ALIX has been involved in exosome biogenesis in multiple studies. One study observed that during reticulocyte maturation, the chaperone protein HSP70 binds to the newly endocytosed transferrin receptor via the cytoplasmic domain of the adaptor protein 2 (AP2), which undergoes degradation by the proteasome (Géminard et al., 2004). Binding of ALIX on the transferrin receptor within the same cytoplasmic domain in the absence of AP2, suggests to link the receptor to the ESCRT machinery for cargo sorting into the ILVs. Supporting this notion, it was reported that exosomes contain syndecans, that can bind to heparan sulphate from the extracellular matrix, but also to syntenin (small scaffolding protein) via their cytoplasmic domain and ALIX, which in turns interacts with syntenin (Baietti et al., 2012). Syntenin overexpression increased exosome secretion (elevated CD63 and HSP70), which was dependent on ALIX. Silencing either syndecan, syntenin or ALIX attenuated exosome secretion. Supporting these findings, two regulators of this syntenin-ALIX complex, GTPase ADP ribosylation factor 6 (ARF6) and its effector phospholipase D2 (PLD2), demonstrated a role for affecting exosome biogenesis and budding into MVEs (Ghossoub et al., 2014). Data suggest that ALIX might be responsible for loading and packaging of miRNA into ILVs (Iavello et al., 2016); and recruiting ESCRT-III components to ESCRT-I domains on the endosome membrane. Interestingly, these data support a role for ESCRT-related proteins (HRS or ALIX) in exosome biogenesis, but the relationship between ESCRT-dependent exosome formation and their cargo load remains poorly understood.

ESCRT-Independent Mechanisms

The presence of different MVE subpopulations in a single cell has suggested that different mechanisms may operate in cells to generate these distinct endosomal compartments, thus challenging the concept that the ESCRT machinery always mediates MVE biogenesis. To

address whether ESCRT are necessary for ILV biogenesis, a study silenced four ESCRT proteins (HRS, TSG101, VPS22 and VPS24) implicated in all ESCRT complexes, to abolish ESCRT-related function (Stuffers et al., 2009). Inhibition of all four ESCRT proteins revealed changes in the endosomal compartments, with the presence of enlarged MVEs and with few internal vesicles next to the limiting membrane. Though, ILVs were still formed in these altered structures, indicating that independent ESCRT pathways can ensure MVE formation.

In one study, it was demonstrated in an oligodendroglial cell line that budding of ILVs into MVEs was independent of ESCRT function and required the sphingolipid ceramide (Trajkovic et al., 2008). Inhibition of neutral sphingomyelinases (nSMase; enzyme hydrolysing sphingomyelin to ceramide) with GW4869 decreased proteolipid protein (PLP)-associated exosome release. This suggested that PLP sorting into ILVs required ceramide and independent of ESCRT. Treatment of embryonic kidney (Chairoungdua et al., 2010, Kosaka et al., 2010) with GW4869 also reduced secretion of exosomal associated protein markers (CD63, CD81 or TSG101). Though, treatment of cells with GW4869 induces cell death, which provides an inaccurate analysis of exosome secretion. In contrast, in human melanoma cells, the depletion of nSMase impairs neither MVE biogenesis or exosome secretion (van Niel et al., 2011). It was proposed that inhibition of ESCRT function (HRS, TSG101 or VPS4) did not alter the sorting of premelanosomal (PMEL) protein (a component of melanosomes) on ILVs. MVEs were still capable of forming cells where the ESCRT machinery had been disrupted, albeit their morphology was different from that of the control (Theos et al., 2006). Another study has proposed that the tetraspanin, CD63, has a role in sorting PMEL to ILVs (van Niel et al., 2011). In melanoma cells (MNT-1), CD63 is detected with PMEL in MVEs and abundantly on ILVs than on the limiting membrane. Silencing CD63 inhibits ILV formation in MVEs and causes PMEL to accumulate at the limiting membrane, demonstrating that CD63 participates in protein sorting to the ILVs. Other tetraspanins, such as CD9, might have an effect, but remains poorly understood in the context of exosome secretion. These results and other studies suggests that MVEs and subsequent sorting mechanisms for the sorting cargo can be performed via ESRCT-dependent and independent mechanisms, that gives rise to a heterogeneous population of MVEs.

1.4.3 Exosome Secretion

The process of exosome secretion involves the trafficking of MVEs or late endosomes to the vicinity of the plasma membrane for docking and fusion; and consequently, ILV release into the extracellular space. This complex process involves multiple molecules that are responsible for different steps: cytoskeleton proteins (actin or tubulin), molecular motor proteins (kinesin) mediates transport to the plasma membrane, the Rab protein family will be heavily involved in endosomal membrane trafficking; and the SNARE protein family will be involved in the final phases of fusion. The precise molecular machinery behind exosome secretion is not fully understood, however, multiple studies have identified potential proteins involved and this will be discussed in greater detail below.

Several studies have analysed whether exosome secretion is constitutive or regulated in various cell types. Exosome secretion can be induced by a rise in intracellular calcium levels in the haematopoietic cell line (K562) (Savina et al., 2003) or in mast cells (Valadi et al., 2007). Degranulation of mast cells has been related to increased exosome secretion (Laulagnier et al., 2004). Alternatively, exosome secretion is normally analysed at the steady state (absence of stimulus), which remains difficult to exclude the possibility that some unsuspected signal or stimulus may trigger or modify this secretion. In one study, exosome secretion might be increased by cognate interactions with antigen-specific CD4+ T lymphocytes (Buschow et al., 2009). Exosome secretion by rat cortical neurons can be stimulated by depolarisation of the cells (Faure et al., 2006). Furthermore, γ-irradiation induced deoxyribonucleic acid (DNA) damage can promote exosome secretion through activation of the p53-regulated protein, TSPAN6 (Yu et al., 2006).

Rab Protein Family

The Rab protein family are small monomeric GTPases which are regulators of trafficking different endosomal compartments within the cell; Rabs can be involved in either vesicle budding, tethering to the membrane of an acceptor compartment or motility through the cytoskeleton, which will ultimately fuse with the target compartment (Pfeffer, 2001, Stenmark, 2009). There are over 70 Rab GTPases, each of which are associated with a specific endosomal compartment. The regulatory function of these Rab proteins is based on their capacity to switch between an inactive GDP-bound form to an active GTP-bound form, considered to be the active conformation (Pereira-Leal and Seabra, 2001). This cycle is regulated by guanine nucleotide exchange factors (GEFs), which facilitate GDP release and subsequent GTP binding. Alternatively, GTP hydrolysis can be catalysed by the Rab GTPases themselves or by GTPase activating proteins (GAPs).

The first study that provided evidence for Rab proteins involvement in exosome secretion came from studying the erythroleukaemia cell line, K562, which releases exosomes containing the transferrin receptor (Savina et al., 2002). Overexpression of the dominant negative form of Rab11 (unable to hydrolyse GTP), resulted in attenuated secretion of HSP70-associated exosomes, suggesting a role for Rab11. This follow up study suggested that Rab11 was involved in tethering MVEs to the plasma membrane, with the final fusion step requiring calcium ions (Savina et al., 2005).

Later, a screening approach was performed in HeLa-CIITA cells to target multiple Rab GTPases in their role in exosome secretion (Ostrowski et al., 2010). A total of 59 Rab proteins were targeted by an RNAi approach and proposed that Rab2b, Rab5a, Rab9a appeared to modulate exosome secretion, with Rab27a and Rab27b, however, having the greatest role. It was shown that silencing these Rab proteins decreased the secretion of exosomes bearing CD63, CD81 and MHC-II. Additional analysis unravelled that silencing Rab27a, increased MVE size and altered its docking to the plasma membrane. However, silencing Rab27b altered docking of smaller MVEs to accumulate in the perinuclear region of the plasma membrane. Alternatively, another screen was performed that targeted Rab-activating proteins (Rab-GAPs) in oligodendroglial cell lines (Hsu et al., 2010), revealing that TBC1D10A-C act as regulators of exosome secretion. Rab35 was identified as a target of TBC1D10A-C and Rab35 inhibition (either by siRNA or by using a dominant negative mutant) indicated a significant decrease in secretion of PLP-exosomes. Rab35-dependent exosome secretion was also confirmed in another study by using primary oligodendrocytes (Fruhbeis et al., 2013).

Interestingly, different observations were reported in various cell types. In *Drosophila* S2 cells, inhibition of Rab11 by dsRNA attenuate the secretion of small EVs containing wingless or Evi (Beckett et al., 2013), whereas Rab27 or Rab35 did not. In another study, inhibition of Rab11 or Rab35 in retinal epithelial cells attenuated the secretion of flotillin associated EVs, whereas Rab27a/b did not play a role (Abrami et al., 2013). In multiple tumour cell lines of various origins (prostate, breast or melanoma), silencing Rab27a decreased the secretion of exosomes pelletable by ultracentrifugation (Bobrie et al., 2012, Peinado et al., 2012, Webber et al., 2015). According to the literature (Stenmark, 2009), Rab11 and Rab35 are proposed to associate with the recycling endosomes and Rab27a to the late endosome, as shown in Figure 1.9. The conflicting observations in various studies suggests that heterogeneous MVEs can generate different subpopulations of secreted exosomes, that may vary from cell type

and become enriched with specific proteins (CD63, ALIX, TSG101) or other cell-specific proteins (PLP, transferrin receptor or Wnt-associated). Additional investigation will be required to elucidate the roles of Rab11b or Rab35 in the context of prostate cancer cells.

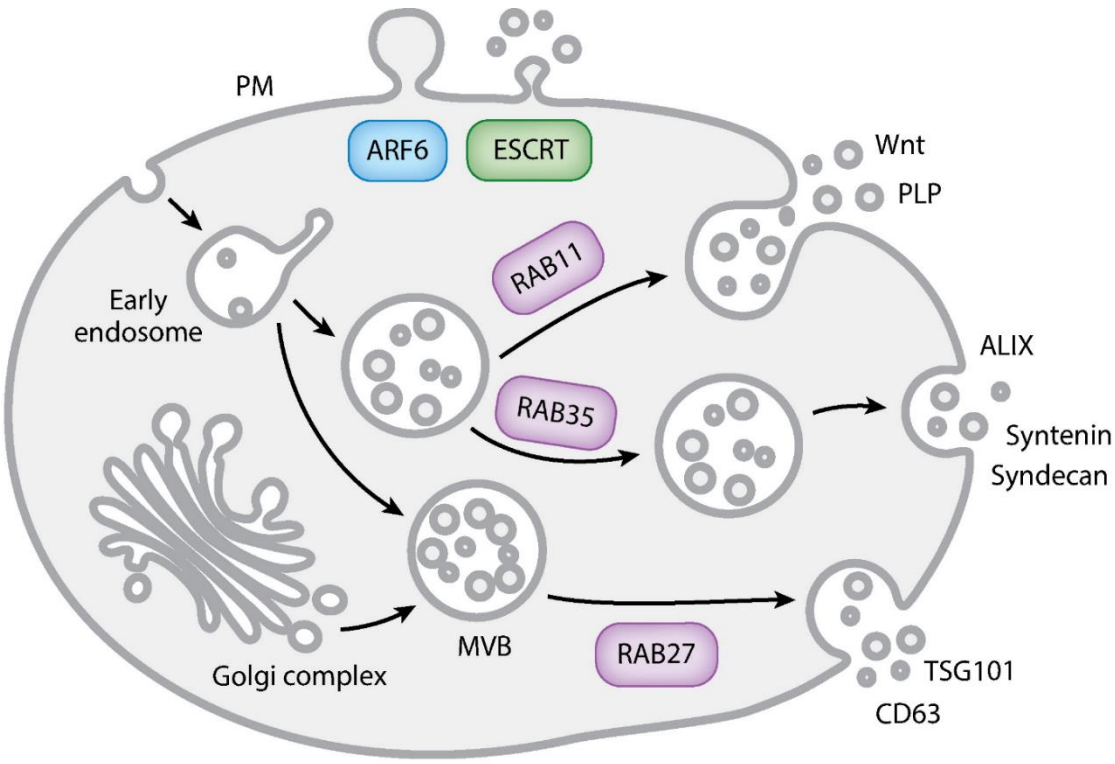

Figure 1.9: The multiple molecular machineries of exosome secretion. Multiple molecular machineries of exosome secretion have been described. For MVE-dependent secretion, the Rab protein family (Rab11, Rab27 and Rab35) has been documented to promote secretion of exosomes and may act on specific MVEs along the endocytic pathway. Other related plasma membrane EVs, ARF6 and some ESCRT components has been proposed to regulated outward budding. *Adapted from Source: (Colombo et al., 2014).*

SNARE Protein

During intracellular vesicle trafficking, the final step fusion of the vesicle with the acceptor membrane depends on a family of proteins called SNARE (soluble N-ethylmaleimide-sensitive fusion attachment protein (SNAP) receptors) (Jahn and Scheller, 2006). SNARE proteins were originally categorised as vesicular SNAREs (v-SNARE: vesicular-associated membrane proteins), if they were located on the vesicle's membrane; and target SNAREs (t-SNARE), if located on the membrane of acceptor compartments (Rao et al., 2004, Chaineau et al., 2009). It has been proposed SNARE proteins form complexes with SNAPs between two membranes and mediate membrane fusion between the two organelles. In multiple studies, calcium regulated fusion of secretory lysosomes with the plasma membrane has been shown to involve SNAP-23 at the plasma membrane and lysosomal vesicle-associated membrane protein (VAMP)7 in epithelial cells (Rao et al., 2004) or VAMP8 in mastocytes (Puri and Roche, 2008), but the SNARE complex involved with MVE fusion with the plasma membrane to modulate exosome secretion has not been thoroughly investigated. One study proposed the role for VAMP7 to promote the secretion of MVEs to release acetylcholinesterase containing exosomes in the human leukaemic cell line, K562 (Fader et al., 2009). Other studies performed in *Drosophila* identified YKT6, a SNARE protein involved in endoplasmic reticulum to golgi apparatus transport, as required for MVEs to fuse with the plasma membrane to release Wnt positive exosomes (Meiringer et al., 2008) or Evi positive exosomes (Koles et al., 2012). More recently, inhibition of YKT6 from the lung cancer cell line, A549, significantly attenuated exosome secretion, characterised by a loss of TSG101 associated exosomes (Ruiz-Martinez et al., 2016), but additional investigations will be required in other cell lines to confirm these findings.

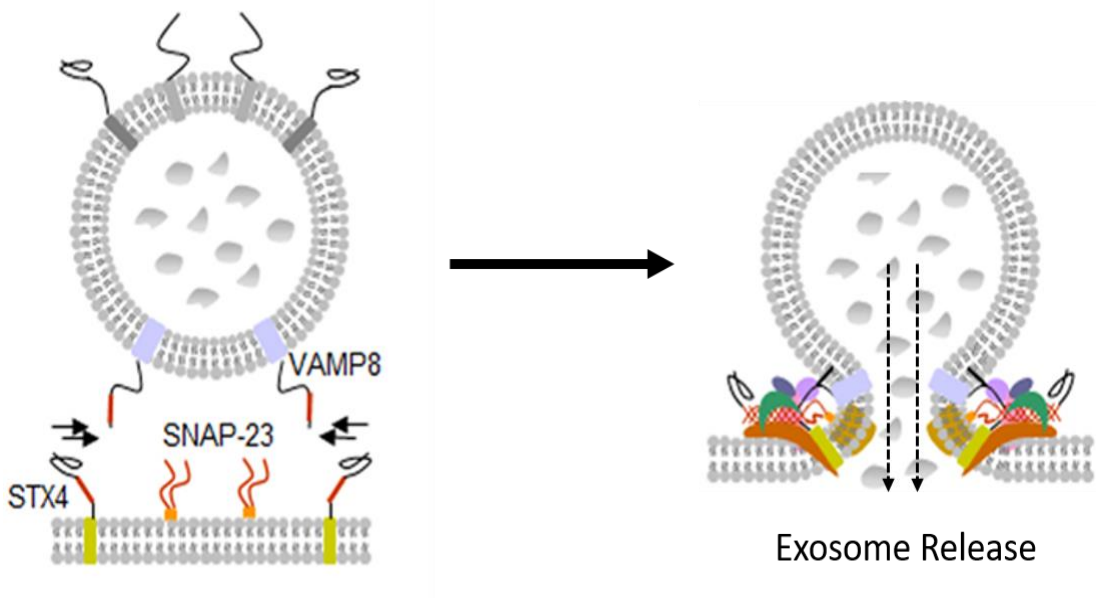

Figure 1.10: Model of fusion machinery on an endosomal membrane. The two membrane are within the vicinity of each other, but the SNAREs are not yet in contact. Once membranes are primed for fusion, the SNARE complexes begin to start zipping, drawing the membranes closer to each other. The lateral tension in the transbilayer contact area induces membrane breakdown, yielding a fusion pore and the release of exosome. *Adapted from Source: (Lorentz et al., 2012).*

1.5 Hypothesis and Thesis Aims

I hypothesise that cancer cells secrete distinct sub-populations of exosomes and that these may impart distinct molecular phenotypes and functions.

The main objective of my Thesis is to gain an insight on the components putatively implicated in exosome biogenesis and secretion. I have focussed on proteins involved in four protein families: tetraspanin, ESCRT, Rab and SNARE. Given their involvement in ILV formation in yeast and mammalian models, it is proposed that the ESCRT family are involved in exosome biogenesis and secretion. Though, studies have challenged the concept that ILV formation solely by ESCRT complexes is not entirely true, with the notion that ESCRT-independent mechanisms must exist. It has been proposed that Rab and SNARE proteins have roles in endosomal trafficking of ILVs between different subcellular compartments and subsequent fusion with the plasma membrane to secrete exosomes. This proposes the idea that vesicle heterogeneity is present, where exosome subpopulations may co-exist and be regulated by specific proteins. Here, I will investigate the roles of these proteins: CD9, Rab5a, Rab11b, Rab35, VAMP7 and VPS25 in one cell type and understand the impact they have upon exosome secretion.

Many studies have highlighted the role for exosomes secreted by cancer cells, as modulators of cancer associated stroma, angiogenesis and metastatic priming; promoting a disease associated phenotype. It remains unclear whether the factors responsible for generating this disease associated phenotype or whether this is due soluble factors or specific vesicle subpopulations driving this phenotype. I will assess the outcome of knockdown on secreted vesicles and their role in stromal-cell activation capacity.

Lastly, the exosome generated myofibroblasts may also be considered as a direct stimulus for tumour growth, supporting tumour cell expansion, migration and invasion. I will be establishing 3D-spheroid culture incorporating tumour cells and fibroblasts, to mimic an *in vivo* 3D microenvironment. It remains poorly understood if the outcome of knockdowns on secreted vesicles will affect the 3D tumour spheroid growth and their ability to invade. Much of the *in vitro* experiments we investigate, will be assessed to see if it is translated into the *in vivo* setting.

CHAPTER 2:

MATERIALS AND METHODS

2.1 Culture of Human Cell Lines

2.1.1 Monolayer Culture

DU145 is a prostate cancer cell line derived from a metastatic brain tumour and purchased from American Tissue Culture Collection (ATCC, USA). The cells were cultured in Roswell Park Memorial Institute (RPMI)-1640 (Lonza, Slough, UK) media, supplemented with 100 U/ml penicillin (Lonza), 100 µg/ml streptomycin (Lonza) and 10% foetal calf serum (FBS; ThermoFisher Scientific, Loughborough, UK). FBS was depleted of bovine exosomes by overnight centrifugation at 100,000 x *g* for 24 hours, followed by filtration though 0.22 µm and then 0.1 µm vacuum filters (Millipore, Watford, UK). Adult lung fibroblasts (Coriell Institute for Medical Research, USA) were cultured in DMEM/F12 (Lonza) containing 100 U/ml penicillin (Lonza), 100 µg/ml streptomycin (Lonza) and 10% exosome-depleted FBS (ThermoFisher Scientific). Human umbilical vein endothelial cells (HUVEC) were purchased from Lonza, and maintained using the endothelial cell growth medium (EGM)-2 BulletKit™ (Lonza). Cell lines were all maintained at 37°C in an atmosphere of 5% CO_2 in a humidified CO_2 incubator. Mycoplasma test was carried out using a MycoAlert™ Mycoplasma Detection Kit (Lonza) every 2 months. All tissue culture work was carried out in a class II biosafety cabinet.

2.1.2 Bioreactor Flasks for Prostate Cancer Cell Line (DU145)

DU145 cells were seeded into bioreactor flasks (Wheaton, New Jersey, USA); and maintained at a high-density culture for exosome production. The bioreactor flask has two compartments; a cell and a medium compartment, which is separated by a 10kDa semi-permeable membrane (Figure 2.1). This membrane allows the continuous diffusion of nutrients into the cell compartment with the removal of any waste products in the medium compartment. The medium compartment contains 500ml of culture media and the cell compartment contains 15ml of culture media which maintains cells. The cells are attached to a woven, polyethylene terephthalate (PET) matrix providing a large surface area for attachment; allowing secreted exosomes to be present in the cell CM. A low volume present in the cell compartment from these bioreactor flasks allows exosomes to 8 – 10 more concentrated per ml, compared to monolayer T-75cm^2 flasks, thus reducing cost, labour and time (Mitchell et al., 2008).

Cells were seeded into the cell compartment of the bioreactor flasks at an initial density of 1.5 – 3.0 x 10^7 cells in 15ml of required supplemental culture media and 10% exosome-depleted FBS. The medium compartment was filled with 500ml RPMI-1640 with required

supplements and 10% FBS. DU145 cell CM from these bioreactor flasks were collected and replaced with fresh media on a weekly basis. The CM containing exosomes from the cell compartment were centrifuged at 400 x *g* for 7 minutes at 4°C, an additional 400 x *g* for 7 minutes at 4°C, followed by a 2000 x *g* for 15 minutes at 4°C to remove dead cells and cellular debris. The CM was collected and filtered using a 0.22µm Millex GP syringe filter (Merck Millipore, Massachusetts, USA), to remove any remaining debris and larger vesicles. The CM was stored at -80°C, until required for exosome purification.

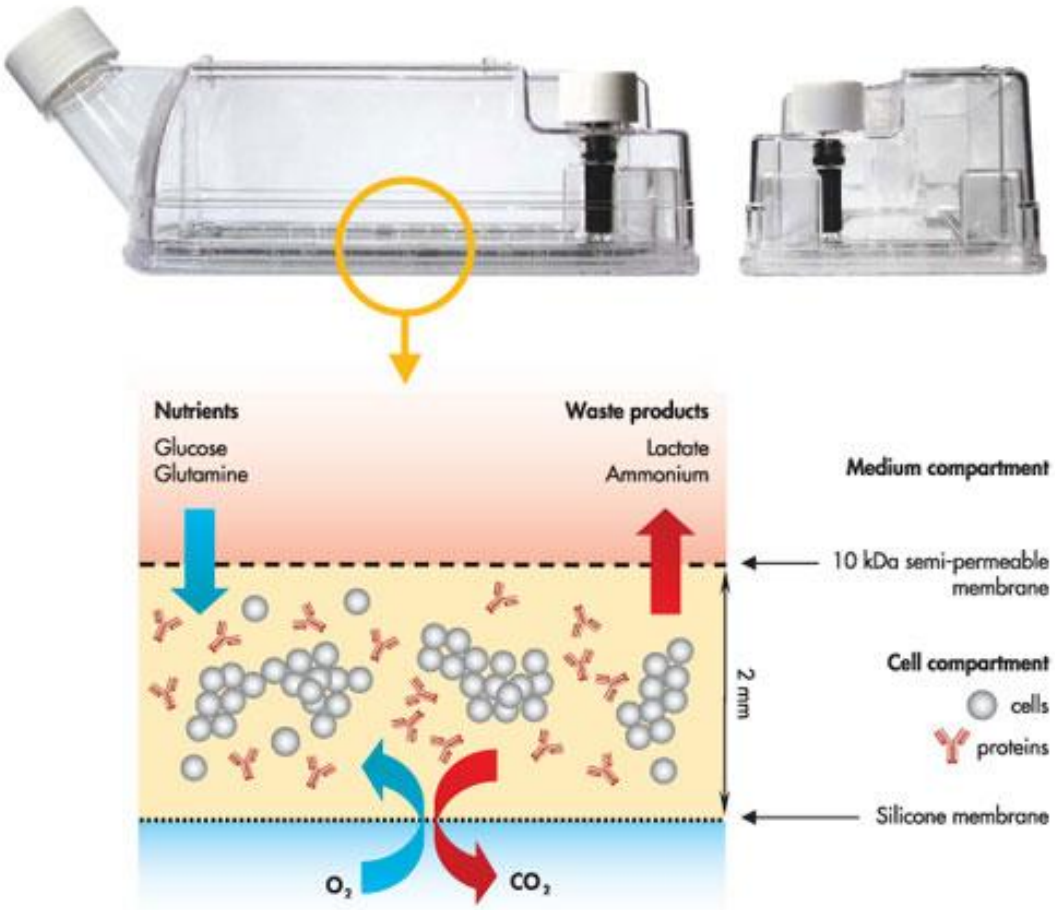

Figure 2.1: Integra Bioreactor Flask. The bioreactor flask contains two compartments: the cell compartment containing the exosomes (maximum 20ml) and the medium compartment (500 – 1000ml) separated by a 10kDa semi-permeable membrane. The membrane allows continuous diffusion of nutrients and waste products between both compartments. Efficient gas exchange is ensured by a silicone membrane which forms the compartment base. This provides an optimal oxygen supply and control of carbon dioxide by providing a short diffusion pathway with the cell compartment. *Source: (Scientific Laboratory Supplies, 2017)*.

2.2 Isolation and Characterisation of Exosomes

2.2.1 Sucrose Cushion Method

For all experiments, unless stated otherwise, exosomes were isolated from cell CM using the sucrose cushion method, as this is less labourious for exosome isolation, compared to the sucrose gradient method. Pre-cleared DU145 cell CM samples were obtained from -80°C and defrosted at 37°C.

The CM was underlain with 4ml of 30% sucrose/D_2O (density of 1.2 g/ml) and ultracentrifuged at 100,000 x *g* (SW-32 rotor, Beckman Coulter, High Wycombe, UK) for 2 hours at 4°C. Approximately 2 - 3ml of the central base of the sucrose cushion solution was collected and diluted in excess phosphate buffered saline (PBS). The exosomes were pelleted by ultracentrifugation again at 100,000 x *g* for 2 hours at 4°C (fixed angle 70Ti rotor, Beckman Coulter). Exosome pellets were resuspended in PBS and stored at -80°C, until required for further experimental use.

The protein concentration for exosome samples were evaluated using the MicroBCA Protein Assay (ThermoFisher Scientific). A standard curve was performed by serial dilution from 2000µg/ml BSA to 0µg/ml. Exosomes were diluted 1:8 with PBS and absorbance values were calculated from the standard curve, to determine the protein content from exosome preparations. Unless stated otherwise, exosomes isolated from the sucrose cushion protocol will be described as purified DU145 exosomes. These exosomes are used in fibroblast differentiation experiments at a dose of 200µg/ml, which is equivalent to a dose of 1.5ng/ml rhTGF-β1, as described previously (Clayton et al., 2007, Webber et al., 2010).

2.2.2 Cryo-Electron Microscopy

For cryo-EM, this was performed in collaboration with Prof. Juan Falcon-Perez (CIC bioGUNE, Derio, Spain). Exosome or vesicle concentrates were directly adsorbed onto glow-discharged holey carbon grids (QUANTIFOIL, Großlöbichau, Germany). Grids were blotted at 95% humidity and rapidly plunged into liquid ethane with the aid of VITROBOT (Maastricht Instruments BV, Maastricht, The Netherlands). Vitrified samples were imaged at liquid nitrogen temperature using a JEM-2200FS/CR Transmission Electron Microscope (JEOL, Tokyo, Japan), equipped with a field emission gun and operated at an acceleration voltage of 200 kV.

2.2.3 Microplate Immuno-Phenotyping Assay

Exosomes or vesicle concentrates were diluted in PBS and bound onto high protein binding ELISA strip 96-well plates (Greiner Bio-One, Frickenhausen, Germany), at a dose of 1µg/well and incubated overnight at 4°C. The wells were washed 3 times using a Tris-based wash buffer (Kaivogen, Turku, Finland), to remove unbound particles. Blocking solution (1% BSA/PBS; weight/volume: w/v) was added for 2 hours, before being washed 3 times. Primary antibodies were added at 1µg/ml (Table 2.1), for 2 hours at room temperature (RT). After washing wells 3 times, primary antibodies were detected by goat anti-mouse biotinylated antibody (Perkin Elmer, Massachusetts, USA) (diluted in 0.1% BSA/PBS w/v), at a 200ng/ml working concentration for 1 hour at RT. The wells were washed 3 times, before adding a europium-streptavidin conjugate (Perkin Elmer) in assay buffer (Kaivogen), for 45 minutes at RT. The wells were washed 6 times, before adding enhancement intensifier (Kaivogen), for 5 minutes at RT and signal assessed by time-resolved fluorescence (TRF) on a PHERAstar FS Microplate Reader (BMG Labtech, Aylesbury, UK).

2.2.4 Development of Permeabilised Exosomes for Microplate Immuno-Phenotyping Assay

Exosomes were diluted in PBS and bound onto high protein binding ELISA strip plate (Greiner Bio-One) at a dose of 1µg/well and incubated overnight at 4°C. The wells were washed 3 times using a wash buffer (Kaivogen), to remove unbound particles. Blocking solution (1% BSA/PBS, w/v) was added for 2 hours, before washed 3 times. Radioimmunoprecipitation assay (RIPA) lysis buffer (Santa Cruz, Texas, USA) was added for 1 hour at RT, before being washed 3 times. Primary antibodies (ALIX and TSG101) were added at 1µg/ml (Table 2.1), for 2 hour at RT. After washing wells 3 times, the primary antibodies were detected by goat anti-mouse biotinylated antibody (Perkin Elmer) (diluted in 0.1% BSA/PBS, w/v), at a 200ng/ml working concentration for 1 hour at RT. The wells were washed 3 times, before adding a europium-streptavidin conjugate (Perkin Elmer) in assay buffer (Kaivogen) for 45 minutes at RT. The wells were washed 6 times, before adding enhancement intensifier (Kaivogen) for 5 minutes at RT and signal assessed by TRF on a PHERAstar FS Microplate Reader (BMG Labtech).

2.2.5 Western Blotting

Cell lysates were extracted from whole cells (1 x 10^6) and prepared by resuspending in RIPA lysis buffer (Santa Cruz, Texas, USA) containing: 1X protease inhibitor cocktail, 200mM phenylmethane sulfonyl fluoride (PMSF), 100mM sodium orthovanadate and 1X lysis buffer (All from Santa Cruz). Insoluble material was removed by centrifuging samples at 10,000 x *g* for 10 minutes at 4°C, split into aliquots and stored at -80°C for future use. Protein concentration was determined by Bradford Protein Assay (BioRad, Hemel Hempstead, UK).

20µg of cell lysate or exosomes (isolated from the sucrose cushion method) or vesicle concentrates (isolated from ultracentrifugation) were boiled in lithium dodecyl sulphate (LDS) sample buffer (Invitrogen, USA), either reducing with 20mM dithiothreitol (DTT; Santa Cruz) or under non-reducing conditions. Boiled samples and molecular weight markers (Magic Mark™ XP and SeeBlue® Plus 2 Precision Stain; Life Technologies, USA) were loaded, and subjected to electrophoresis for 45 minutes on NuPAGE™ precast 4-12% Bis-Tris gradient gels (Life Technologies). The gels were run using 1x NuPAGE™ MOPS sodium dodecyl sulphate (SDS) running buffer (Life Technologies) and an Invitrogen™ PowerEase® 500 (ThermoFisher Scientific) power supply. Proteins were transferred onto methanol activated polyvinylidene fluoride (PVDF) membranes (GE Life Sciences, UK), using 25mM Tris, 192mM glycine (both Sigma-Aldrich, St Louis, USA) and a BioRad Mini Trans-Blot Electrophoretic Transfer Cell (BioRad). Furthermore, the tank was placed in ice to optimise recommended cooling conditions and the blots were run for 90 minutes at a constant 80V. The membranes were blocked overnight at 4°C in PBS containing 0.5% (w/v) Tween®20 (Sigma-Aldrich) and 5% (w/v) non-fat powdered milk (Marvel, London, UK). The membrane was incubated with primary antibodies (Table 2.1), at 1µg/ml for 2 hour at RT. Membranes were washed 3 x 5 minutes with 0.5% Tween®20 (Sigma-Aldrich) in PBS and incubated with a goat anti-mouse-HRP conjugate (Santa Cruz) for 1 hour at RT. After a further 3 x 5 minutes wash, the bands were detected using C-Digit blot scanner (Li-Cor, Lincoln, USA) and an enhanced chemiluminescent substrate (Li-Cor).

Primary Antibody Specificity:	Isotype	Size (kDa)	Catalogue Number	Company
ALIX	IgG_1	95	Sc-166952	Santa Cruz
Calnexin	IgG_1	90	Sc-23954	Santa Cruz
CD9	IgG_{2B}	27	MAB1880	R&D Systems
CD63	IgG_1	25	MCA2142	AbD Serotec
CD81	IgG_1	26	MCA1847EL	BioRad
GAPDH	IgG	40	#Y3322	BioChain
HSP70	IgG_1	70	Sc-66048	Santa Cruz
HSP90	IgG_1	90	Sc-69703	Santa Cruz
LAMP1	IgG_1	120	Sc-20011	Santa Cruz
LAMP2	IgG_1	120	Sc-18822	Santa Cruz
MHC-I	IgG_{2A}	45	16-9983-85	eBioscience
Rab5a	IgG_{2B}	25	Sc-130010	Santa Cruz
Rab11b	IgG	26	PA5-31348	ThermoFisher Scientific
Rab35	IgG	25	PA5-31674	ThermoFisher Scientific
TSG101	IgG_{2A}	43	Sc-7964	Santa Cruz
VAMP7	IgG_{2A}	25	MAB6117	R&D Systems
VPS25	IgG_1	21	Sc-271648	Santa Cruz

Table 2.1: Table of primary antibodies used for Western Blot and plate-based assays.

2.2.6 Nanoparticle Tracking Analysis

NTA is a method that visualises and analyses nanometre particles (10 – 1000 nm) in liquids. Based on a laser-illuminated microscopical technique, NTA utilises the properties of light scattering and Brownian motion to analyse nanoparticles in real-time. Brownian motion is defined as the random motion of nanoparticles suspended in liquid; their rate of movement is related to the temperature and viscosity of the liquid. NTA uses high-intensity laser beams sent through the sample chamber, the particles in suspension in the path of this beam can scatter light and can be detected by a highly sensitive camera over multiple frames (Figure 2.2). The NTA software can track each particle on a frame-by-frame basis and the velocity of particle movement is used to calculate particle size by applying the Stokes-Einstein equation:

$$Dt = TK_B / 3\pi\eta d$$

Dt: Diffusion constant (product of diffusion coefficient *D* and time *t*)

T: Sample temperature

K_B: Boltzmann's constant

η: Solvent viscosity

***d*: Diameter of spherical particle**

Each particle is visualised and analysed separately; and the resulting estimate of particle size distribution and particle size does not suffer in terms of intensity distribution, which is often observed in another method, such as DLS. The use of high intensity laser beams combined with a low-background optical configuration, allows particles of nanometre dimensions to be visualised, though this is dependent on the particle refractive index (Ri; dictates the interactions between light and nanoparticles). Particles with very high Ri (colloidal gold) can often determine size down to 15nm diameter for lower Ri particles, such as those of biological origin (exosomes), the smallest detectable size can only be around 30nm.

Here, exosomes can be modelled as nanoparticles by determining the light scattering intensities of nanoparticles, temperature and liquid viscosity. Each exosome preparation was analysed, where size distribution profiles and particle counts were determined using NTA (Malvern Instruments, Malvern, UK). The analysis was performed on a NanoSight™ NS300, but configured with a temperature controlled 488nm laser module and a high-sensitivity sCMOS Camera System (OrcaFlash 2.8, Hamamatsu C11440, Hamamatsu City, Japan) and a syringe-pump system (Malvern Instruments).

100nm standard latex beads (Malvern Instruments) were tested to confirm the NTA measurements were accurate. Samples were administered and recorded under controlled flow using the NanoSight™ syringe pump (set to 50) and script control system for each sample. Six replicate videos of 30 seconds were taken and temperatures were set at 25°C. Videos were batch analysed using NTA 3.1 software (version 3.1 build 3.1.54), with the camera's sensitivity and detection threshold set at 14-16 and 1-3, respectively, to reveal small particles taken in light scatter mode. On some occasions, videos were also taken following application of long fluorescence filter, so that only particles emitting light at >500nm were visible. Samples were diluted in nanoparticle-free water (Fresenius Kabi, Runcorn, UK), so that the particle concentration (particles / ml) was within the linear range of the instrument. The area under the histogram for each triplicate measurement was averaged to be used as a particle concentration measurement and corrected for cell number.

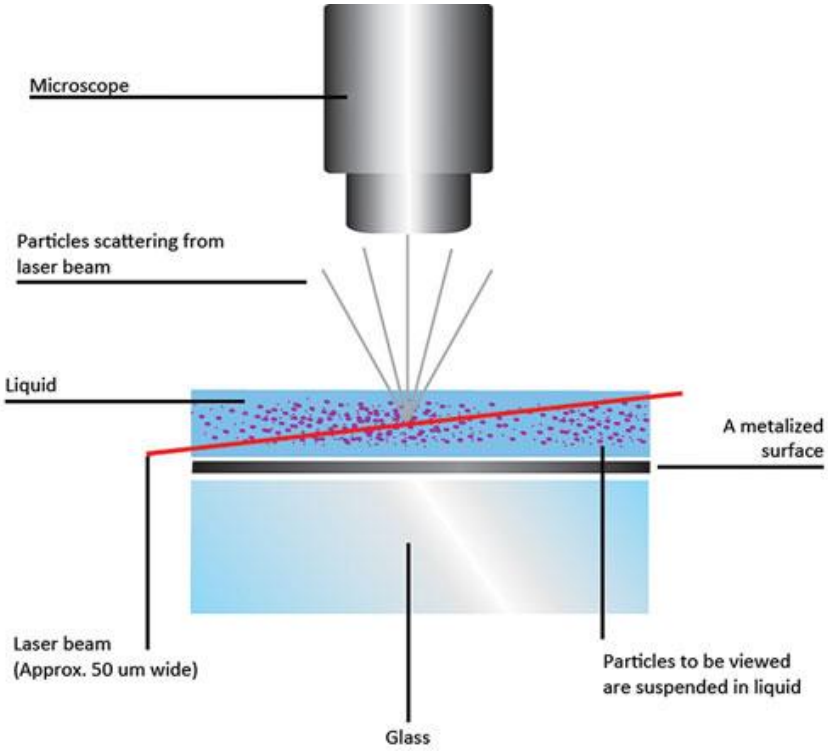

Figure 2.2: Nanoparticle Tracking Analysis (NTA): A laser beam is passed through the sample chamber and the particles in suspension in the path of the beam scatter light that can visualised by a x20 magnification microscope, which is mounted a video camera. The camera captures a video file of the particles moving under Brownian motion. The NTA software tracks particles individually and can calculate their hydrodynamic diameters using the Stokes Einstein equation. The NanoSight™ provides high resolution particle size, concentration and provides real time monitoring in the heterogeneous particle population observed by visual. *Source: (Malvern Instruments, 2017)*.

2.3 Generation of Lentiviral Transduced DU145 Cell Lines

2.3.1 shRNA Lentiviral Particle Transduction

Gene silencing and knockdown using RNAi interference (RNAi) technology is a commonly used tool to stably silence gene expression. The introduction of small interfering (siRNAs) into cultured cells provides a quick and efficient method of knocking down gene expression and is a ubiquitous tool in molecular biology. However, siRNA has been shown to be effective only in the short term for gene inhibition and in certain transformed mammalian cell lines, while short hairpin RNA (shRNA; sequence of RNA that forms a tight hairpin turn), offers a possibility to stably and potently silence gene expression.

Using shRNA can offer stable and long term gene silencing that is often achieved by using clonal selection methodologies, such as the pLKO.1 plasmid containing the puromycin resistance gene, followed by selection. The MISSION® shRNA lentiviral transduction particles (Sigma-Aldrich) can often permit efficient transduction and integration of the specific shRNA construct into the host cells. The host genome can transcribe the target shRNA in the nucleus, export it from the nucleus to be processed by Dicer (endoribonuclease), that is primed into the RNA-inducing silencing complex (RISC). This complex cleaves their designated target mRNA and represses mRNA translation, resulting in target gene silencing (Figure 2.3).

Wild type DU145 cells were seeded into 96-well flat bottomed plates at 5,000 cells/well, exosome-depleted media. At day 1, the DU145 cells were stably transduced with MISSION® shRNA lentiviral transduction particles (Table 2.2) (Multiplicity of Infection (MOI): 20) in the presence of hexadimethrine bromide (8µg/ml) (Sigma-Aldrich). At day 2, puromycin (1.25µg/ml) (Sigma-Aldrich) was added and media was changed daily, where each knockdown was confirmed at both the mRNA and protein level. The cells were cultured in the presence of puromycin until passage 6, when deemed free of lentiviral particles for experimental use. For my Thesis, the non-mammalian (NM) DU145 control (CTR) (transduced with a non-mammalian control shRNA) and knockdown of CD9 ($CD9^{KD}$), Rab5a ($Rab5a^{KD}$), Rab11b ($Rab11b^{KD}$), Rab35 ($Rab35^{KD}$), VAMP7 ($VAMP7^{KD}$) and VPS25 ($VPS25^{KD}$) cells, were generated and selected for additional experiments.

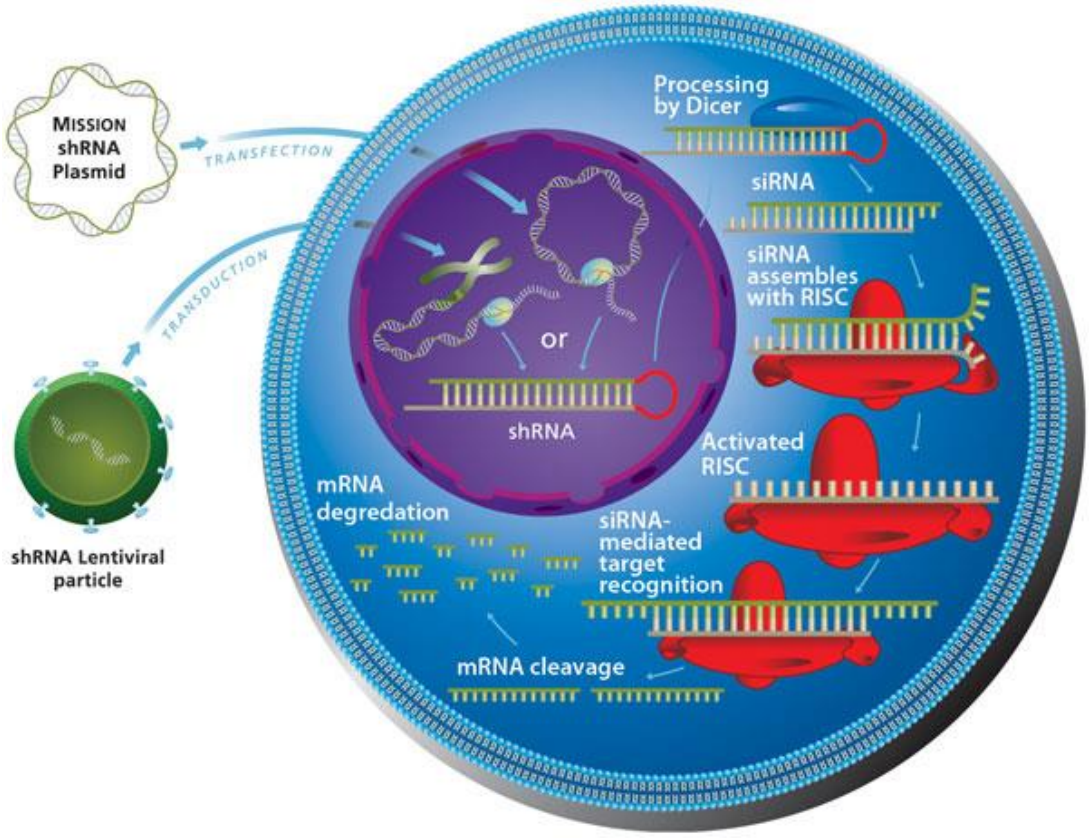

Figure 2.3: shRNA-mediated gene silencing via lentiviral transduction particles. The shRNA are incorporated into the lentiviral particle systems, which permit the transduction of the viral genome into the cytoplasm, where they are reverse transcribed. The DNA intermediate is imported into the nucleus, where it is stably integrated in the host genome. Following transcription, the shRNA sequence is exported to the cytoplasm where Dicer, processes the shRNA into the siRNA duplexes. This endogenously derived siRNA binds to the target mRNA and is incorporated into the RISC complex for target-specific mRNA degradation; thus preventing protein translation. *Source: (Sigma, 2016)*.

Target	TRC Number	Sequence	Clone ID
CD9	TRCN0000296953 (#953)	CCGGTTCTACACAGGAGTCTATATTCTCGAGAATATAGACTCCTGTGTAGAATTTTTG	NM_001769.2-277s21c1
	TRCN0000296958 (#958)	CCGGCCTGCAATGAAAGGTACTATACTCGAGTATAGTACCTTTCATTGCAGGTTTTTG	NM_001769.2-1072s21c1
	TRCN0000291711 (#711)	CCGGGCTGTTCGGATTTAACTTCATCTCGAGATGAAGTTAAATCCGAACAGCTTTTTG	NM_001769.2-150s21c1
	TRCN0000057469 (#469)	CCGGCATTGGACTATGGCTCCGATTCTCGAGAATCGGAGCCATAGTCCAATGTTTTTG	NM_001769.2-201s1c1
	TRCN0000057470 (#470)	CCGGGCTGTTCGGATTTAACTTCATCTCGAGATGAAGTTAAATCCGAACAGCTTTTTG	NM_001769.2-150s1c1
Rab5a	TRCN0000380597 (#597)	GTACCGGGAGAGTCCGCTGTTGGCAAATCTCGAGATTTGCCAACAGCGGACTCTCTTTTTTG	NM_004162.4-615s21c1
	TRCN0000380466 (#466)	GTACCGGCAAGGCCGACCTAGCAAATAACTCGAGTTATTTGCTAGGTCGGCCTTGTTTTTTG	NM_004162.4-934s21c1
	TRCN0000273641 (#641)	CCGGGCAGCCTTCCTTTCCAAAGTTCTCGAGAACTTTGGAAAGGAAGGCTGCTTTTTG	NM_004162.4-2298s21c1
	TRCN0000011215 (#215)	CCGGGCAGCCTTCCTTTCCAAAGTTCTCGAGAACTTTGGAAAGGAAGGCTGCTTTTT	NM_004162.3-2139s1c1
	TRCN0000007974 (#974)	CCGGCCAGGAATCAGTGTTGTAGTACTCGAGTACTACAACACTGATTCCTGGTTTTT	NM_004162.3-999s1c1
Rab11b	TRCN0000381919 (#919)	GTACCGGTTTGCTGCACCCATGAAACTCCTCGAGGAGTTTCATGGGTGCAGCAAATTTTTTG	NM_004218.3-951s21c1
	TRCN0000381558 (#558)	GTACCGGAGACAGCAACATCGTCATCATCTCGAGATGATGACGATGTTGCTGTCTTTTTTTG	NM_004218.3-435s21c1
	TRCN0000380618 (#618)	GTACCGGCATTCAAGAACATCCTCACAGCTCGAGCTGTGAGGATGTTCTTGAATGTTTTTTG	NM_004218.3-587s21c1
	TRCN0000029185 (#185)	CCGGCCTATTCAAAGTGGTGCTCATCTCGAGATGAGCACCACTTTGAATAGGTTTTT	NM_004218.1-36s1c1
	TRCN0000029188 (#188)	CCGGCAAGCACCTGACCTATGAGAACTCGAGTTCTCATAGGTCAGGTGCTTGTTTTT	NM_004218.1-288s1c1
Rab35	TRCN0000380335 (#335)	GTACCGGTGATGATGTGTGCCGAATATTCTCGAGAATATTCGGCACACATCATCATTTTTTG	NM_006861.4-475s21c1
	TRCN0000380080 (#080)	GTACCGGTTCACGAAATCAACCAGAACTCTCGAGAGTTCTGGTTGATTTCGTGAATTTTTTG	NM_006861.4-453s21c1
	TRCN0000380003 (#003)	GTACCGGGGAGAATGTCAACGTGGAAGACTCGAGTCTTCCACGTTGACATTCTCCTTTTTTG	NM_006861.4-601s21c1
	TRCN0000047796 (#796)	CCGGAGAGCAGTTTACTGTTGCGTTCTCGAGAACGCAACAGTAAACTGCTCTTTTTTG	NM_006861.4-207s1c1
	TRCN0000047794 (#794)	CCGGCCTCCGAGCAAAGAAAGACAACTCGAGTTGTCTTTCTTTGCTCGGAGGTTTTTG	NM_006861.4-649s1c1
VAMP7	TRCN0000379810 (#810)	GTACCGGATGAGAGAACAAGGAGTTAAACTCGAGTTTAACTCCTTGTTCTCTCATTTTTTTG	NM_005638.4-867s21c1
	TRCN0000298636 (#636)	CCGGGCGAGTTCTCAAGTGTCTTAGCTCGAGCTAAGACACTTGAGAACTCGCTTTTTG	NM_005638.4-485s21c1
	TRCN0000298637 (#637)	CCGGTCTTATGAGCTATCTACTAAACTCGAGTTTAGTAGATAGCTCATAAGATTTTTG	NM_005638.4-1157s21c1
	TRCN0000293928 (#928)	CCGGGGAAAGAAGAAGTTACCATTACTCGAGTAATGGTAACTTCTTCTTTCCTTTTTG	NM_005638.4-837s21c1
	TRCN0000059888 (#888)	CCGGGCGAGGAGAAAGATTGGAATTCTCGAGAATTCCAATCTTTCTCCTCGCTTTTTG	NM_005638.3-561s1c1
VPS25	TRCN0000381980 (#980)	GTACCGGAGTCCAGCTTCCTGATCATGTCTCGAGACATGATCAGGAAGCTGGACTTTTTTTG	NM_032353.2-321s21c1
	TRCN0000322763 (#763)	CCGGCCCTTTACTTCTTACCTCCCACTCGAGTGGGAGGTAAGAAGTAAAGGGTTTTTG	NM_032353.2-585s21c1
	TRCN0000322707 (#707)	CCGGAGTCGATCCAGATTGTATTAGCTCGAGCTAATACAATCTGGATCGACTTTTTTG	NM_032353.2-255s21c1
	TRCN0000144757 (#757)	CCGGGAGTCGATCCAGATTGTATTACTCGAGTAATACAATCTGGATCGACTCTTTTTTG	NM_032353.2-254s1c1
	TRCN0000143764 (#764)	CCGGCCTGTCTCCCTTTACTTCTTACTCGAGTAAGAAGTAAAGGGAGACAGGTTTTTTG	NM_032353.2-578s1c1

Table 2.2: Table of MISSION® lentiviral particles (Sigma-Aldrich) used to transduce DU145 cells.

2.3.2 Reverse Transcription and Quantitative Polymerase Chain Reaction

RNA Extraction

RNA was extracted from confluent lentiviral transduced DU145 cell lines or 3D spheroids, using 1ml TRI Reagent® per well (Sigma-Aldrich). Afterwards, 200µl of chloroform was added (Sigma-Aldrich) to each sample and mixed by inverting the sample numerous times in eppendorf tubes (Greiner Bio-One). The samples were centrifuged at 16,000 x *g* for 20 minutes at 4°C, to allow the separation of both aqueous and phenol phases. The colourless aqueous layer was removed and mixed with ice-cold isopropanol at -20°C for 24 hours, to allow precipitation of RNA. Samples were centrifuged at 16,000 x *g* for 20 minutes at 4°C, to wash away the isopropanol and the RNA pellets were washed in ice-cold 70% ethanol (volume/volume: v/v). This washing step was repeated twice and afterwards, the RNA pellets were air dried at RT and dissolved in 11µl molecular biology grade water.

1µl of RNA sample was administered onto the NanoDrop™ 2000 Spectrometer (ThermoFisher Scientific) which obtains a ratio of absorbance measured at 260nm and 280nm. RNA and DNA both will absorb at 260nm, they will contribute to the total absorbance of the sample. A ratio $\geq$1.7 is generally accepted as 'pure' RNA and used for analysis. If the ratio is considerably lower, it may indicate the presence of protein, phenol or other contaminants that absorb strongly near 280nm. For nucleic acid quantification, the extinction coefficient for RNA is 40 and the modified Beer-Lambert equation used is:

$$\textbf{C (Nucleic acid concentration µg/ml)} = \frac{\textbf{A (Absorbance) * ε (Extinction Coefficient)}}{\textbf{b (Path length in cm)}}$$

Reverse Transcription

Reverse transcription was performed using the random primer method in a final volume of 20µl per reaction, containing 1µg of RNA of the sample, 2µl of 10X reverse transcription buffer, 0.8µl of 25X deoxynucleotide triphosphates (dNTPs) (mixed nucleotides of dATP, dCTP, dGTP and dTTP) mix, 2µl of 10X reverse transcription random primers, 1µl of Multiscribe™ reverse transcriptase and 1µl of RNase Inhibitor (all from ThermoFisher Scientific). A negative control was included, which substituted RNA sample for molecular biology grade H_2O. The samples were loaded onto the S1000 Thermal Cycler (BioRad) to begin reverse transcription, which involved incubation at 25°C for 10 minutes to allow the primers to anneal to the RNA. The primers were then extended in the presence of dNTPs using reverse transcriptase at 37°C for 2 hours, generating cDNA. The cDNA was then heated at 85°C for 5 seconds to deactivate the RT. The cDNA samples were stored at -20°C.

Quantitative Polymerase Chain Reaction (qPCR)

qPCR was carried out with 20µl per reaction, containing 1µl of sample cDNA, 10µl of TaqMan® Universal Master Mix (20X) (ThermoFisher Scientific), 8µl of H_2O and 1µl of a TaqMan® gene expression assay primer and probe mix (all from ThermoFisher Scientific) (Table 2.3). A negative control was prepared using H_2O substitute for the cDNA. The PCR amplification was performed in a StepOnePlus™ Real-Time PCR System Thermocycler (ThermoFisher Scientific). Samples were amplified by heating them to 50°C for 2 minutes, then at 95°C for 15 seconds and 60°C for 1 minute, for a total of 40 cycles. The comparative C_T method was used for relative quantification of target gene expression. The C_T (threshold cycle where amplification is in the linear range of the amplification curve) for the standard reference gene (glyceraldehyde 3-phosphate dehydrogenase: GAPDH) were subtracted from the target gene C_T to obtain the ΔC_T for each sample. Target gene expression was calculated in each experimental sample relative to control samples by:

$$\textbf{Relative Expression} = 2^{-((\Delta CT\ TARGET\ 1) - (\Delta CT\ TARGET\ 2))}$$

The 'ΔCT 1' is the mean ΔCT value calculated for the experimental samples, whereas the 'ΔCT 2' is the mean ΔCT value calculated for the control samples (GAPDH). The data was analysed using the StepOnePlus™ Software (Version 2.0, ThermoFisher Scientific).

Primer and Probe Mix	Assay ID	Amplicon Length	Catalogue Number
CD9	Hs00233521_m1	72	#4331182
GAPDH	Hs02758991_g1	93	#4331182
MMP-1	Hs00899658_m1	64	#4331182
MMP-13	Hs00233992_m1	91	#4331182
Rab5a	Hs00991290_m1	157	#4331182
Rab11b	Hs00188448_m1	72	#4331182
Rab35	Hs00900055_m1	66	#4331182
TIMP-3	Hs00165949_m1	59	#4331182
VAMP7	Hs00194568_m1	80	#4331182
VPS25	Hs00260613_m1	92	#4331182

Table 2.3: Table of primers used for qPCR.

2.3.3 Collecting DU145 Cell Conditioned Media or Vesicle Concentrates

Obtaining Cell Conditioned Media

DU145 control or lentiviral transduced cell lines were seeded into 6-well plates (Greiner Bio-One), at equal densities (1 x 10^5) and cultured until 80% confluency. Media was removed from the flasks and replaced with 1.5ml of fresh RPMI-1640 media only. These plates were left at 37°C for 7 days, to allow the accumulation of vesicles in cell CM. Cell CM was collected and centrifuged at 400 x *g* for 7 minutes at RT, an additional 400 x *g* for 7 minutes at RT, followed by an additional at 2000 x *g* for 15 minutes at RT, to remove dead cells and cellular debris. The remaining CM were filtered using a 0.22µm millex GP syringe filter (Merck Millipore), to remove any remaining debris and larger vesicles. Filtered CM was used for experimental use or stored at -80°C until required.

Obtaining Vesicle Concentrates

The CM from above underwent ultracentrifugation at 200,000 x *g* for 2 hours at 4°C (fixed angle 70Ti rotor, Beckman Coulter). Vesicle concentrates were resuspended in PBS and stored at -80°C, until required for further experimental use.

Normalisation of CM/Vesicle Concentrates to Cell Number

One method of normalisation would be based on protein quantification (BCA Assay) of either cell CM or vesicle concentrates. Though, if the knockdown of interest did attenuate exosome secretion, normalisation based on protein content would not be a fair representation of vesicle loss and may negate its effect in downstream experiments. As protein normalisation would be based upon other vesicle subpopulations, this is not a fair representation of the impact of knockdown on vesicle secretion. As an alternative, we normalised lentiviral transduced DU145 cell CM/vesicle concentrates based on cell number, as this gives a fairer representation of secreted number of vesicle per cell.

First, cell counts were performed for the DU145 NM CTR, after collecting cell CM from T-75cm^2 culture flasks for ultracentrifugation. This gives an accurate count of cells that manufacture 100% of the control vesicle present in cell CM.

Secondly, cell counts were performed for lentiviral transduced DU145 cells, after collecting cell CM from T-75cm^2 culture flasks for ultracentrifugation. This give an accurate count of cells that manufacture a certain % of the vesicle present in cell CM following knockdown.

As examples for correcting cell CM to cell number:

	Control	Knockdown 1	Knockdown 2	Knockdown 3
Collected Cell CM	1ml	1ml	1ml	1ml
Cell Counts	100000	50000	200000	140000
Correction Factor	1x	2.0x	0.5x	0.71x
Normalise Samples to Cell Number				
-	Control	Knockdown 1	Knockdown 2	Knockdown 3
CM from Sample	0.5ml	1ml	0.25ml	0.35ml
PBS	0.5ml	0ml	0.75ml	0.65ml
Sample Normalised to 50,000 Cell Counts				

For characterisation or functional experiments, DU145 control vesicle concentrates was quantified to 20µg/ml or 200µg/ml by performing a MicroBCA Protein Assay (Thermo Scientific), as previously described. The vesicles derived from each DU145 CD9^{KD}, Rab5a^{KD}, Rab11b^{KD}, Rab35^{KD}, VAMP7^{KD} or VPS25^{KD} cell line would be adjusted to achieve an equivalent cell count versus controls.

As examples for correcting vesicle concentrates to cell number:

	Control	Knockdown 1	Knockdown 2	Knockdown 3
Vesicle Concentrates	10µl = 20µg/ml	(Unknown)	(Unknown)	(Unknown)
Correction Factor	1x	2.0x	0.5x	0.71x
Normalise Vesicle Concentrates to Correction Factor				
	Control	Knockdown 1	Knockdown 2	Knockdown 3
Corrected Vesicle Concentrates to Use	10µl	20µl	5µl	7.1µl
Corrected Volume of Vesicle Concentrates				

Normalisation based on secreted vesicles per cell number would give an accurate count of the influence following knockdown has upon vesicle secretion.

2.4 Characterising and Phenotyping Cells and Vesicles

2.4.1 Cell Viability Assay

The cell viability reagent, water soluble tetrazolium (WST)-1 (Roche, Basel, Switzerland) was used to examine cell viability. In principle, the stable tetrazolium salt, WST-1, is cleaved to a soluble dependent on the NAD(P)H in viable cells. Thus, the amount of formazan dye formed directly correlates to the number of metabolically viable cells in culture.

DU145 control or knockdown cells were seeded at 5,000 cells/well in 96-well flat-bottom plates (Greiner Bio-One) and incubated with 10µl of WST-1 reagent for 0.5 – 4 hours to determine the optimal time. Subsequently, seeded cells were left for 24, 48 and 72 hours respectively and plates were incubated up to 1 hour at 37°C. After this incubation period, the amount of formazan dye was quantitated by measuring absorbance at 420 nm by the PHERAstar FS Microplate Reader.

2.4.2 Light Microscopy and Immunofluorescence Microscopy

Light microscopy was used to examine general cellular morphology *in vitro*. DU145 cells, fibroblasts and HUVECs in 96-well plates, 25cm^3 or 75cm^3 culture flasks at 60 – 100% confluence, were visualised by phase contrast and images were captured using the Axio Observer Z1 (Zeiss, Oberkochen, Germany).

For immunofluorescence analysis, a monolayer of lentiviral transduced DU145 cells were seeded at 20,000 cells/well in Nunc™ Lab-Tek™ 8-Well Chamber Glass Slides (ThermoFisher Scientific) and incubated until 70% confluent. Likewise, following various treatments, stromal cells, such as endothelial cells and fibroblasts were washed gently with pre-warmed PBS (Lonza) three times and fixed in ice-cold acetone-methanol (1:1 v/v) (ThermoFisher Scientific) for 5 minutes and allowed to air dry at RT. The cells were washed three times with PBS and blocked for 1.5 hours at RT in 1% BSA (R&D Systems, Minneapolis, USA) in Hanks' Balanced Salt Solution (HBSS) (Sigma-Aldrich). The cells were washed three times using 0.1% BSA/HBSS (w/v) and were stained with unconjugated anti-mouse monoclonal antibodies (Figure 2.6), at 1µg/ml (in 0.1% BSA/HBSS) for 2 hours at RT. The cells were washed three times and stained with a goat anti-mouse secondary antibody (Alexa-488 conjugate) (ThermoFisher Scientific), at 10µg/ml for 45 minutes at RT, in the dark. Subsequently, following three washes, the cells were counterstained 4',6-diamidino-2-phenylindole (DAPI) (14.3mM) (ThermoFisher Scientific), diluted 1:50,000 in 0.1% BSA/HBSS (w/v) for 5 minutes, followed by three further washes and the cells were visualised by wide-field fluorescence Axio Observer Z1 with apotome using the Zen Blue Software (Zeiss).

2.4.3 Flow Cytometry

Lentiviral transduced DU145 cells were seeded in 6-well plates at 100,000 cells/well. Once confluent, cells were harvested using trypsin (Lonza) and centrifuged to obtain cell pellets, which were resuspended in PBS in form a homogenous cell suspension. The cells were fixed in IC Fixation Buffer (ThermoFisher Scientific), for 15 minutes at RT and washed twice with PBS. The resuspended cell pellets were incubated with unconjugated primary antibodies or matched isotype controls (Table 2.4) at 1µg/ml (in PBS) for 1 hour at RT, either with 2X Permeabilisation Buffer (ThermoFisher Scientific) or without. Following two washes, the cells were incubated with a goat anti-mouse secondary antibody (Alexa-488 conjugate) (ThermoFisher Scientific) at 10µg/ml for 45 minutes at RT, in the dark. Following a further two washes, cells were analysed using a FACSverse (BD Biosciences, New Jersey, USA).

Primary Antibody Specificity:	**Isotype**	**Catalogue Number**	**Company**
α-SMA	IgG_1	Sc-166952	Santa Cruz
CD9	IgG_{2B}	MAB1880	R&D Systems
CD31 (PECAM-1)	IgG_1	Sc-6520	Santa Cruz
CD63	IgG_1	MCA2142	AbD Serotec
CD81	IgG_1	MCA1847EL	BioRad
EEA1	IgG_1	610456	BD Bioscience
LAMP1	IgG_1	Sc-20011	Santa Cruz
LAMP2	IgG_1	Sc-18822	Santa Cruz

Table 2.4: Table of primary antibodies used for flow cytometry and immunofluorescent microscopy.

2.4.4 Enzyme-Linked Immunosorbent Assay (ELISA)

Quantification of FGF-2, HGF, uPA and VEGF-A in DU145 or treated fibroblasts cell CM was assayed using the DuoSet ELISA systems (R&D Systems). The manufacturer's instructions were followed except for the detection of the colourimetric change in the substrate solution, that was substituted for europium streptavidin and amended to detect TRF. The FGF-2, HGF, uPA and VEGF-A capture antibody at a dose of 1µg/ml (mouse anti-human against FGF-2, HGF, uPA and VEGF-A) were added to a high protein binding ELISA strip 96-well plate (Greiner Bio-One), at 100µl per well and incubated overnight at RT. Wells were aspirated and washed three times with Delfia® Wash Buffer (1X in water) (Perkin Elmer) to remove unbound antibody. Blocking buffer (1% BSA in PBS) was added to wells for 2 hours at RT, where wells were washed three times with Delfia® Wash Buffer. This was followed by the addition of a serial dilution human recombinant FGF-2, HGF, uPA and VEGF-A standard (diluted in 0.1% BSA in PBS) starting from 1000pg/ml (FGF-2), 2000pg/ml (VEGF-A), 4000pg/ml (uPA) or 8000pg/ml (HGF), respectively to 0pg/ml to create an eight-point standard curve.

Furthermore, DU145 or treated fibroblasts cell CM were added to the coated wells and incubated for 2 hours at RT, where wells were aspirated and washed. This was followed by the addition of the FGF-2, HGF, uPA and VEGF-A detection antibody (biotinylated goat anti-human antibody against FGF-2, HGF, uPA or VEGF-A) at 100ng/ml (VEGF-A), 200ng/ml (HGF), 250ng/ml (FGF-2), 400ng/ml (uPA), was added respectively for 2 hours at RT. Wells were washed 3 times, before adding a europium-streptavidin conjugate (Perkin Elmer) in a red buffer solution (Kaivogen) for 45 minutes at RT. Wells were washed 6 times, before adding enhancement solution (Kaivogen) for 5 minutes at RT; and the signal assessed by time resolved fluorescence (TRF) on a PHERAstar FS Microplate Reader. The absorbance values were extrapolated from the standard curve to calculate the FGF-2, HGF, uPA or VEGF-A protein concentration in each sample.

TGF-β1 ELISA

Quantification of TGF-β1 in treated fibroblasts cell CM was assayed using the DuoSet ELISA systems. The manufacturer's instructions were followed except for the detection of the colourimetric change in the substrate solution, that was substituted for europium streptavidin and amended to detect TRF. The TGF-β1 capture antibody at a dose of 1µg/ml were added to a high protein binding ELISA strip 96-well plate (Greiner Bio-One), at 100µl per well and incubated overnight at RT. Wells were aspirated and washed three times with Delfia® Wash Buffer (1X in water) (Perkin Elmer), to remove unbound antibody. Blocking buffer (1% BSA in PBS) was added to wells for 2 hours at RT, where wells were washed three

times with Delfia® Wash Buffer. This was followed by the addition of a serial dilution human recombinant TGF-β1 standard (diluted in 0.1% BSA in PBS), starting from 2000pg/ml to 0pg/ml to create an eight-point standard curve.

To activate latent TGF-β1 to the immunoreactive form detectable by the TGF-β1 DuoSet ELISA kit, treated fibroblasts cell CM or vesicle concentrates were acid activated using 20µl of 1N hydrochloric acid (HCL), vortexed and incubated for 10 minutes at RT. The acidified samples were neutralised by adding 20µl of 1.2N sodium hydroxide (NaOH)/0.5 M HEPES, the pH was measured to ensure neutralisation was within 7.0 – 7.6. Once neutralised, 100µl of sample were added to the wells and incubated for 2 hours at RT, where wells were aspirated and washed. Biotinylated goat anti-human TGF-β1 detection antibody at 300ng/ml was added for 2 hours at RT. Wells were washed 3 times, before adding a europium-streptavidin conjugate in a red buffer solution for 45 minutes at RT. Wells were washed 6 times, before adding enhancement solution for 5 minutes at RT; and the signal assessed by TRF on a PHERAstar FS Microplate Reader. The absorbance values were extrapolated from the standard curve to calculate the TGF-β1 protein concentration in each sample.

MMP-1 and MMP-13 ELISA

Quantification of MMP-1 and MMP-13 in 3D spheroids cell CM was assayed using the RayBio® Human MMP-1 and MMP-13 ELISA kit (both from RayBio® Tech, Georgia, USA). The manufacturer's instructions were followed except for the detection of the colourimetric change in the substrate solution, that was substituted for europium streptavidin and amended to detect TRF. A serial dilution of human recombinant MMP-1 and MMP-13 (diluted in 0.1% BSA in PBS) starting from 18000pg/ml (MMP-1) or 6000pg/ml (MMP-13) to 0pg/ml created an eight-point standard curve in pre-coated MMP-1 and MMP-13 microplates (RayBio® Tech). 100µl of 3D spheroids cell CM were added to the wells and incubated for 2.5 hours at RT, where wells were aspirated and washed three times with Delfia® Wash Buffer (1X in water). MMP-1 or MMP-13 detection antibody (biotinylated goat anti-human antibody against MMP-1 or MMP-13) was added at 1:80 dilution for both MMP-1 and MMP-13 for 1 hour at RT. Wells were washed 3 times, before adding an europium-streptavidin conjugate in a red buffer solution, for 45 minutes at RT. Wells were washed 6 times, before adding enhancement solution for 5 minutes at RT; and the signal assessed by TRF on a PHERAstar FS Microplate Reader. The absorbance values were extrapolated from the standard curve to calculate the MMP-1 and MMP-13 protein concentration in each sample.

2.4.5 Protein Profiling Array

Vesicle concentrates (20µl) from DU145 control, Rab11b^{KD} or Rab35^{KD} cells were subject to lysis (20µl of RIPA buffer); and analysed by a sensitive Proximity Ligation Assay Configure, in the form of a 92-Plex Array. Alternatively, cell CM normalised for cell number, without concentrating, were used. The Olink Proseek® Multiplex Inflammation I^{96x96} Panel comprises 92 inflammation-related protein analytes as it gave a good coverage of potentially relevant factors (Olink Bioscience, Uppsala, Sweden). The Limit Of Detection (LOD) was defined as 1.5 standard deviations above background and values below this limit were reported as <LOD. The data were filtered to remove analytes below the limit of detection and comparisons were made between control and knockdowns, based on fold change and t-test.

2.5 Functional Experiments

2.5.1 Growth Arrest

Prior to all functional experiments, fibroblasts were growth-arrested in serum-free media for 72 hours to allow fibroblast depletion of growth factors, otherwise any remanence of growth factors in the media would allow fibroblasts the potential capacity to express α-SMA. Seeded fibroblasts were washed with serum-free DMEM/F12 (Lonza) to remove any residual FBS. Fresh serum-free DMEM/F12 medium was added to fibroblasts for 72 hours and unless stated otherwise, fibroblasts were cultured in DMEM/F12 media.

2.5.2 Fibroblast Differentiation

Fibroblasts were cultured in Nunc™ Lab-Tek™ 8-Well Chamber Glass Slides (ThermoFisher Scientific) or 24-well plates (Greiner Bio-One) in DMEM/F12 media with supplement mixture (as described in 2.1.1) and once 80% confluent, the cells were growth-arrested for 72 hours. The fibroblasts were treated with either the equivalent of recombinant human TGF-β1 (rhTGF-β1) (1.5ng/ml), 200µg/ml of purified DU145 exosomes, cell-number normalised vesicle concentrates (DU145 NM CTR, Rab11b^{KD} or Rab35^{KD}), in DMEM 10% exosome-depleted FBS for 72 hours. In other experiments, fibroblasts were also treated in DU145 NM CTR, Rab11b^{KD} or Rab35^{KD} cell CM normalised to cell number. Treated fibroblasts cell CM after 72 hours treatment was used for ELISAs or to treat endothelial cells in a migration assay. The cells were fixed and subsequently stained for α-SMA (Santa Cruz) and visualised with the Axio Observer Z1 with apotome.

2.5.3 Migration Assay

A confluent monolayer of HUVEC cells was cultured in 96-well plates and serum-starved for 24 hours in growth-factor free conditions. The confluent monolayer was subject to a single vertical scratch using a 200µl pipette tip. The wells were gently washed with PBS and treated with CM taken from fibroblast cultures and wells were microscopically monitored at 0, 6, 12, 24 hours. The width of the scratch in triplicate wells was measured at 6 points for each well, using Image-J (National Institutes of Health, Bethesda, USA) and the rate of monolayer recovery plotted as relative to the original scratch width (% closure).

2.5.4 Vessel-like Formation Assay

Formation of endothelial vessel-like structures was performed with endothelial cells (20,000 per well), serum-starved for 24 hours. These were added in triplicate to monolayers of fibroblasts (100,000 cells per well), that had been previously treated with rhTGF-β1, exosomes or vesicle concentrates for 72 hours. A 1:1 volume ratio of DMEM/F12:EGM-2

media in the absence of exogenous factors was used. After a further 4 days of culture, structures formed by endothelial cells were visualised by immunofluorescent labelling of CD31 (Santa Cruz). The total area occupied by CD31-positive structures was quantified using Zen Blue Software to calculate the area occupied by stained cells in each well. Data shows the average from triplicate wells per treatment and are representative of three such experiments.

2.5.5 Spheroid Generation for Invasion and Growth Assessment

Spheroid Generation

Spheroids were generated in a 96-well u-bottom polyhydroxyethylmethacrylate (Poly-HEMA)-coated plate (Sigma-Aldrich) or cell-repellent surface plate (Greiner Bio-One). To generate homotypic or heterotypic spheroids, tumour cells (DU145 NM CTR, Rab11b^{KD} or Rab35^{KD}) were incubated alone or together with fibroblasts at a ratio of 4:1 (tumour cells:fibroblast), in poly-HEMA or cell-repellent surface plates and centrifuged at 400 x *g* for 10 minutes at RT. This ratio was previously used *in vivo* experiments specifically revealing a tumour growth benefit of fibroblasts (Webber et al., 2015). 10,000 cells were seeded in total per well for each generated spheroids and the medium consisted of RPMI-1640 in 10% exosome-depleted FBS. After 72 hours, the cell established 3D spheroidal structures.

Growth Assessment

3D cell spheroids were cultured in RPMI-1640 with 10% exosome-depleted FBS and every other day, 50% of the culture media was replaced by fresh media. Over a 24-day period, spheroid area and diameter was measured every 3-4 days by using Image J.

Invasion Assay

100µl of Matrigel™ (Corning, UK) was added to each well of a 24-well flat glass bottom plate. The basement membrane matrix consists of laminin, collagen IV, entactin and heparan sulphate proteoglycans. The matrigel-coated plates were set for 30 minutes at 37°C and medium was added. Spheroids were transferred to freshly matrigel-coated, 24-well plates to explore the potential invasive behaviours of these cells and the wells were monitored for 96 hours thereafter. To evaluate the magnitude out from the spheroid, the free-hold selection tool in Image-J was used to draw the circumference of the central sphere. This was subtracted from the circumference of the region occupied by invading cells. This gives an approximation of Matrigel™ invaded by cells, as it does not consider the volumetric aspect of the 3D culture and is likely then to underestimate the true differences across the experimental groups.

2.6 *In vivo* Experiments

2.6.1 Animal Maintenance

In vivo experiments were conducted in accordance with the Animal (Scientific Procedures) Act 1986 and the United Kingdom Co-ordinating Committee on Cancer Research (UKCCCR) guidelines for the welfare of animals in experimental neoplasia. 8-week-old male CD1 athymic mice were housed under standard laboratory conditions in a temperature controlled (22°C; 50-55% humidity) pathogen free environment, with a 12-hour light-dark cycle. 4 mice were used per experimental group. Food and water was supplied *ad libitum*. All procedures were performed under aseptic conditions and the body temperature of animals was kept constant using heated pads.

2.6.2 Xenograft Establishment and Tumour Growth Delay

For *in vivo* xenograft experiments, this was performed in collaboration with Prof. Jenny Worthington (Axis Bioservices, Coleraine, Northern Ireland). DU145 control or Rab11b^{KD} or Rab35^{KD} cells with fibroblasts xenografts (4 tumour cells:1 fibroblast ratio) were established on the dorsal flank by subcutaneous injection of 5 x 10^6 cells suspended in 100µl of matrigel with a 21g needle (Becton Dickinson, Oxford, UK). Once the tumour became palpable, dimensions were measured using Vernier calipers every two to three days, to determine the volume, up to the severity limits at day 46. Tumour volume was calculated using tumour volume = 0.523 x width^2 x length. Total body weight was also taken and this did not change for any mouse during the procedures. At 46 days, tumours were excised and photographed.

2.7 Statistical Analysis

Statistical analyses were performed using Prism-5 Software V5.01 (Graph Pad, San Diego, USA). In experiments with more than two experimental groups, 1-way ANOVA with Tukey's post-test was used, except for kinetic experiments where a 2-way ANOVA with Bonferroni post-test was used. Experiments with two experimental groups were evaluated using students *t* test. P values less than 0.05 were considered significant *$p<0.05$, **$p<0.01$, ***$p<0.001$. Graphs depict mean±SEM, from one representative experiment of at least three similar experiments, unless stated otherwise.

CHAPTER 3:

CHARACTERISATION OF EXOSOMES FROM WILD-TYPE DU145 CELLS

3.1 Characterisation of Exosomes from Wild Type DU145 Cells

3.1.1 Introduction

Cells communicate via soluble, secreted factors or via membrane vesicles, collectively referred to as EVs. Exosomes are endosome-derived EVs and correspond to the ILVs released into the extracellular space, by fusion of MVEs with the plasma membrane. The prostate cancer cell line chosen for this study were DU145 cells, derived from prostate adenocarcinoma metastatic to the brain (Stone et al., 1978), as they are commonly used for studying prostate cancer in several studies (Alimirah et al., 2006, Clayton et al., 2007, Webber et al., 2010); and their exosomes are well-characterised by the Clayton group.

To broaden our understanding of exosomes, great efforts have been made for characterisation. In general, exosomes are isolated from either cell CM or biological fluids; and several protocols have been developed. This includes one that was used in initial studies describing exosomes (Johnstone et al., 1987, Raposo et al., 1996); and involves several centrifugation steps to separate vesicles (Théry et al., 2006): 400 x *g* and 2000 x *g* were used to eliminate unwanted cells and debris; and 10,000 x *g* to eliminate microvesicles, which are larger than exosomes (100 – 1000nm in diameter vs 30 – 150nm for exosomes). Exosomes are then pelleted at 100,000 – 200,000 x *g*. Alternatively, many variations are implemented in practice. Some protocols utilise serial filtration or others use 0.22µm filters prior to exosome pelleting, as this provides a quicker isolation step compared to additional spins. This protocol leads to a pellet that is concentrated with vesicles. Furthermore, density gradient-based isolation using the continuous sucrose gradient (Raposo et al., 1996, Caby et al., 2005), 30% sucrose cushion method (Lamparski et al., 2002) and iodixanol (OptiPrep™) (Cantin et al., 2008, Tauro et al., 2012), can be applied to obtain purer exosome preparations, by allowing separation based on density, rather than size or sedimentation rates by ultracentrifugation.

Here, wild type DU145 exosomes were isolated based on a combination of ultracentrifugation and through a 30% sucrose cushion. Once isolated, characterisation of exosomes using a combination of techniques aimed at observing size/morphology and enrichment in exosomal-associated proteins (Western blotting or plate-based assays) was performed. These techniques fit the minimum experimental requirements for the definition of exosomes as set out by ISEV (Lotvall et al., 2014). NTA is a light-scattering technique, that is useful for size distribution and concentration measurements of exosomes (Dragovic et al., 2011). In combination, cryo-EM was used to observe exosome morphology and

heterogeneity present within samples (Sokolova et al., 2011). Validation of exosomal-associated markers include: the tetraspanins (CD9, CD63 and CD81); ESCRT-associated proteins (ALIX and TSG101); lysosomal-associated membrane proteins (LAMP1 and LAMP2); heat shock proteins (HSP70 and HSP90); and major histocompatibility complex-I (MHC-I). In addition, the presence of proteins not expected to be enriched in exosomes of endosomal origin should be determined and this simple aspect is often overlooked in the field. Contaminating soluble proteins such as calnexin (endoplasmic reticulum associated protein), cannot be detected by cryo-EM or NTA, and can be assessed by Western blot or other methods. One other method that discriminates purer vesicle preparations from those containing contaminating proteins is to compare the ratio of nanoparticle counts to protein concentration (P:P ratio) (Webber and Clayton, 2013). By being able to estimate purity and compare sample purity in relatively simple and general quantitative manner, will be useful. As this tool broadly defines what is an acceptably pure vesicle sample. A P:P ratio that is less than 1×10^{10} is considered to be unpure and will be used as a basis to quality control check exosome preparations.

Here, in this Chapter, we will characterise wild type DU145 exosomes by using multiple approaches, which include cryo-EM, an immune-phenotyping plate assay, Western blot, NTA and by determining P:P ratios. These methods will form as a basis for analysing exosomes, by determining the quantity and phenotype of vesicles. These methods will act as a platform to examine whether exosome secretion is modulated by silencing putative regulators of exosome biogenesis and secretion.

3.1.2 Characterisation of DU145 Exosomes

The DU145 cell line (originally derived from the metastatic site of the brain) was purchased from ATCC. A monolayer of DU145 epithelial cells were examined by phase contrast microscopy (Figure 3.1), revealing cells to be adherent to plastic and consisting of a flat polygonal shape in appearance; sometimes referred to as a cobble-stone like pattern when fully confluent (Stone et al., 1978). These morphological observations agreed with other studies on the DU145 cell line (Hayward et al., 2001, Alimirah et al., 2006).

Isolating exosomes from DU145 cell CM by a combination of ultracentrifugation and purifying exosomes on a density-based gradient or cushion, based on their floatation property, is a commonly used analytical tool (Raposo et al., 1996, Théry et al., 2006). Traditionally, the continuous sucrose gradient is a commonly used method, however, it is labourious and there is variability with the exosome yields obtained (Lamparski et al., 2002). Alternatively, the sucrose cushion is a quicker method for isolating exosomes compared to the sucrose gradient method. This method utilises both ultracentrifugation and a 30% sucrose cushion to purify exosomes based on their flotational density in sucrose of 1.1 – 1.2g/ml. Exosomes were captured in a small density cushion, composed of 30% sucrose/D_2O. D_2O can readily diffuse with H_2O, which allows the formation of the minigradient between 1.1 – 1.8g/cm^3 and for enrichment and increased purity of exosomes because of the decreased soluble proteins present. The cushions containing exosomes were collected and went through an additional PBS wash. This resulted in an exosomal pellet which was characterised.

First, the morphology of DU145 exosomes was examined by cryo-EM, in collaboration with Prof. Juan Manuel Falcon-Perez (CIC bioGUNE, Derio, Spain). This was carried out by resuspending exosome pellets in PBS and placed onto carbon grids. Grids were vitrified with the aid of a Vitrobot. Vitrified samples were imaged quickly at liquid nitrogen temperature to prevent the formation of ice crystals. The image reveal heterogeneous populations of rounded structures of vesicles with a thick outer boundary, indicative of a lipid bilayer (Figure 3.2). The diameter of DU145 exosomes agrees with the typically observed diameter range for exosomes, often found between 30 – 150nm, as reported by other studies (Raposo et al., 1996, Welton et al., 2010, Yuana et al., 2013).

Additionally, the phenotype of DU145 exosomes was examined using a microplate immune-phenotype assay. Exosomes were coated onto ELISA plates overnight and were assessed for their expression of proteins commonly found on exosomes. The expression of CD9, CD81 and

MHC-I on the DU145 exosomes were expressed at just over 3.5 x 10^6 TRF (Figure 3.3 A). The DU145 exosomes still showed expressed levels of CD63, but to a lesser extent compared to the other tetraspanins (3-fold less). The expression of other markers LAMP1, LAMP2, HSP70 and HSP90 revealed DU145 exosomes exhibit a lower positive expression (< 5 x 10^5 TRF). However, it remained difficult to detect ALIX and TSG101 (ESCRT-related proteins) on the surface DU145 exosomes with this method, as these are ESCRT-related markers typically found on exosome's internal side. Next, we attempted to refine this immune-phenotype assay by lysing exosomes coated onto ELISA plate to detect levels of ALIX and TSG101 (Figure 3.3 B). The signal of ALIX and TSG101 was 4-fold greater when lysing exosomes with RIPA, compared to the standard method ($P<0.001$). Here we showed the isolated DU145 exosomes express proteins typically found on the exosome's surface similar to other studies (Escola et al., 1998, Théry et al., 1999).

To ensure that a specific protein is enriched in exosomes, a comparison in proteins between whole cell lysates and exosomes were prepared from the same parent cell (DU145) on the same gel. Cell lysates and exosomes from DU145 cells were compared by Western blot and probed with an assortment of antibodies. The expression of exosome-associated markers, such as ESCRT-related proteins (ALIX and TSG101) and MHC-I were highly enriched in exosomes, compared to cell lysates (Figure 3.4). LAMP1 and LAMP2 expression was found to be positively expressed in both cell lysates and exosomes, slightly enriched in the exosomes. In contrast, the endoplasmic reticulum protein, calnexin, was only present in the cell lysates. The expression of the cytosolic marker, GAPDH, was found in cell lysates and exosomes, as expected. By phenotyping the DU145 exosomes, these results agree with similar documented studies in characterising exosomal-associated proteins (Raposo et al., 1996, Escola et al., 1998). The method provides a means of differences in the endosomal/lysosomal origin of exosomes; and potentially as a means of defining if any change in their pathways arise if interferences with secretion.

To provide an indication of the heterogeneity present within our purified DU145 exosome preparations, Nanosight™ NTA was used. First, we analysed the size distribution of vesicles present in DU145 cell CM and show a modal diameter of 99nm (Figure 3.5 A). This observation is comparable to the cryo-EM images presented in Figure 3.2, showing a heterogeneous population of exosomes with a diameter within the range of 30 – 150nm (Raposo et al., 1996, Filipe et al., 2010, Sokolova et al., 2011). Similarly, the isolated purified DU145 exosomes had a modal diameter of 131nm (Figure 3.5 B), comparable with the cryo-EM images. No major differences in the modal size characteristics of exosomes were present

between both methods. Despite showing no presence of larger sized vesicles or cellular aggregates present (>500nm) in purified exosomes, there remains a broader range of detected vesicles (up to 500nm), compared to cell CM which ranges up to 300nm. This data suggests that characterising vesicles in cell CM gives similar size distribution profiles present in purified DU145 exosomes, with the benefit of having fewer peaks for larger size nanoparticles (>300nm). On the other hand, it is important to consider the purity of isolated exosomes from cell CM, as it is often dependent on the protocol utilised.

Estimation of the exosome purity can be measured based on the P:P ratio, using a combination of NTA and a colourimetric BCA assay, to determine the particle per ml and protein concentration respectively (Webber and Clayton, 2013). A study has demonstrated that an exosome preparation containing protein contaminants, resulted in a reduced P:P ratio, compared to an exosome sample with no contamination. It was proposed that a P:P ratio that was below 1.0×10^{10} were impure and a P:P ratio $\geq 1.0 \times 10^{10}$ were considered of low to high purity. The quality threshold of our exosome preparations were routinely used on isolated exosomes from the sucrose cushion preparation (Table 3.1). By characterising vesicles from cell CM alone, a P:P ratio of 1.78×10^{8} was obtained and indicates the sample would be impure and could contain other soluble proteins that may not be vesicle-based (Figure 3.5 A). In contrast, a P:P ratio of 1.11×10^{10} was obtained from a purified DU145 exosome preparation (Figure 3.5 B), passing the arbitrary threshold for a pure preparation.

Many exosome preparations exceeded the quality threshold and were used for subsequent characterisation and functional experiments. In contrast, the preparations that failed the quality control were not used for experiments and this could be explained by some contamination of collecting the sucrose cushion containing exosomes during isolation. Exosomes isolated from prostate cancer DU145 cells using the sucrose cushion method are of good purity and largely free of contaminating proteins.

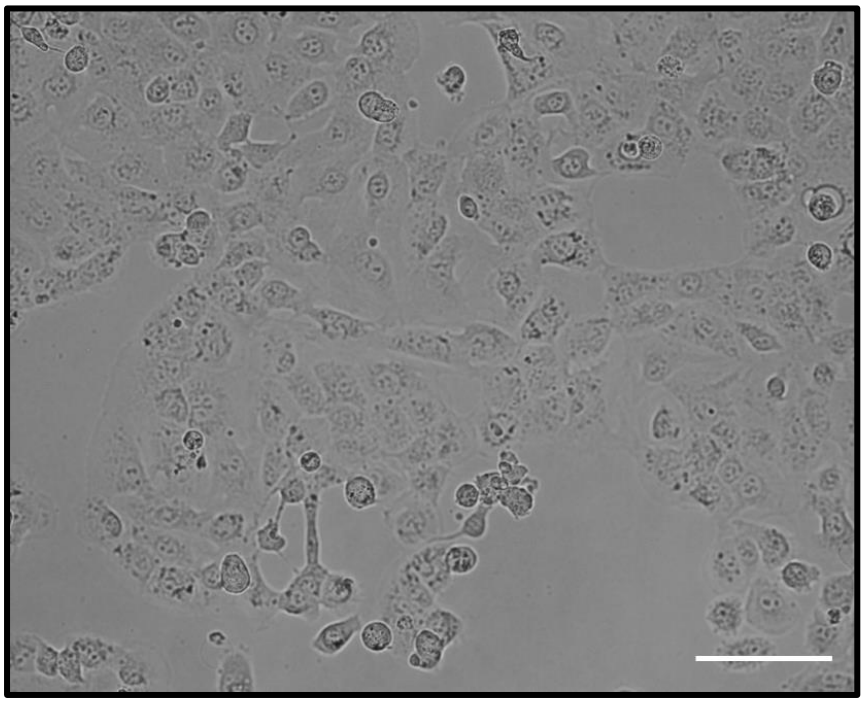

Figure 3.1: Morphology of prostate cancer cell line (DU145). Monolayer of live prostate cancer cell (DU145) were imaged using phase contrast microscopy to confirm cobblestone morphology of the epithelial cells. Scale Bar: 100µm.

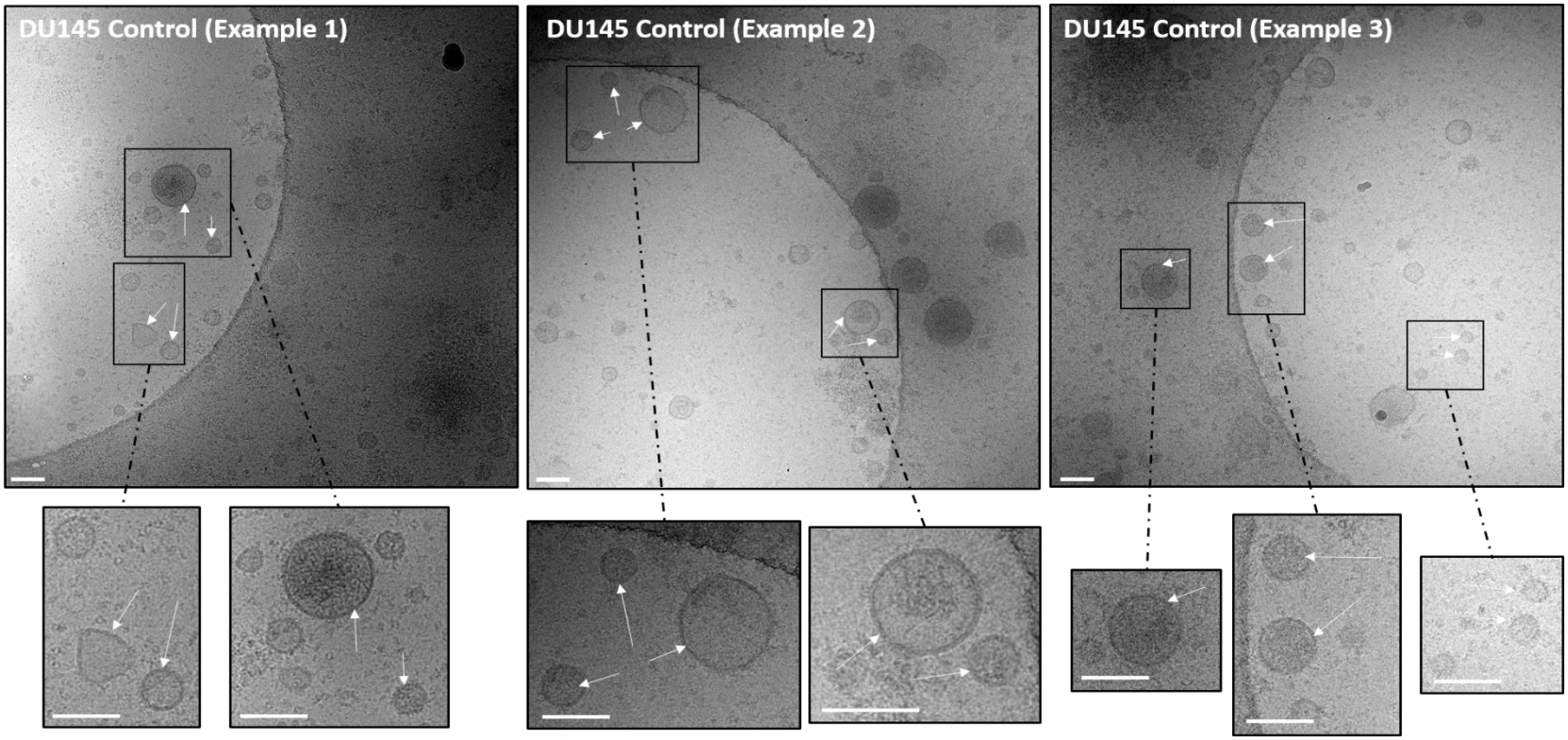

Figure 3.2: Cryo electron microscopy images of DU145 exosomes. DU145 exosomes were adsorbed onto glow-discharging holey carbon 200-mesh copper grids (QUANTIFOIL, Germany). Grids were blotted at 95% humidity and rapidly plunged into liquid ethane with the aid of VITROBOT (Maastricht Instruments BV, The Netherlands). Vitrified samples were imaged at liquid nitrogen temperature using a JEM-2200FS/CR Transmission Electron Microscope (JEOL, Japan), equipped with a field emission gun and operated at an acceleration voltage of 200 kV. Multiple samples were viewed under cryo-EM, confirming the presence of vesicle structures (white arrows) typical of exosomes. Scale bar: 100µm.

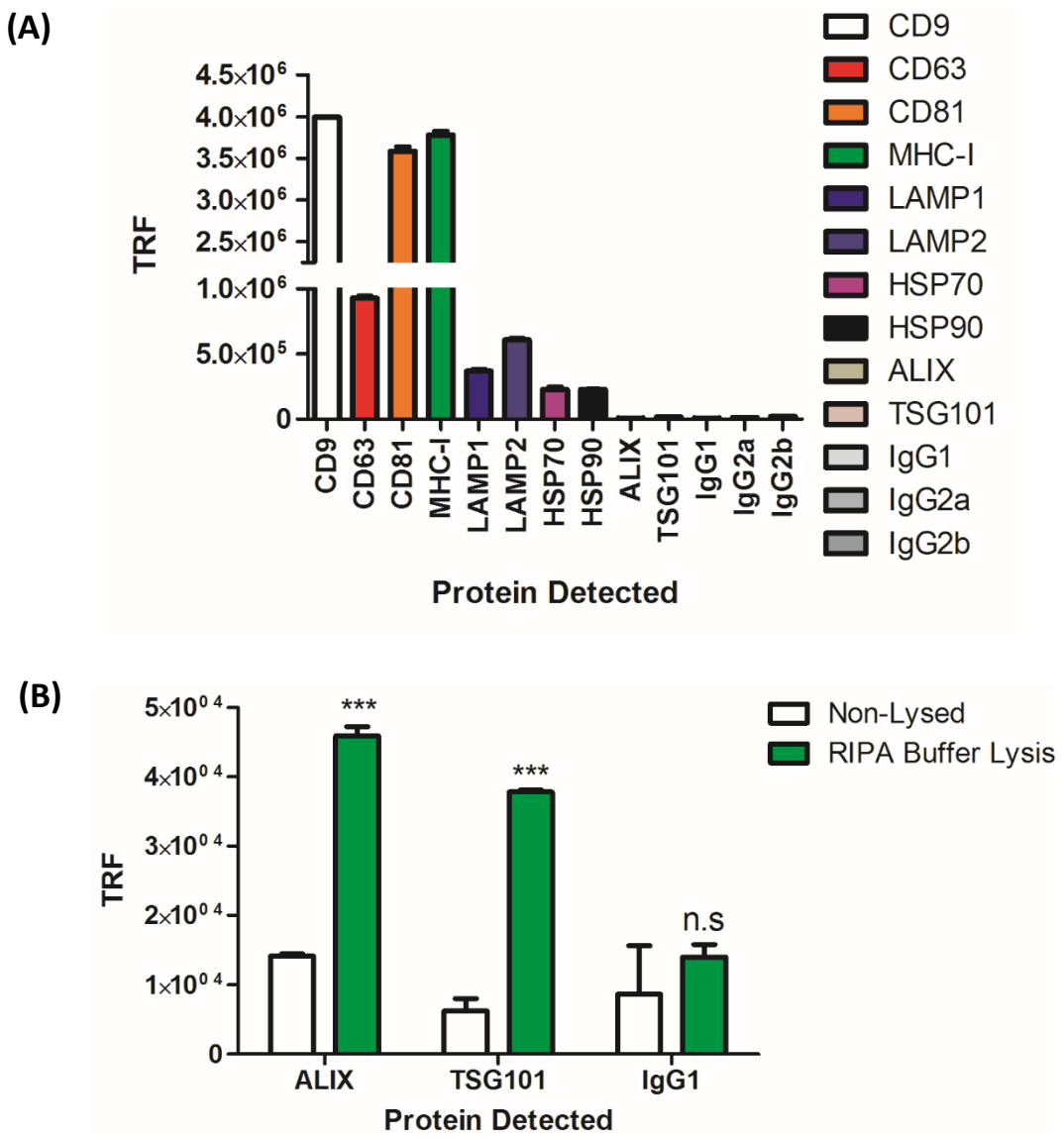

Figure 3.3: Characterisation of DU145 exosomes by an immune-phenotype plate assay. **(A)** DU145 exosomes were captured onto high protein binding ELISA plates (1µg/well). They were analysed for the expression exosome-associated proteins: tetraspanins (CD9, CD63 and CD81), MHC-I, lysosomal associated membrane proteins (LAMP1 and LAMP2), heat-shock proteins (HSP70 and HSP90), ESCRT-related proteins (ALIX and TSG101) with isotype controls. Graph shows mean + SEM, based on duplicate wells. **(B)** DU145 exosomes were lysed with RIPA and analysed for the expression of ALIX and TSG101. Time resolved fluorescence (TRF) is shown. Graph shows mean + SEM, based on duplicate wells. n.s: non-significant, **<0.01 and ***P<0.001. One-way ANOVA with Tukey's multiple comparison test.

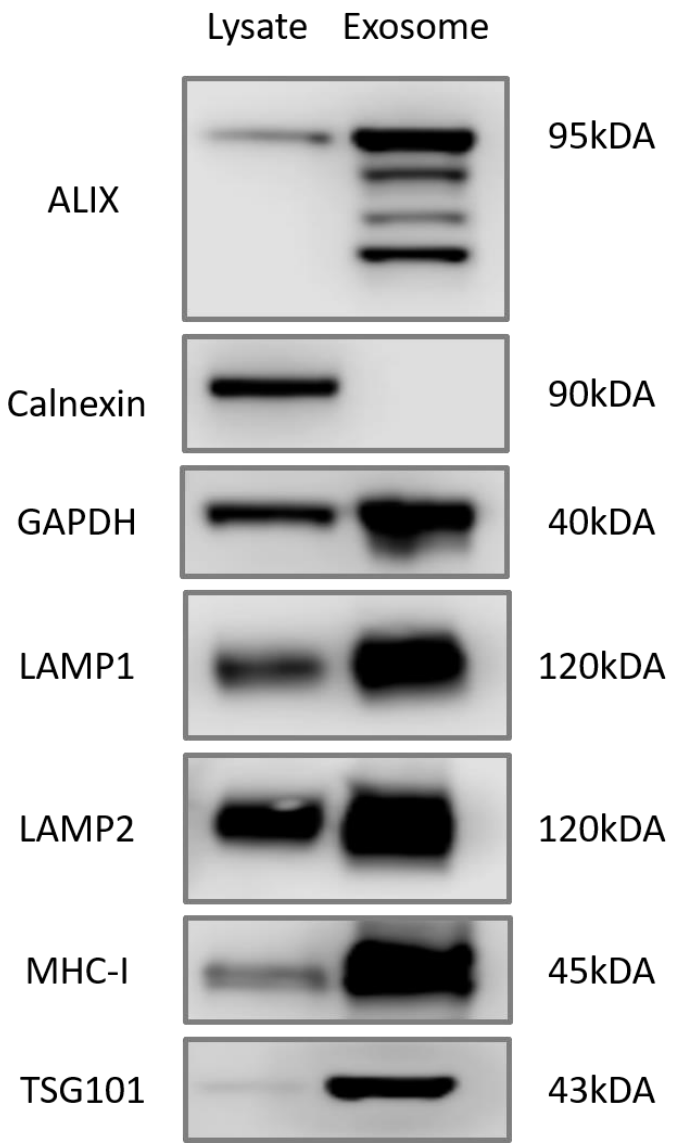

Figure 3.4: Characterisation of DU145 exosomes by Western blot. DU145 exosomes (20µg) and whole cell lysates (20µg), were subjected to SDS-PAGE and Western blotting. They were probed for exosomal associated proteins: ALIX, GAPDH, LAMP1, LAMP2, MHC-I, TSG101. The presence of a protein not expected of endosomal origin was determined by calnexin a marker for the endoplasmic reticulum.

(A)

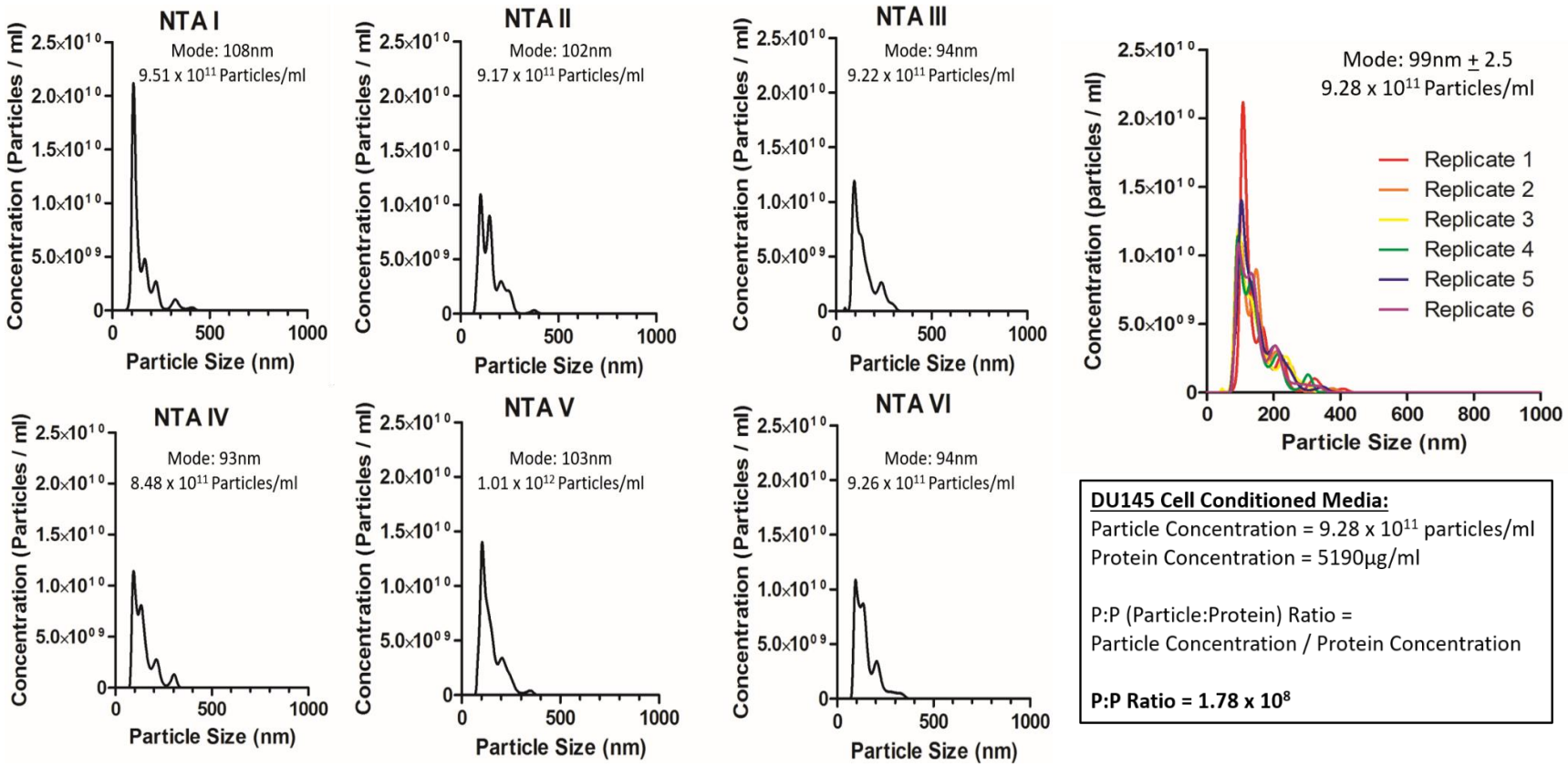

DU145 Cell Conditioned Media:
Particle Concentration = 9.28 x 10^{11} particles/ml
Protein Concentration = 5190µg/ml

P:P (Particle:Protein) Ratio =
Particle Concentration / Protein Concentration

P:P Ratio = 1.78 x 10^{8}

(B)

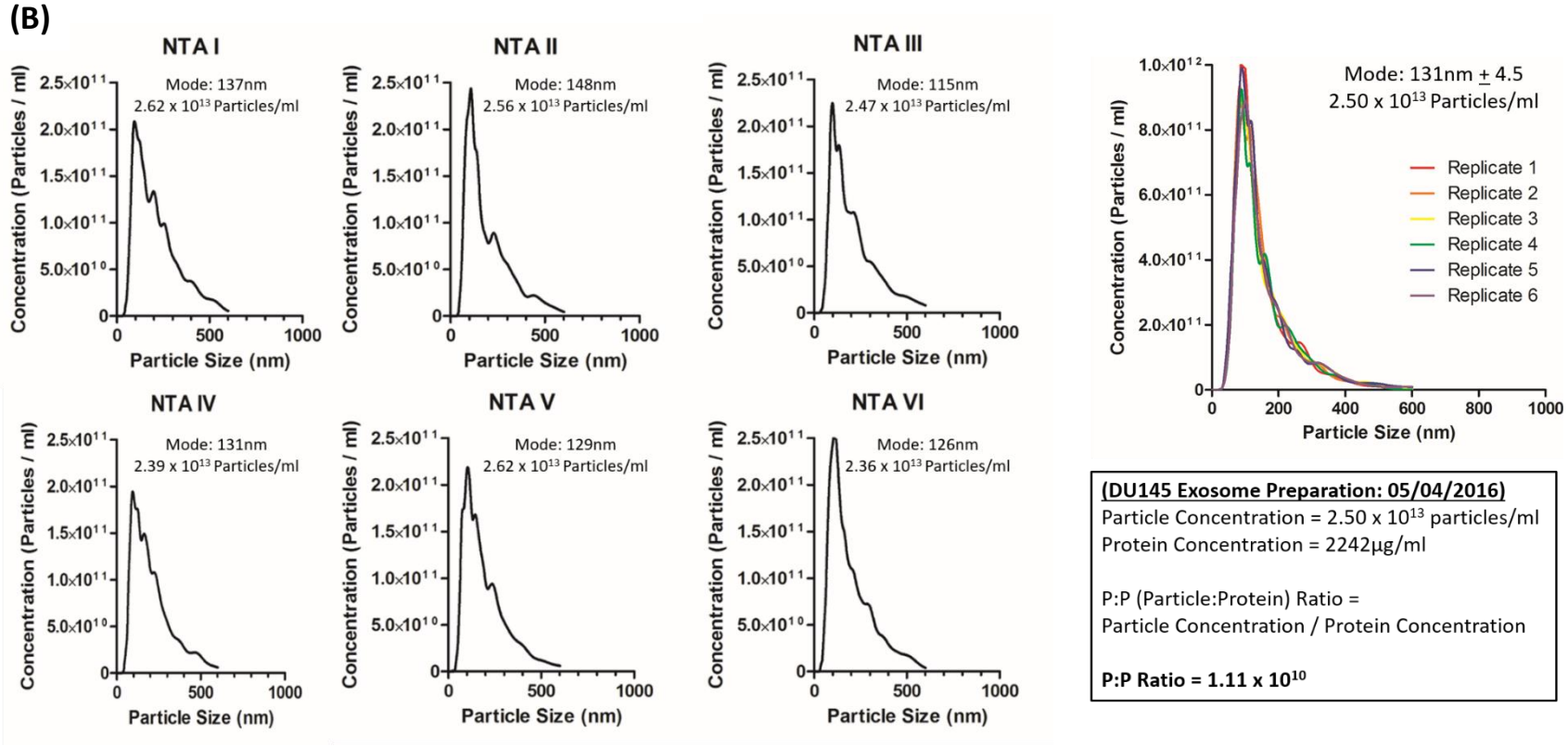

Figure 3.5: Isolated DU145 exosomes using the sucrose cushion are of high purity. (A) DU145 cell CM or **(B)** sucrose cushion purified exosomes were measured under flow conditions using Nanosight™ NTA. Data from each repeat measurement is shown, revealing the overall size distribution (histograms) and particle counts (particles/ml). 6 replicate measurements were carried out and overlaid to show the consistency across repeat measurements. BCA assay was used to quantify the protein concentration (µg/ml) of the exosomes. The purity of exosomes was assessed by the P:P ratio.

Date	Protein Concentration (µg/ml)	Particle Concentration (particles/ml)	Ratio (Particle/µg)	Quality Control
14/02/2014	3518	3.86×10^{13}	1.09×10^{10}	**PASS**
26/03/2014	4239	1.48×10^{14}	3.49×10^{10}	**PASS**
30/06/2014	6018	1.53×10^{14}	2.54×10^{10}	**PASS**
30/07/2014	7281	2.20×10^{12}	3.02×10^{8}	**FAIL**
11/09/2014	6390	1.86×10^{13}	2.91×10^{9}	**FAIL**
18/11/2014	10273	2.51×10^{14}	2.44×10^{10}	**PASS**
30/01/2015	2262	3.12×10^{13}	1.38×10^{10}	**PASS**
20/02/2015	4456	6.87×10^{13}	1.54×10^{10}	**PASS**
18/06/2015	9099	4.30×10^{14}	4.73×10^{10}	**PASS**
17/08/2015	9748	2.27×10^{13}	3.70×10^{9}	**FAIL**
21/10/2015	5164	6.11×10^{13}	1.18×10^{10}	**PASS**
04/11/2015	1760	3.73×10^{13}	2.12×10^{10}	**PASS**
03/12/2015	903	8.31×10^{12}	9.20×10^{9}	**FAIL**
06/01/2016	677	8.54×10^{12}	1.30×10^{10}	**PASS**
15/02/2016	2053	4.27×10^{13}	2.07×10^{10}	**PASS**
10/03/2016	2758	3.63×10^{13}	1.32×10^{10}	**PASS**
05/04/2016	2242	2.50×10^{13}	1.11×10^{10}	**PASS**
24/05/2016	6398	6.40×10^{13}	1.00×10^{10}	**PASS**
18/07/2016	11019	1.40×10^{14}	1.27×10^{10}	**PASS**
04/10/2016	2003	3.86×10^{13}	1.97×10^{10}	**PASS**
21/11/2016	3159	5.90×10^{13}	1.77×10^{10}	**PASS**
22/12/2016	5014	7.02×10^{13}	1.39×10^{10}	**PASS**

Table 3.1: Quality of isolated DU145 exosomes from the sucrose cushion. Protein and particle concentration of DU145 exosomes were measured using the BCA Assay and Nanosight™ nanoparticle tracking analysis respectively, to calculate the particle:protein (P:P) ratio. Isolated exosome samples with a P:P ratio of $\geq 1 \times 10^{10}$ passed the arbitrary quality threshold for a pure exosome preparation (Webber and Clayton, 2013).

3.2 Discussion

In this Chapter, we used purified DU145 exosomes as a basis to characterise vesicles for future experiments, to determine whether silencing putative regulators of exosome biogenesis and secretion will impact vesicle secretion.

Here, we showed that the prostate cancer cell line, DU145, was confirmed to have a cobble-stone like morphology (Stone et al., 1978), similarly shown in other studies with prostate cancer cells (Hayward et al., 2001, Alimirah et al., 2006). Exosomes from DU145 cells were isolated using the sucrose cushion method and revealed circular structures, demonstrating the presence of a lipid bilayer. The DU145 exosomes were a heterogeneous population, in which the size of vesicles ranged between 30 – 150nm in diameter, in agreement with NTA analysis. The NTA enabled size distribution measurements of nanoparticles in fluid phase, as opposed to dehydrated and fixed exosome samples used in traditional (non-cryo) EM. This observation may give a greater representation of exosomes, as they are in their native state. The NTA data indicated a broad nanoparticle size ranging up to 500nm for purified DU145 exosomes, despite passing through 220nm-pore filters. The purity of this method of isolating exosomes has been previously questioned as high molecular weight complexes and apoptotic blebs may co-sediment with these exosomes. Though, other studies have demonstrated the purity of these isolated exosomes contain minimal contaminating organelles (Mitchell et al., 2008, Webber and Clayton, 2013, Jeppesen et al., 2014). In contrast, we observed fewer size distribution peaks that are >300nm in size with nanoparticles in cell CM as detected by NTA. It could be possible that cell CM is less concentrated with EVs that may not co-isolate as many mixed EV populations. Both NTA and cryo-EM gave evidence that nanoparticles greater than >500nm were not present, suggesting the absence of apoptotic bodies or large organelles. Both these methods provide an indication of the heterogeneity present within samples that can characterise individual exosomes. NTA alone cannot distinguish EVs from co-isolated, non-membranous particles of similar size and should be compared with cryo-EM to acquire wide-field images of exosomes in question. Other methods to determine the presence of exosome-associated proteins must be considered to ascertain the isolated samples are in fact exosomes.

Typically, a general overview of the protein composition of each exosome preparation should be provided in a semi-quantitative manner, with exosomal-associated proteins expected to be present and components not necessarily expected. Although numerous proteomics studies have highlighted proteins commonly found in exosome preparations, it is becoming

clear that these do not represent exosome 'specific' markers, but rather exosome 'enriched' proteins (Mathivanan and Simpson, 2009, Kalra et al., 2012). Within the literature, the relative proportion of exosomal-associated proteins varies with different EVs or cell types. It has been proposed that several proteins (three or more) in a semi-quantitative manner should be reported to characterise EVs (Lotvall et al., 2014). The expression of these tetraspanins: CD9, CD63, CD81 were detected on our purified DU145 exosomes, commonly found on the surface of exosomes from various cell types (Raposo et al., 1996, Escola et al., 1998, Lamparski et al., 2002). These findings were similar to other studies with prostate and bladder cancer cells (Zoller, 2009, Welton et al., 2010). The microplate immune-phenotype assay and Western blot analysis revealed DU145 exosomes to be enriched with LAMP1 and LAMP2. The LAMP proteins are markers for lysosomes and could reflect the late endosomes containing ILVs, although the presence of LAMPs varies for most cell types. Some studies only demonstrate the presence of LAMP proteins in exosomes, as reported in tumour cells (Wolfers et al., 2001), but absent in DC-derived exosomes (Zitvogel et al., 1998). DU145 exosomes also showed an enrichment of HSP70 and HSP90. These proteins are involved in antigen presentation and participate in loading peptides to MHC molecules (Srivastava, 2002). Here, MHC-I was also present on exosomes and it is normally present in exosomes from most cell types. In general, the level of cellular contamination present within the exosome preparation was minimal, as the calnexin protein (ER marker) was absent in exosome samples. Within these DU145 exosomes, the presence of CD9, CD63, CD81, ALIX, TSG101, LAMP1, LAMP2, HSP70 and HSP90, in combination of the absence of calnexin, strongly suggests that the studied vesicles are exosomes.

One other approach to determine sample purity of exosome preparations is by determining the levels of particle to protein (P:P) ratio (Webber and Clayton, 2013). It has been shown that vesicle preparation that are considered pure exhibit a relatively high ratio of particles to protein and thus contaminating protein within samples should have a negative effect on this ratio. Typically, an arbitrary P:P ratio of $<1 \times 10^{10}$ would be considered an impure isolated vesicle sample. From the data, isolated DU145 exosomes from the sucrose cushion method as one example, demonstrated a P:P ratio of 1.11×10^{10} compared to cell CM with a ratio of 1.78×10^{8}. This suggests the exosome preparation from the sucrose cushion would be deemed purer. In contrast, analysing cell CM indicates an impure exosome preparation, possibly indicating a greater level of soluble proteins present. Applying the ratio method provides a relatively simple and quantitative manner to estimate and compare purity. Though, there are some caveats using the P:P ratio as a sole method to analyse exosomes.

There it is difficulty in discriminating vesicles from non-vesicular particular material, there is an assumption that all detected particles are vesicles and there could be an overestimation of particles present within the sample. Furthermore, there is an assumption that each vesicle has a comparable and stable quantity of protein; though different disease states may alter the protein content to some degree, but this remains poorly understood. Nevertheless, bearing issues in mind, the P:P ratio method does provide an additional method to determine the purity of the vesicle preparation for future experiments.

Other methods to isolate exosomes have claimed to isolate pure exosomes from cell CM, such the commercially available ExoQuick® (EQ) or Total Exosome Isolation Reagent (TEI). Though, the main caveat is that these reagents co-precipitates exosomes with non-vesicular proteins, leading to a low yield of impure exosomes (Van Deun et al., 2014). It has been shown that isolating vesicles based only on ultracentrifugation can retain a relatively moderate pure sample of vesicles, compared to density-based methods. One of the main advantages of ultracentrifugation method is it shows a greater protein yield, compared to other methods and remains enriched in exosomal-associated proteins. The ease of obtaining high overall yields of vesicles will be important for future experiments, as it will be utilised to not only be characterised by various methods, but also to perform functional experiments.

In this Chapter, we have demonstrated different methods used to determine the phenotype of exosomes and the amount or concentration of exosomes present. All these methods act to analyse exosomes. By doing so, these methods act as a platform to evaluate whether exosomes are modulated by silencing putative regulators of exosome biogenesis and secretion in future Chapters.

CHAPTER 4:

GENERATING EXOSOME-DEFICIENT CANCER CELLS

4.1 Generating Exosome-Deficient Cancer Cells

4.1.1 Introduction

Exosomes were first defined as EVs of heterogeneous sizes including one population with diameters between 500 and 1000nm (Trams et al., 1981); although this definition changes with exosomes originating from the endocytic pathway during early endosome maturation, to form MVEs (Harding et al., 1983, Pan et al., 1985). The formation of ILVs, within MVEs, involves inwardly budding vesicles with the incorporation of selected cargo. Once ILV formation is completed, fusion of MVEs with the plasma membrane secretes ILVs into the extracellular space; thus exosome secretion (Stoorvogel et al., 2002). However, MVEs that do not fuse with the plasma membrane can often be redirected to lysosomes for degradation (Futter et al., 1996). Currently, a great amount of effort has been made towards identifying the molecular machinery responsible for this process.

One of the first mechanisms described for MVE formation was the ESCRT complex (Babst et al., 2002a). It contains four protein complexes (ESCRT-0, -I, -II and -III) and interacting accessory proteins, transiently engaged to the endosome's limiting membrane. It is proposed that ESCRT-0, -I and -II are involved in clustering cargo in ILVs; and ESCRT-III in vesicle budding and scission (Wollert et al., 2009). The ESCRT-II complex contains two core VPS25 protein subunits, interacting heavily with both ESCRT-I and -III protein complexes (Wernimont and Weissenhorn, 2004). VPS25, as part of the ESCRT-II complex, appears to play a role in MVE formation (Katzmann et al., 2002); and localisation of ESCRT-III to late endosomes (Babst et al., 2002a). The formation of late endosome, ESCRT components (ALIX and TSG101), as well as ubiquitinated proteins, have been proposed to load cargo into ILVs. As examples, ALIX and TSG101 mediate epidermal growth factor (EGFR) and transferrin receptor loading into exosomes, respectively (Lu et al., 2003, Géminard et al., 2004); and are exosome-associated protein markers. Furthermore, the presence of cytosolic proteins into the ILVs can be due to co-sorting with other proteins. This mechanism is suggested for chaperones, such as HSP-70 and HSP-90, found on exosome surfaces in some cell types (Théry et al., 1999, Gastpar et al., 2005).

In contrast, depletion of certain ESCRT subunits does not completely impair MVE formation, indicating other mechanisms independent of ESCRT may operate in ILV formation (Stuffers et al., 2009). It was demonstrated that inhibition of neutral sphingomyelinase, decreased the levels of PLP-associated exosome secretion (Trajkovic et al., 2008), independent of ESCRT function. Exosomes are often enriched with tetraspanins, such as CD9, CD63 and CD81,

dependent on cell type; although a recent report suggests that only CD81 is exosome-specific (Kowal et al., 2016). More recently, the tetraspanin, CD63, known to be expressed on the exosome surface, directly participates in ESCRT-independent sorting of the PMEL, as PMEL localises to CD63-containing ILVs, even in ESCRT-I depleted cells (van Niel et al., 2011). In the absence of functional CD63, ILV formation, PMEL sequestration and downstream melanosome biogenesis are severely reduced. Similarly, silencing another member of the tetraspanin family, CD9, results in a significant decrease in secreted exosomes from DCs (Chairoungdua et al., 2010) and Nalm-6 pre-B cells (Mazurov et al., 2013). Although CD9 is a commonly expressed tetraspanin on DU145 exosomes (Hosseini-Beheshti et al., 2012, Webber et al., 2014), the role they play on MVE biogenesis and exosome secretion is poorly understood. CD9 may function, in a similar manner to CD63 with melanosome secretion (van Niel et al., 2011). This suggests that distinct ESCRT-independent mechanisms might coexist with the ESCRT machinery on MVEs in different cells, reflecting multiple MVE subpopulations fated for degradation or exosome secretion (Buschow et al., 2009, Ostrowski et al., 2010, Hurley and Odorizzi, 2012).

Rab proteins are small GTPases and essential regulators of transporting different endosomes between different endosomal compartments. Rabs can be involved endosomal budding, motility or tethering to the membrane of an acceptor compartment. The Rab family is composed of greater than 70 GTPases, each of which is potentially associated with one intracellular compartment, depending on cell type. Rab5 is proposed to be involved in early endosome formation and maturation of these compartments into late endosomes (Gorvel et al., 1991, Chen et al., 2009). It was first reported that silencing Rab11 in K562 cells attenuated exosome secretion (Savina et al., 2002); and their follow-up study showed Rab11 to promote docking and fusion of MVE with the plasma membrane (Savina et al., 2005). These studies created an interest in Rab protein roles in exosome secretion. Rab27 was initially explored in HeLa cells, found to function in MVE docking at the plasma membrane (Ostrowski et al., 2010) and silencing Rab27a inhibited exosome secretion, as shown in various studies (Peinado et al., 2012, Bobrie et al., 2012, Ostenfeld et al., 2014, Webber et al., 2015). Similarly, silencing Rab35 demonstrated an accumulation of intracellular endosomes within the cell, whilst attenuating exosome secretion (Hsu et al., 2010). These proteins, Rab11, Rab27a and Rab35 are proposed to stimulate tethering and fusion of recycling or late endosomes to the plasma membrane, though it remains poorly understood whether Rab11 or Rab35 have the same role in trafficking MVEs with the plasma membrane in one given cell type.

In addition to Rab proteins, SNARE proteins localise to exosomes with CD63 and lipid rafts (Salaun et al., 2005, Perez-Hernandez et al., 2013). SNARE proteins are proposed to mediate membrane fusion, including transport between organelles (Jahn and Scheller, 2006). As a v-SNARE protein, VAMP7 is suggested to assist in MVE docking and fusion with the plasma membrane; and subsequent release of exosomes into the extracellular space (Fader et al., 2009). Some of these components are involved in MVE fusion with the plasma membrane during exosome release, although the specific SNARE complex has yet to be discovered.

Here, we will transduce DU145 cells with lentiviral particles with a specific shRNA sequence targeting: CD9, Rab5a, Rab11b, Rab35, VAMP7 and VPS25. Confirmation of knockdown will be assessed at the mRNA and protein level; and possible cytopathic consequence of the knockdowns. Multiple approaches will be utilised to assess the outcome of knockdown on secreted vesicles; and be any distribution changes in endo/lysosomal compartments. Currently, there appears to few distinct mechanisms for exosome biogenesis, trafficking and release. It remains poorly understood whether different mechanisms may explain the heterogeneity of exosomes produced in each cell. However, one question that remains is whether it is possible to manipulate cells and force them to produce an altered repertoire of vesicle subpopulations, whilst understanding if there is a hierarchy of which mechanism is most relevant? As shown in Figure 4.1, the hypothesis is that blockade of one pathway (pathway A for example) may lead to a loss of a specific subpopulation. This may still enable the secretion of other vesicle subpopulations, pathway B and C as examples, that may impart a different cancer cell function.

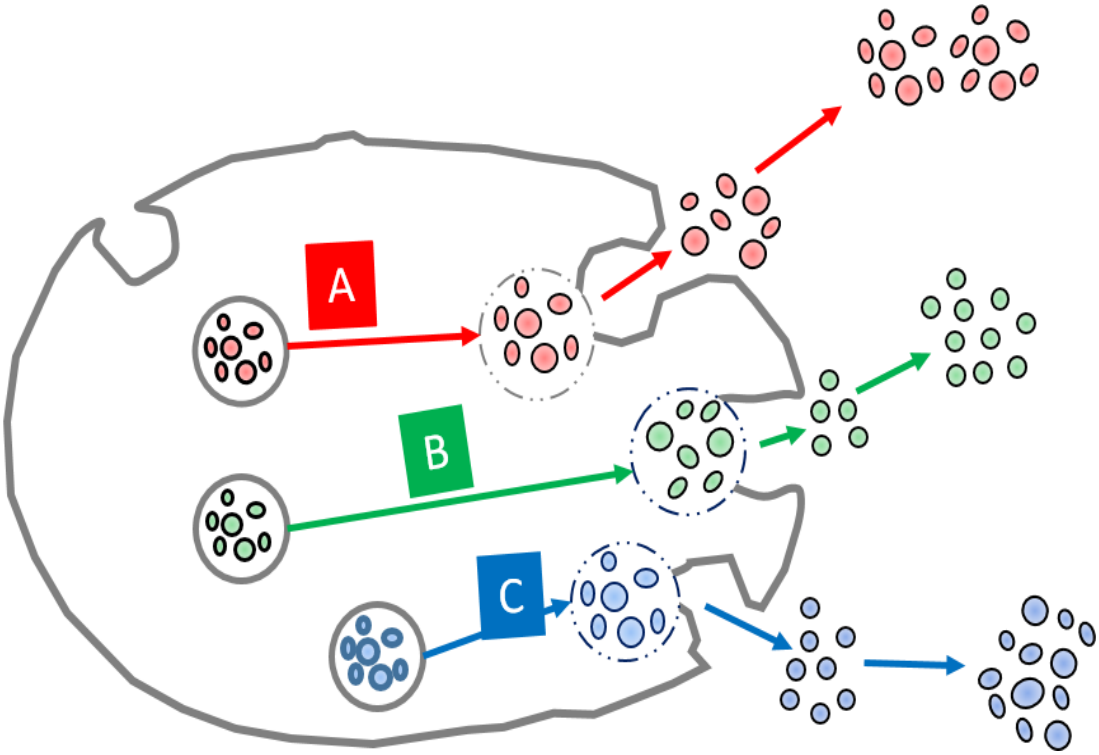

Figure 4.1: Simplified diagram of MVE and vesicle heterogeneity. The cell has distinct pathways that generate complex heterogeneity in secretion of exosomes. Blockade of one pathway, for example pathway A, may result in a loss of subpopulation and impact the cancer cells function.

4.1.2 Puromycin Kill Curve for DU145 Cells

For my initial studies, MISSION® shRNA lentiviral particles (Sigma-Aldrich) were used to transduce DU145 cells with a shRNA sequence against each respective target. Each lentiviral plasmid vector contains a puromycin resistance gene for mammalian selection. Therefore, puromycin was used in gene selection for mammalian host cells. First, a puromycin kill curve was performed to determine the minimum puromycin concentration required to kill all non-resistant cells. Here, the WST-1 assay (measuring cell metabolic activity) was used to determine the minimum puromycin concentration required for efficiently selecting transduced cells. Incremental doses of puromycin (0 – 10µg/ml) were used to treat DU145 cells (Figure 4.2). Absorbance was measured, based by the cleavage of the stable tetrazolium salt, WST-1, into a soluble formazan by cellular mitochondrial dehydrogenases present in viable cells. The quantity of released formazan dye correlates to the number of metabolically active cells in culture. Here, 1.25µg/ml was the minimal puromycin dose observed, that was sufficient to kill all DU145 cells.

4.1.3 Confirmation of Knockdown at the mRNA and Protein Level

Here, we used lentiviral particles with a specific shRNA sequence to silence targets putatively involved in exosome biogenesis and secretion to transduce DU145 cells. A multiplicity of infection (MOI) of 20 was used. MOI is defined as the number of transducing lentiviral particles per cell. DU145 cell were transduced with lentiviral particles containing shRNA, treated with puromycin for six passages before assessing levels of target mRNA and protein. We tested five different shRNA sequences for each target (Figure 4.3) that included: CD9, Rab5a, Rab11b, Rab35, VAMP7 and VPS25. Lentiviral particles delivering a shRNA sequence targeting a non-mammalian RNA was used as a control. Confirmation of each knockdown was carried using gene expression assays to show relative quantification (RQ) of the target mRNA to the control. For this, GAPDH mRNA was used as an internal control.

The five shRNA sequences targeting CD9 showed variable mRNA knockdown, ranging from 45% - 87% (Figure 4.3 A). Targeting Rab5a showed mRNA knockdown ranging from 85% - 97% (Figure 4.3 B). Targeting Rab11b showed mRNA knockdown ranging from 71% - 95% (Figure 4.3 C). Targeting Rab35 showed mRNA knockdown ranging from 78% - 95% (Figure 4.3 D). Targeting VAMP7 showed mRNA knockdown ranging from 87% - 92% (Figure 4.3 E). Lastly, targeting VPS25 showed mRNA knockdown ranging from 78% - 93% (Figure 4.3 F). These results indicated that we had successful knockdown of each target at the mRNA level. However, confirming knockdown at the mRNA level may not necessarily correlate to changes at the protein level.

Next, the protein level was investigated by Western blotting. First, analysis of whole cell lysates derived from each cell line demonstrated attenuated expression of target proteins. With the CD9 target, the clone #953 showed the greatest mRNA knockdown of 87% (Figure 4.3 A), but did not show the greatest attenuation at the protein level (Figure 4.4 A). The clone #470 showed the greatest attenuation for CD9 at the protein level (Figure 4.4 A), despite only having a mRNA knockdown of 70%. All clones for the Rab5a target showed no detectable protein levels (Figure 4.4 B). The clone #466 was selected based on the mRNA knockdown at 97%. With the Rab11b target, the clone #919 showed the greatest attenuation at the protein level (Figure 4.4 C), with a mRNA knockdown of 95%. Knockdown of Rab35 was less obvious when detecting levels of Rab35 protein (Figure 4.4 D). Although mRNA knockdown ranged from 78% - 95% for Rab35; the Rab35 clone #335 was selected based on 95% knockdown at the mRNA level. All clones for the VAMP7 target showed no detectable protein levels (Figure 4.4 E). Therefore, clone #928 was selected based on the mRNA knockdown at 92%. For the VPS25 target, clone #757 showed the greatest attenuation at the protein level (Figure 4.4 F), with a mRNA knockdown of 93%. In Figures 4.3 and 4.4, the selected clones (denoted by a ↓), CD9 (#470), Rab5a (#466), Rab11b (#919), Rab35 (#335), VAMP7 (#928) and VPS25 (#757) were chosen for future experiments, based on a combination of both the mRNA and protein data.

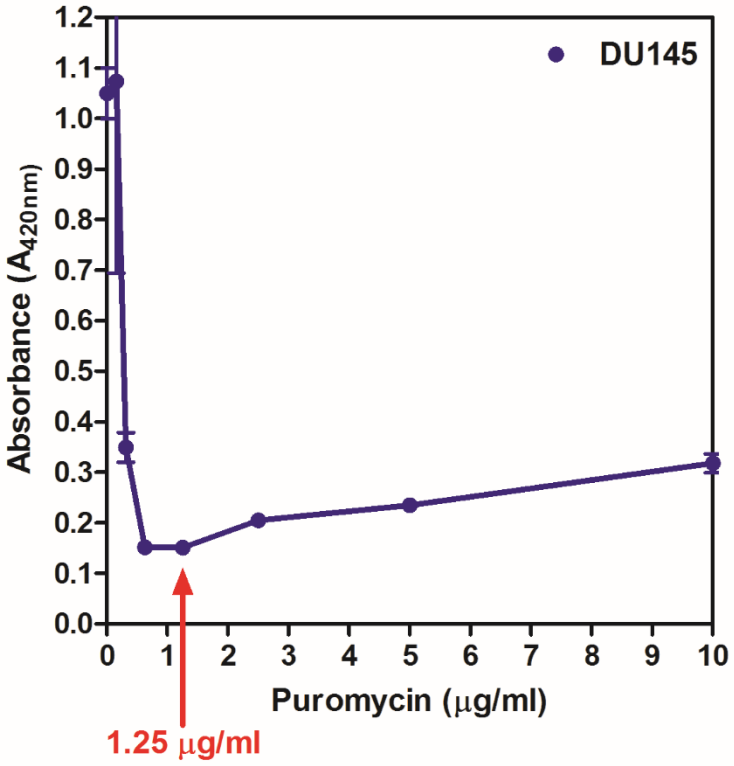

Figure 4.2: Puromycin kill curve for DU145 cells. DU145 cells were seeded at a density of 5,000 cells per well in a 96-well plate. Wells were subjected to a range of puromycin concentrations (0 -10μg/ml) and incubated for 2 hours. After this incubation period, cell viability was measured using the WST-1 assay. Wells were incubated with WST-1 for 1 hour, to quantify the release of formazan by measuring absorbance at 420nm by the PHERAstar FS Microplate Reader. Graph shows mean ± SEM, based on 5 wells.

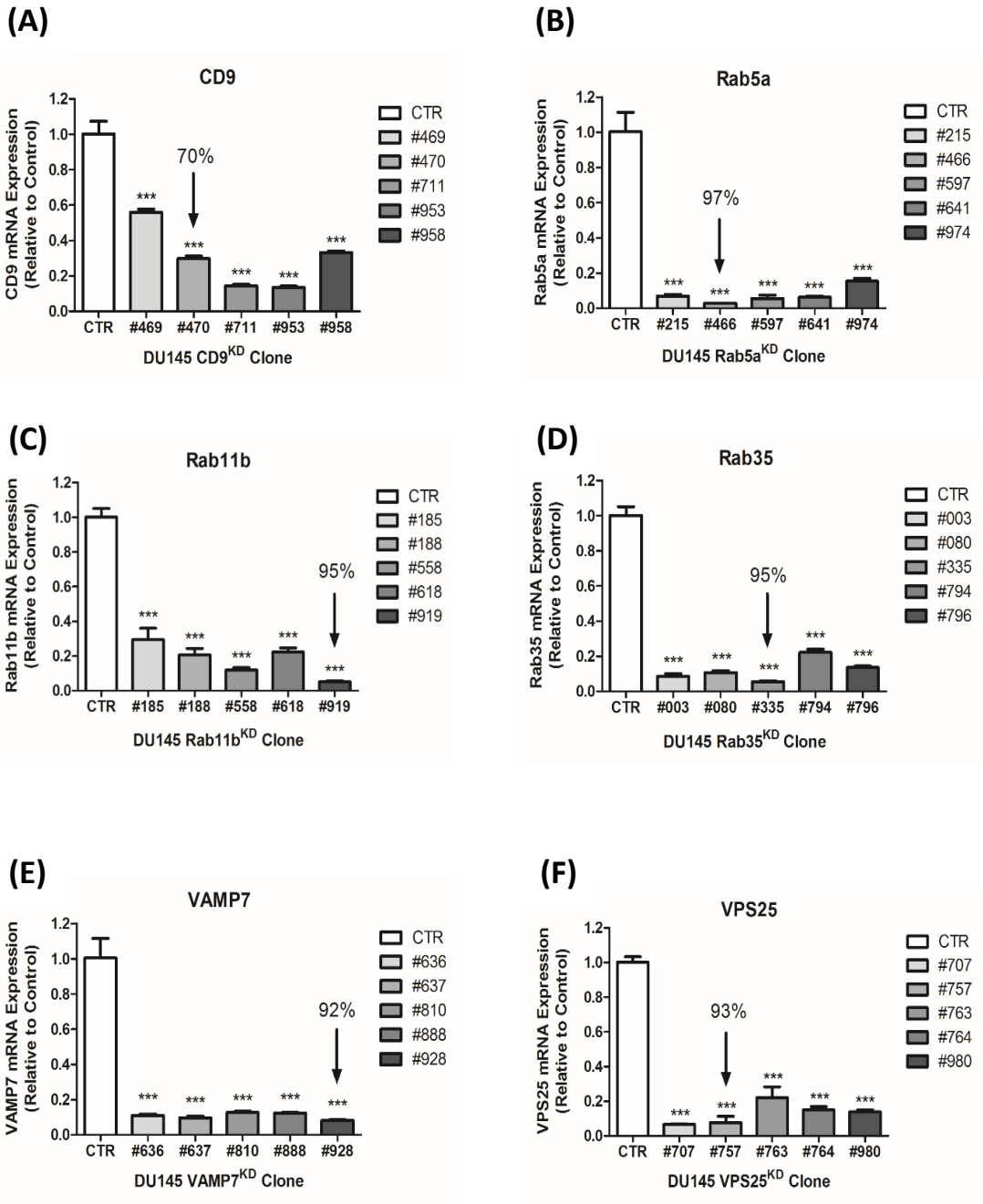

Figure 4.3: Confirmation of knockdown of target mRNA by qPCR. DU145 cells were stably transduced with MISSION® shRNA lentiviral transduction particles expressing a non-mammalian control (CTR) or shRNA against the indicated target: **(A)** CD9, **(B)** Rab5a, **(C)** Rab11b, **(D)** Rab35, **(E)** VAMP7 and **(F)** VPS25. Relative expression of target mRNA was evaluated using qPCR, with GAPDH as the internal control. Arrows indicate selected clones demonstrating greatest knockdown at the mRNA level and subsequent protein level taken forward for experiments. Graph shows mean ± SEM, based on triplicate wells. ***P<0.001. One-way ANOVA with Tukey's post hoc test.

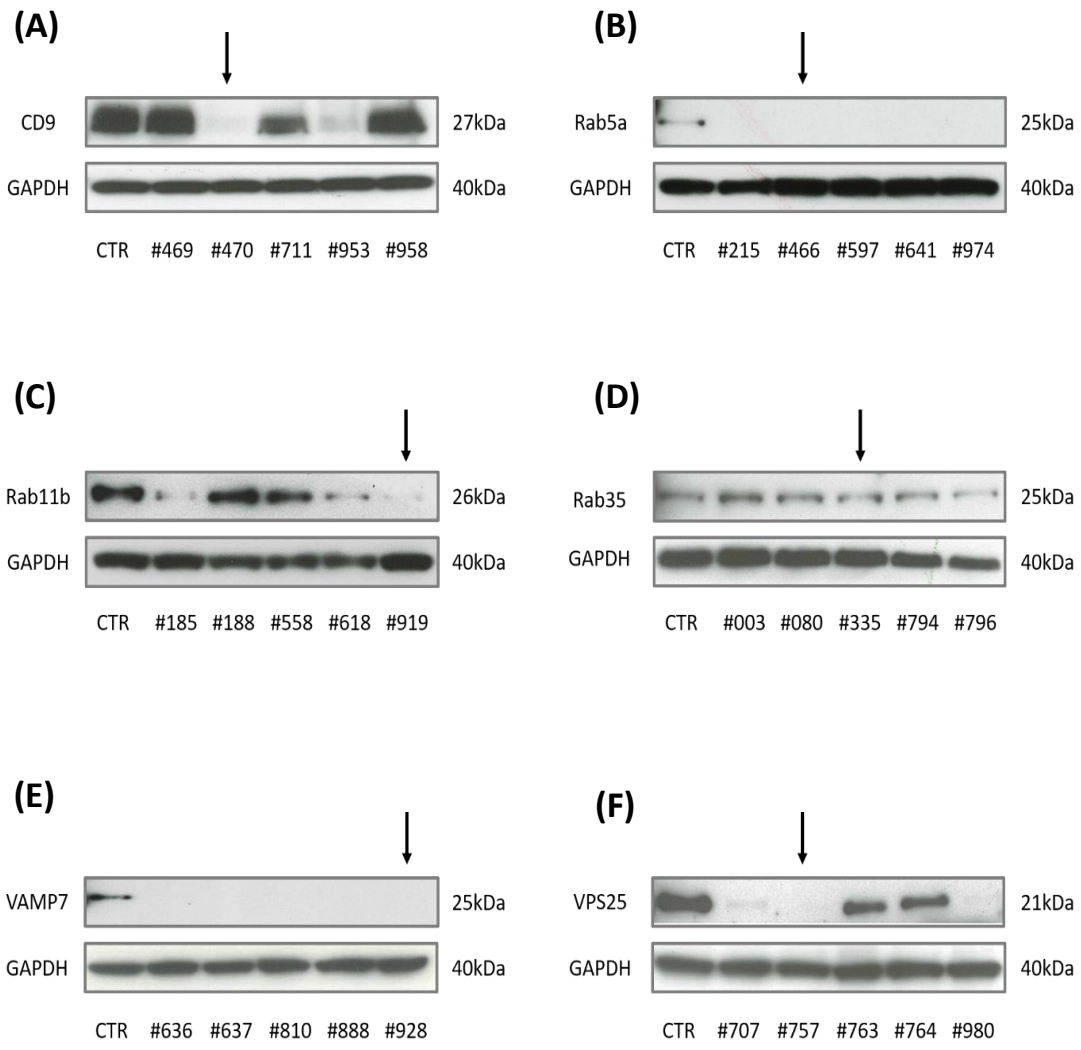

Figure 4.4: Confirmation of knockdown by Western blot. Cell lysates (20µg) from each cell lines was probed for their respective target protein: **(A)** CD9, **(B)** Rab5a, **(C)** Rab11b, **(D)** Rab35, **(E)** VAMP7 and **(F)** VPS25. GAPDH was used as a protein loading control. Arrows indicate the selected clones which showed greatest knockdown at both the mRNA and protein level.

4.1.4 The Impact of Knockdowns on Cell Viability

We next explored some of the general properties of cells, to understand if the knockdowns have any cytopathic impact. A monolayer of lentiviral transduced DU145 cells were seeded and examined by phase contrast microscopy (Figure 4.5). All the cells display a flat polygonal morphology typically shown in DU145 control cells, forming discrete islands when sub-confluent (shown) and a cobblestone-monolayer pattern, when confluent. This was indeed the case regardless of attenuated target proteins. The knockdowns, therefore, did not impart gross effects on cell shape or the capacity to attach or form monolayers.

Next, we examined the proliferation properties of these lentiviral transduced cells, using the cell proliferation reagent, WST-1. DU145 cells were seeded equally and incubated with the WST-1 reagent for 0.5 – 4 hours. This determined the optimal incubation time required to detect formazan levels above the background and below the maximum thresholds (Figure 4.6 A). Here, we observed that doubling of DU145 cell numbers, indicated by the absorbance values showed a sigmoidal curve with a signal plateau at 50,000 cells/well or greater; although there was a dose-dependent relationship within a range of 6,000 – 50,000 cells. Here, there is no advantages in signal strength when incubating for different times. Therefore, a time of 1 hour was chosen to incubate cells to ensure the signal is present or does not plateau.

Next, we seeded 5,000 lentiviral transduced DU145 cells into 96-well plates and monitored cell proliferation over 72 hours. WST-1 was incubated for 1 hour at each timepoint to measure formazan absorbance. Here, knockdown of CD9 and Rab5a in DU145 cells appeared to show weak inhibition of cell proliferation (Figure 4.6 B and C) over 72 hours, compared to controls. Knockdown of Rab11b and Rab35 (Figure 4.6 D and E) in DU145 cells appears to be negligible on cell proliferation over 72 hours compared to the control. In contrast, knockdown of VAMP7 in DU145 cells appeared to show a modest increase in cell proliferation (Figure 4.6 F). On the other hand, there was a significant decrease in cell proliferation with the knockdown of VPS25 (Figure 4.6 G), compared to controls. The majority of knockdowns showed a minimal impact upon cell viability, except for VPS25. Therefore, any observed changes with vesicle secretion with the VPS25 knockdown will be difficult to assess, as the impact on vesicle secretion may be accounted for by toxic, rather than specific effects on vesicle biogenesis/traffic function.

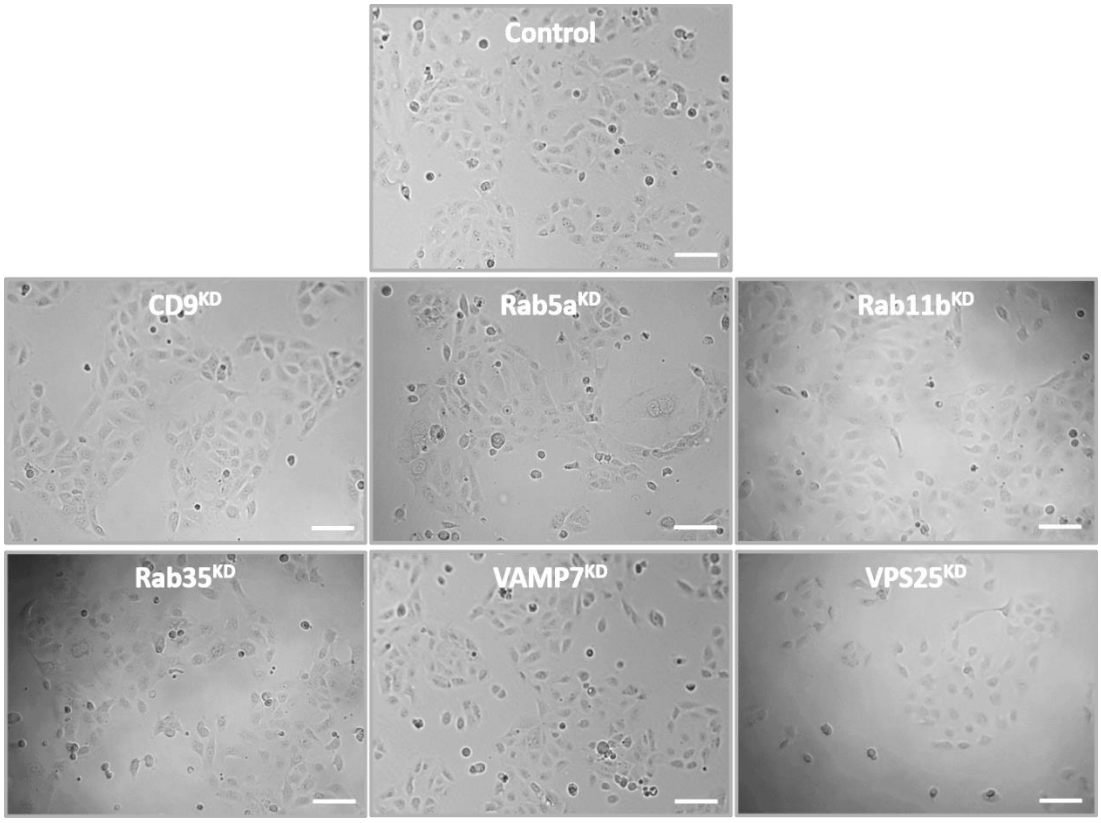

Figure 4.5: Transduced DU145 cells maintain cobblestone-like morphology. Monolayer of live transduced DU145 cell lines were imaged using phase-contrast microscopy, to visualise the cobblestone-like morphology within the epithelial cells. Scale bar: 100µm. Representative fields are shown.

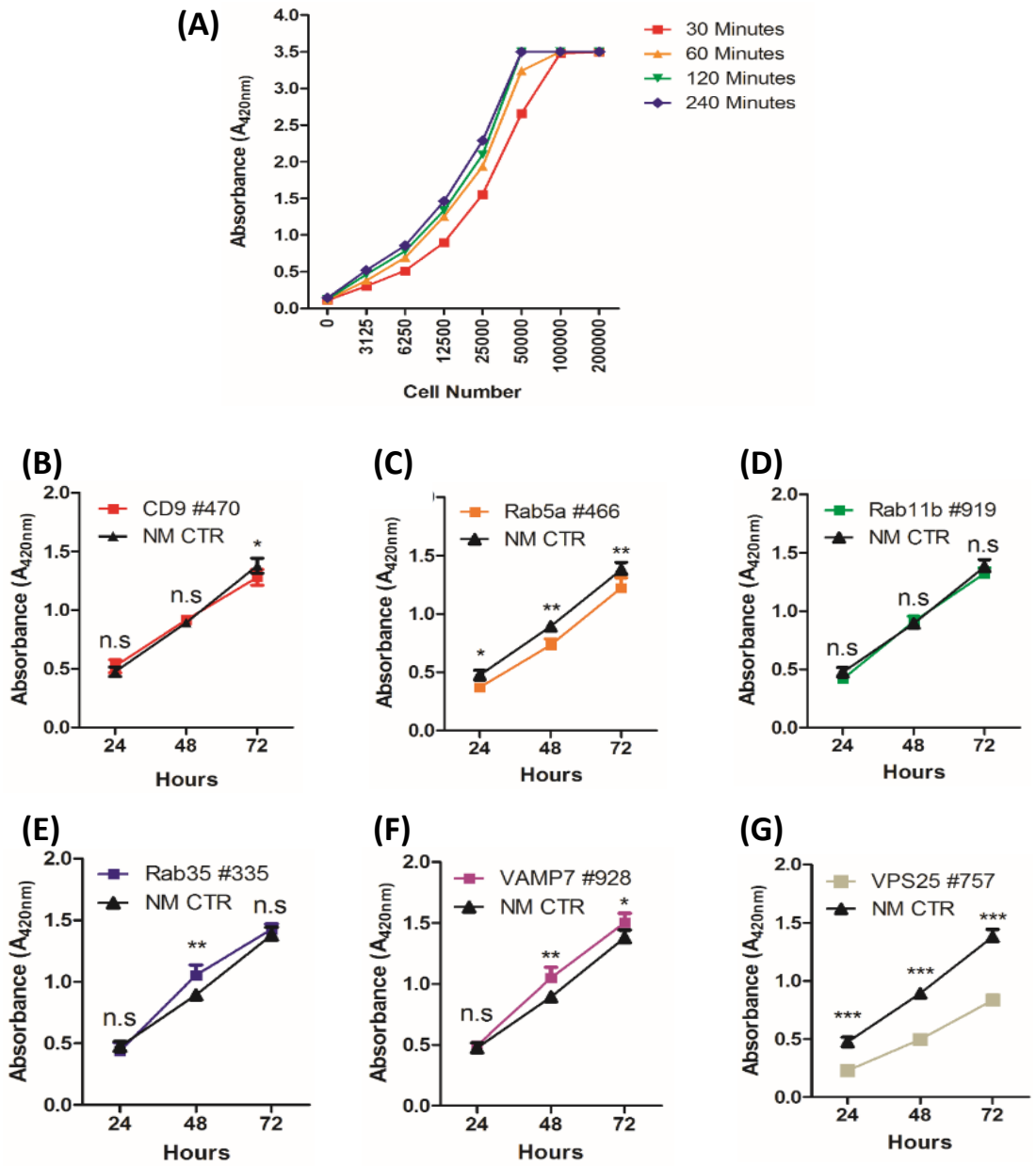

Figure 4.6: Confirmation of lentiviral transduced DU145 cell viability. (A) Lentiviral transduced DU145 cell lines were seeded at various cell densities (0 – 200,000 cells per well) in a 96-well plate; and subjected to different incubation times (30 - 240 minutes) with WST-1 reagent. After incubation, absorbance was measured at 420nm, quantifying formazan release, using the PHERAstar FS Microplate Reader. 5,000 cells were seeded into 96-well plates for each lentiviral transduced DU145 cell lines: **(B)** CD9, **(C)** Rab5a, **(D)** Rab11b, **(E)** Rab35, **(F)** VAMP7 and **(G)** VPS25. Cells were subjected to the WST-1 reagent at 24, 48 and 72 hours. Graph shows mean ± SEM, based on quadruplicate wells. n.s: non-significant, *P<0.05, **P<0.01 and ***P≤0.001. Two-way ANOVA with Bonferroni post hoc test.

4.1.5 Confirmation of Knockdown Cell Stability

Previously, we demonstrated that puromycin selection eliminated non-transduced DU145 cells and knockdown of CD9, Rab5a, Rab11b, Rab35, VAMP7 and VPS25 was validated at both the mRNA and protein levels. Selected sequences with successful knockdown demonstrated a mRNA reduction between 70% - 97%. However, if shRNA-mediated depletion of the target caused a growth disadvantage over time, the cells bearing knockdowns might be overgrown with cells not exhibiting the knockdown from this heterogeneous cell population. This may limit the experimental timeframe available to us, if loss of the knockdown phenotype over time is apparent. To test the stability of each knockdown within the populations of transduced DU145 cells, we compared target mRNA expression between two time-points. Newly transduced DU145 cell lines, free from lentiviral particles at week 6, were compared to cells maintained in continuous culture for 15 weeks, longer than any other experiments conducted in this study.

The CD9 mRNA transcript expression levels were decreased by 86% in DU145 $CD9^{KD}$ cell populations at 15 weeks after transduction (Figure 4.7 A), compared to a 70% decrease at week 6. Transduction of other targets showed decreased expression of target mRNA that still maintained very good knockdown stability, as in all cases, the target mRNA remains >78% decreased below controls, although this shows a slight increase in target mRNA expression levels than at the initial 6-week time-point, for Rab5a, Rab11b, VAMP7 and VPS25 (Figure 4.7 B – C and E – F). For Rab35, however, the cloning levels was faster for wild type, showing expression levels at 5% at week 6 and 45% at week 15; but remained significantly down (Figure 4.7 D). In all cases, besides CD9, the mRNA knockdown decayed over time, indicating cells can maintain their stability over a given time, although all experiments were performed prior to week 15.

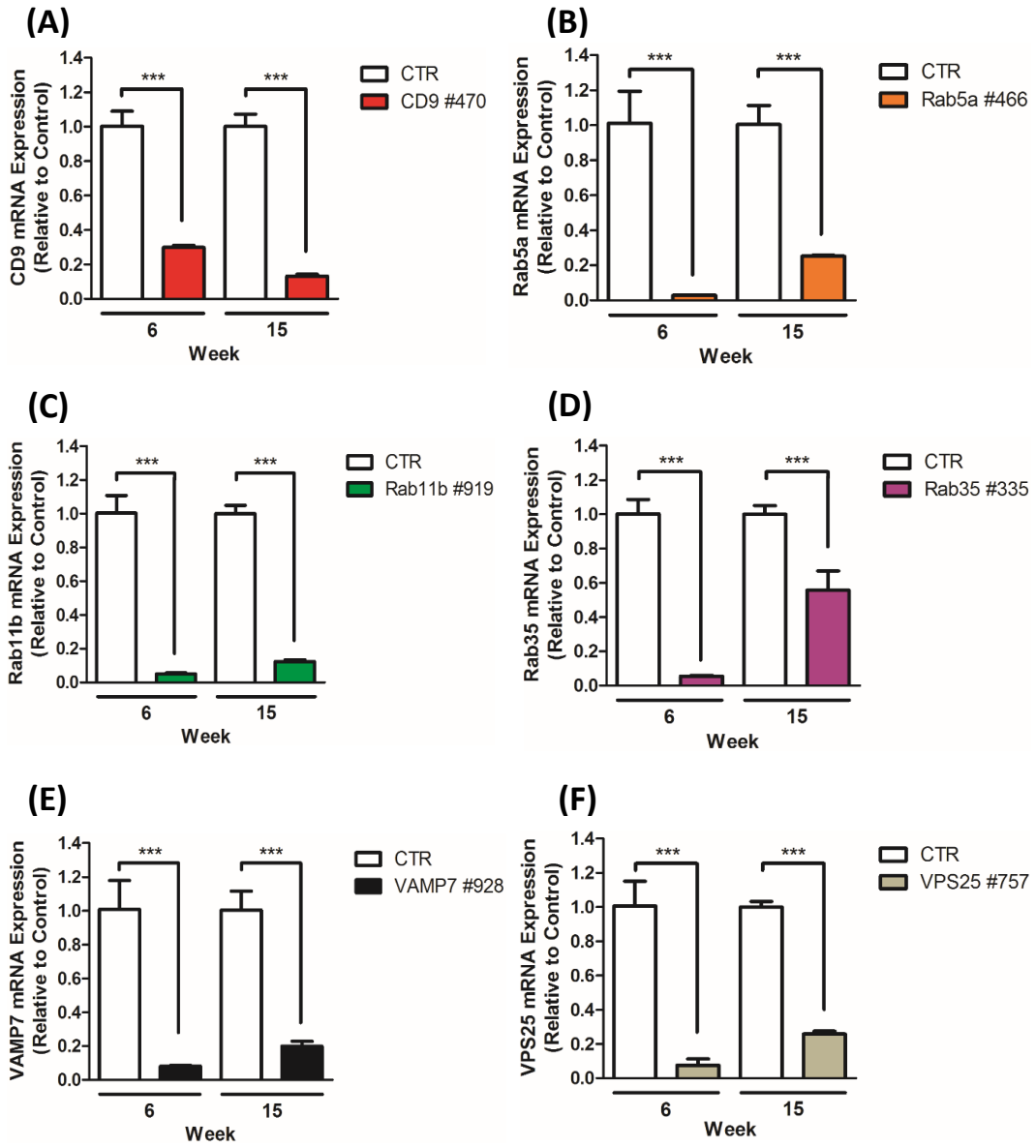

Figure 4.7: Confirmation of shRNA silencing stability in lentiviral transduced DU145 cells. mRNA was extracted from lentiviral transduced DU145 cell lines at week 6 or 15, to confirm the stability of each target at the mRNA level. Relative expression of target mRNA; **(A)** CD9, **(B)** Rab5a, **(C)** Rab11b, **(D)** Rab35, **(E)** VAMP7 and **(F)** VPS25 were evaluated using qPCR, with GAPDH as the internal control. Graph shows mean ± SEM, based on triplicate wells. ***P<0.001. One-way ANOVA with Tukey's post hoc test.

4.1.6 Characterisation of Vesicles Derived from Lentiviral Transduced DU145 Cells

We investigated whether silencing CD9, Rab5a, Rab11b, Rab35, VAMP7 or VPS25 attenuated exosome secretion. We characterised the number and size of nano-particulate material present in cell CM using the Nanosight™ NTA platform for each lentiviral-transduced DU145 cells. First, cell CM was collected from DU145 CD9^{KD}, Rab5a^{KD}, Rab11b^{KD}, Rab35^{KD}, VAMP7^{KD} and VPS25^{KD} cells, cultured at identical densities. Cellular debris was removed by serial centrifugation (400 x *g* for 7 minutes, 2000 x *g* spins for 15 minutes); and the removal of large non-exosomal particles by filtration (0.22µm filter). The resultant cell CM was analysed by NTA. Otherwise, cell CM underwent ultracentrifugation (200,000 x *g* for 2 hours), to obtain vesicle concentrates that were characterised for exosomal-associated proteins.

Traditionally, estimates of the relative expression of proteins of interest are often made by comparison against the signal observed by internal standards (housekeeping proteins). Conventionally, such proteins are considered to be ubiquitously and constitutively expressed in every tissue, presumed necessary for normal cellular function. Classical examples include GAPDH or β-actin. This allows normalisation of signals so that expression of genes/proteins between samples can be compared, eliminating variations arising from technical reasons, such as sample loading or transfer. However, there is currently no ubiquitously and constitutively expressed housekeeping protein on exosomes, derived from various cell types. Here, by investigating multiple targets putatively implicated in exosome biogenesis and secretion, comparisons made between secreted exosomes from lentiviral transduced DU145 cells were difficult. Normalisation of the secreted exosomes based on protein concentration would not give a true representation of the knockdown effect, as this may incorporate other exosome subpopulations. Thus, the cell CM or vesicle concentrate pellet were corrected for cell number. By normalising for cell number, we can analyse the exosome quantity arising from each lentiviral transduced DU145 cells, that will give a fair comparison between the exosome subpopulations.

First, we performed size distribution measurements of vesicles by NTA in the DU145 control, CD9^{KD}, Rab5a^{KD}, Rab11b^{KD}, Rab35^{KD}, VAMP7^{KD} and VPS25^{KD} cell CM, corrected for cell number (particle/cells). We observed that nanoparticle size distribution profiles were similar irrespective of knockdown; and revealed a population of particles ranging between 50 – 200nm in diameter, while not exceeding 300nm (Figure 4.8 A). The histogram mode of the control cells was around 110nm and this was comparable with other knockdowns, with a tendency for larger nanoparticles in the VAMP7^{KD} (125nm) and VPS25^{KD} (135nm) (Figure 4.8 B). When examining the quantity of particles per cell, some significant differences were

present. We observed no significant differences in the CD9^{KD}, but surprisingly an elevation (24%) in particles/cell (P<0.01) was evident in the Rab5a^{KD}. In contrast, there was a modest attenuation in particles/cell with respect to the Rab11b^{KD} (24%) (P<0.01), Rab35^{KD} (23%) (P<0.05), VAMP7^{KD} (32%) (P<0.001) and VPS25^{KD} (20%) (P<0.01), respectively (Figure 4.8 C). The selected knockdowns, therefore, appeared to have an impact on the cell-derived, nanoparticles produced, except for the CD9^{KD}.

Solely relying on NTA to characterise vesicles based on size distribution profiles is not sufficient, as it does not discriminate vesicles from other nanoparticles or any other non-vesicular aggregates of protein/cell debris. Therefore, other related assays (Western blot or plate-based assays) are used to confirm the vesicle levels in the total secretome. To confirm vesicle loss from DU145 control, CD9^{KD}, Rab5a^{KD}, Rab11b^{KD}, Rab35^{KD}, VAMP7^{KD} and VPS25^{KD} cells, we used ultracentrifugation to concentrate vesicles in bulk. For the following experiments, cell counts were used as a basis for correcting differences in cell numbers at the CM harvesting time. Pelleted vesicle concentrates were obtained from cell CM, as previously described. Western blot was performed to observe the presence of any exosomal-associated proteins in the vesicles derived from knockdowns. Membranes were probed for ESCRT-related proteins; ALIX and TSG101; lysosomal associated membrane proteins, LAMP1 and LAMP2; heat shock proteins HSP70 and HSP90; and GAPDH. Data for the CD9^{KD} in terms of Western blot, matched the NTA dataset to some degree, where we observed little change in the levels of ALIX, GAPDH, HSP90 and TSG101, despite a modest reduction in intensity for HSP70, LAMP1 and LAMP2 (Figure 4.9). Following Rab5a^{KD}, the Western blots pointed to a general increase in intensity for ALIX, GAPDH, HSP90, LAMP1 and LAMP2, despite little change in HSP70 or TSG101, consistent with NTA data showing an increase in particles/cell. In contrast, the Western blots revealed a general reduction in levels of ALIX, HSP70, HSP90, GAPDH, LAMP1, LAMP2 and TSG101 for the Rab11b^{KD}, Rab35^{KD} or VPS25^{KD}. This agreed with the NTA data and would be consistent with a partial attenuation in exosome secretion. Similarly, VAMP7^{KD} followed this trend, despite showing little change in ALIX and TSG101 protein. Despite these trends, it remains difficult to assess changes in protein target levels, as it depends on the knockdown target.

Next, we characterised these vesicle concentrates from the DU145 control, CD9^{KD}, Rab5a^{KD}, Rab11b^{KD}, Rab35^{KD}, VAMP7^{KD} and VPS25^{KD} cell CM (described previously), using a plate-based assay to examine surface expressing tetraspanins (CD9 and CD81). Vesicle concentrates were corrected to cell number, as previously described. We examined the relative level of tetraspanin positive vesicles, compared to controls. Vesicles derived from the CD9^{KD},

demonstrated a significant reduction in CD9 signal (P<0.001); as expected (Figure 4.10). Similarly, there was an attenuation (<50%) in CD9 signal with the Rab11b^{KD}, Rab35^{KD} and VAMP7^{KD} (P<0.01); and likewise, with the VPS25^{KD} (P<0.001), compared to controls. Consistently, there was an increase (80%) in CD9 signal for the Rab5a^{KD} (P<0.001), similar to the Western blot and NTA data. Despite showing no significant differences in CD81 signal, we observed the same trends with each knockdown, as we saw for CD9-signal (Figure 4.10).

In summary, stable knockdown of at least >70% was achieved for each target, without unleashing gross cytopathic or toxic effects. Although the mRNA was effectively diminished, exosome concentrates for Rab11b or Rab35 resulted in a modest 23% decrease only. VAMP7^{KD} was similar, but gave no changes in levels of ALIX or TSG101. These are difficult to interpret, whether indicative of a protein and/or a vesicle effect. The CD9^{KD} demonstrated little changes in vesicle number, but may have some effect in controlling protein-cargo loading onto vesicles, although this remains difficult to understand. In contrast, Rab5a^{KD} showed increased levels of exosome concentrates, though this is unknown whether this is due to increased exocytosis or blockade of endocytosis. Silencing VPS25, however, remains difficult to assess, whether this is due to the toxic cellular effect or genuine vesicle function. Based on our evidence, we decided to explore the importance of Rab11b and Rab35, in terms of vesicle structure and endosomal/lysosomal distribution in cells.

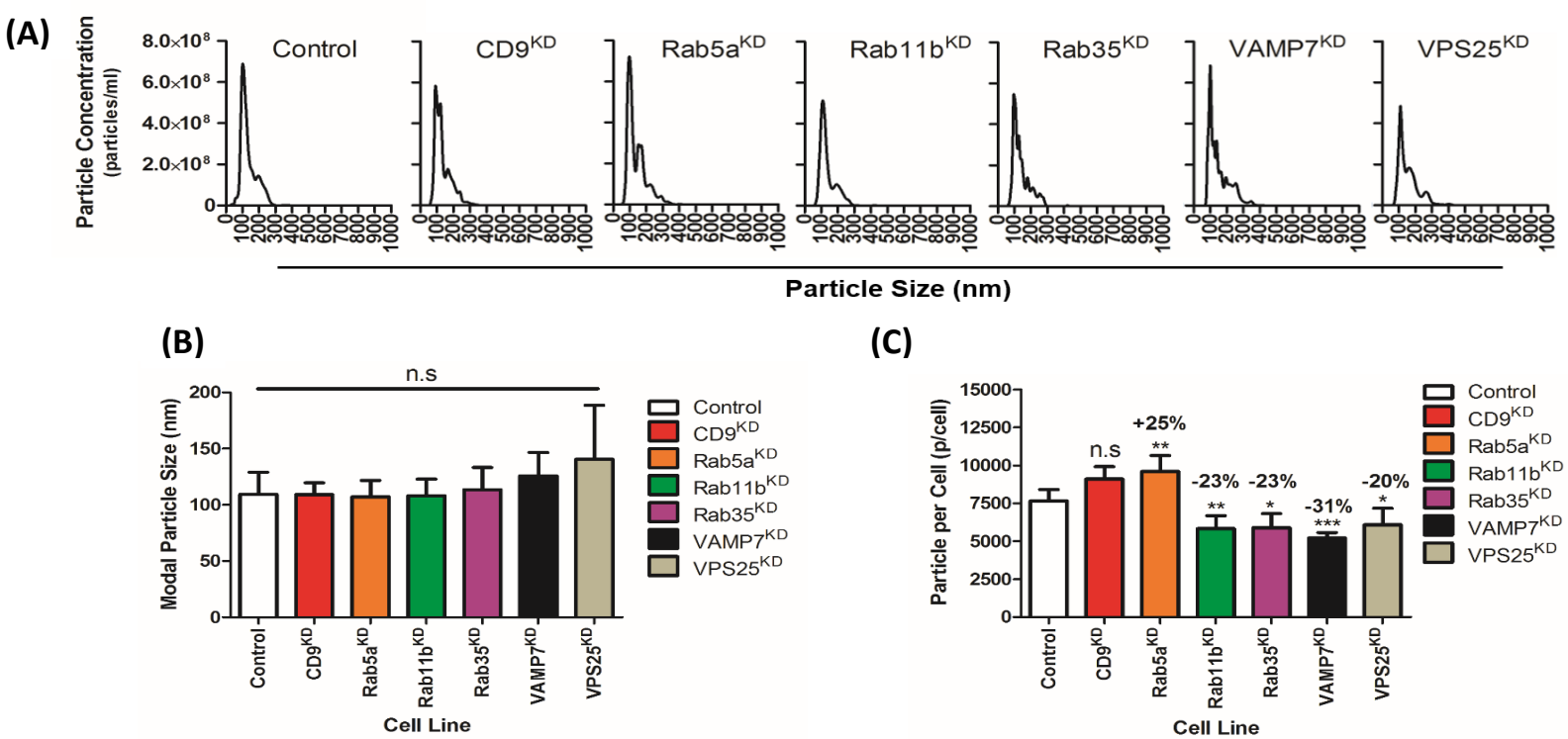

Figure 4.8: Characterising vesicles from lentiviral transduced DU145 cell CM by NTA. Cell CM was collected from DU145 control, CD9^{KD}, Rab5a^{KD}, Rab11b^{KD}, Rab35^{KD}, VAMP7^{KD} and VPS25^{KD} cells, cultured for 7 days. CM was analysed by NTA and six replicate measurements, revealing **(A)** the overall size distribution (histogram), **(B)** modal particle size and **(C)** the number of particles, adjusted for cell number (particles per cell: p/cell) is shown. The background of particles in the culture medium has been subtracted. These data are from a contiguous experiment and are representative of three such experiments. Graph shows mean ± SEM, based on 6 replicates. n.s: non-significant, *P<0.05, **<0.01 and ***P<0.001. One-way ANOVA with Tukey's post hoc test.

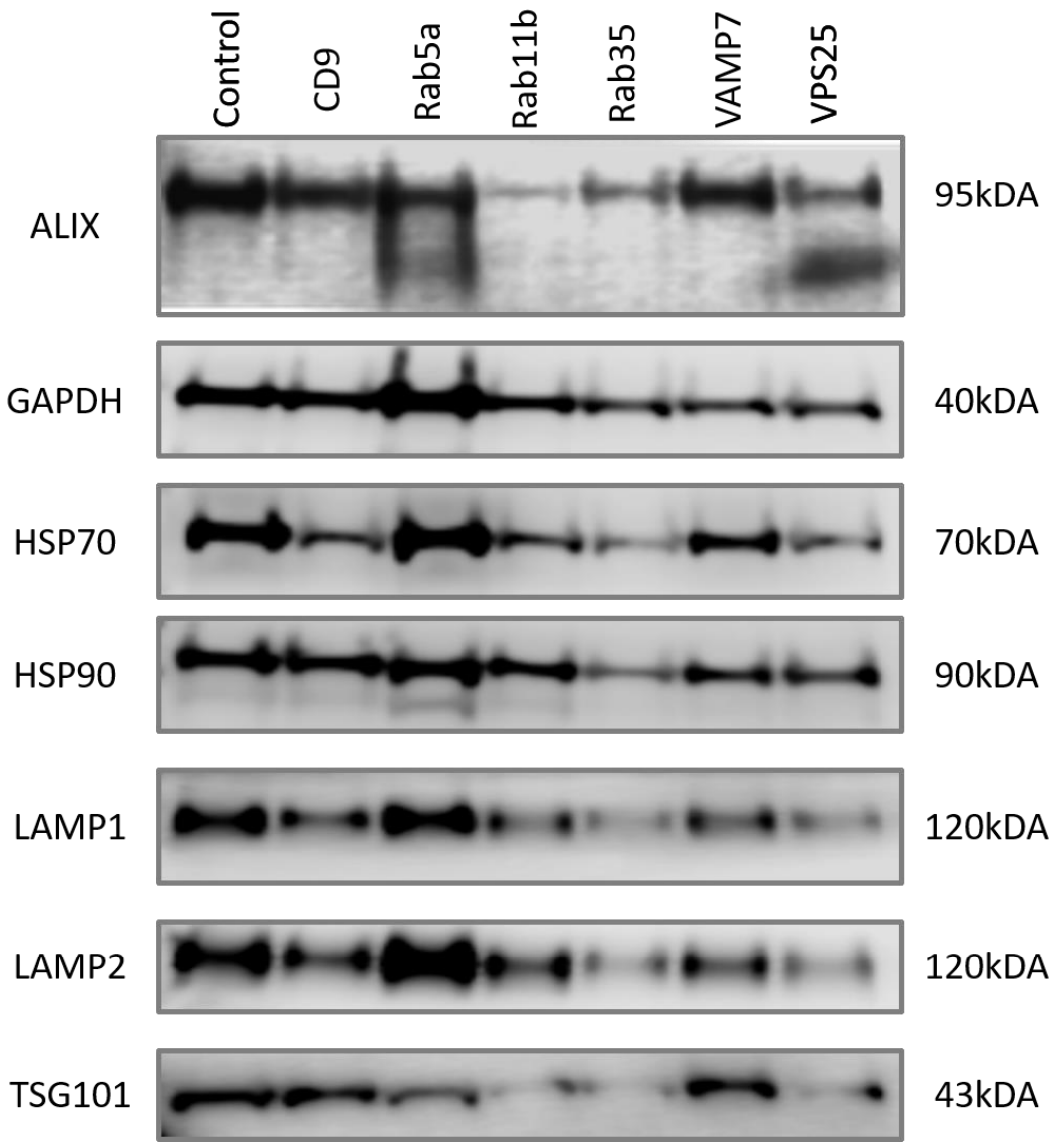

Figure 4.9: Characterising vesicles from lentiviral transduced DU145 cell CM by Western blot. Cell CM was collected from DU145 control, CD9^{KD}, Rab5a^{KD}, Rab11b^{KD}, Rab35^{KD}, VAMP7^{KD} and VPS25^{KD} cells, cultured for 7 days. CM underwent a basic differential ultracentrifugation method, followed by filtration through a 0.22µm filter, before ultracentrifugation at 200,000 x *g* for 2 hours in a fixed angle 70Ti rotor to obtain vesicle concentrates. Vesicle concentrates corrected for cell number were loaded. Six different exosomal-associated proteins (ALIX, HSP70, HSP90, LAMP1, LAMP2 and TSG101) were probed by Western blot.

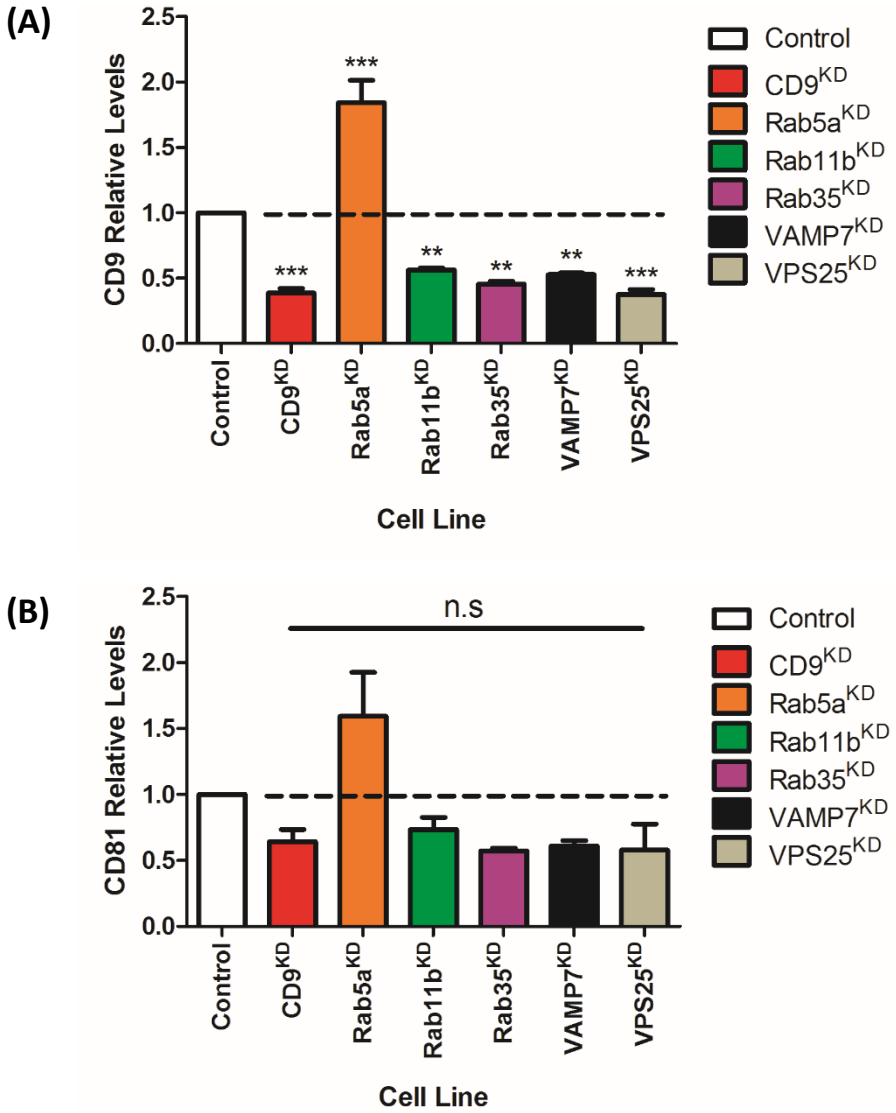

Figure 4.10: Characterising vesicles from lentiviral transduced DU145 cell CM by a plate-based assay. Cell CM was collected from DU145 control, CD9^{KD}, Rab5a^{KD}, Rab11b^{KD}, Rab35^{KD}, VAMP7^{KD} and VPS25^{KD} cells, cultured for 7 days. CM underwent a basic differential ultracentrifugation method, followed by filtration through a 0.22µm filter, before ultracentrifugation at 200,000 x *g* for 2 hours in a fixed angle 70Ti rotor to obtain vesicle concentrates. Vesicle concentrates corrected for cell number were captured onto high protein binding ELISA plates. Expression of **(A)** CD9 and **(B)** CD81 were analysed and plotted as relative levels, compared to control cells. Graph shows mean ± SEM, based on duplicate wells, due to the limitation of sample availability. n.s: non-significant, **<0.01 and ***P<0.001. One-way ANOVA with Tukey's post hoc test.

4.1.7 Characterising Vesicle Structures by Cryo-EM From DU145 Control or Rab11b^{KD} or Rab35^{KD} Cells

To understand the structure of nanometre sized vesicles, direct imaging would be a preferred characterisation technique. However, due to the limitation of their nanometre size, vesicles are at the lower limit of resolution for conventional light microscopy techniques. Although confocal or fluorescence microscopy can detect the larger nanometre-sized vesicles (>200nm), the fine details cannot be resolved (Piccin et al., 2007); although attempts have been made, but none seem quite successful. One of the commonly used methods to determine vesicle's size and structure is TEM. Though some concerns about the reliability of analysis of pelleted vesicles (dehydration and fixation) for TEM may alter vesicle size and morphology. Other 'newer' methods, such as cryo-EM, led to finding that the 'cup-shaped' morphology of exosomes was an artefact related to fixation for TEM (Théry et al., 2006). Despite these concerns, cryo-EM is the only method by which the nature of the vesicles size and structure may be determined at the same time. Here, the morphology of vesicles derived from DU145 control, Rab11b^{KD} or Rab35^{KD} cell CM were examined using cryo-EM in collaboration with Prof. Juan Manuel Falcón-Pérez (CIC bioGUNE, Derio, Spain). To perform this, vesicle concentrates were resuspended in PBS and placed onto glow-discharged holey carbon grids. Grids were blotted at 95% humidity and rapidly plunged into liquid ethane with the aid of VITROBOT. Vitrified samples were imaged at liquid nitrogen temperature, using a JEM-2200FS/CR cryo-TEM (JEOL, Japan), equipped with a field emission gun and operated at an acceleration voltage of 200 kV. Vesicle samples were viewed, revealing circular vesicle structure with a thick outer boundary, typical of a lipid bilayer.

Representative images are presented from DU145 control, Rab11b^{KD-} or Rab35^{KD-} derived vesicle concentrates, showed the presence of exosomes (Figure 4.11 A - C). The vesicles were heterogeneous in size, demonstrating that the population of vesicles from either control or knockdowns are not uniform as expected; and comparable to other reports of vesicle analysis by others (Caby et al., 2005, Yuana et al., 2013, Royo et al., 2017). From these representative images, there appeared to be fewer smaller sized (<50nm) vesicles in the Rab11b^{KD} images (Figure 4.11 B), compared to controls. Though, there appears to be an increase in smaller sized vesicle-like structures (<20nm) in the Rab35^{KD} (Figure 4.11 C), that may reflect the impact of knockdown on vesicle heterogeneity. Overall, these representative images appear to show the presence of vesicles, with all well recognised within the established diameter range of exosomes at 30nm - 150nm reported by various studies (Raposo et al., 1996, Escola et al., 1998, Yuana et al., 2013).

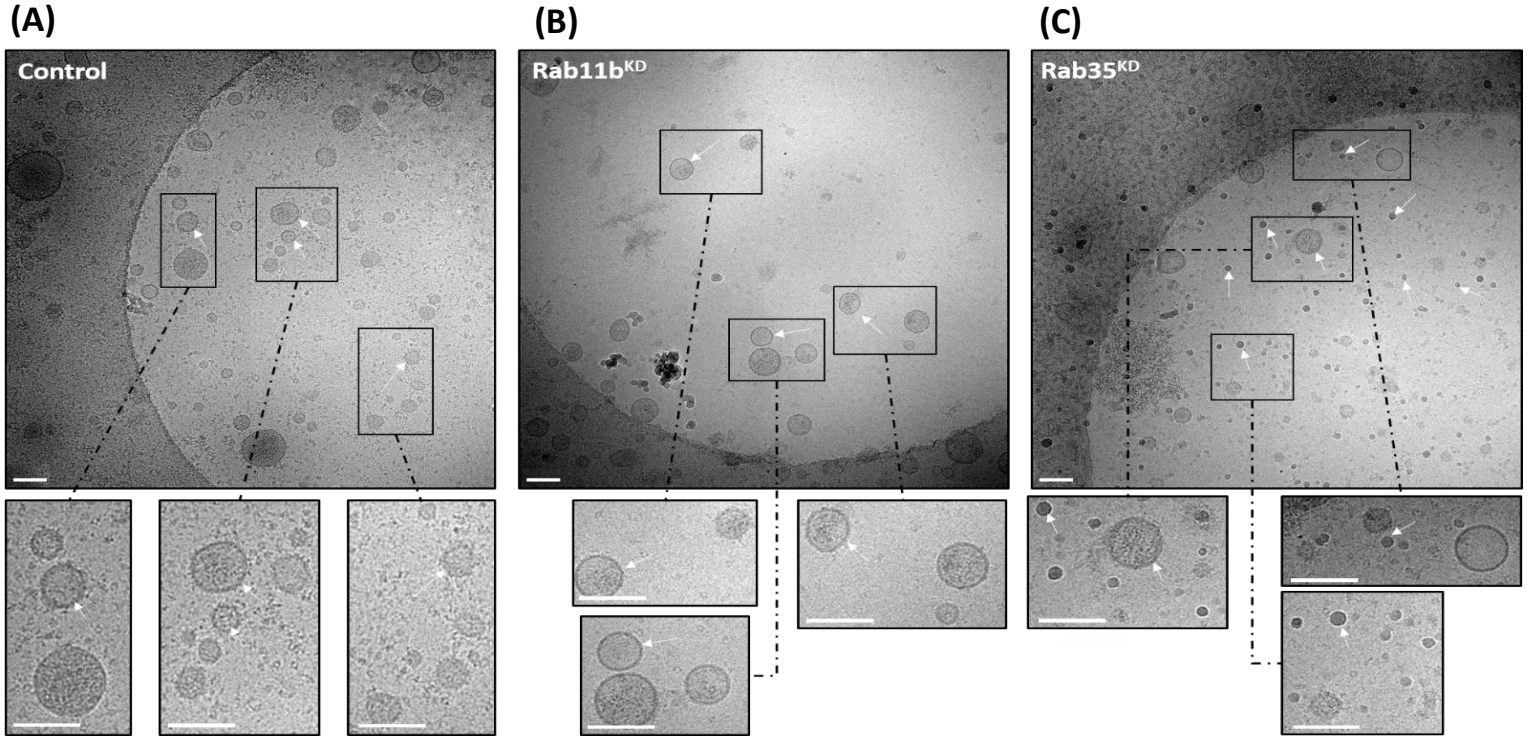

Figure 4.11: Characterisation of vesicles from DU145 control, Rab11b^{KD} or Rab35^{KD} cells by cryo-EM. CM from **(A)** control, **(B)** Rab11b^{KD} or **(C)** Rab35^{KD} cells were concentrated by 200,000 x *g* ultracentrifugation into vesicle pellets, that were resuspended in PBS and placed onto glow-discharged holey carbon grids. Grids were blotted at 95% humidity and rapidly plunged into liquid ethane with the aid of Vitrobot. Samples were imaged at liquid nitrogen temperature using a JEM-2200FS/CR cryo-TEM (JEOL), equipped with a field emission gun. The vesicles were viewed under cryo-EM, confirming the presence of lipid-bounded vesicle structures typical of exosomes. Scale bar: 100nm.

4.1.8 Distribution of Endosomal/Lysosomal Markers in DU145 Rab11b^{KD} or Rab35^{KD} Cells

Previous studies have demonstrated that silencing Rab27a (Ostrowski et al., 2010) or Rab35 (Hsu et al., 2010), results in an accumulation of MVEs within the cell, because of attenuated exosome secretion. These alterations are often associated in distribution changes with endosomal/lysosomal compartments, revealing MVE accumulation that may otherwise be exosomally-secreted. We next investigated the impact of knocking down Rab11b and Rab35 upon the endosomal compartments in DU145 cells. These following experiments involved immunofluorescent microscopy and flow cytometry staining for the tetraspanins (CD63 and CD81) and LAMP2. We also included early endosome antigen 1 (EEA1), as a marker for the early endosome. For assessing whole cell populations, flow cytometry was carried out on fixed/permeabilised cells for the markers, as described.

Here, we examined the impact of Rab11b^{KD} or Rab35^{KD}, in relation to any alteration in size or distribution and accumulation of proteins in late endosomes/lysosomes. There was clear evidence for an elevation in intracellular CD63, LAMP1 and CD81, following knockdown of Rab11b or Rab35 (Figure 4.12 A - C), compared to controls. The weak and diffuse punctate staining of CD63, LAMP1 and CD81 in control cells became more intense, with increased peri-nuclear accumulation. On the other hand, staining for EEA1 (Figure 4.12 D) remained punctate and diffuse within the cytosol with no significant alteration in intensity or distribution, suggestive of the early endosomes remaining unaffected following knockdown.

Next, we performed flow cytometric analysis on control and knockdown cells, showing similar results to immunofluorescent staining. However, the results indicated the median fluorescent intensity (MFI) are weak and this may be due to sub-optimal staining or sub-optimal cell permeabilisation (Figure 4.13 A - C). Nevertheless, we observed a significant elevation (40%) in the MFI of CD63 (Figure 4.13 D) was observed in both Rab11b^{KD} and Rab35^{KD} ($P<0.001$), compared to controls. This was also true for LAMP1 staining accumulation (40% increase) (Figure 4.13 E), in Rab11b^{KD} ($P<0.05$) and Rab35^{KD} ($P<0.01$). Interestingly, data for CD81 (Figure 4.13 F), showed a significant difference in Rab11b^{KD} ($P<0.05$), but not for Rab35^{KD}. Consistently, EEA1 (Figure 4.13 G) MFI remained not significantly altered following either knockdown, suggesting that early endosomes are not affected. Here, the cells demonstrate that knockdown of Rab11b or Rab35 impacts the organisation of the late endosomal or lysosomal compartments and not early endosomes, consistent with the previous published data related to attenuated exosome secretion.

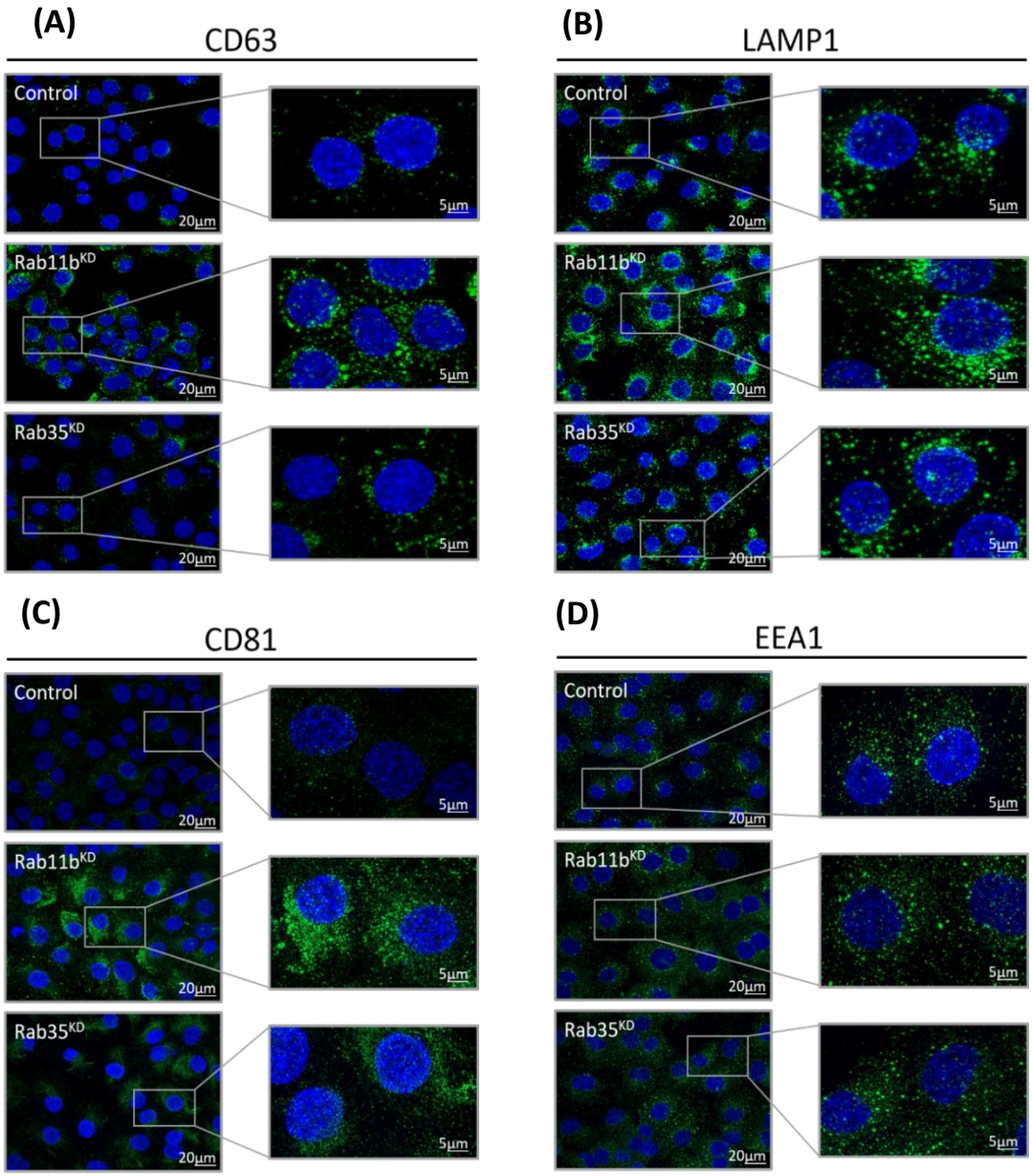

Figure 4.12: Immunofluorescent staining of endosomal/lysosomal markers in DU145 control, Rab11b^{KD} or Rab35^{KD} cells. Fixed-permeabilised DU145 control or Rab11b^{KD} or Rab35^{KD} cells were stained for markers of late endosomes/lysosomes: **(A)** CD63, **(B)** LAMP1, **(C)** CD81, or a marker of early/recycling endosomes EEA1 (D) and labelled with Alexa-488, and DAPI. Wide-field fluorescence microscopy, with structured illumination was performed, and images show representative microscopic fields, as Z-axis sections overlaid to generate maximum projection images. The grey box shows selected regions at higher magnification. Scale bar: 20µm and 5µm respectively. Representative fields are shown.

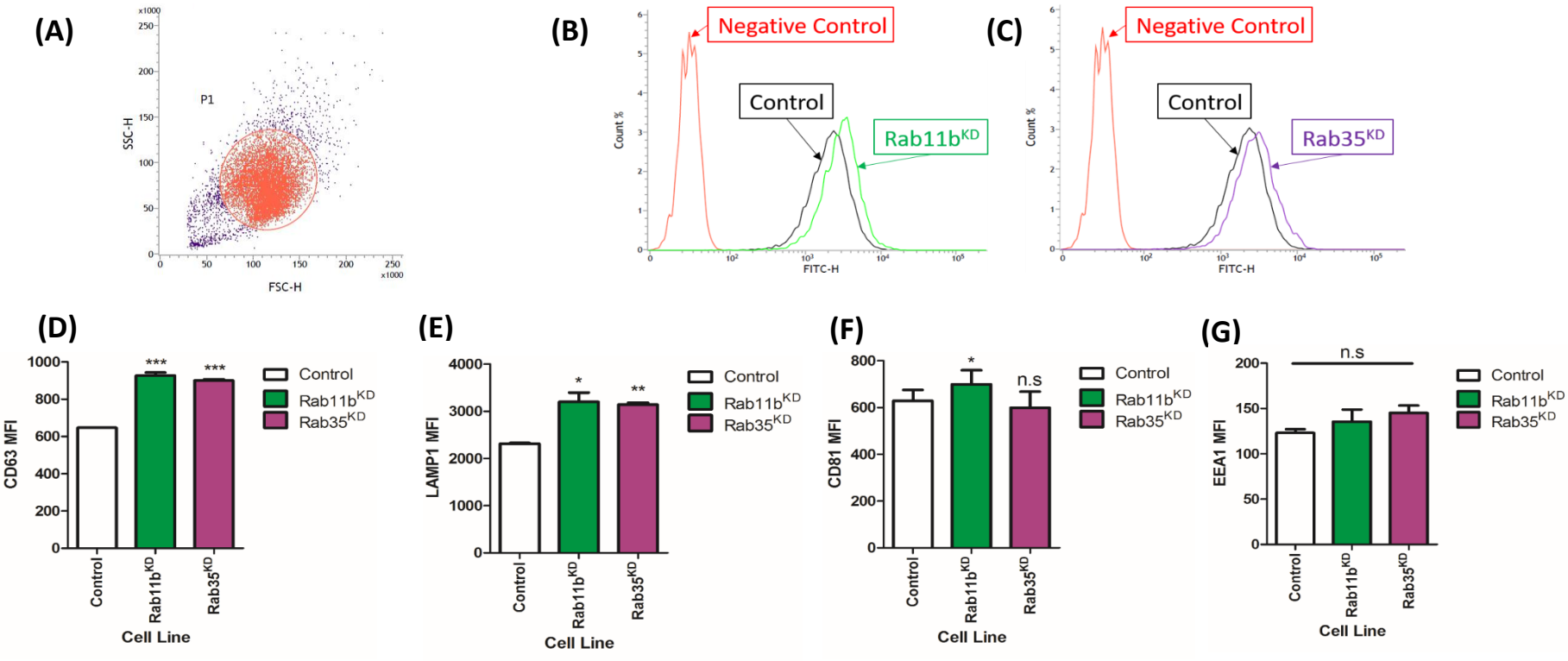

Figure 4.13: Flow cytometric analysis of endosomal/lysosomal markers in DU145 control, Rab11b^{KD} or Rab35^{KD} cells. Flow cytometry analysis of fixed-permeabilised DU145 control, Rab11b^{KD} or Rab35^{KD} cells. **(A)** Representative dot plot image of size and granularity distribution of cells. Region of interest (P1) was selected to include single and viable cell populations. Representative histograms shows an example of LAMP1 staining in fix/permeabilised DU145 control and **(B)** Rab11b^{KD} and **(C)** Rab35^{KD} cells. Median fluorescent intensities (MFI) were plotted after isotype subtraction (based on 5,000 events), based on other primary antibodies against: **(D)** CD63, **(E)** LAMP1, **(F)** CD81 and **(G)** EEA1. Graph shows mean ± SEM, based on duplicate samples. n.s: non-significant, *P<0.05, **<0.01 and ***P<0.001. One-way ANOVA with Tukey's post hoc test.

4.1.9 Protein Profiling of Vesicles or the Soluble Secretome Following Rab11b or Rab35 Knockdown

The Rab proteins are known to function collectively in regulating a myriad of membrane transport processes. However, disrupting the intracellular traffic regulators may have unexpected effects on the secretome. In one report, silencing Rab27a resulted in effective exosome attenuation, although, this also impacted on the secretion of a subset of cytokines. For example, the secretion of pro-MMP-9 were significantly reduced, or in contrast cells displayed increased tendencies to secrete granulocyte-colony stimulating factor (G-CSF); but none were secreted in associated with vesicles (Bobrie et al., 2012). These results highlight silencing Rab27a not only impacts the secretion of MVE derived exosomes, but also regulates the secretion of a subset of soluble proteins.

Here, we investigated whether the secretion of non-exosome associated secreted factors present in cell CM (total secretome) and changes arising in the vesicle concentrates, could also be affected upon knockdown of Rab11b or Rab35. We performed a sensitive Proximity Ligation Array (Proseek® Multiplex Immuno-Onc I^{96x96}) for this experiment, which measured the expression of 92 proteins across various samples, to sub picogram sensitivity. This sensitive array was performed because soluble factors are often at low concentrations that are difficult to detect by the Array. From the Array, many proteins were reported below the LOD, whilst detectable signal was present for 46 proteins in the total secretome. With respect to the vesicle concentrates a total of 38 proteins were detected (Figure 4.14).

First, we compared the profile of vesicle-rich pellets from DU145 control cells, compared to vesicle pellets from Rab11b or Rab35 knockdowns. The data is presented as fold-changes compared to control cells; and revealed around 18 analytes exhibiting greater than 2-fold changes in relative abundance following knockdown (Figure 4.15 A). Though the extent of change was dissimilar, the direction of change was similar for both Rab11b and Rab35 knockdowns, all except for some cases. For example, CXCL6 was >3.8 fold decreased in vesicles derived from the Rab11b knockdown, compared to >2 fold increased from the Rab35 knockdown. The factors were significantly different ($P<0.05$) compared to control cells, as shown in the volcano plot (Figure 4.15 B). This highlights a reduction in MMP-1, but an elevation in CXCL6, IL18R1, TGFα, TNFRSF3, TRAIL and VEGF-A in vesicle pellets derived from Rab35 knockdowns. In contrast, vesicle concentrates from the Rab11b knockdown demonstrated decreased levels of AXL1N, CXCL6, TRAIL and TWEAK; and showed an elevation in 4E-BP1. This data revealed that despite showing similarities across vesicle

samples, there are examples where the vesicle populations following knockdown of Rab11b or Rab35, are not identical.

Similar comparisons were made comparing with cell CM (Figure 4.15 C). We observed numerous changes with the DU145 Rab11b^{KD} and Rab35^{KD} cells, compared to controls. As examples, LIF (>30 fold) and IL-6 (>36 fold) expression were significantly elevated in the Rab35 knockdown cell secretome, but were not a feature of the vesicle-rich pellets. This suggests that these are present as soluble rather than in association with vesicles. Changes in CXCL6 and 4E-BP1 in the Rab11b knockdown, or CXCL6, IL18R1 in the Rab35 knockdown (Figure 4.15 D), however, agreed in both the general secretome and vesicle pellets; which were at least partially vesicle-related. Protein profiling the secretome highlights several examples of dissimilarity and showed Rab11b or Rab35 knockdown imparts distinct effects on the general secretome and which are not vesicle exclusive.

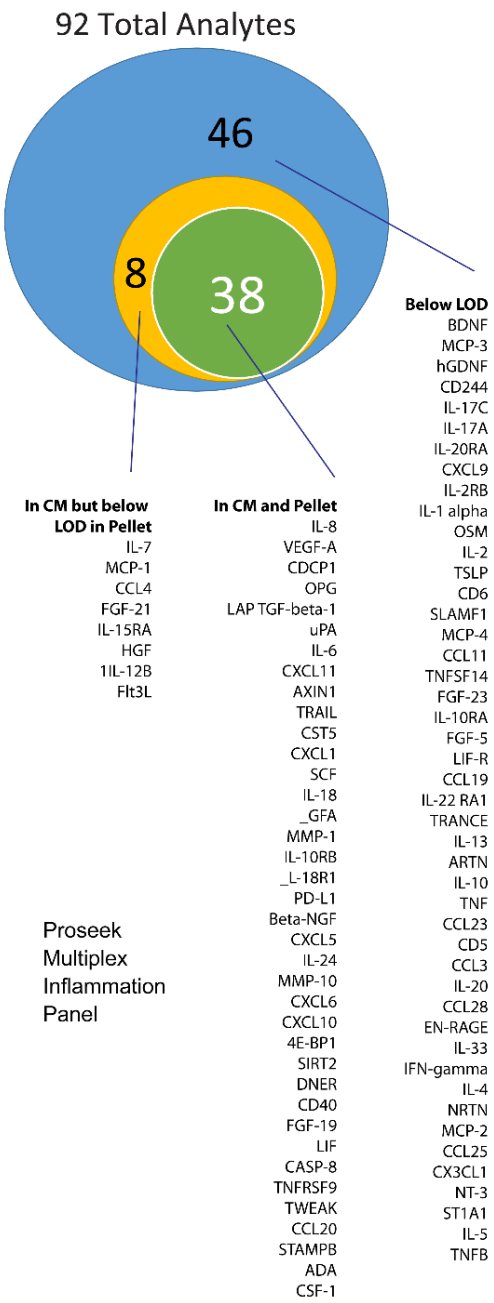

Figure 4.14: Venn diagram depicting the Protein Array in CM and vesicle pellets. The Venn diagram depicts the entire Proseek® (Multiplex Immuno-Onc I^{96x96}) Protein Array menu (of 92 analytes); and shows those identified with signal above the limits of detection in cell conditioned media and vesicle pellets (green, 38 analytes), or those found in cell conditioned media but reported with no signal in vesicle pellets (orange, 8 analytes). Half of the menu (blue, 46 analytes), were below detection limits. Specific identifications in each category are shown.

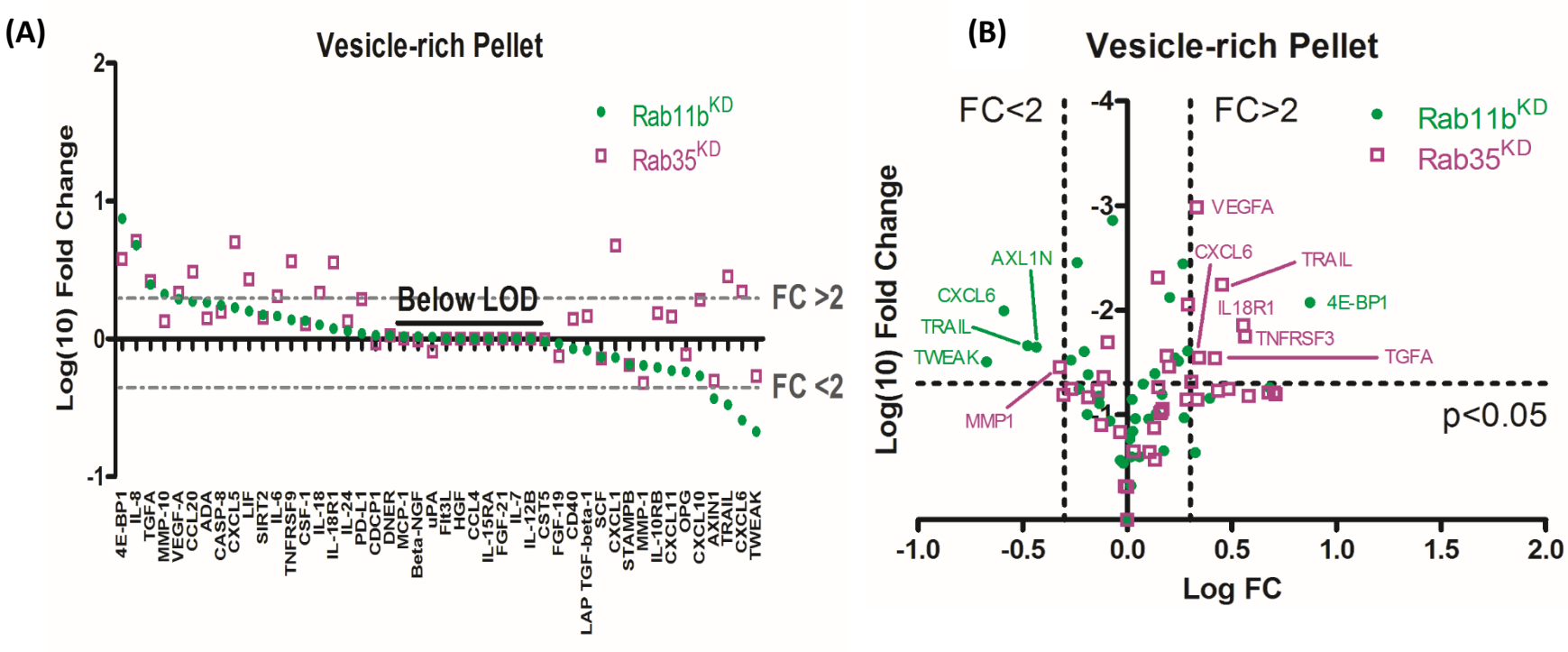
(A)
Vesicle-rich Pellet
Log(10) Fold Change
Rab11b^KD
Rab35^KD
Below LOD
FC >2
FC <2
4E-BP1
IL-8
TGFA
MMP-10
VEGF-A
CCL20
ADA
CASP-8
CXCL5
LIF
SIRT2
IL-6
TNFRSF9
CSF-1
IL-18
IL-18R1
IL-24
PD-L1
CDCP1
DNER
MCP-1
Beta-NGF
uPA
Flt3L
HGF
CCL4
IL-15RA
FGF-21
IL-7
IL-12B
CST5
FGF-19
CD40
LAP TGF-beta-1
SCF
CXCL1
STAMPB
MMP-1
IL-10RB
CXCL11
OPG
CXCL10
AXIN1
TRAIL
CXCL6
TWEAK
(B)
Vesicle-rich Pellet
FC<2
FC>2
Rab11b^KD
Rab35^KD
Log(10) Fold Change
VEGFA
AXL1N
CXCL6
TRAIL
IL18R1
4E-BP1
TNFRSF3
TGFA
TWEAK
MMP1
p<0.05
Log FC

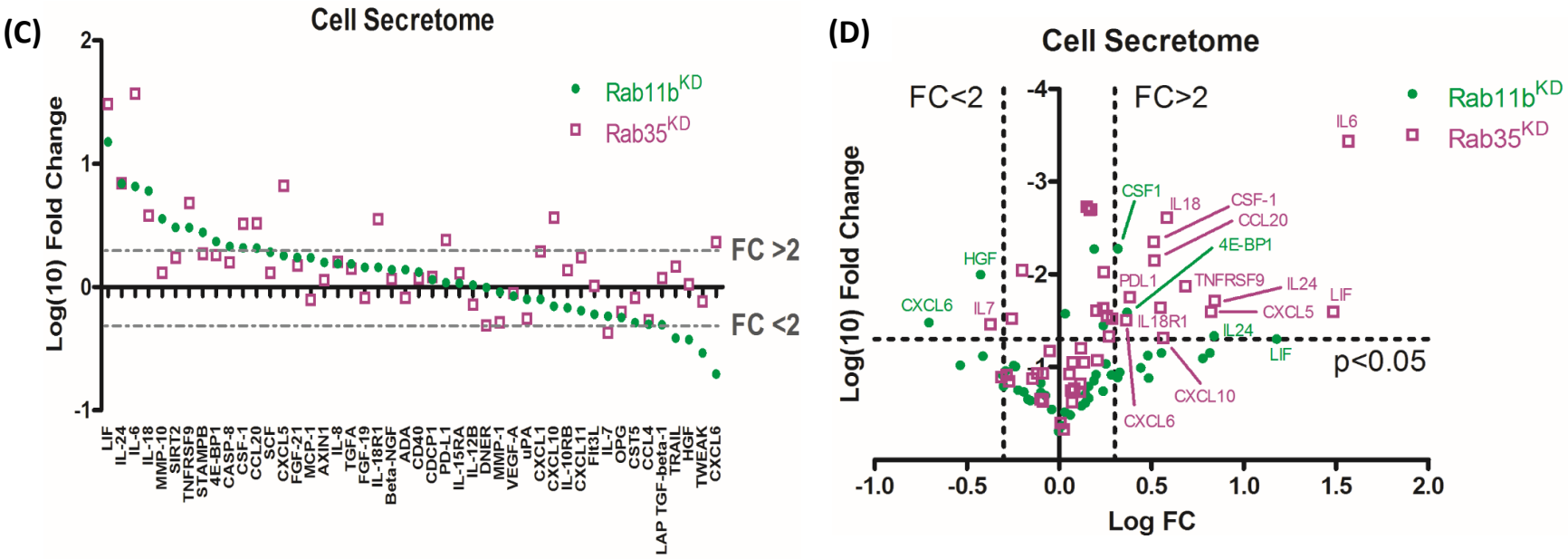

Figure 4.15: Knockdown of Rab11b or Rab35 alters the protein profile of vesicle concentrates and the general secretome. Cell CM from control or knockdown cells were concentrated by 200,000 x *g* ultracentrifugation and pellets normalised for protein, were analysed using the Proseek Multiplex Proximity Ligation Array, with coverage of 92 analytes related to inflammation. Analysis represent differences in levels of those 38 analytes reporting with signals above the assay limits of detection (LOD), comparing the vesicle-pellets derived from RAB11b or Rab35 relative to control. **(A)** The waterfall plot lists the analytes, and plots log10-fold change compared to control levels. **(B)** The volcano-plot identifies differentially expressed analytes with a fold change>2 and a P value<0.5 (T-test). Similarly, cell conditioned media was analysed (without concentrating vesicles), representing the secretome, showing **(C)** waterfall and **(D)** a volcano-plot as above for the 48 analytes reporting with signals above the LOD.

4.2 Discussion

In this Chapter, we investigated whether our choice of factors putatively implicated in exosome biogenesis and secretion can be successfully knocked down using lentiviral particles delivering specific shRNAs. Puromycin was used in gene selection for mammalian host cells and identified the minimal puromycin concentration to kill all non-resistant cells, which was used to conditioned transduced DU145 cells with specific shRNA clones.

RNA-mediated silencing is an evolutionary conserved mechanism, through which dsRNA induces inactivation of specific gene sequences. The discovery of RNAi provided researchers with a rapid rise in identified genes underlying many biological processes and produced phenotypes that revealed gene function (Moffat et al., 2006). Its success is attributed to an evolutionary endogenous pathway present in all cell types, that regulates gene expression commonly achieved by siRNA or shRNA. The use of exogenously supplied siRNA that mimic the functions of miRNAs, but are designed to have a greater specificity to their targets by having complementary sequences, can assemble with RISC and have siRNA-mediated target recognition; thus mRNA cleavage and degradation (Brennecke et al., 2005). One drawback to using this is the depletion of siRNA over a few days and a loss of effect, with recovery of cells to the wild-type phenotype. As an alternative to this method, we used shRNA and its delivery through a lentiviral vector-expressing plasmid, which contains a selection marker (puromycin). This produces a dsRNA structure that is similar to the pri-miRNA of the cell and is produced accordingly to the miRNA mimic, the siRNA. Hence, we achieved continuous stable expression of shRNA for suppressing the target gene (Lee et al., 2003, Sigma, 2016). Many studies have utilised shRNA as a powerful tool to study gene function in both *in vitro* and *vivo* models (Stewart, 2003, Van den Haute et al., 2003, Singer and Verma, 2008, Wilson et al., 2013). Similarly, our knockdowns still remain stable over 15 weeks and all characterisation and functional experiments were performed, prior to 15 weeks.

Our results initially confirmed that knockdown targets were reduced (70 - 97%) at the mRNA level; and we evaluated if these knockdowns would translate into attenuated protein levels. We demonstrated attenuated expression of target proteins in lentiviral transduced DU145 cells, with an overall agreement of the mRNA knockdown. As one example showing mRNA expression was strongly decreased by 86% in DU145 $CD9^{KD}$ (#711 clone) cells, it's impact on protein was not similar, compared to the #470 clone. Since biological processes are typically driven by proteins, mRNA expression signatures results are thought of as a proxy for functional pathway changes, involving changes in protein levels. This requires the

assumption that global differences in mRNA levels reflect differences in protein levels. Comparisons attempting to directly determine how closely mRNA expression levels reflect those corresponding to proteins, have revealed weak to moderate correlations between both mRNA and protein markers (Anderson and Seilhamer, 1997, Tian et al., 2004, Pascal et al., 2008, Koussounadis et al., 2015). Differences in the mRNA vs protein correlation show a surprisingly weak correlation of 0.40; signifying that only ~40% of protein concentration can be explained by knowing mRNA abundance (de Sousa Abreu et al., 2009, Schwanhausser et al., 2011). The other ~60% of the variation could be explained by a combination of post-transcriptional and post-translational regulation, half-life of different proteins varying from minutes to days; and by measurement errors (Maier et al., 2009, Vogel and Marcotte, 2012). Thus, we felt it was important to evaluate and select our knockdowns sequences on a combination of diminished mRNA and protein levels.

We next determined whether the phenotypic consequence of gene knockdown would impact cell proliferation or morphology. Similar cobblestone-like cell morphology was observed in all lentiviral transduced DU145 cells. There was slightly reduced cell proliferation seen with knockdown of CD9 and Rab5a in DU145 cells; and this was more pronounced with the knockdown of VPS25. The connection between VPS25 knockdown and cell proliferation extends to fungal species, where VPS25 inhibition interrupts the division of cells and invasive growth (Sarode et al., 2011). In *Drosophila* models, many of the mutations related to VPS-related proteins and in particular VPS25 mutant cells, are very sensitive to apoptosis (Herz et al., 2006). With this evidence, we proposed that VPS25 have roles in reducing cell proliferation and a slower rate of reaching confluency. However, to assess vesicle secretion, DU145 VPS25^{KD} cells experienced some toxicities, which is extremely difficult to assess, as these cells are undergoing cell death that can produce apoptotic blebs and cellular debris to confound analysis of exosome secretion. We did not, therefore, evaluate the remaining vesicle population in detail for this cell line.

CD9 was first documented in exosomes derived from dendritic cells (Théry et al., 1999). Several studies describe CD63 and CD81 as the most frequently identified proteins in exosomes, which are considered classical markers (Kobayashi et al., 2000, Caby et al., 2005, Logozzi et al., 2009). Here, silencing CD9 showed a partial decrease in protein content of LAMP1, LAMP2 and HSP70, whilst no significant changes in particles/cell. There are, however, some conflicting studies. In one report, exosome release from dendritic cells generated from CD9 knockout (CD9^{KO}) mice was reduced, compared to wild type dendritic cells (Chairoungdua et al., 2010). In a different model, knockdown of CD9 in Nalm-6 pre B-

cells resulted in a decrease in CD10-associated vesicles (Mazurov et al., 2013). In a similar tetraspanin model, in the absence of CD63 expression, ILV formation and downstream MVE biogenesis were severely reduced, but not any MVEs requiring sphingomyelinase expression or activity (van Niel et al., 2011). The results we observed differs from other studies and suggests that knockdown of CD9 has little effect on vesicle number, but some effect in controlling the protein-cargo loading onto the vesicle. Perhaps, CD9 may contain a population of vesicles that are independent of ALIX and TSG101, but are important for LAMP1, LAMP2 and HSP70. This data reveals there is a full complex mechanism for vesicle manufacture by the cells and the data do not possess a definite explanation yet of the CD9 role.

Also, we next investigated the impact of the SNARE protein (VAMP7) in exosome secretion by DU145 cells. Silencing VAMP7 caused a modest decrease in particles/cell and other exosomal-associated markers (CD9, LAMP1 and LAMP2) in the remaining vesicle pellet. With a role in membrane fusion between intracellular endosomal compartments, VAMP7 is potentially involved in the final steps of exosome secretion. Currently, there are few studies to address the requirement of SNAREs in exosome secretion. Our results are consistent with the finding that VAMP7 is involved in exosome secretion by K562 cells (Fader et al., 2009). Expression of the N-terminal domain of VAMP7, which impairs the formation of the SNARE complex, induced the accumulation of enlarged MVEs at the cell periphery and reduced exosome secretion, similar to other studies targeting exosome secretion by other means (Bobrie et al., 2012, Webber et al., 2015). Likewise, YKT6 is another SNARE protein implicated in membrane fusion, YKT6 inhibition led to a reduction in exosome release in lung cancer models (Ruiz-Martinez et al., 2016). There are some conflicting studies demonstrating that VAMP7 is not required for exosome secretion (Rao et al., 2004). In one report, expression of the longin domain (N-terminus) of VAMP7 inhibits the secretion of lysosomes, but not of exosomes (Proux-Gillardeaux et al., 2007). These findings indicate that different SNARE complexes may function differently in specific cell types and might be involved in fusion of certain endosomal compartments. Therefore, different SNARE complexes could mediate only a certain subpopulation of MVEs within a single cell type, as highlighted by another group (Colombo et al., 2013); and VAMP7 downregulation might only affect a specific exosome subpopulation. Our data shows quantification of some exosomal-associated markers (ALIX and TSG101) remains unaltered in the knockdown of VAMP7, compared to controls. The results we observe differ from other studies, and suggests that knockdown of VAMP7 attenuates vesicles secretion by 31%, but show little changes in the levels of ALIX

and TSG101. Perhaps VAMP7 may contain a population of vesicles that are dependent of ESCRT-related proteins, but not important for LAMP1, LAMP2, HSP70 and HSP90. It could be possible that VAMP7 may govern a specific MVE subpopulation, though this data reveals the complex mechanism for vesicle secretion and does not provide a definitive role of VAMP7.

In contrast, silencing Rab5a induced an increase in exosome secretion by 25%, which may be a potential candidate for enhancing the extracellular vesicle content, either through enhanced accelerated secretion, or equally by dysregulating the cell's capability to endocytose and process vesicles through an autocrine fashion. Some studies reveal overexpression of Rab5 impairs early intra-endosomal trafficking and causes MVEs to enlarge, severely reducing exosome secretion and respective markers (ALIX, CD63 and syntenin) in MCF-7 cells (Baietti et al., 2012). Likewise, knockdown of endogenous Rab5 increased the number of secretory granules per mast cell in the immunological setting (Azouz et al., 2014). These findings conflicted with other observations, where exosome secretion is decreased upon Rab5a targeting (Ostrowski et al., 2010). Multiple studies, however, have documented that knockdown of Rab5 decreased uptake levels of horseradish peroxidase in NIH3T3 cells (Su et al., 2006), low-density lipoproteins in primary mouse hepatocytes (Zeigerer et al., 2012) and *Staphylococcus aureus* (*S. aureus*) uptake in Cos-7 cells (Hagiwara et al., 2014). These studies suggests Rab5 plays potential roles in endocytic uptake. Other studies have also shown the role for Rab5a-mediated autophagy, together with a key autophagic protein (Beclin-1), between the early stages of autophagosome-mediated fusion with the lysosome (Maroni et al., 2016, Tan et al., 2016). Different Rab5 isoforms for endosomal trafficking show that in HeLa cells, Rab5a^{KD} or Rab5b^{KD} impairs and delays EGFR degradation and consequently delays early to late endosome trafficking, whereas Rab5c^{KD} does not affect EGFR degradation (Chen et al., 2009). With no direct evidence to these speculations, it could be hypothesised that cargo in the early endosome is typically fated for Rab5a-mediated autophagic degradation. Rab5a inhibition could potentially redirect endosomal compartments to a different pathway (exocytosis), hence increased exosome secretion, yet this should be investigated in further detail.

From our data, silencing either Rab11b and Rab35 appears to have attenuated exosome secretion from DU145 cells, confirmed by a reduction in exosomal-associated proteins (ALIX, HSP70, HSP90, LAMP1, LAMP2 and TSG101) and tetraspanins (CD9 and CD81) within the remaining vesicle pellet and a modest reduction (20%) in particle/cell. Supporting these findings, other studies focusing on Rab11 in K562 cells and Rab35 in oligodendrocytes, have demonstrated that silencing either protein appears to attenuate exosome secretion (Savina

et al., 2002, Hsu et al., 2010). Given the amount of evidence available, we generated knockdowns of Rab11b or Rab35 to give a genuine, but modest, perturbation on exosome secretion and provided the basis of selected target for future investigation.

There was no general failure in trafficking machinery following Rab11b or Rab35 knockdown, as early endosomes appeared unaffected and the knockdowns showed only a limited impact on exosome secretion. Silencing Rab11b or Rab35 also accumulated levels of CD63, LAMP1 and CD81 around the nuclei, signifying an accumulation of potential MVEs in the cells, which agreed with other studies in a similar Rab27a knockdown model (Ostrowski et al., 2010, Webber et al., 2015, Grimsey et al., 2016). Similarly, it was noted that knockdown of Rab27a demonstrated reduced MVE docking, despite an increase in MVE size (Ostrowski et al., 2010). This could be explained by a lack of motor linkage resulting in enlarged compartments. Myosin Va is a widely expressed actin-based protein, binding only to a subset of Rab proteins (Rab8, Rab11b and Rab27a), associated with either endocytic recycling and post-golgi secretory systems (Desnos et al., 2003, Lindsay et al., 2013). In contrast, myosin Va does not directly bind to Rab35 (Rahajeng et al., 2012). However, Rab35 promotes the recruitment of Rab8 with MICAL-L1, a multiple Rab-binding protein mediating exocytosis (Kobayashi et al., 2014). This may explain that a myosin Va-driven specific-Rab exchange mechanism is only conceivable during the late stages of exocytosis, as is the case for Rab11b or Rab35, transporting MVEs to the cell periphery by a kinase-driven mechanism; thus modulating exosome secretion.

Visualisation of the nanometre-sized structures of the vesicles derived from either DU145 control, Rab11b^{KD} or Rab35^{KD} cells was performed by cryo-TEM. As observed for controls, the 200,000 x *g* vesicle pellet showed the presence of different populations of vesicles with different sizes ranging from 30nm-150nm. The existence of morphologically different exosome subpopulations among secreted vesicles is in agreement with other reports, showing the presence of different MVEs in a single cell (Möbius et al., 2003, White et al., 2006, Bobrie et al., 2012, Willms et al., 2016), as these distinct exosomes may be formed in diverse MVEs. Alternatively, smaller sized vesicle-like structures (<10nm), exhibit a dense centre without a distinctive bilayer membrane was observed in the knockdown of Rab35. It was demonstrated that mutant Rab35 redirects many receptors to be found in smaller sized vesicles (<30nm in diameter), suggesting an accumulation in transport intermediates (Sato et al., 2008). In contrast, no smaller size vesicles were detected in the knockdown of Rab11b. From these images, there could possibly be an underestimation of the particle/cells in the knockdown of Rab35. NTA enables the analysis of nanoparticles around 20nm, provided the

samples have a high refractive index (Gardiner et al., 2014), but biological samples are often complex and in reality, the limit of detection is often around 40 - 50nm. Despite showing the differences behind the knockdown of Rab35 in generating <20nm vesicles, the mechanism behind this remains unknown and has not been addressed, but these images show the presence of distinct vesicle subpopulations as a result from each respective knockdown.

Because of the similarities in data for Rab11b^{KD} and Rab35^{KD}, in terms of a partial attenuation of exosome secretion, characterised by exosomal-associated markers and NTA analysis, described above; the hypothesis is whether both Rab11b and Rab35 co-regulate an identical pathway. Here, a highly sensitive multiplexed proximity-ligation array was used to address this. There were significant changes in the protein profile of DU145 Rab11b^{KD}-derived vesicles, with many overlapping similarities following knockdown of Rab35, but the phenotype between vesicles were not identical. The Array showed that CXCL6, TRAIL and TWEAK are proteins found in the DU145 Rab35^{KD}-derived vesicles, compared to their decrease in DU145 Rab11b^{KD} derived vesicles. These observations support the concept that different endosomal compartments and subsequent secreted vesicles, display different protein compositions (Bobrie et al., 2012, Colombo et al., 2013), governed by these Rab proteins. It remains difficult, however, to characterise specific markers to analyse different vesicle populations, either based on different isolation techniques or different endosomal-derived vesicles. Published reports have highlighted the presence of vesicle heterogeneity (Lazaro-Ibanez et al., 2014, Smith et al., 2015, Willms et al., 2016); and one study has attempted to distinguish different vesicles by a proteomic comparison, attempting to define new markers (Kowal et al., 2016). Here, our data reveals vesicle heterogeneity, with respect to remaining vesicles enriched with distinct proteins, following knockdown of Rab11b or Rab35 in DU145 cells.

Inhibition of Rab11b or Rab35, however, for assessing subsequent exosome function should be taken with a degree of caution, as this may impact secretion of soluble factors. It is not completely understood what interplay between vesicles that are truly separate from the soluble secretome. However, many databases, such as ExoCarta (Mathivanan and Simpson, 2009) and Vesiclepedia (Kalra et al., 2012), highlight vesicle association with various cytokines, eicosanoids and growth factors. Hence, the loss of a vesicle subpopulation may impact on the soluble secretome, as these are no longer available to tether molecules to their surface as a manner of sequestration. In a breast carcinoma model, secretion of other non-exosome-associated proteins, such as MMP-9, was decreased, with the Rab27a knockdown model (Bobrie et al., 2012). Likewise, other secreted soluble factors such as PDGF

and placental growth factor (PGF), in melanoma cells were decreased following Rab27a knockdown (Peinado et al., 2012). Control of MVE trafficking by Rab GTPases have potential broad effects on exocytic events, that cannot be assumed to be exosome-selective.

In this Chapter, we have successfully transduced DU145 cells with specific shRNA and validated these DU145 knockdown cell lines at the mRNA and protein level. We have demonstrated that Rab11b and Rab35 play minor roles in terms of overall secretion of exosomes and abrogate distinct subpopulations of exosomes. We will take forward both DU145 Rab11b^{KD} and Rab35^{KD} cells, to explore the functional impact of a loss of these exosome subpopulations has upon the cancer-associated stroma.

CHAPTER 5:

THE IMPACT OF EXOSOME-DEFICIENT TUMOUR CELLS ON THE STROMA

5.1 The Impact of Exosome-Deficient Tumour Cells on the Stroma

5.1.1 Introduction

Tumours are complex structures of malignant cancer cells surrounded by stroma, pivotal for cancer growth and progression (Hanahan and Weinberg, 2011). The tumour stroma consists of cellular and non-cellular components. Cellular components include immune cells, endothelial cells, mesenchymal stem cells and fibroblasts, whereby non-cellular components include growth factors and other signalling molecules (Kalluri and Zeisberg, 2006). While none of these cells are themselves malignant, their complex reciprocal interaction with each other and tumour cells, creates a tumour microenvironment that supports local growth, invasion and ultimately dissemination. Exosomes plays large roles in intercellular communication, between cancer and stromal cells, resulting in tumour microenvironment maturation, aiding tumour growth in a variety of systems (Chowdhury et al., 2015, Saleem and Abdel-Mageed, 2015, Webber et al., 2015, Baglio et al., 2017).

Fibroblasts are one of the dominant cell types within the tumour microenvironment of many solid cancers and then play pivotal roles in dictating the nature of cancer-activated stromal tissues. For this study, we relied on an extensively well-characterised primary cell as a model, to assess stromal-fibroblast phenotypes under the influence of cancer cells. The AG02262 normal diploid adult lung fibroblasts (from Coriell Institute) were used, as these have limited population doubling levels and become senescent post-passage 10. They have previously been studied for their capacity to differentiate to myofibroblasts (Webber et al., 2009, Webber et al., 2010, Midgley et al., 2013, Chowdhury et al., 2015, Webber et al., 2015). These fibroblasts can differentiate into myofibroblasts under the control of recombinant human TGF-β1 (rhTGF-β1) and have been used in studying exosome-controlled differentiation (Webber et al., 2010, Webber et al., 2015). Myofibroblasts are determined by the acquisition of alpha-smooth muscle actin (α-SMA), together with cell contractility (Hinz et al., 2012).

Since the classic observations of many histological similarities between the tumour microenvironment and wound healing, it has been proposed that the tumour stroma is “wound healing gone awry” (Dvorak, 1986). During normal wound healing, coagulation of extravasated blood initiate an intricate cascade of signals that recruit inflammatory cells, stimulate fibroblasts and epithelial cell proliferation, direct cell migration and induce angiogenesis to restore tissue integrity (Kalluri and Zeisberg, 2006). This permits re-epithelialisation of the injured region and the myofibroblasts undergo apoptosis when the injured site is fully covered by a new epidermis (Shaw and Martin, 2009). In the context of

carcinomas, this process is not self-limiting. As it is often associated with the chronic persistence of α-SMA positive myofibroblasts (Orimo et al., 2005), increased proliferation and invasion of epithelial cells, resulting in uncontrollable tumour growth and eventual metastatic spread (Coussens and Werb, 2002).

For the metastatic spread of cancer tissue, the formation of a supportive vascular network is important. Tumour cells can penetrate into newly-formed and poorly organised blood or lymphatic vessels, pass through the lymphatic or peripheral circulation and then localise at other sites (Folkman, 1971). Angiogenesis occurs in a multi-step process involving endothelial cell activation by angiogenic factors, migration, proliferation and organisation of endothelial cells into vessel-like structures (Carmeliet and Jain, 2000). Tumour angiogenesis, however, relies on many of the same processes involved in physiological angiogenesis. This is associated with excessive growth-promoting signals and a lack of sufficient cues to spatially and temporally coordinate vessel growth, remodelling and maturation, fuelled in part by tumour-secreted factors and tumour hypoxia (Carmeliet and Jain, 2000, Trojan et al., 2004). The blood vessels produced by tumours are typically aberrant, where the tumour neovasculature is marked by distorted and enlarged vessels, leakiness and abnormal endothelial cell proliferation (Nagy et al., 2010). Numerous studies have demonstrated that angiogenesis directly associates with aggressive carcinomas and increasing incidences of tumour metastasis (Weidner et al., 1993, Jaeger et al., 1995, Parangi et al., 1996). Therefore, angiogenesis is considered an important aspect for primary tumour growth that provides a continual supply of nutrients, as one of the hallmarks for cancer (Hanahan and Weinberg, 2011).

A host of pro-angiogenic growth factors secreted from cancer epithelial and stroma cells have been identified. The VEGF family and their receptors (VEGFR) are powerful angiogenic mediators in cancerous tissues and adjacent stroma. Elevated expression of VEGF and VEGFR correlates with aggressive metastatic cancer, compared to non-metastatic tumours (Takahashi et al., 1995, Hoeben et al., 2004, Caballero et al., 2007). Expression of hepatocyte growth factor (HGF), has been shown to positively correlate with enhanced vessel formation in various *in vitro* and *in vivo* models (Xin et al., 2001, Abounader and Laterra, 2005). Basic fibroblast growth factor (bFGF) and epidermal growth factor (EGF) were expressed in malignant carcinomas, associating with increased CD31 (endothelial cell marker) expression, compared to non-tumour tissues (Dunn et al., 2000, Bajou et al., 2002, Trojan et al., 2004, van Cruijsen et al., 2005). Various studies showed that different growth factors are released from epithelial cells, or cells within the stroma, such as endothelial cells, mast cells or

fibroblasts (McNeil et al., 1989, Leon et al., 1994, Stadnyk, 1994, Grugan et al., 2010). These cellular components may therefore play a role in support of vessel formation, but the principal source of these growth factors should be explored.

Fibroblasts within the tumour stroma have an activated phenotype, known to produce growth factors and chemokines, supporting ECM remodelling and facilitating the angiogenic recruitment of endothelial cells (Kalluri and Zeisberg, 2006). Breast cancer cells co-cultured with tumour-associated myofibroblasts demonstrated extensive vascular formation *in vivo* (Orimo et al., 2005). However, capillaries were far less established when tumour cells were co-cultured with normal fibroblasts. In intestinal tumours, tumour-associated myofibroblasts strongly stimulated the migration and vessel formation of vascular endothelial cells (Shao et al., 2006); and this has also been shown in gastric cancer *in vivo* models (Guo et al., 2008). However, not all myofibroblasts are pro-angiogenic. Current studies have shown that α-SMA positive myofibroblasts generated from rhTGF-β1 induced fibroblasts did not elevate angiogenic growth factors or support formation of endothelial vessel-like structures *in vitro* (Webber et al., 2015). In contrast, prostate cancer exosomes induced myofibroblasts, which were pro-angiogenic, exhibited elevated HGF and VEGF secretion and encouraged formation of endothelial vessel-like structures *in vitro* (Webber et al., 2015). In the *in vivo* setting, co-administration of diseased prostate stromal myofibroblasts with tumour cells in mice enhanced tumour growth, in contrast to rhTGF-β1-treated fibroblasts or exosome-activated, normal stromal fibroblasts (Webber et al., 2015). These findings show the role of exosomes in communicating between tumour cells and the surrounding stroma, directing stromal differentiation to a tumour supporting phenotype.

Previously, I have demonstrated that knockdown of Rab11b or Rab35 appeared to impact a distinct subpopulation of exosomes from DU145 cells. It remains unknown, however, whether the effect has any functional relevance in terms of cancer cell influence on stromal fibroblasts. The hypothesis is that the remaining vesicles, following Rab11b or Rab35 attenuation, lose their stromal activating potency.

5.1.2 The Cancer Cell Secretome Triggers a Poor Fibroblast Differentiation Response

We first measured secreted growth factor levels from the cancer conditioned media (CM) (control or Rab11b^{KD} or Rab35^{KD}), corrected for cell number (as described in Chapter 4). There were no significant differences in secreted levels of FGF-2, HGF, uPA and VEGF-A (Figure 5.1 A-D) in either Rab11b^{KD} or Rab35^{KD} in comparison to controls. These observations are important, as it demonstrates that exocytic modulation by knocking down Rab11b or Rab35 does not have a major effect on these important angiogenic factors.

Next, we determined the fate of fibroblast differentiation in response to cancer cell CM (control or Rab11b^{KD} or Rab35^{KD}). Fibroblasts were grown until 70% confluent and growth-arrested for 72 hours. Subsequently, fibroblasts were grown in DMEM-F12 media alone or with a single stimulation with rhTGF-β1 (1.5ng/ml), purified DU145 exosomes at an equivalent TGF-β1 dosage (200µg/ml) or cell CM (control or Rab11b^{KD} or Rab35^{KD}), corrected for cell number. After 72 hours, fibroblasts were fixed, stained and analysed by immunofluorescent microscopy, to explore α-SMA expression. The number of α-SMA positive cells was assessed over 6 microscopic fields and in duplicate treatments. Fibroblasts treated with either rhTGF-β1 or purified DU145 exosomes increased the number α-SMA positive cells, compared to untreated fibroblasts (Figure 5.2). Control cell CM had a negligible effect on α-SMA onset, where weak staining was evident in a small proportion of cells. There was a total absence of α-SMA-positivity in fibroblasts treated with Rab11b^{KD} or Rab35^{KD} cell CM. Thus, unlike rhTGF-β1 or purified exosomes, the soluble secretome appears insufficient to trigger a robust fibroblast differentiation response into α-SMA positive myofibroblastic cells under these conditions.

The levels of growth factors, FGF-2, HGF, uPA and VEGF-A, secreted by untreated fibroblasts or fibroblasts treated with cancer CM were investigated (Figure 5.3). There was a significant reduction in HGF levels, following treatment with CM from Rab11b^{KD} ($P \leq 0.01$) or Rab35^{KD} ($P \leq 0.001$) cells, compared to the control (Figure 5.3 B). Similarly, levels of activated VEGF-A secretion followed the comparable trend of HGF and did not quite reach statistical significance when using knockdown cell CM (Figure 5.3 D). In contrast, levels of activated FGF-2 and uPA secretion (Figure 5.3 A & C), exhibited negligible changes in both control and knockdown conditions. These observations are important, as the cell CM effects are apparent following knockdown of Rab11b or Rab35. A full-blown differentiation was not observed and there were indeed, documented differences in the functional influence of the CM, following knockdown. For example diminished HGF and VEGF levels, suggestive that Rab11b or Rab35 must have a role in attenuating growth factor release.

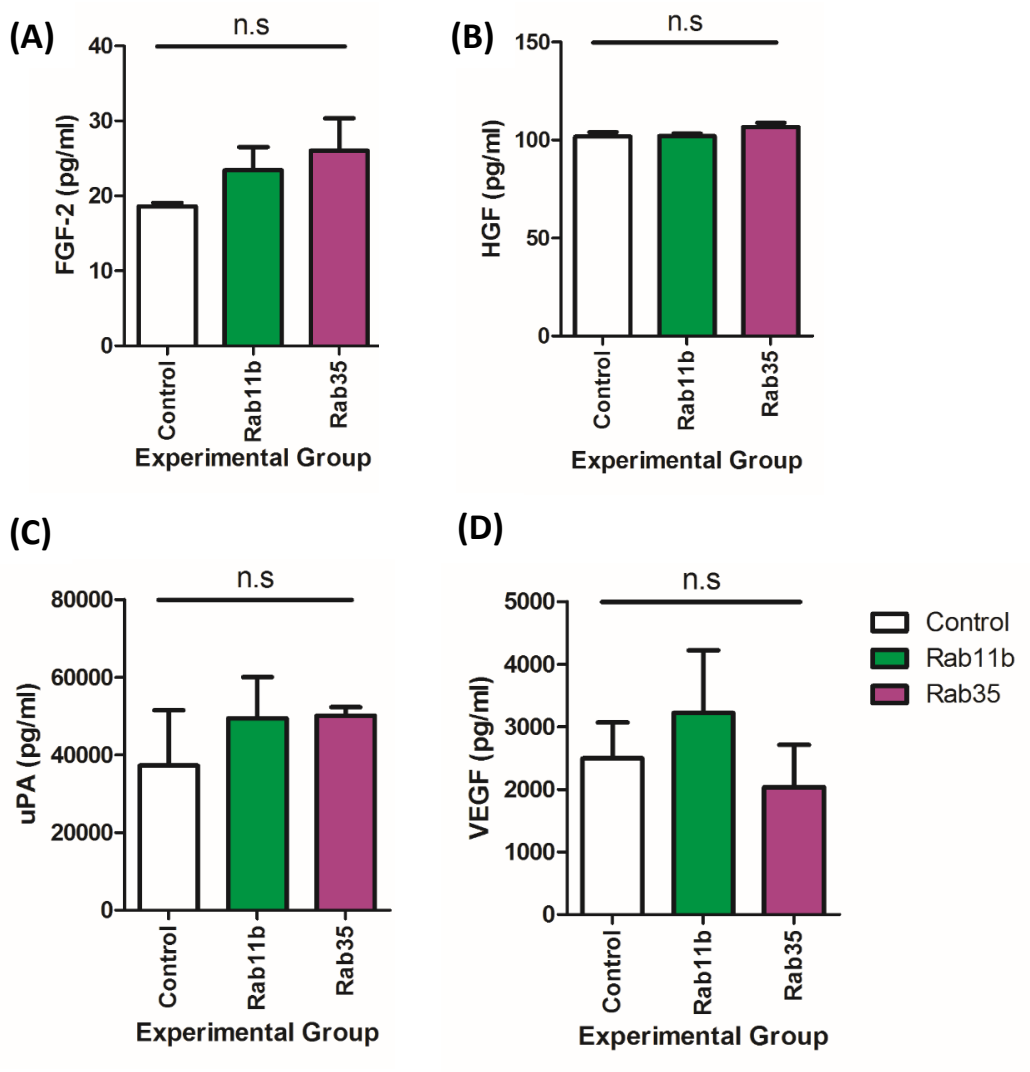

Figure 5.1: Assessment of growth factor secretion from exosome competent and deficient tumour cells. Cell CM from DU145 control or knockdowns (Rab11b or Rab35; corrected for cell number), after 5 days of culture were analysed by ELISA for **(A)** FGF-2, **(B)** HGF, **(C)** uPA and **(D)** VEGF levels. Graph shows mean ± SEM, based on triplicate wells. n.s: non-significant. One-way ANOVA with Tukey's post hoc test.

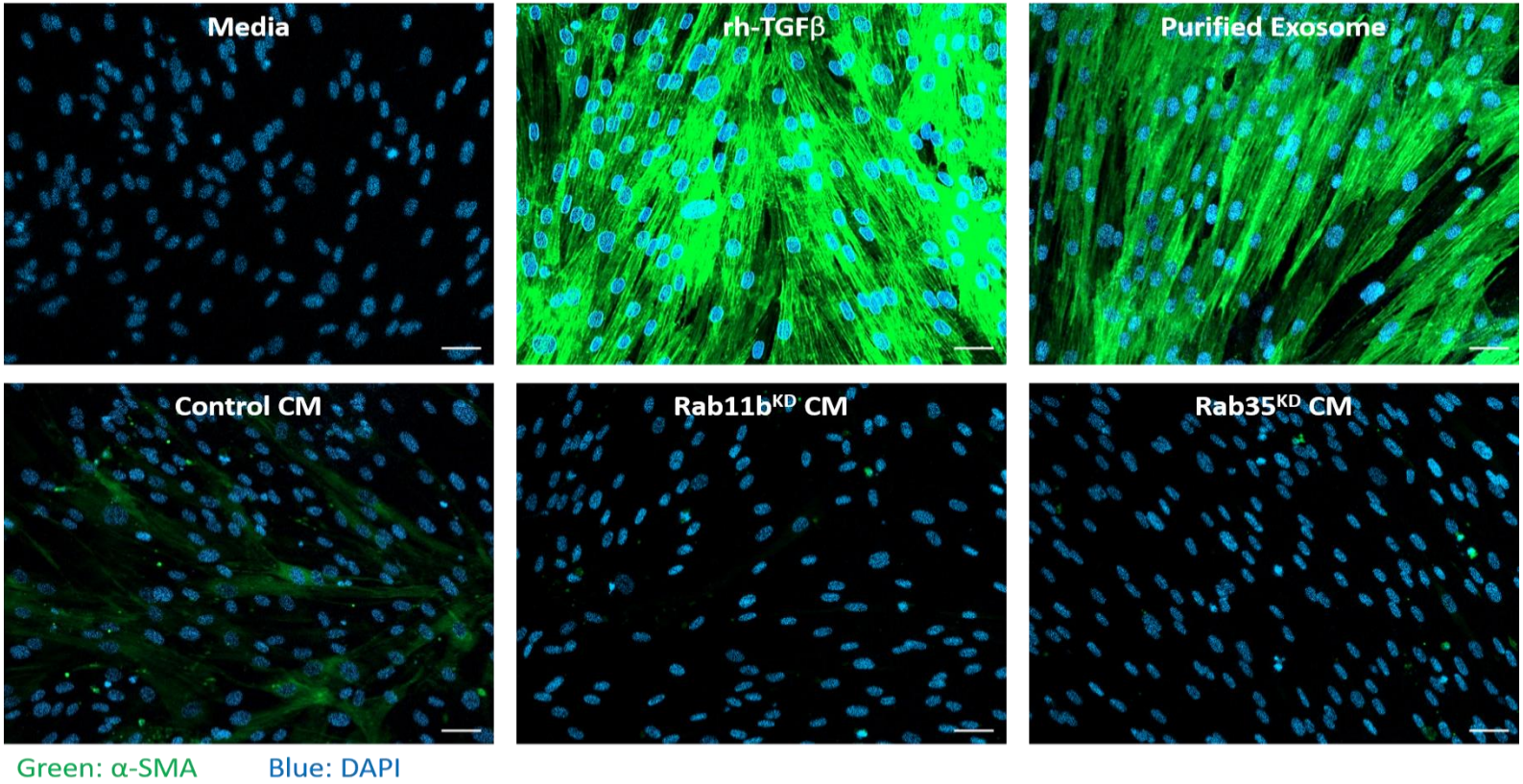

Figure 5.2: Cancer cell secretome triggers a poor fibroblast differentiation response. Fibroblasts at passage 7 were growth-arrested (72 hours) and were either left untreated, or treated in the presence of rhTGF-β1 (1.5ng/ml), purified DU145 exosomes (200ug/ml) or DU145 (CTR, Rab11b^{KD} or Rab35^{KD}) cell CM, corrected for cell number in DMEM-F12 media. Fibroblasts were examined by immunofluorescent microscopy for the expression of α-SMA (green) and DAPI (blue). Scale bar: 50µm. α-SMA positive cells over 6 microscopic fields were examined in duplicate wells per treatment. Representative fields are shown. Data are representative of three independent experiments.

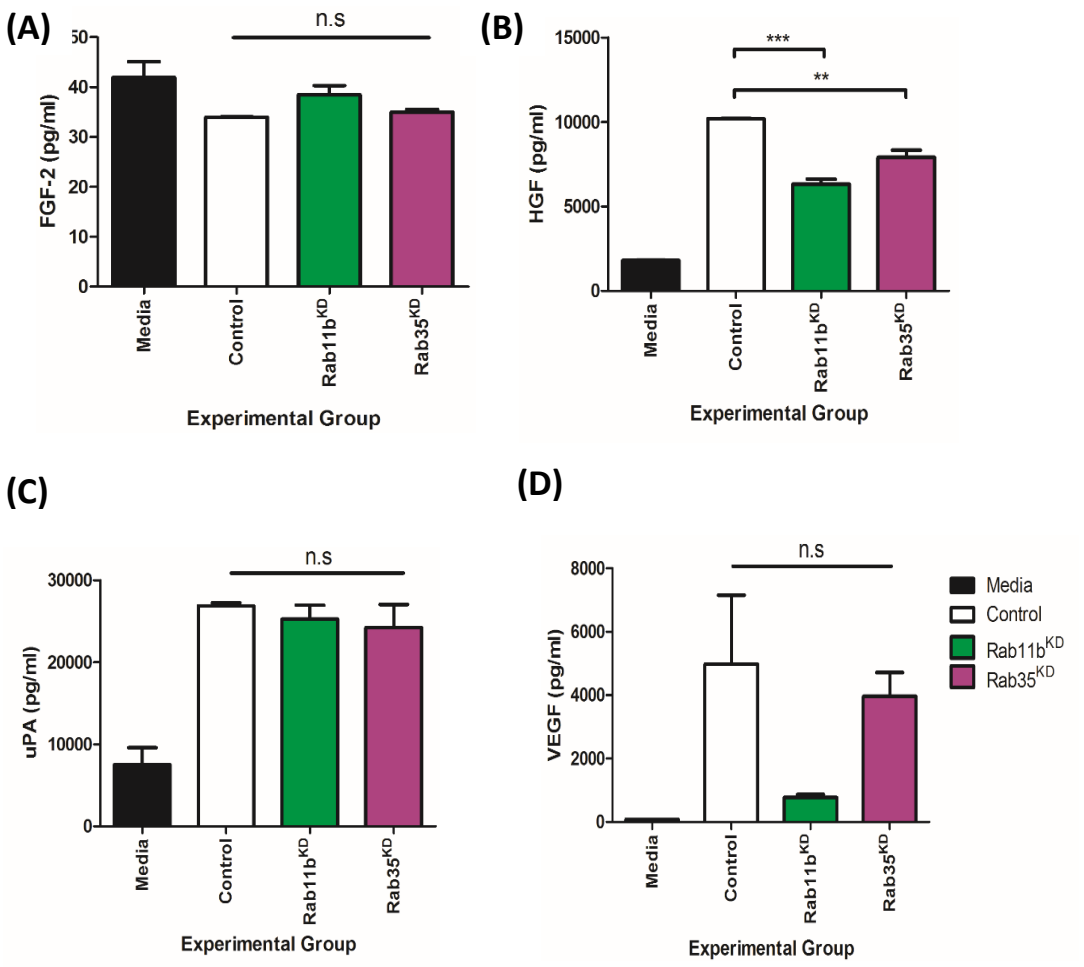

Figure 5.3: Fibroblasts treated with DU145 Rab11b^{KD} or Rab35^{KD} cell CM generate reduced pro-angiogenic growth factors. Fibroblasts at passage 7 were growth arrested (72 hours) and were either left untreated, or treated in the presence of the DU145 (control, Rab11b^{KD} or Rab35^{KD}) cell CM, corrected for cell number in DMEM-F12 media. CM collected from different treated fibroblast conditions was analysed by ELISA for levels of **(A)** FGF-2, **(B)** HGF, **(C)** uPA and **(D)** VEGF. Graph shows mean ± SEM, based on triplicate wells. n.s: non-significant, **P≤0.01 and ***P≤0.001. One-way ANOVA with Tukey's post hoc test. Data are representative of three independent experiments.

5.1.3 Vesicle Concentrates From Rab11b^{KD} or Rab35^{KD} Cell CM Lose Their Stroma-Activating Potency

Previously it was shown that the cell CM influenced fibroblast secretion. As such, we proposed that this may be due to a vesicle-driven process, as demonstrated with cancer exosomes holding the capacity to drive stromal fibroblast differentiation into myofibroblasts (Webber et al., 2010, Webber et al., 2015). We, therefore, concentrated vesicles from cell CM and examined the effects on fibroblasts, as we did for the treatment of cell CM.

Fibroblasts were grown in DMEM-F12 media alone, with a single stimulation with rhTGF-β1 (1.5ng/ml) or purified DU145 exosomes at an equivalent TGF-β1 dosage (200µg/ml). Vesicle concentrates (control or Rab11b^{KD} or Rab35^{KD}) corrected for cell number also were compared. Untreated fibroblasts exhibited low level/negligible staining of α-SMA, whilst purified exosomes from wild-type DU145 cancer cells stimulated the onset of α-SMA in the entire cell population (Figure 5.4). Similarly, stimulation with rhTGF-β1 generated a robust differentiation response. Vesicle concentrates obtained from control cell CM triggered a strong differentiation response, involving the majority of the fibroblasts in the population. In contrast, treating fibroblasts with remaining vesicle concentrates deriving from Rab11b^{KD} or Rab35^{KD} cells, revealed a poorly convincing differentiation response; whilst some of the α-SMA was detectable, this was weaker in intensity and not all cells had responded (Figure 5.4). Hence, we proposed that the remaining vesicles from Rab11b^{KD} or Rab35^{KD} cells resulted in an attenuated fibroblast differentiation response.

We next explored levels of FGF-2, HGF, uPA and VEGF-A, secreted by treated fibroblasts (Figure 5.5). We observed a significant increase in both HGF and VEGF secretion when using vesicle concentrates from control cells (Figure 5.5 B & D). In contrast, there was a significant reduction in secreted HGF (Figure 5.5 B) in treated conditions for Rab11b^{KD} ($P \leq 0.001$) and Rab35^{KD} ($P \leq 0.01$). Also, levels of VEGF secretion (Figure 5.5 D) followed this pattern, when using either Rab11b^{KD} ($P \leq 0.05$) or Rab35^{KD} ($P \leq 0.01$). Levels of FGF-2 increased with the Rab11b^{KD} ($P \leq 0.01$) (Figure 5.5 A), secreted uPA levels were reduced with the Rab35^{KD} ($P \leq 0.05$) (Figure 5.5 C). This highlights that the fibroblasts treated with distinct vesicle concentrates following knockdown of Rab11b or Rab35 are different in the effects on fibroblasts. It supports the idea of vesicle subpopulations dictate distinct functions.

Overall, there appears to be a significant attenuation when using vesicles concentrated from either Rab11b^{KD} or Rab35^{KD}, in terms of the acquisition of the α-SMA positive phenotype and in terms of the secretory phenotype of the fibroblasts.

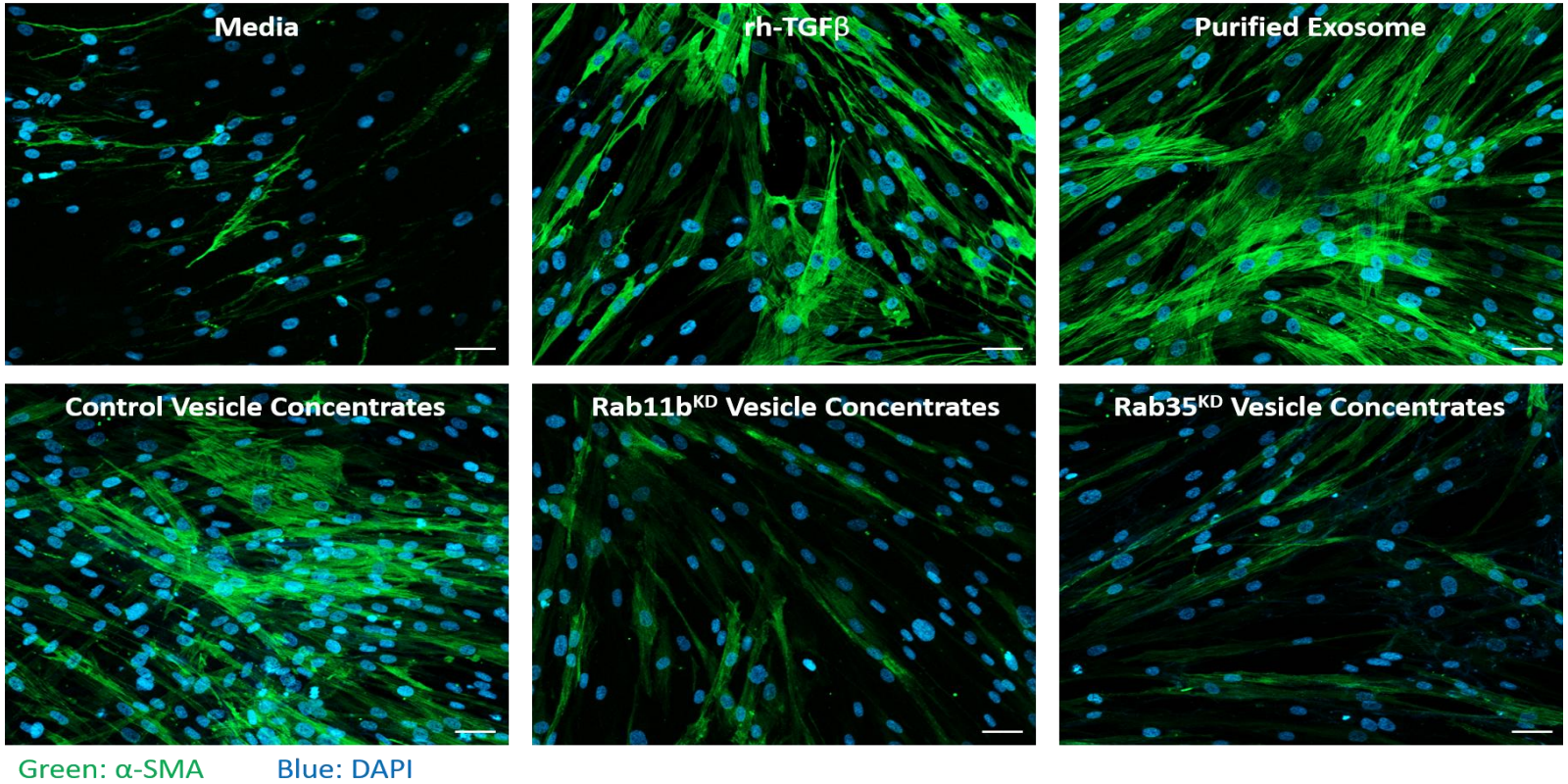

Figure 5.4: Vesicle concentrates from Rab11b^{KD} or Rab35^{KD} cell CM triggers a poor fibroblast differentiation response. Fibroblasts at passage 7 were growth arrested (72 hours) and were either left untreated, treated in the presence of rhTGF-β1 (1.5ng/ml), purified DU145 exosomes (200µg/ml), or DU145 vesicle concentrates (control, Rab11b^{KD} or Rab35^{KD}) corrected for cell number in DMEM-F12 media. Fibroblasts were examined by immunofluorescent microscopy for the expression of α-SMA (green) and DAPI (blue). Scale bar 50µm. Images of α-SMA positive cells over 6 microscopic fields were examined in duplicates per treatment. Representative fields are shown.

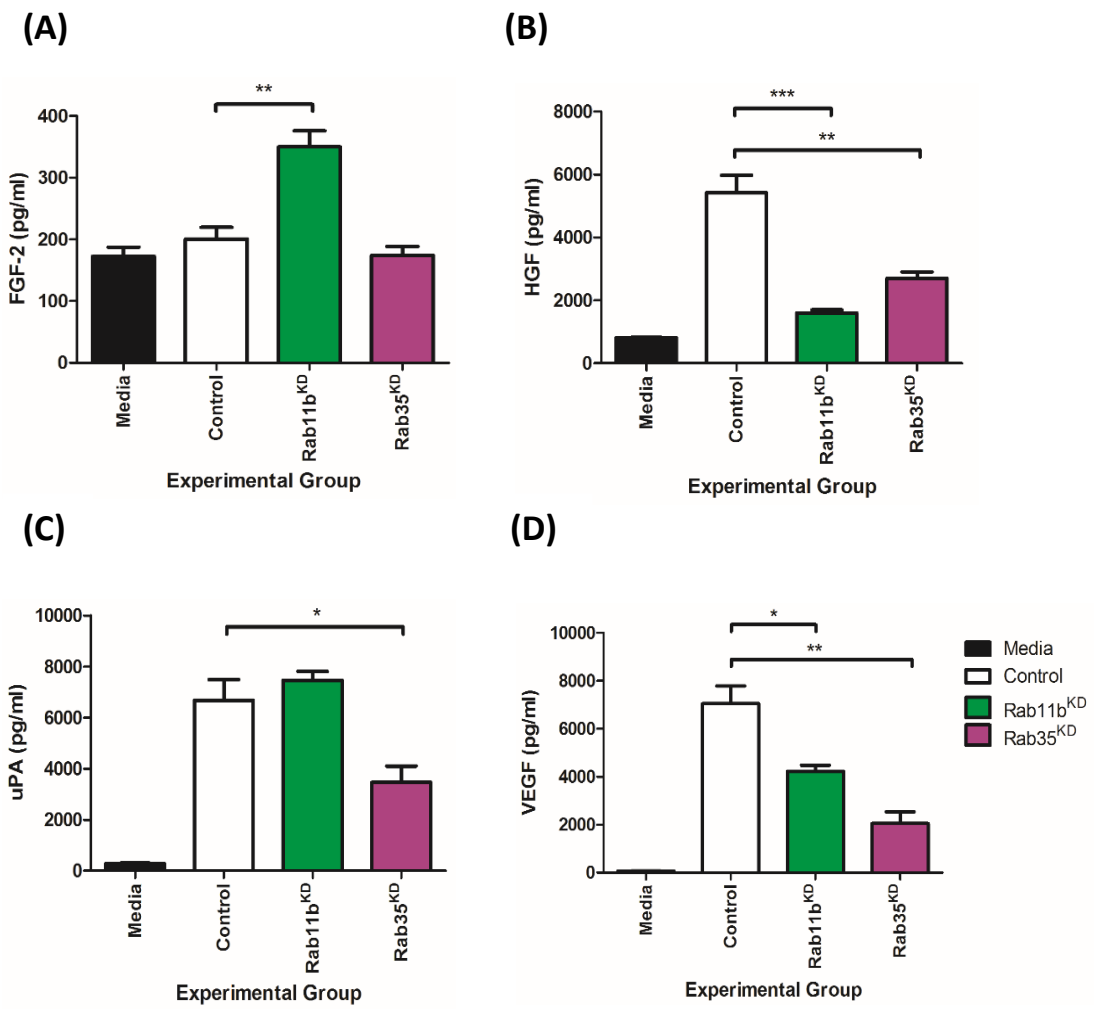

Figure 5.5: Vesicle concentrates from Rab11b^{KD} or Rab35^{KD} cell CM fail to fully induce fibroblast secretion of pro-angiogenic factors. Fibroblasts at passage 7 were growth arrested (72 hours) and were either left untreated, or treated in the presence of the DU145 vesicle concentrates (control, Rab11b^{KD} or Rab35^{KD}) corrected for cell number in DMEM-F12 media. CM collected from undifferentiated and differentiated fibroblasts was analysed by ELISA for levels of **(A)** FGF-2, **(B)** HGF, **(C)** uPA and **(D)** VEGF. Graph shows mean ± SEM, based on triplicate wells. n.s: non-significant, *P<0.05, **P≤0.01 and ***P≤0.001. One-way ANOVA with Tukey's post hoc test.

5.1.4 Quantification of Remaining TGF-β1 Positive Vesicles following Knockdown

Previously, as we observed a different fate in α-SMA expression, following treatment with vesicles following knockdown of Rab11b or Rab35, we examined if there were any changes in vesicle-associated TGF-β1 which accounted for this.

Vesicles derived from control or knockdown cells were treated with HCl, to activate the latent TGF-β1 on the vesicle's surface to the immunoreactive form, detectable by the TGF-β1 ELISA (Figure 5.6). A consistent expression of TGF-β1 was observed among the control vesicle, in which 7.2pg of TGF-β1 was expressed per µg of DU145 vesicles, similar to previous studies (Clayton et al., 2007, Webber et al., 2010). We, therefore, questioned if perturbation of the Rab GTPases would interfere the TGF-β1-positive signal on vesicles. We revealed there was 4.8pg of TGF-β1 expressed per µg of DU145 Rab11b^{KD} derived vesicles (33% decrease) ($P<0.01$), compared to controls. Similarly, 4.1pg of TGF-β1 was detected in DU145 Rab35^{KD} derived vesicles (44% decrease) ($P<0.001$), compared to controls. This suggests that the presence of Rab11b or Rab35 must be required for vesicles that are expressing high TGF-β1 content, in relation to the entire vesicle population.

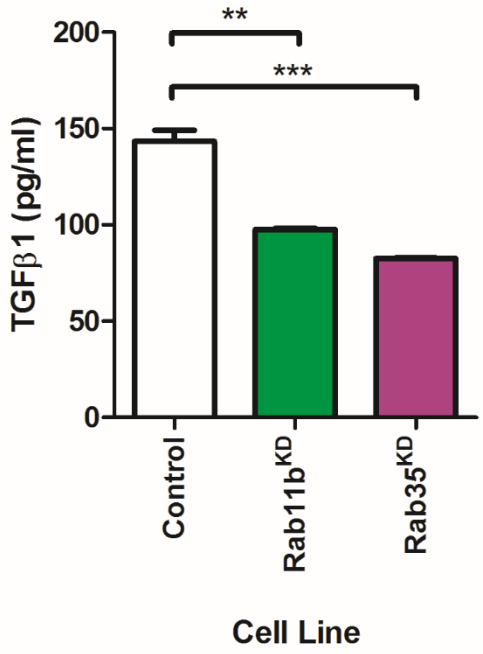

Figure 5.6: Reduced TGF-β1 expression on vesicles derived from DU145 Rab11b^{KD} or Rab35^{KD} cells. CM underwent a differential ultracentrifugation method, followed by filtration through a 0.22µm filter, before ultracentrifugation at 200,000 x *g* for 2 hours in a fixed angle 70Ti rotor to obtain vesicle concentrates. Vesicle concentrates from DU145 control or Rab11b^{KD} or Rab35^{KD} cells (20µg/well) and corrected for cell number were added to a 96-well plate coated with a TGF-β1 capture antibody. Vesicles were subjected to acid activation and expression of active TGF-β1 were measured using a TGF-β1 ELISA. Graph shows mean ± SEM, based on duplicate wells. **P≤0.01 and ***P≤0.001. One-way ANOVA with Tukey's post hoc test.

5.1.5 Rab11b- and Rab35-Dependent Vesicles are Required for Stromal Activation

Previously we have shown that knockdown of Rab11b or Rab35 results in a loss of TGF-β1 positive vesicles from DU145 cells, which results in a poor differentiation response. We, therefore, examined if this functionality is dependent on the exosome dose required to trigger a fibroblast differentiation response or if it were due alterations in the vesicle's phenotype following knockdown.

Fibroblasts were grown and growth-arrested as described previously. Briefly, fibroblasts were grown in DMEM-F12 media alone or with a single stimulation with rhTGF-β1 (1.5ng/ml) or purified DU145 exosomes at an equivalent TGF-β1 dosage (200µg/ml). Importantly, unlike our previous experiments, the vesicle concentrates were added at equal quantities (200µg/ml) to the fibroblasts, to negate any effects on knockdown on vesicle secretion amount. Untreated fibroblasts exhibited low level/negligible staining of α-SMA and positive control exosomes from wild-type DU145 cancer cells stimulated the onset of α-SMA in the entire cell population (Figure 5.7). Similarly, stimulation with rhTGF-β1 generated a robust differentiation response. Vesicle concentrates obtained from DU145 control cell CM triggered a strong differentiation response, involving the majority of the fibroblasts in the population. Treating fibroblasts with vesicle concentrates derived from knockdown of Rab11b showed a moderate differentiation response; whilst some α-SMA was detectable. Though, vesicles derived from knockdown of Rab35 showed a poor differentiation response. Whilst some α-SMA was detectable, this was weaker in intensity and not all cells had responded. Here, adding the identical quantity of vesicle from the cancer cell CM gives a different fibroblast response. We concluded that the knockdowns modulate a distinct vesicle phenotype and this results in defective cancer cell stromal influence.

We also observed a significant increase in both HGF and VEGF secretion when using vesicle concentrates from control cells. In contrast, there was a significant reduction in secreted HGF (Figure 5.8 A) in treated conditions for $Rab11b^{KD}$ ($P \leq 0.01$) and $Rab35^{KD}$ ($P \leq 0.05$). Also, levels of VEGF secretion (Figure 5.8 B) followed this trend, when using either knockdown of Rab11b ($P \leq 0.05$) or Rab35 ($P \leq 0.05$). By equalising vesicle quantity, it was not sufficient to negate the effects of the knockdowns. These effects, therefore, must be due to the changes occurring in the vesicle's molecular phenotype, following attenuation of Rab11b or Rab35.

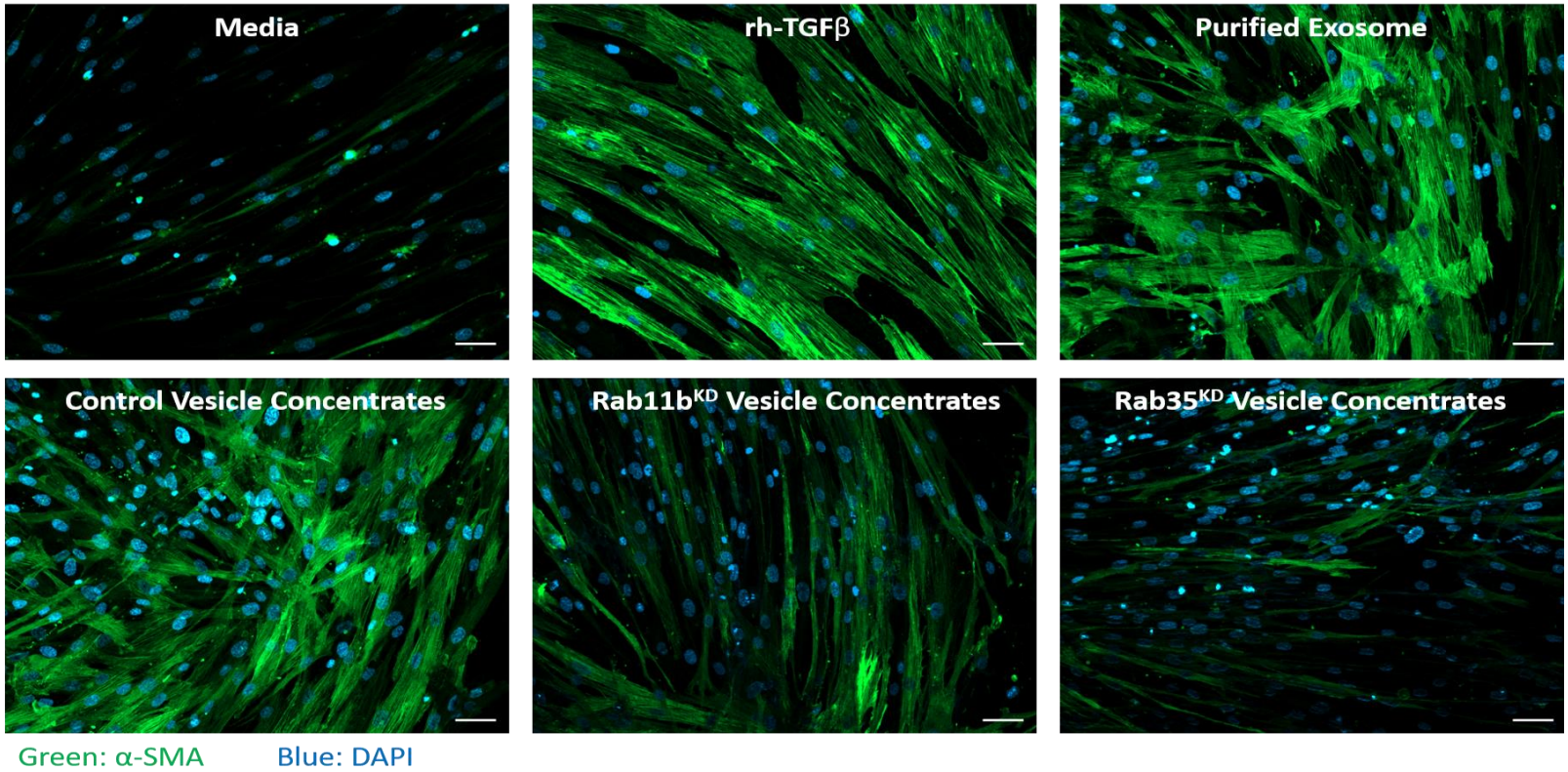

Figure 5.7: Rab11b- or Rab35-dependent vesicles are still required for stromal activation. Fibroblasts at passage 7 were growth arrested (72 hours) and were either left untreated, treated in the presence of rhTGF-β1 (1.5ng/ml), purified DU145 exosomes (200µg/ml), or DU145 vesicle concentrates (control, Rab11b^{KD} or Rab35^{KD}) corrected for protein (200µg/ml) in DMEM-F12 media. Fibroblasts were examined by immunofluorescent microscopy for the expression of α-SMA (green) and DAPI (blue). Scale bar 50µm. Images of α-SMA positive cells over 6 microscopic fields were examined in duplicates per treatment. Representative fields are shown.

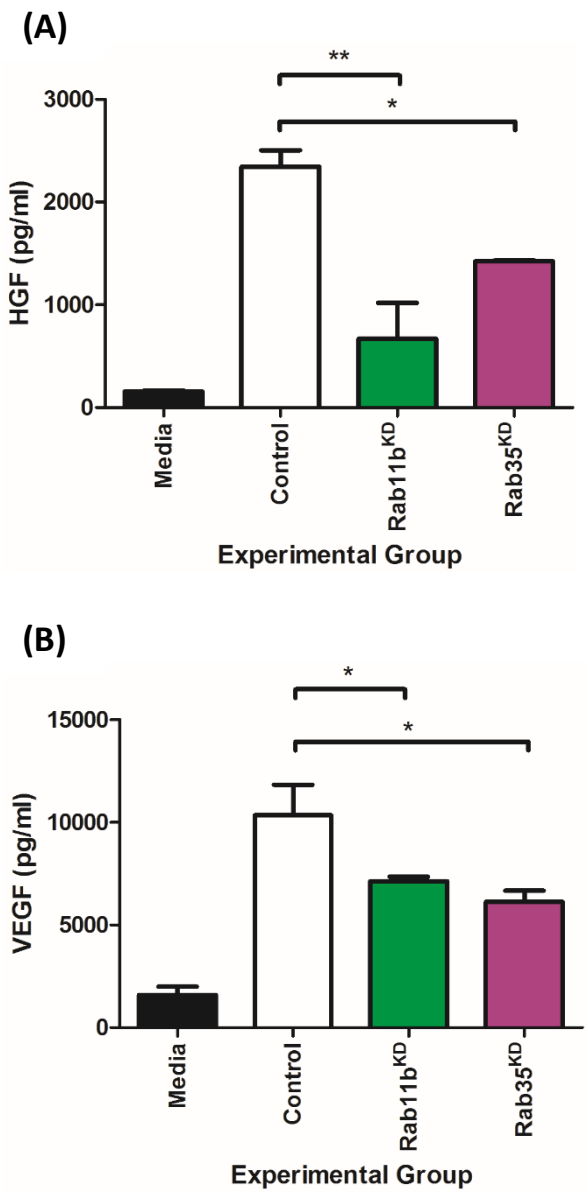

Figure 5.8: Normalised vesicle concentrates by quantity from Rab11b^{KD} or Rab35^{KD} CM, reduces fibroblast secretion of pro-angiogenic factors. Fibroblasts at passage 7 were growth arrested (72 hours) and were either left untreated, or treated in DU145 vesicle concentrates (control, Rab11b^{KD} or Rab35^{KD}) corrected for protein (200µg/ml) in DMEM-F12 media. CM collected from undifferentiated and differentiated fibroblasts was analysed by ELISA for levels of **(A)** HGF and **(B)** VEGF. Graph shows mean ± SEM, based on duplicate wells. *P<0.05 and **P≤0.01. One-way ANOVA with Tukey's post hoc test.

5.1.6 Fibroblasts Treated with Vesicles From Knockdown of Rab11b or Rab35 are not Pro-Motile

One key aspect of tumour-associated myofibroblasts is their influence on an angiogenic response. Previously, our group demonstrated that purified cancer exosomes can generate a pro-angiogenic stromal microenvironment (Webber et al., 2015). For angiogenesis to occur, endothelial cell migration is crucial and a simple method to quantify this, is the 'scratch' migration assay (Liang et al., 2007). The creation of an artificial gap to an endothelial cell monolayer so called 'scratch', allows the cells on the newly created edge to migrate to close the 'scratch', until new cell-to-cell contacts are re-established. This motility may be heightened by a particular stimulus. Here, we assessed the effects of CM from fibroblasts following treatments with either cancer cell secretome or vesicle concentrates (control or Rab11b^{KD} or Rab35^{KD} derived) on endothelial cell motility, using a monolayer scratch assay.

A monolayer of HUVEC cells, cultured in EBM-2 media was established. Once fully confluent, these were growth-arrested for 24 hours to remove pro-motility factors in the supplemented media, followed by formation of a vertical scratch by a 200µl pipette tip. The endothelial cell media was replaced with CM from either untreated (EBM-2 only) or fibroblasts treated with the cell secretome (control or Rab11b^{KD} or Rab35^{KD}). Endothelial cell motility in response to the different treatments was examined by imaging and measuring scratch closure over the 24-hour period (Figure 5.9 A). From an early timepoint of 6 hours, the endothelial scratch closure in response to untreated or CM from treated fibroblasts with knockdown cell secretome was less than 10% (Figure 5.9 B). In contrast, the endothelial cell response to the CM from fibroblasts treated with the control cell secretome showed an accelerated response of 30% closure by 6 hours; achieving almost 70% closure within 24 hours. In contrast, untreated or knockdown-treated CM was slower in closure, reaching only around 30% closure in the same timeframe ($P \leq 0.001$).

Next, we, therefore, questioned if CM from vesicle-treated fibroblasts would accelerate endothelial cell motility, compared to the cancer cell secretome-treated fibroblasts. HUVEC monolayers were established, as described previously, but endothelial cell media was replaced with CM, from untreated or DU145 vesicle concentrates (control or Rab11b^{KD} or Rab35^{KD}) treated fibroblasts (Figure 5.10 A). Endothelial cell motility was markedly quicker (30%~) at 6 hours in response to CM from vesicle-treated fibroblasts, compared to the cancer cell secretome-treated fibroblasts (~10%) (Figure 5.9 B). From an early timepoint at 6 hours, endothelial scratch closure in response to CM from untreated or CM from treated fibroblasts with Rab11b^{KD} or Rab35^{KD} vesicle concentrates was less than 30% (Figure 5.10 B). In contrast,

the endothelial cell response to CM from normal vesicle-treated fibroblasts marked an accelerated response of 60% closure, achieving full closure by 18 hours; quicker than fibroblasts treated with the cancer cell secretome (50%) (Figure 5.9 B). In contrast, the closure rate was slower at 18 hours, reaching only <40% in untreated ($P<0.001$) and <60% in knockdown of Rab11b and Rab35 in the same timeframe ($P\leq0.001$).

Therefore, the soluble factors secreted from fibroblasts treated with vesicles accelerated endothelial cell migration, compared to fibroblasts treated with the cancer cell secretome; indicating this stimulus is enhanced by vesicles. This influence, suggests that to promote a highly pro-motile influence over endothelial cell, stromal cells activated by vesicles is required and the effect is strongly attenuated using knockdown of Rab11b or Rab35.

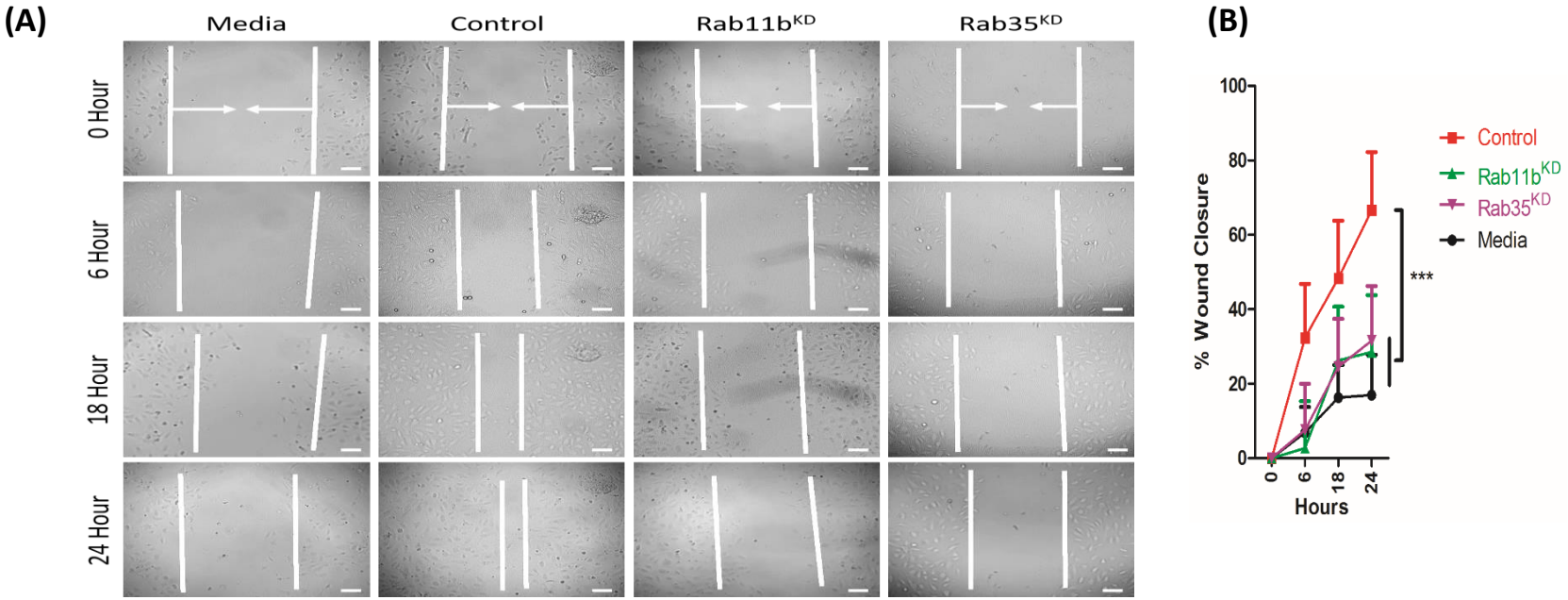

Figure 5.9: CM from fibroblasts treated with Rab11b^{KD} or Rab35^{KD} cell secretome, slows endothelial cell motility. (A) Growth-arrested primary fibroblasts were treated with the control or Rab11b^{KD} or Rab35^{KD} cancer cell secretome, normalised for input cell number. After 3 days, the fibroblast CM was harvested and added to monolayers of human endothelial cells that had been freshly scratched using a 200µl pipette tip. The closure of the scratch was monitored microscopically up to 24 hours thereafter. Representative images of wells at scratch initiation and at 24 hours are shown and the margin of the scratch emphasised by the white lines. Scale bar: 100µm. **(B)** Measurements of scratch gap were taken throughout the time course and are plotted as the proportion of scratch width relative to that at 0 hours, at each time point. Graph shows mean ± SEM, based on quadruplicate wells. ***P≤0.001. Two-way ANOVA with Bonferroni post hoc test.

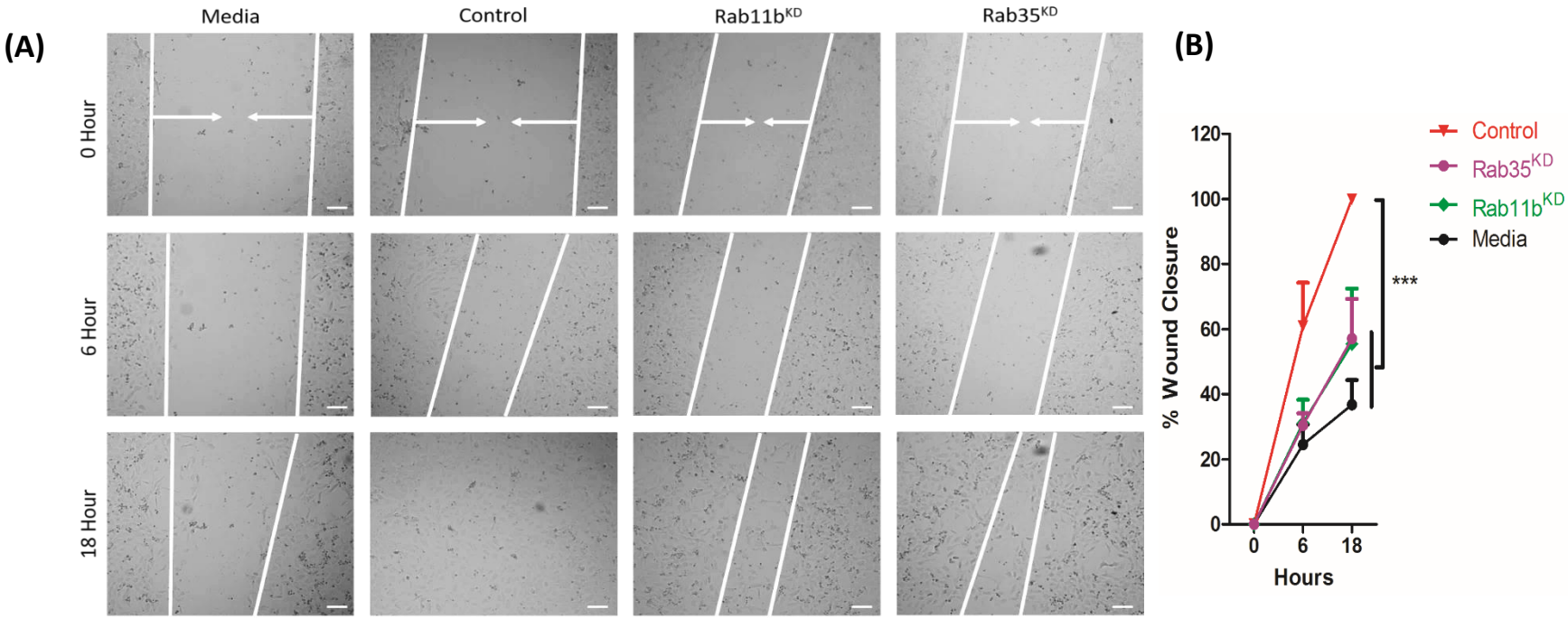

Figure 5.10: CM from fibroblast treated with vesicles from Rab11b^{KD} or Rab35^{KD} cells, slows endothelial cell motility. (A) Growth-arrested primary fibroblasts were treated with vesicles from control or Rab11b^{KD} or Rab35^{KD} cells, normalised for input cell number. After 3 days, the fibroblast CM was harvested and added to monolayers of human endothelial cells that had been freshly scratched using a 200µl pipette tip. The closure of the scratch was monitored microscopically up to 18 hours thereafter. Representative images of wells at scratch initiation and at 18 hours are shown and the margin of the scratch emphasised by the white lines. Scale bar: 100µm. **(B)** Measurements of scratch gap were taken throughout the time course and are plotted as the proportion of scratch width relative to that at 0 hours, at each time point. Graph shows mean ± SEM, based on quadruplicate wells. ***P≤0.001. Two-way ANOVA with Bonferroni post hoc test.

5.1.7 Rab11b^{KD-} or Rab35^{KD-} Derived Vesicles Fail to Trigger Angiogenesis-Promoting Stroma

The formation of blood vessels coordinates a combination of endothelial cell proliferation, migration and structural organisation into vessel-like structures (Adams and Alitalo, 2007). To investigate the potential for endothelial cells to not only migrate, but to organise into vessel-like structure, was performed through co-culture of pre-treated fibroblasts with endothelial cells (Sheldon et al., 2010). Fibroblasts were left untreated with DMEM-F12 media alone or treated for 72 hours with a single stimulation with rhTGF-β1 (1.5ng/ml), purified DU145 exosomes at an equivalent TGF-β1 dosage (200µg/ml) or vesicle concentrates (control or Rab11b^{KD} or Rab35^{KD}) corrected for cell number. After stimulation, endothelial cells were added in a random drop-wise fashion to the wells and left untreated for 96 hours. The cells were fixed and stained for the endothelial cell marker, CD31, absent in fibroblasts.

The data demonstrated in either untreated or rhTGF-β1 treated fibroblasts, there were rare clusters of CD31-positive cells formed, with little evidence of newly developed structures (Figure 5.11). In contrast, purified wild type DU145 exosomes showed the generation of often thick, elaborate CD31-positive structures, comprising hundreds of individual cells. There was little evidence of structures generated with the fibroblasts treated with the control cell secretome or with knockdown of Rab11b or Rab35. It suggested that although the CM could support motility, their influence is limited and fails to promote a more sophisticated and mature endothelial structure, with limited effects on vessel formation. We, therefore, questioned whether vesicles dependent on Rab11b or Rab35, can support these vessel-like structures to form.

Similarly, untreated or rhTGF-β1 treated fibroblasts gave rare clusters of CD31-positive cells, with little evidence of endothelial cell structures (Figure 5.12 A). In contrast, purified wild type DU145 exosomes and control vesicle concentrates showed the generation of often thick, elaborate CD31-positive structures comprising hundreds of individual cells and occupying most of the microscopic field. There were a relative lack of structures generated with either DU145 Rab11b^{KD-} or Rab35^{KD-} derived vesicles. These were comprised of tens, rather than hundreds, of cells. Measuring the area occupied by the CD31-positive structures allowed for a straightforward means of quantifying this pro-angiogenic behaviour (Figure 5.12 B). This revealed a significant increase in CD31-positive surface area in response to controls, compared to the knockdown of Rab11b or Rab35 ($P<0.001$). Therefore, the vesicles which remain following knockdown of Rab11b or Rab35 are insufficient in numbers and/or

molecular composition, to trigger formation of a fibroblast with a positive influence on vessel forming capacity of endothelial cells. Together, these findings suggest that Rab11b- or Rab35-dependent vesicles play roles in activating the stroma, in terms of fibroblast differentiation and supporting the formation of vessel-like structures.

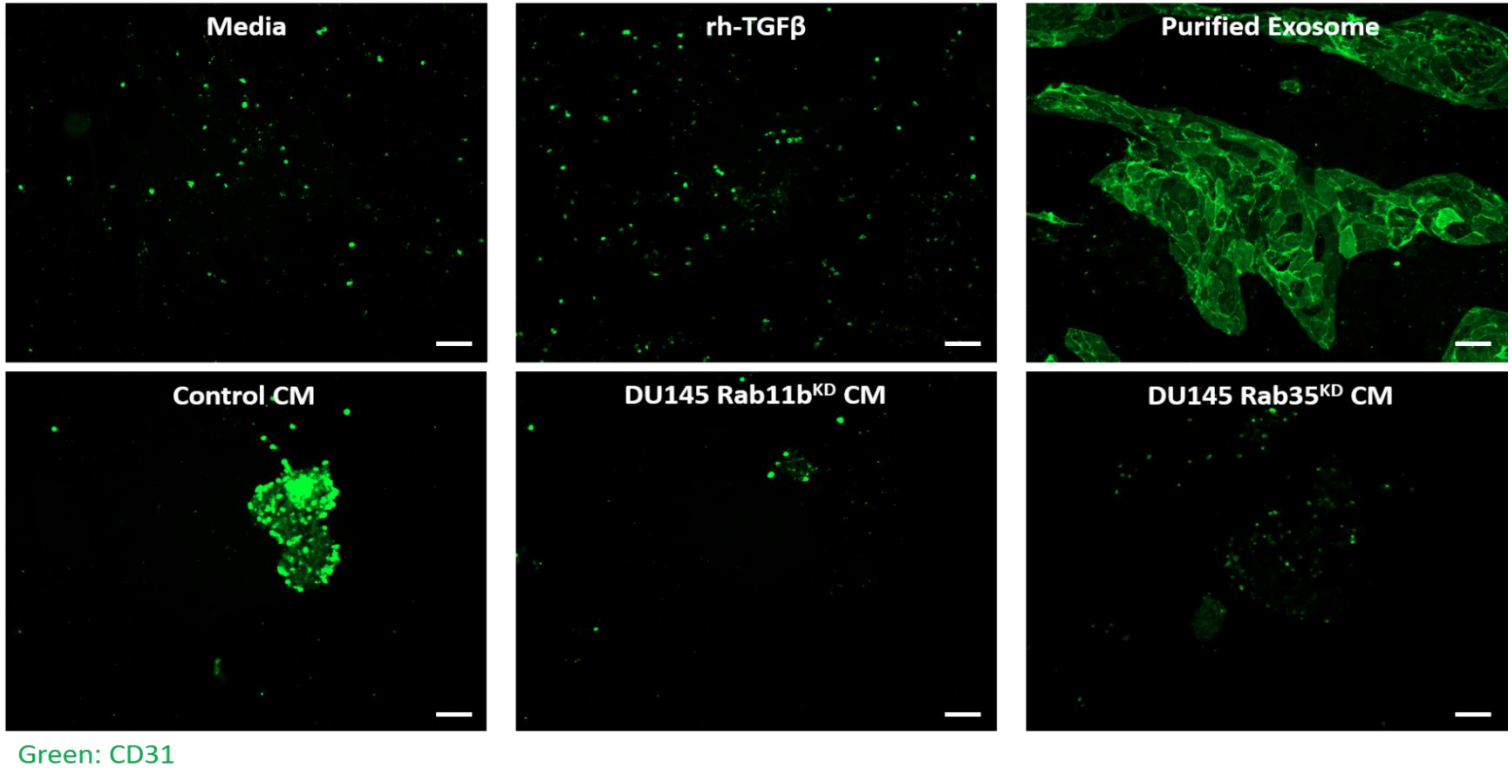

Figure 5.11: Cancer cell secretome fails to stimulate fibroblasts to support endothelial vessel-like structure formation. Growth-arrested primary fibroblasts were treated with the cancer cell secretome derived from control or Rab11b^{KD} or Rab35^{KD} cells, normalised for input cell number. Similarly treated fibroblasts at day 3 were subject to the addition of endothelial cells (20,000 cells/well), in a randomly placed, drop-wise fashion. Co-cultures were maintained undisturbed for a further 4 days, before fixation and immunofluorescent staining with antibody against CD31. Images of CD31 positive cells were examined in duplicates per treatment are shown. Scale Bar: 100µm. Data are representative of three independent experiments.

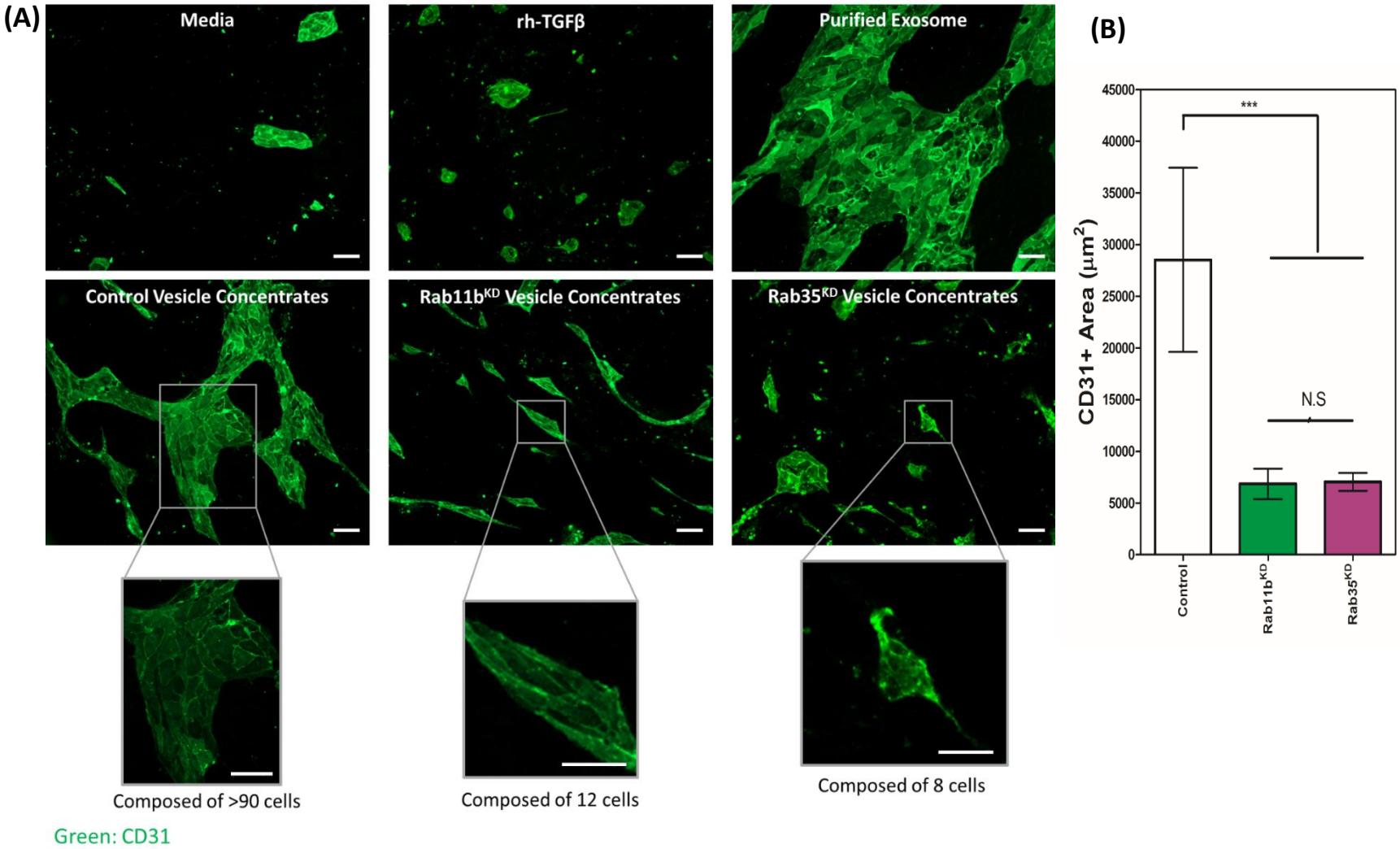
(A)
Media
rh-TGFβ
Purified Exosome
Control Vesicle Concentrates
Rab11b^KD Vesicle Concentrates
Rab35^KD Vesicle Concentrates
Composed of >90 cells
Composed of 12 cells
Composed of 8 cells
Green: CD31
(B)
CD31+ Area (μm²)
45000
40000
35000
30000
25000
20000
15000
10000
5000
0
***
N.S
Control
Rab11b^KD
Rab35^KD

Figure 5.12: DU145 Rab11b^{KD-} or Rab35^{KD-} derived vesicles render the stroma poorly angiogenic. (A) Growth-arrested primary fibroblasts were treated with vesicle concentrates derived from control or Rab11b^{KD} or Rab35^{KD} cells, normalised for input cell number. Similarly, treated fibroblasts at day 3 were subject to the addition of endothelial cells (20,000 cells/well), in a randomly placed, drop-wise fashion. Co-cultures were maintained undisturbed for a further 4 days, before fixation and immunofluorescent staining with antibody against CD31. Fluorescence (CD31-alexa-488) images of representative microscopic fields are shown. Selection from image showing endothelial vessel-like structures comprising of hundreds or tens of endothelial cells (inset). Scale Bar: 100µm. **(B)** The regions of CD31-positivity were measured using intensity thresholding in the Alexa-488 channel (Zeiss Zen software), to calculate the area occupied by endothelial cells. This was done on 4-microscopic fields in each well. Graph shows mean ± SEM, based on triplicate wells. n.s: non-significant ***P≤0.001. One-way ANOVA with Tukey's post hoc test.

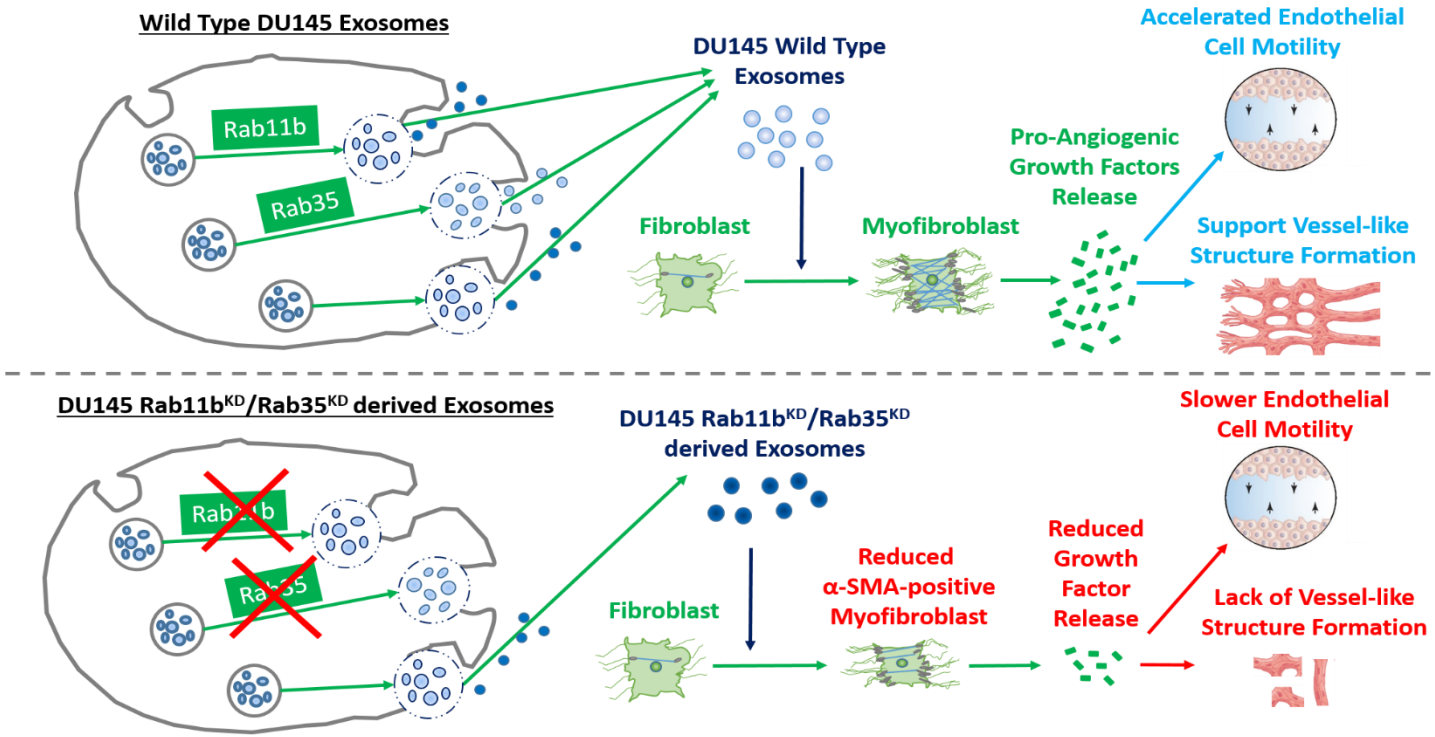

Figure 5.13: Diagram of the importance of Rab11b- or Rab35-dependent tumour vesicles on the stroma. Wild type exosomes can drive fibroblast differentiation into α-SMA positive myofibroblasts, secreting growth factors, accelerating endothelial cell motility and vessel-like structure formation. Here, we propose that in the absence of either Rab11b^{KD}/Rab35^{KD} derived vesicles, a reduction in α-SMA positive myofibroblastic cells are present, showing a reduction in secreted pro-angiogenic growth factors from myofibroblasts, thus slower endothelial motility and a lack of vessel like-structures formed.

5.2 Discussion

In this Chapter, we investigated the functional importance of tumour-derived Rab11b- and Rab35-dependent, vesicle subpopulations, by highlighting the vesicle populations following Rab11b or Rab35 knockdown and their interaction with the stroma, in terms of fibroblast differentiation and promotion of angiogenic properties.

Traditionally, TGF-β1 is an established cytokine essential for regulating fibroblast differentiation (Desmoulière et al., 1993, Sime et al., 1997, Thannickal et al., 2003). rhTGF-β1 treated fibroblasts, resulted in high levels of α-SMA positive cells, but secrete low levels of both HGF and VEGF (Chowdhury et al., 2015, Webber et al., 2015). In contrast, purified prostate cancer exosomes had the potent capacity to trigger fibroblast differentiation, as noted by the onset of α-SMA stress fibres, consistent with a previous study (Webber et al., 2010). Furthermore, exosome-treated fibroblasts secreted elevated levels of pro-angiogenic growth factors, HGF and VEGF, consistent with features akin to myofibroblastic stromal cells extracted from prostate cancer tissues, that have been 'educated' *in vivo* under the direction of the cancer milieu (Webber et al., 2015). These findings agree with lung cancer-derived, vesicles stimulating the stromal cells to produce factors that induce the expression of several pro-angiogenic factors, such as VEGF and MMP-9, that can enhance metastatic spread (Wysoczynski and Ratajczak, 2009). Similarly, melanoma derived vesicles, promoted fibroblast differentiation to myofibroblasts, that potentially regulates VCAM-1 and activates extracellular signal-regulated kinase 1/2 (ERK1/2) signalling pathways, promoting endothelial cell proliferation and migration during angiogenesis (Srinivasan et al., 2009, Zhao et al., 2015, Shin et al., 2016). Likewise, pancreatic cancer cell-derived vesicles, containing miR-155, also can trigger fibroblast differentiation (Pang et al., 2015). Taken together, the literature suggest that cancer-derived exosomes are crucial for generating tumour-associated myofibroblasts, conditioning the tumour microenvironment in promoting angiogenesis and metastasis.

Growing evidence suggests that the cancer cell secretome itself containing cancer exosomes, can promote fibroblast differentiation into myofibroblasts. CM taken from aggressive breast tumour cells induces fibroblast differentiation by potentiating TGF-β1 signalling, in both *in vitro* and *in vivo* models (Valenti et al., 2001, Avgustinova et al., 2016). Similarly, fibroblast treatment with ovarian cancer cell secretome resulted in α-SMA positive myofibroblastic-like cells, secreting elevated levels of HGF and VEGF (Yao et al., 2009). The cancer cell secretome from ovarian and cancer cells appear sufficient to trigger fibroblast

differentiation. Equally, with the prostate cancer model, our group have previously shown that the cell secretome is sufficient to trigger fibroblast differentiation and secreting elevated growth factors (Webber et al., 2015). However, our data demonstrates the cell secretome appears insufficient to trigger fibroblast differentiation, despite differences in the secretory profile. One explanation for this, could be the collection of the cancer cell CM was from densely seeded cell numbers in other studies, therefore a concentrated cell secretome, sufficient to trigger these responses. In contrast, our experiments may have been conducted using lower density of cell numbers, producing therefore a diluted cell secretome, insufficient to trigger the onset of fibroblast differentiation.

Initially, the first indications for Rab GTPases in exosome secretion were from reticulocyte cell lines, which required the function of Rab11 for exosome secretion (Savina et al., 2002). In an RNAi screen in HeLa cells targeting a host of Rab GTPase family members, silencing Rab27a reduced MVE docking, which significantly reduced the levels of secreted exosomes (Ostrowski et al., 2010). However, other studies using the Rab27a knockdown model have demonstrated that silencing Rab27a does not exclusively affect exosome secretion, but impacts other secretory routes for the cell, such as pro-MMP-9 secretion (Bobrie et al., 2012). Similarly, observations in another Rab27a knockdown model, reveal attenuated levels of exosome secretion, which also reduced secretion of pro-angiogenic soluble factors (PDGF-AA and osteopontin), derived from tumour cells, hindering bone marrow derived cells mobilisation and tumour growth (Peinado et al., 2012). Therefore, this makes interpretation of the data difficult, as findings may be due to soluble factors and not due to loss of vesicles. However, I found much of the stromal-activating activity is focused to the vesicular content of the secretome, observing stronger differentiation effects and a stronger angiogenic promoting phenotype. This demonstrates the effects on the soluble-secretome are not solely responsible for the functional defect arising (Webber et al., 2015). In our data, concentrating vesicles from the cell secretome triggered fibroblast differentiation, in much of the fibroblast population. The knockdowns, however, could not trigger differentiation similar to the control, even following vesicle concentration. Myofibroblastic differentiation is predominantly a vesicle-mediated effect and not governed by other factors derived from cancer cells. For this critical activation of tumour-associated myofibroblasts, we showed that vesicle secretion controlled by Rab11b or Rab35 is required.

Understanding precisely how myofibroblastic traits of the cancer-associated stroma are initiated, altering stroma from a normal homeostatic function towards a malevolent, or indeed, a protective phenotype; remains unclear. Although TGF-β, secreted by tumour cells

has remained a principal factor, studies from our group (Webber et al., 2010, Chowdhury et al., 2015, Webber et al., 2015), and others (Gu et al., 2012, Borges et al., 2013), have reported exosomes delivering TGF-β1 elicit robust stromal modulation in cancer. In our data, we demonstrate a 20% loss of vesicles following knockdown of either Rab11b or Rab35, that demonstrates defective α-SMA differentiation. Attenuating the vesicle population even by 20% may be sufficient to disrupt the required threshold for differentiation. The vesicles following knockdown of Rab11b or Rab35 show a loss of 30 – 40% of TGF-β1 positive vesicles, and it appears that these are needed to generate the robust differentiation response. Alternatively, there could be alterations in the vesicle's phenotype following knockdown of Rab11b or Rab35, that renders the remaining population deficient in fibroblast differentiation. In a simple experiment, normalising vesicles to a quantity to reach a threshold for activation was shown; and knockdown of Rab11b were still capable of driving differentiation. However, vesicles following knockdown of Rab35 remained deficient in differentiation ability, irrespective of normalisation. The data highlights that the vesicles following Rab11b knockdown are distinct in protein profile and differentiation capacity, compared to vesicle produced following Rab35 knockdown. This suggests that the Rab35-dependent vesicle subpopulation are required for fibroblast differentiation to myofibroblasts.

Angiogenesis is a complex process in which growth of new blood vessels can be described by multiple steps. Firstly, angiogenic stimuli cause increased endothelial cell permeability and cellular proliferation, which is followed by proteolysis of the basement membrane and ECM. Endothelial cell migration into the stroma of the neighbouring tissue, requires the cooperative MMP and plasminogen activator system, before endothelial cells trigger lumen formation as the sprout forms a vessel-like structure (Hoeben et al., 2004).

In this Chapter, I have demonstrated that CM from fibroblasts treated with the DU145 knockdown (Rab11b or Rab35) cell secretome can significantly slow endothelial cell migration, in comparison to controls. Here, the *in vitro* scratch assay is a frequently used technique to investigate endothelial cell motility (Xu and Deng, 2006, Shi et al., 2013, Chronopoulos et al., 2016). One downfall is that it does not replace well-established chemotaxis studies, such as the Boyden Chamber assay (Liang et al., 2007) and there is little physiological relevance. Still, the *in vitro* scratch assay is an inexpensive and straightforward method to study cell migration. Here, we show endothelial cells cultured in CM from untreated fibroblasts were poorly motile. This effect was similar to CM from fibroblasts

treated with vesicle concentrates from knockdown of Rab11b or Rab35, only achieving 50%~ closure by 18 hours; in contrast where full closure was seen in the control.

Endothelial cell migration is one essential aspect of angiogenesis and many different cytokines are involved in chemotactic endothelial cell migration. Some of the main promoters of actin-based motility include HGF, VEGF, bFGF, angiopoietins and other contributing factors, such as: PDGF, EGF, TGF-β, uPA and many more (Lamalice et al., 2007). VEGF is a potent inducer of endothelial cell proliferation and migration *in vitro* and *in vivo* (Ferrara, 1993, Bernatchez et al., 1999). Endothelial cell sensitivity to VEGF is exemplified, by the lethal vascular abnormalities that result from disrupting a single VEGF allele in mice (Carmeliet et al., 1996). Furthermore, VEGF-A is capable of binding onto multiple VEGFRs including VEGF-R1 and VEGF-R2. Upon VEGF binding, phosphorylation of tyrosine kinase residues on VEGF-R, activates the ERK pathway and p38/mitogen-activated protein kinase (MAPK) which induces cell proliferation, migration and increases vascular permeability (Murphy et al., 2006). Furthermore, HGF is a powerful motility factor in different cells, acting through the tyrosine kinase receptor, encoded by the MET oncogene (Bussolino et al., 1992). In various studies, heightened HGF levels interacts with its cognate receptor, c-Met; and promotes angiogenesis by elevating VEGF expression; and by stimulating endothelial cell migration and growth (Cai et al., 2000, Duan et al., 2004, Usatyuk et al., 2014). Interestingly, analysis of tumour-associated myofibroblasts showed elevated levels of both PDGF and PDGFR in a colorectal cancer model (Pena et al., 2013). PDGF appears to play a critical role in increasing endothelial cell migration during angiogenesis *in vitro*, by activating protein kinase A (PKA), increasing downstream vasodilator-stimulated phosphoprotein (VASP) phosphorylation; thus, increasing endothelial cell migration (Thommen et al., 1997, Zhang et al., 2010).

At the molecular level, HGF/c-Met signalling is proposed to activate multiple signal transduction pathways, including the p120/STAT3, the PI3K/Akt pathway, the Ras/MEK pathway and phosphorylating annexin-1 supporting angiogenesis. The p120/STAT3 pathway stimulates branching morphogenesis of cells (Boccaccio et al., 1998), the PI3K/Akt pathway activates cell motility and survival (Potempa and Ridley, 1998, Xiao et al., 2001), the Ras/MEK pathway mediates HGF-induced scattering and proliferation of cells (Ivan et al., 1997) and phosphorylating annexin-1 induces endothelial cell proliferation and migration (Pin et al., 2012). Therefore, these pathways may directly or indirectly stimulate endothelial cells: directly by morphogenic effects and indirectly by regulation of other angiogenic factors. As demonstrated in various studies, tumour-associated myofibroblasts can secrete various

growth factors and cytokines supporting angiogenesis (Kalluri and Zeisberg, 2006, Clark et al., 2013, Webber et al., 2015, Chowdhury et al., 2015). Therefore, we demonstrate that targeting the Rab11b or Rab35 vesicle secretion pathway, triggering a weakened fibroblast differentiation response with decreased levels of secreted HGF and VEGF; and possibly other related growth factors, thereby, slowing endothelial cell motility. The extent by what the fibroblast secretes by sub-optimal stimulation due to Rab vesicles is not yet understood, but a worthwhile avenue for more expansive studies.

As angiogenesis is a complicated event that requires interactions among different cells, growth factors and matrix components, a single “gold standard” assay to capitulates all these events is currently unavailable. More commonly used, the *ex vivo* explant assay involving a 3D mouse aortic ring, is considered more physiological relevant, because the system includes the surrounding non-endothelial cells (pericytes and smooth muscle cells) and a supporting matrix, in contrast to traditional cell-based assays (Bellacen and Lewis, 2009). Also, the endothelial cells have not been altered by repeat passaging, thus making them quiescent at the beginning of explantation, hence, more representative of the *in vivo* situation, where angiogenesis is stimulated and quiescent endothelial cells respond by migration, proliferation from existing vessels and differentiating into tubules (Staton et al., 2004). However, this method has its downfalls, including the necessity for fresh mouse tissue, species differences compared to humans, a lack of non-aortic tissues; and vessel regression over time giving them a restricted time for analysis (Baker et al., 2011). Also, endothelial cells derived from veins, such as HUVECs, are more applicable for studying angiogenesis, as they are prone to generating capillaries, albeit ideally the source should be microvascular endothelial cells best derived from the tissue organs, similar to those found at tumour sites, unlike endothelial cells from aortic vessels (dela Paz and D'Amore, 2009).

Here, we used the co-culture method (fibroblasts with endothelial cells), which allowed us to assess the specific stromal influence on the formation of vessel-like structures, unlike the aortic ring model. Fibroblasts provide critical support for the proliferation and migration of endothelial cells, in part, this is mediated through the secretion of pro-angiogenic growth factors (Jain, 2003, Nagy, 2003). Furthermore, similar observations showed endothelial cell migration, forming branching vessel-like structures that was dependent upon the presence of fibroblasts. Tumour cells that released VEGF could not replace fibroblasts in these interactions (Velazquez et al., 2002). Here, exosome-generated myofibroblasts can secrete pro-angiogenic growth factors, aiding the formation of endothelial vessel-like structures. This was shown in a similar gastric cancer exosome model, inducing VEGF expression in

stromal fibroblasts, which accelerated the vessel formation assay in HUVECs *in vitro* and *vivo* (Guo et al., 2008). Yet, vesicles remaining following attenuation of the Rab11b or Rab35 secretory pathway could only trigger weakened stromal activation, with decreased levels of secreted HGF and VEGF, thus reflecting the failure of these vesicles to promote a pro-angiogenic function in stromal cells. The cancer cell secretome derived from knockdown of Rab27a, also failed to trigger fibroblast differentiation and lacked pro-angiogenic effects, in terms vessel-forming capability (Webber et al., 2015).

Therefore, in this Chapter, I have shown that targeting the Rab11b or Rab35 vesicle sub-population has major effects on cancer to stroma communication. Although there remains notable vesicles secretion (80%) by these cells, this remaining subpopulation is dysfunctional in driving fibroblast differentiation into myofibroblasts. The stromal cells that arise also exhibit attenuated support for angiogenesis. Therefore, the production of vesicle that dependent on Rab11b or Rab35 are important elements in stromal regulation by cancer cells.

CHAPTER 6:

THE IMPACT OF EXOSOME-DEFICIENT TUMOUR CELLS IN A 3D CO-CULTURE MODEL

6.1 The Impact of Exosome-Deficient Tumour Cells and Fibroblasts in a 3D Co-Culture Model

6.1.1 Introduction

Cancer develops in a complex tissue environment, which depend upon continuous growth, invasion and metastasis. Studies have shown that tumour-derived exosomes are capable of "re-educating" fibroblasts within the stroma to an activated phenotype, supporting ECM remodelling and tumour invasion (Yang and Robbins, 2011, Webber et al., 2015). For example, myofibroblasts isolated from breast carcinomas compared to normal mammary fibroblasts from the same patient, contribute to enhanced tumour invasion and growth *in vivo* (Olumi et al., 1999). An altered stromal microenvironment is a feature of many aggressive tumours and consistently, myofibroblasts are commonly found in the stroma of carcinomas, often concentrated at the invasive margin of the tumour (Lewis et al., 2004, Karagiannis et al., 2013, Li et al., 2016). CM from these tumour-associated myofibroblast contains elevated levels of HGF, VEGF or MMPs, suggested to promote the invasive capacity of myofibroblast and carcinoma cells through collagen and matrigel matrices (De Wever et al., 2004, Cat et al., 2006, Ding et al., 2015). This highlights the importance of myofibroblasts in tumour invasion. In particular, interactions between tumour cells and the associated disease stroma represents a powerful relationship that influences disease progression and poor prognosis (Joyce and Pollard, 2009). Currently, information on exosomal communication, controlling the interplay between cancer cells and stromal myofibroblasts remains limited *in vivo*, as it is difficult to recapitulate this exact environment *in vitro*.

Evidence has suggested that three dimensional (3D) cell culture models represent the microenvironment accurately, where cells resides in tissue, compared to 2D culture systems (Kim, 2005). Within 3D culture conditions, there exists a pathophysiological gradient this is representative of that *in vivo*, compared to 2D culture (Benya and Shaffer, 1982, Nelson and Bissell, 2005, Baharvand et al., 2006). This added dimensionality leads to quite different cellular responses, because not only does it influence physical constraints of the cell, but it also promotes the spatial orientation of cell surface receptors engulfed in surrounding cells. These physical and spatial features in 3D culture affects the signal transduction from outside and into the cell, ultimately influencing gene expression and cellular behaviour in a profound manner (Takahashi et al., 2015).

Previous studies have reported the importance of cancer exosomes in activating the stroma (Webber et al., 2010), that can provide a tumour-supporting environment to support tumour invasion *in vitro* (Chowdhury et al., 2015) and growth *in vivo* (Webber et al., 2015). It remains unclear whether a Rab11b- or Rab35-dependent vesicle subpopulations from tumour cells can maintain this crosstalk to fibroblasts within a 3D cell culture model. The previous Chapter provided evidence that the Rab11b- or Rab35-dependent vesicle subpopulations can play roles in stroma activation, that can support a pro-angiogenic phenotype. Whether these functional *in vitro* assays can be recapitulated within a 3D microenvironment will be explored.

In this Chapter, we will first characterise 3D cell spheroid generation methods with tumour cells alone, or co-cultured with fibroblasts. We hypothesise that the remaining vesicle subpopulations, following knockdown of Rab11b or Rab35, can exert an influence on 3D culture models, in terms of spheroid generation and growth as examples. The invasive capacity of these 3D cell spheroids will be explored and their potential mechanism of action will be investigated. The hypothesis is that the vesicles remaining following knockdown of Rab11b or Rab35 in tumour cells, will severely attenuate the capacity for tumour growth in a 3D structure and propose these findings may be recapitulated *in vivo*.

6.1.2 Optimisation of 3D Co-Culture with Tumour Cells and Fibroblasts

3D spheroid growth of established tumour cell lines is regarded as a stringent and representative model when performing *in vitro* drug screening. They possess several *in vivo* features of aggressive solid cancer, such as cell-to-cell interaction (Baker and Chen, 2012), hypoxia (Doublier et al., 2012), production/deposition of ECM (Kimlin et al., 2013) and tumour invasion (Weiswald et al., 2015). Here, homotypic (tumour cells alone) or heterotypic (tumour cells with fibroblasts) spheroids were used to evaluate spheroid growth and the influence of DU145 Rab11b or Rab35 knockdowns.

The DU145 CTR or Rab11b^{KD} or Rab35^{KD} cells were incubated alone or together with fibroblasts at a ratio of 4 tumour cells : 1 fibroblast in cell-repellent plates. Here, two methods were used to generate and characterise 3D spheroid cell culture: a Poly-HEMA coated plate (cell repellent) or CELLSTAR® cell-repellent surfaces, obtained from Greiner Bio-One (GBO, UK). The spheroids were cultured in RPMI-1640 in 10% exosome-depleted FBS and every other day, 50% of the culture media was replaced with fresh media, as other methods used to generate spheroids (Hirschhaeuser et al., 2010, Vinci et al., 2012, Weiswald et al., 2015).

Spheroids were fully established at day 3 (Figure 6.1 A), with cells seeded at a density of either 1,000, 5,000 or 10,000 cells (4 tumour control cell: 1 fibroblast) on a poly-HEMA-coated 96-well round-bottomed plates. Some cellular debris was present around the spheroid's periphery, in different cell seeded conditions. The free hand tool on Image J was used to measure spheroid's diameter and area. The morphology of different cell seeded spheroids looks spherical, comparing day 3 to day 13 images. Cells seeded at 1,000 cells had an average diameter of 220µm; a diameter of 400µm at 3,000 cells; and a diameter of 580µm at 10,000 cells (Figure 6.1 B). In terms of area, a 1,000-cell spheroid had an average area of 50,000µm^2; an area of 100,000µm^2 at 3,000 cells; an area of 260,000µm^2 at day 3 and an area of 200,000µm^2 at day 13 ($P<0.001$) at 10,000 cells (Figure 6.1 C). This showed that as more cell numbers were seeded, diameter and area both increased. It was observed that in replicate 10,000 cell spheroids, they were robust and stable generated spheres that could be handled, compared to smaller cell numbers as they would become fragile, when assessed for other functional experiments. Such smaller sized spheroids that were fragile could not be modelled without disrupting their structure. Therefore, we proceeded seeding 10,000 cells to generate 3D spheroids.

As an example of spheroid generation, time-lapse imaging of cells aggregating together over 72 hours is shown (Figure 6.2). Cells seeded at a density of 10,000 cells (tumour:fibroblast) can aggregate into a compact 3D spheroid, with the spheroid's core becoming darker, compared to the spheroid's periphery by 16 hours. Possibly, the larger seeded cell numbers are shrinking and becoming compact within the inner spheroid core, as light must travel through more thickness.

Next, we measured spheroid growth over a 24-day period, either in spheroids containing DU145 control, Rab11b^{KD} or Rab35^{KD} cells, or in the presence or absence of fibroblasts (Figure 6.3 A) by the Poly-HEMA method. All tumour or tumour:fibroblast spheroids were stable upon generation. By day 4, the spheroid's diameter (Figure 6.3 B) was smaller (650µm) in spheroid's containing fibroblasts, compared to tumour cells alone (750µm). There was a 35% decrease in area (~250,000µm^2), in spheroid's containing fibroblasts (Figure 6.3 C), compared to tumour cells alone (~380,000µm^2) ($P<0.05$). By day 13, all spheroid's diameter and area had shrunk by 20%-30% (~500µm:~200,000µm^2). However, from day 17, all spheroids increased in spheroid size by 20% (~600µm:~250,000µm^2). There were no significant differences in size between spheroids containing exosome-deficient or competent tumour cells, or in the absence or presence of fibroblasts in spheroids. Though, the observed biphasic changes in a 3D sphere was unexpected and is difficult to interpret. Perhaps, this may be related to the uneven coating poly-HEMA to these plates that may explains these changes.

In contrast, spheroids generated with the GBO cell-repellent surfaces plates, coated with a polymer still induced spheroid formation. This method maintained a steady spheroid size increase, showing a darker inner core over 24 days (Figure 6.4 A). Possibly, larger spheroids over time have greater inner quiescent cells that die through necrosis; thus a darker necrotic core. By day 4, the diameter and area (Figure 6.4 B & C) of spheroids were 10%-15% smaller in size (575µm:275,000µm^2), in the presence of fibroblasts, compared to tumour cells alone (675µm:305,000µm^2). By day 24, the diameter and area on average increased by 5%-20% (690µm:350,000µm^2), in fibroblast containing spheroids and similarly shown in spheroids containing tumour cells only. We failed to observe any significantly differences in spheroid growth by comparing spheroids containing or lacking fibroblasts, or the presence or absence of DU145 Rab11b^{KD} or Rab35^{KD} cells. Hence, we failed to discriminate each homotypic or heterotypic spheroid by size alone.

Next, we compared both spheroid generation methods (Poly-HEMA vs GBO). There was a consistent increase in spheroid size by using the GBO method (Figure 6.5), compared to Poly-HEMA. Furthermore, fluctuations in spheroid size by the Poly-HEMA method remained difficult to ascertain, whether this was due to the knockdown effect or spheroid generation method. Over time, we observed a consistent increase in spheroid size with the GBO method and a dark spheroid inner core, proposed to be a necrotic cell core similar with other 3D cell spheroid studies (Hirschhaeuser et al., 2010, Godugu et al., 2013, Takahashi et al., 2015). Therefore, the reliability issues with generating spheroids, together with minimal fluctuations in size parameters, parallel with other studies the GBO method will be implemented for future experiments within this Chapter.

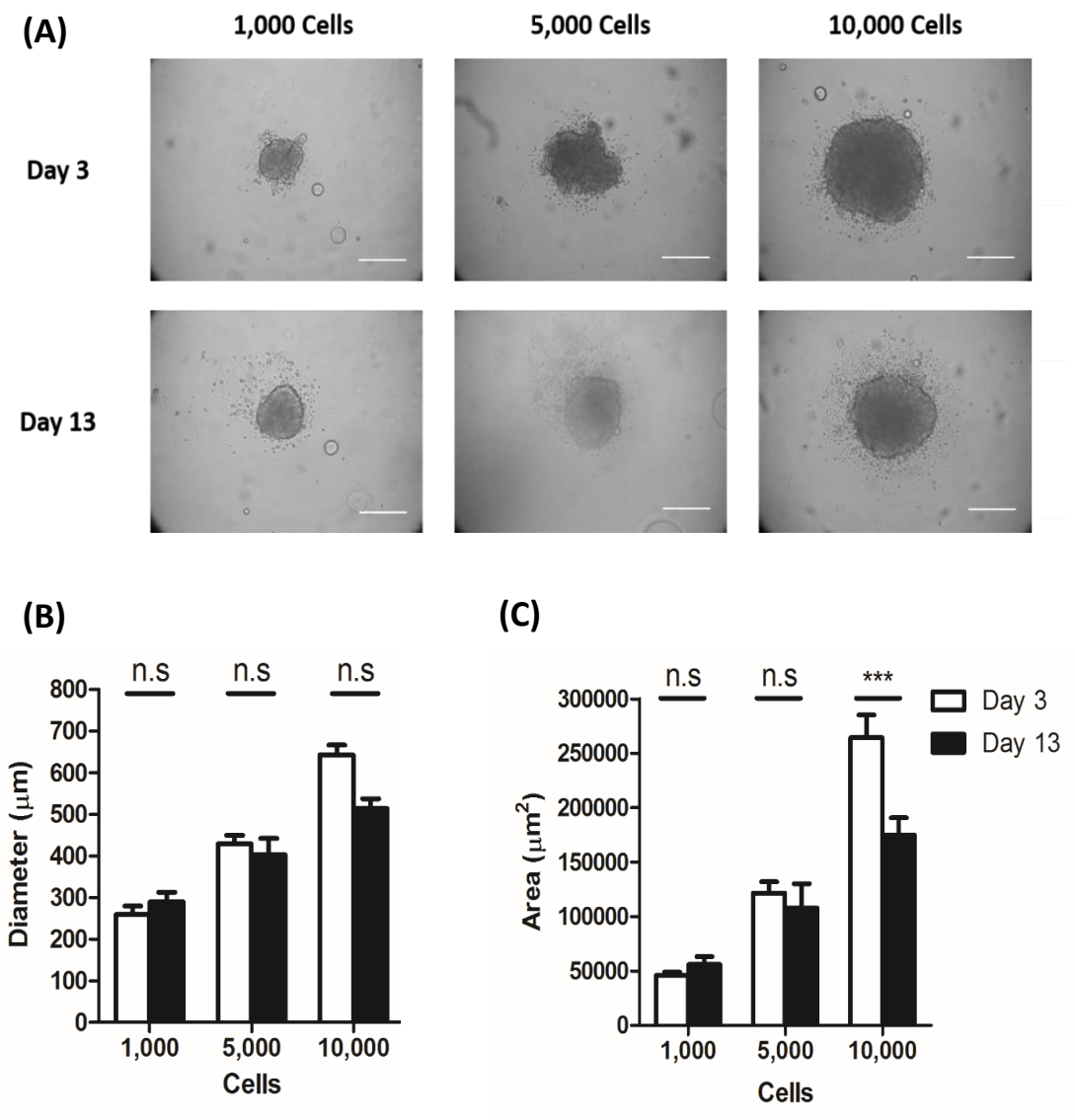

Figure 6.1: Optimising cell number to generate 3D cell spheroids. Cells were seeded at a density of 1,000, 5,000 or 10,000 cells (4 tumour control cell: 1 fibroblast) on poly-HEMA-coated (cell repellent), 96-well round-bottomed plates. After 72 hours, seeded cells aggregated into a compact 3D cell spheroid. **(A)** Representative images of 3D co-cultured spheroids (a single spheroid per well) at day 3 and day 13. Scale bar: 250µm. Representative fields are shown. **(B)** Diameter and **(C)** area measurements were carried out using Image J software at day 3 and 13. Graph shows mean ± SEM, based on 15 wells. n.s: non-significant and ***P<0.001. One-way ANOVA with Tukey's post hoc test. Data are representative of three independent experiments.

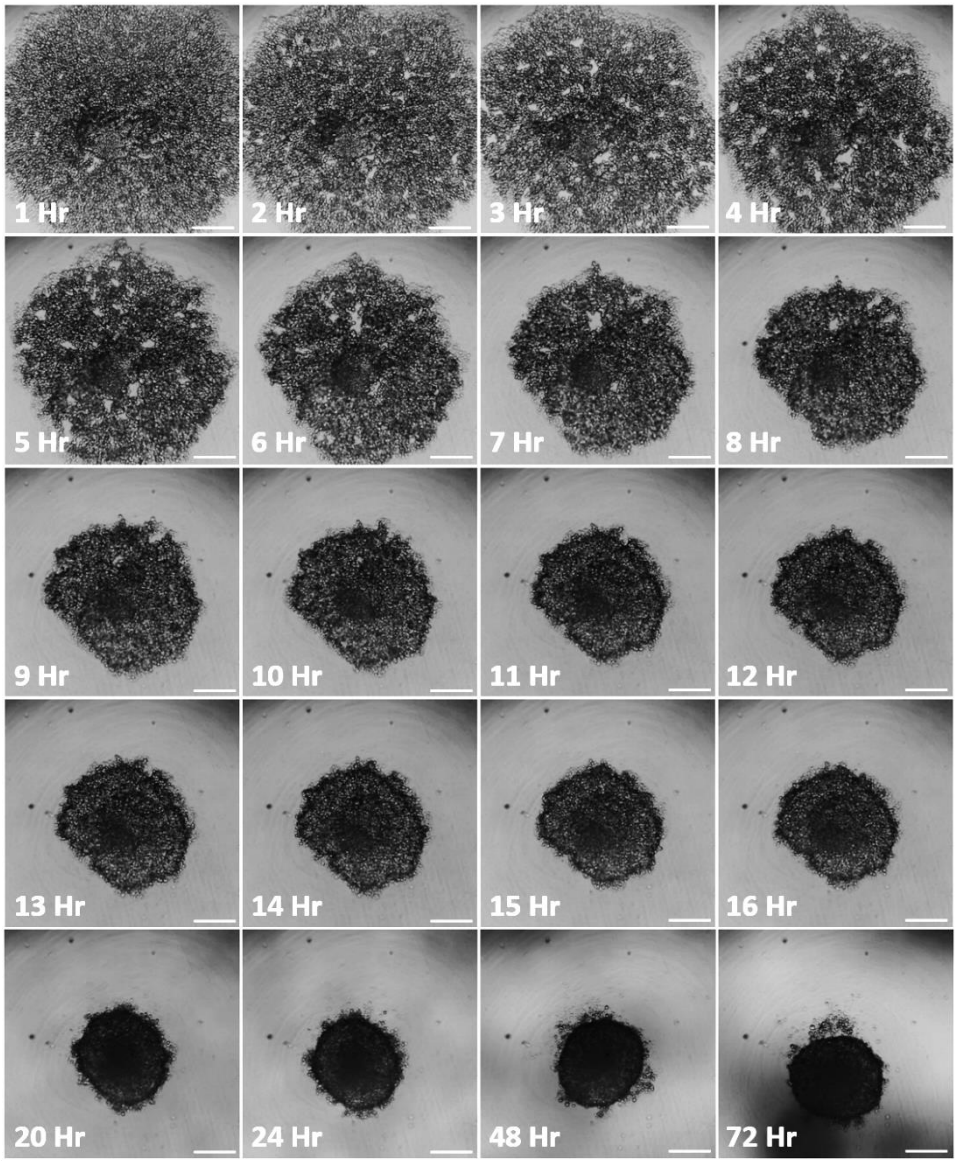

Figure 6.2: Time-lapse images of 3D spheroid generation. Cells were seeded at a density of 10,000 cells (4 tumour cell: 1 fibroblast). Over time, cells suspended on a cell-repellent plate aggregated into a compact 3D cell spheroid. Time-lapse brightfield images were obtained every hour, up to 72 hours by the CytoSmart™ Lux 10X System (pictured: every hour up to 16 hours, and daily up to 72 hours). Representative images are shown. Scale bar: 250µm. Data are representative of three independent experiments.

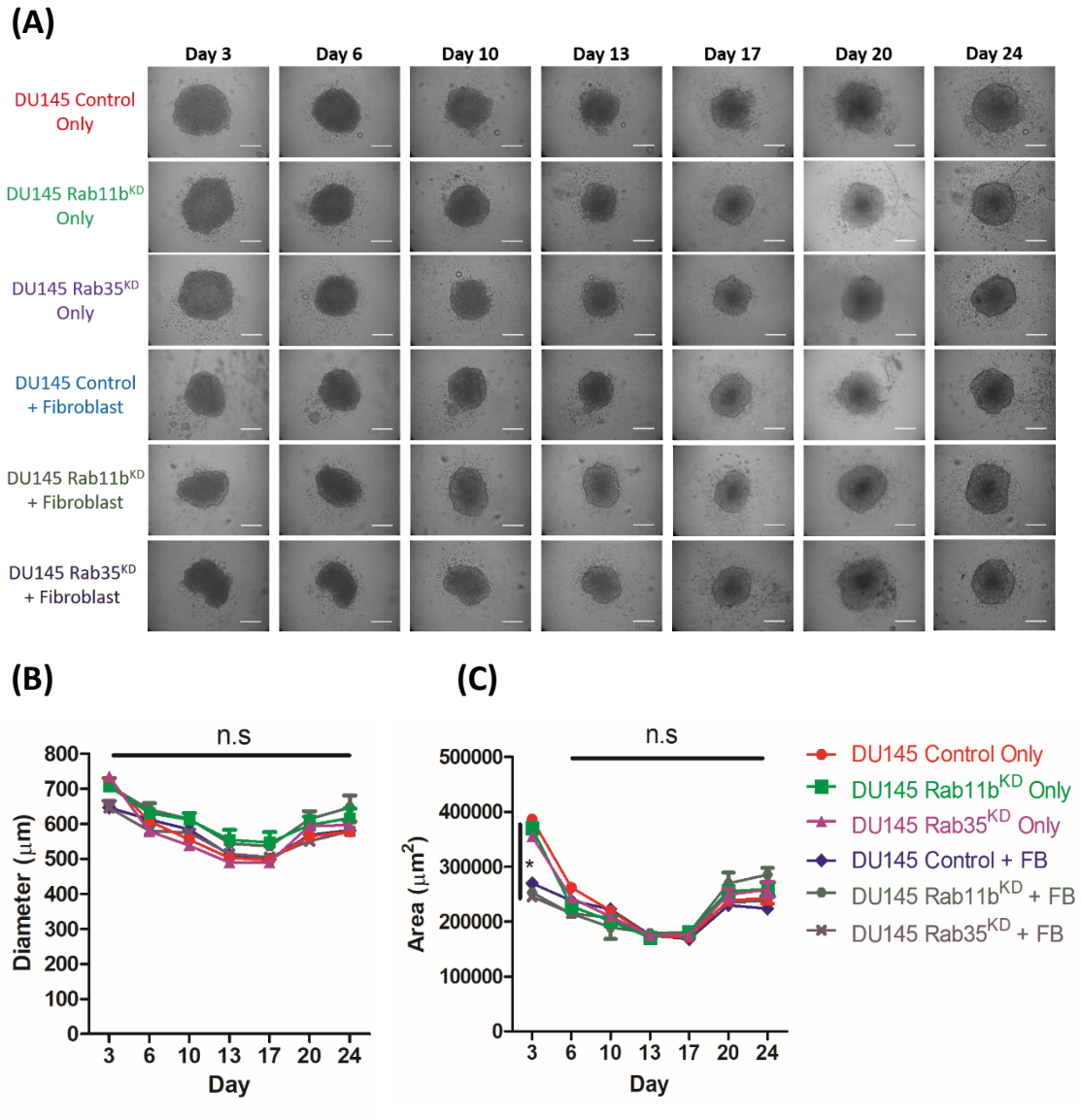

Figure 6.3: Spheroids containing DU145 control, Rab11b^{KD} or Rab35^{KD} cells alone or co-cultured in fibroblasts maintain tumour growth over time (Poly-HEMA method). (A) Starting from day 3 post- initiation, representative images of DU145 control, Rab11b^{KD} or Rab35^{KD} +/- fibroblasts spheroids grown on Poly-HEMA plates, were obtained at indicated time points. Scale bar: 250µm. Representative fields are shown. **(B)** Diameter and **(C)** area measurements were carried out using ImageJ software. Graph shows mean ± SEM, based on 10 wells. n.s: non-significant. Two-way ANOVA with Bonferroni post hoc test. Data are representative of three independent experiments.

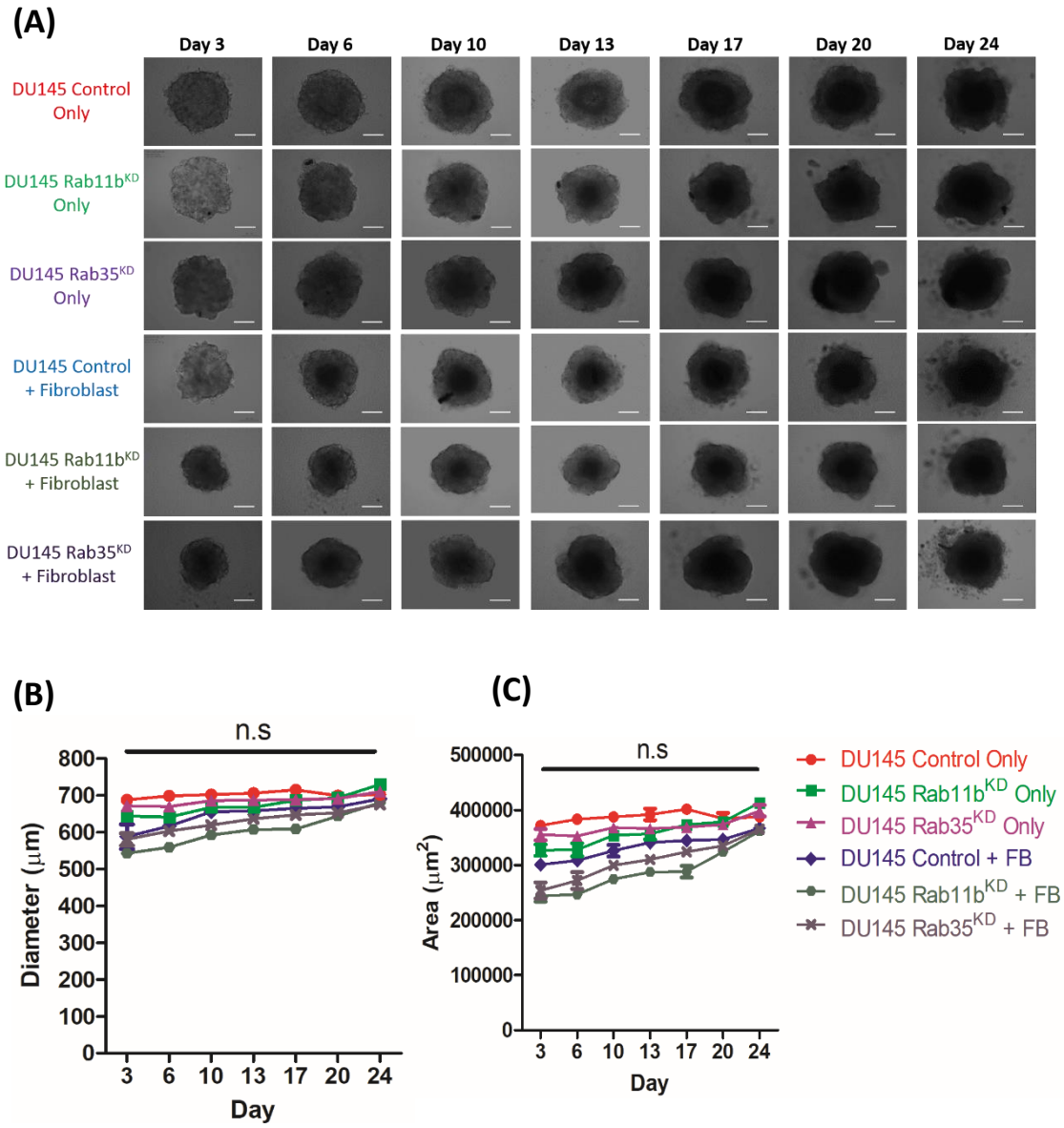

Figure 6.4: Spheroids containing DU145 control, Rab11b^{KD} or Rab35^{KD} cells alone or co-cultured in fibroblasts maintain tumour growth over time (GBO method). Starting from day 3 post initiation, representative images of DU145 control, Rab11b^{KD} or Rab35^{KD} +/- fibroblasts spheroids grown on CELLSTAR® cell-repellent surfaces from Greiner-Bio One (GBO) plates were obtained at indicated time points. Scale bar: 250µm. Representative fields are shown. **(B)** Diameter and **(C)** area measurements were carried out using ImageJ software. Graph shows mean ± SEM, based on 15 wells. n.s: non-significant. Two-way ANOVA with Bonferroni post hoc test. Data are representative of three independent experiments.

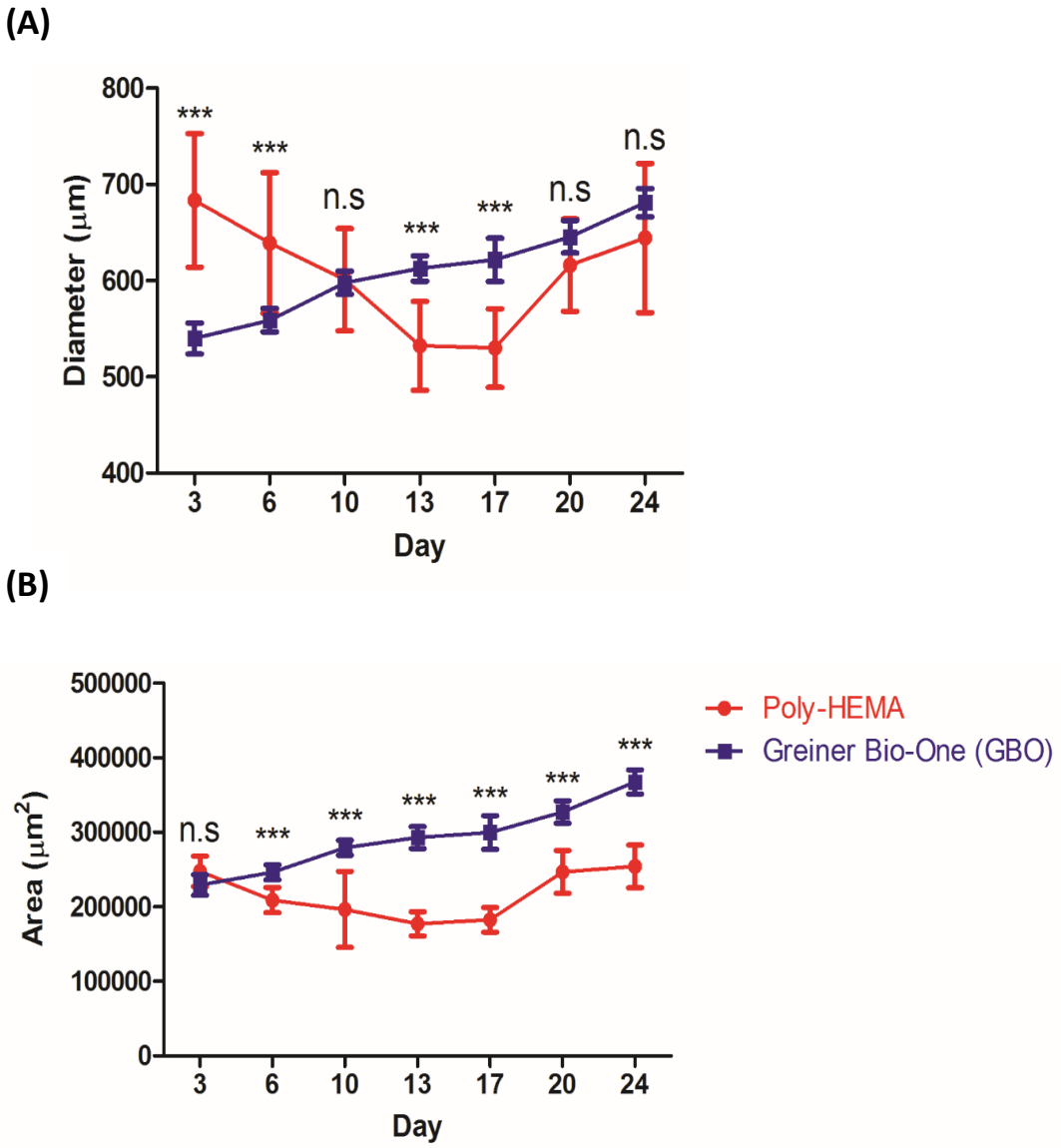

Figure 6.5: Comparing two spheroid generation methods (Poly-HEMA vs GBO) over time. Measurements of **(A)** diameter and **(B)** area of 3D spheroids between the Poly-HEMA and the GBO spheroid method over 24 days. Line graph showing diameter and area of Poly-HEMA spheroids fluctuating compared to GBO's spheroids gradually increasing over time. Graph shows mean ± SEM, based on 15 wells. n.s: non-significant and ***P<0.001. Two-way ANOVA with Bonferroni post hoc test.

6.1.3 Loss of Rab11b- or Rab35-Dependent Tumour Exosomes Attenuates Invasion in 3D Culture

Myofibroblasts orchestrate processes aiding tumour invasion and progression, through paracrine interactions involving the secretion of several soluble growth factors, such as EGF, FGF-2, HGF, VEGF-A (Orimo et al., 2005, Kalluri and Zeisberg, 2006, Webber et al., 2015). Furthermore, myofibroblasts can also secrete MMP enzymes to aid ECM modelling that can potentially recruit cells to facilitate an aggressive invasive functional change of tumour cells.

Here, we explored if loss of Rab11b- or Rab35-dependent exosomes can have any effect on invasivity in 3D culture models. We established 3D tumour (DU145 control or Rab11b^{KD} or Rab35^{KD} cells) spheroids with or without fibroblasts by day 4. Once these spheroids were established, these were transferred to matrigel-coated plates acting as a 3D basement membrane mimic (Figure 6.6 A). Each well contained RPMI-1640 media with 10% exosome-depleted FBS. Each spheroid was examined microscopically daily, up to 96 hours, to determine whether cells escape from the spheroid into the surrounding matrix. Cell outgrowth was observed from the spheroid (DU145 control + fibroblast) as early as 8 hours, growing beyond the field of view (x10 objective) at 32 hours (Figure 6.6 B).

Control tumour cells, in the absence of fibroblasts readily formed compact spheroids, but cells within exhibited a poor capacity to escape into the surrounding matrix. This was true for both knockdown of Rab11b (Figure 6.7 A) or Rab35 (Figure 6.7 C). In contrast, when incorporating fibroblasts into these spheroids, we observed notable cell invasion into the matrix as early as 24 hours; and beyond the x10 field of view as time progressed. By tiling multiple images, we could assess invasion up to 96 hours and quantify % increase in area difference from day 0 spheroid. The formula used to calculate this:

% increase in area difference = Total area of outgrowth (day *n*) / Total area of spheroid at day 0

When measuring these outgrowths, we took into consideration these 3D spheroid structures are viewed as 2D images. Therefore, we are not accounting for any movement in the z-axis. Nonetheless, spheroids comprising fibroblasts and exosome competent tumour cells demonstrated a significant increase in area occupied by extra-spheroid cells (Figure 6.7 B & D), compared to tumour cells containing the Rab11b^{KD} (150% decrease) ($P<0.01$) (Figure 6.7 B) or Rab35^{KD} (350% decrease) ($P<0.001$) (Figure 6.7 D) at 96 hours. Outgrowths were drastically less extensive by 96 hours, with a clear attenuation of invasive capacity in the absence of Rab11b or Rab35 tumour-derived vesicles. Fibroblasts, therefore, are important

mediators of this invasive behaviour. Tumour cells exhibiting knockdown of Rab11b or Rab35 still exhibited an attenuated invasive capacity, even in the presence of fibroblasts, suggesting these regulators are important in communicating between tumour and stromal cells in the context of a 3D spheroid environment, as they are relevant regulators of invasive behaviour.

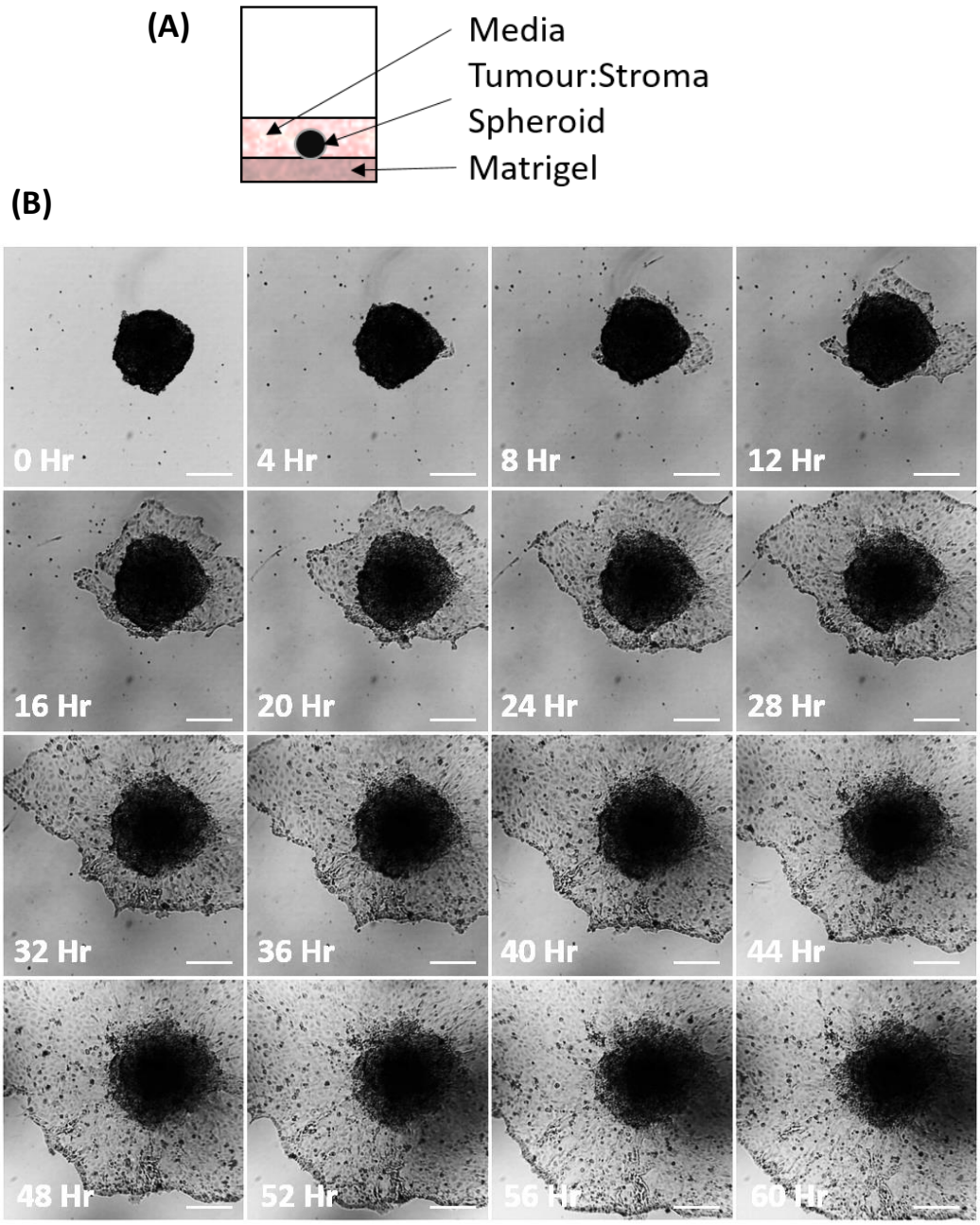

Figure 6.6: Time-lapse imaging of the 3D spheroid invasion assay. (A) Schematic diagram of 3D spheroid matrigel invasion assay: a single day 4 established tumour:stroma spheroid was transferred to each well of a matrigel matrix-coated 24-well, flat bottomed plate. **(B)** Representative time-lapse brightfield images of the 3D spheroid cell outgrowths (pictured: every 4 hours up to 60 hours) were obtained by the CytoSmart™ Lux 10X System. Scale bar: 250µm. Data are representative of three independent experiments.

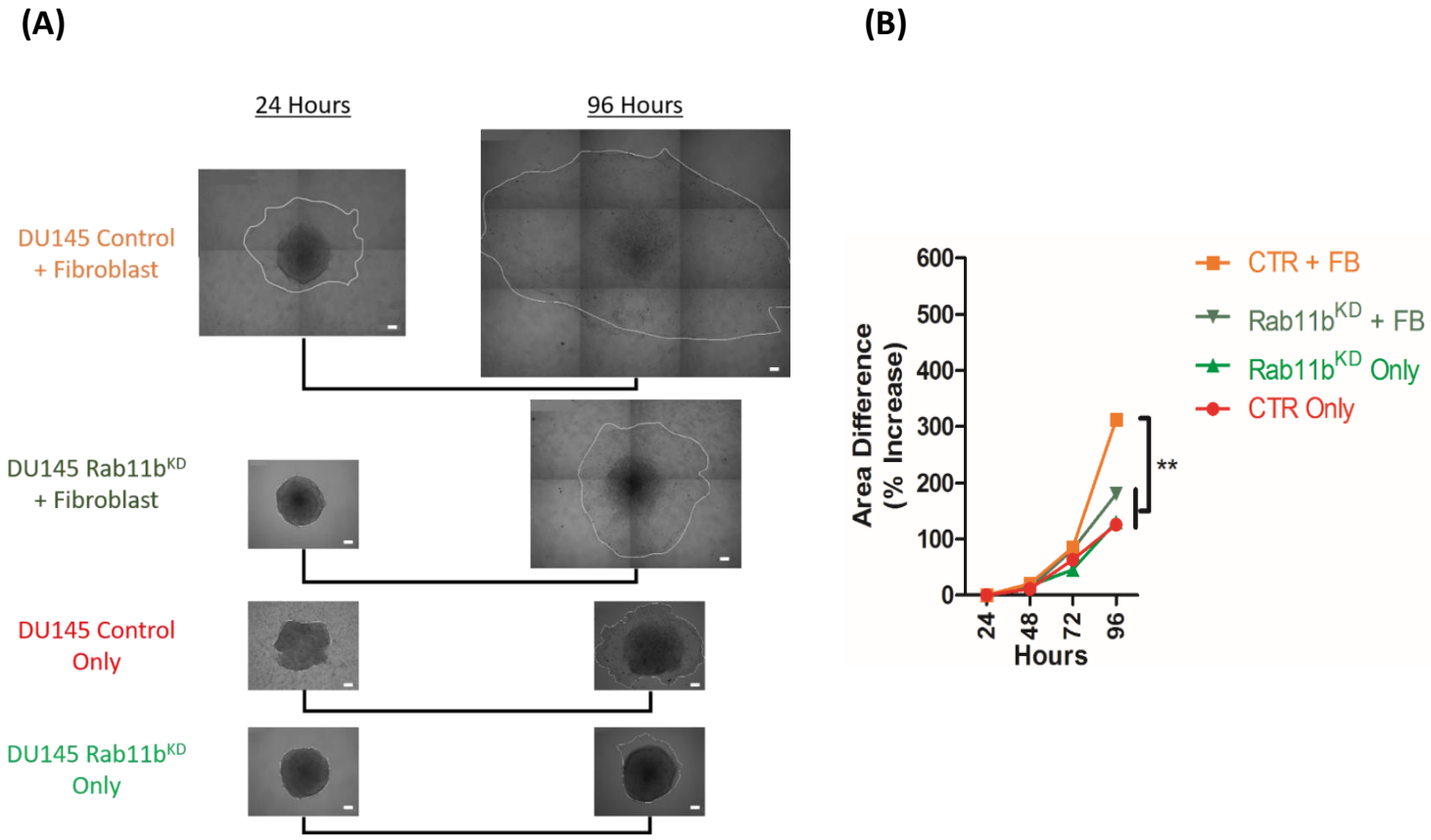
(A)
24 Hours
96 Hours
DU145 Control
+ Fibroblast
DU145 Rab11b^{KD}
+ Fibroblast
DU145 Control
Only
DU145 Rab11b^{KD}
Only
(B)
Area Difference
(% Increase)
600
500
400
300
200
100
0
24
48
72
96
Hours
**
CTR + FB
Rab11b^{KD} + FB
Rab11b^{KD} Only
CTR Only

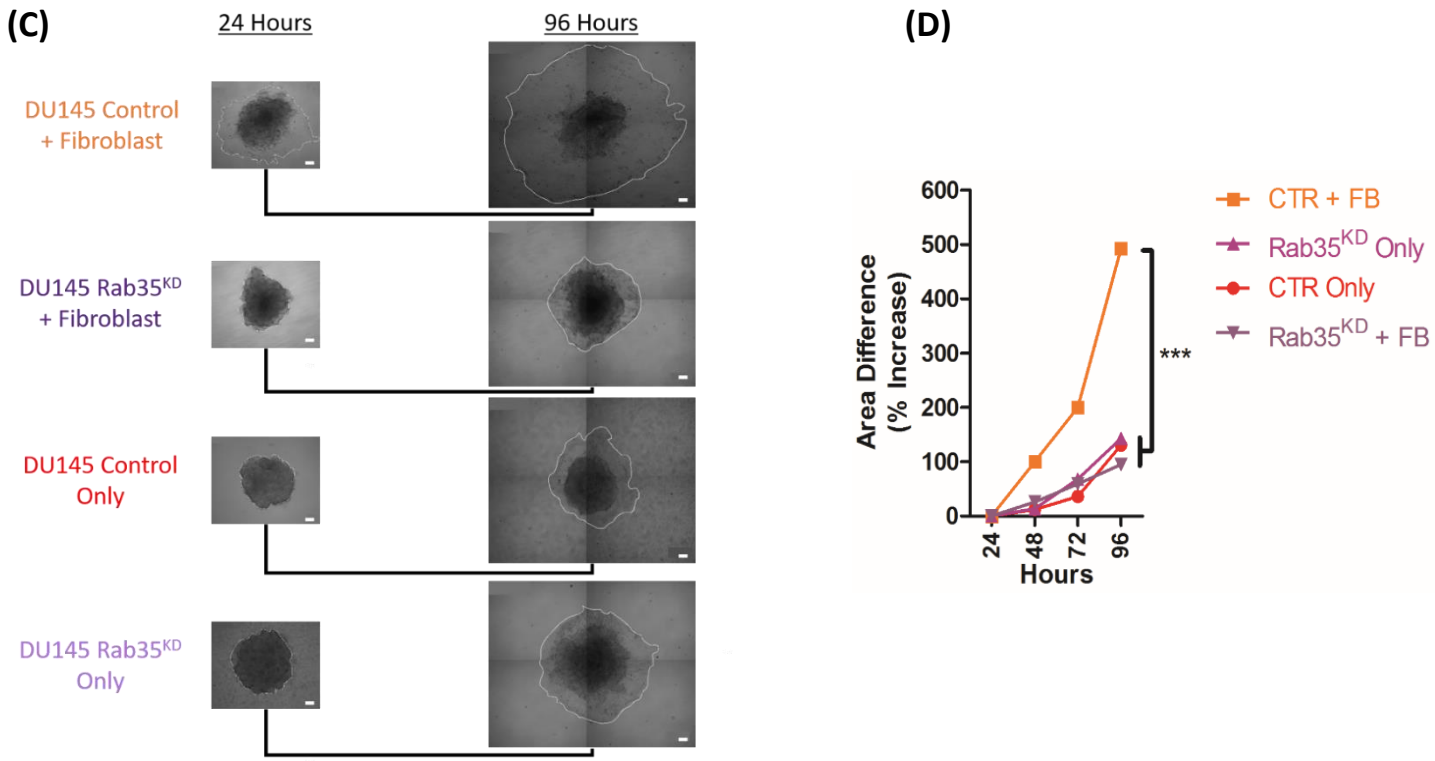

Figure 6.7: DU145 Rab11b^{KD}/Rab35^{KD} cells attenuate aggressive invasion in 3D culture. Spheroid cultures were established, composed of DU145 control and **(A and B)** Rab11b^{KD} or **(C and D)** Rab35^{KD} cells, or a combination of DU145 cells with fibroblasts (at a ratio of 4:1 respectively), at 10^4 total cells/spheroid. The area occupied by extra-spheroidal cell outgrowths was measured daily for up to 96 hours. For late time-points, multiple images of the spheroid-outgrowths were taken and these were tiled to form a composite representation of the full extent of outgrowth. Scale bar: 100µm. Graph shows mean ± SEM, based on 5 spheroids per group. ** P≤0.01 and ***P≤0.001. Two-way ANOVA with Bonferroni post hoc test. Data shown as representative of three experiments.

6.1.4 Tracking Fluorescently Labelled Tumour Cells and Fibroblasts in the Invasion Assay

The tumour margin is an important aspect for invasion, where stromal cells are pivotal in supporting this complex tumour microenvironment. Notably, many tumour cells do not degrade the surrounding matrix and do not secrete high levels of proteases, but are able to disseminate and invade aggressively (Cao et al., 2015). The population of myofibroblasts may provide a significant stromal remodelling capacity, leading the way for invasive tumour cells. However, it remains poorly understood whether tumour cells or fibroblasts concentrate at the leading edge to support cancer invasion. Here, DU145 cells labelled with green fluorescent protein (GFP) and fibroblasts labelled with quantum dots (qDot) were used, to track cells in the spheroid invasion assay.

Previously, we transduced DU145 cells with MISSION® lentiviral particles (Chapter 4) with the pLKO.1-puro vector, allowing stable gene silencing of selected targets. Here, we selected the best knockdowns and used lentiviral particles with an alternative vector backbone; Neo-CMV-tGFP, to fluorescently express our selected DU145 cells with GFP allows for selection of transduced cells using Geneticin® (G418). The 3-(4,5-Dimethylthiazol-2-yl)-2,5-diphenyltetrazolium bromide (MTT) assay was used to determine the lowest G418 dose (eukaryote antibiotic) required for efficiently selecting transduced cells. Here, incremental G418 doses were used to treat DU145 cells (Figure 6.8). 2000µg/ml was the minimal G418 dose observed, sufficient to kill the majority of DU145 cells. These transduced DU145 cells successfully fluorescently expressed GFP.

We initially proposed to use a Neo-CMV-tRFP to fluorescently label our fibroblast cell line with red fluorescent protein (RFP); though this would be redundant as these primary fibroblasts have a limited number of passages. If fibroblasts were RFP positive and be deemed free of lentiviral particles, they would undergo senescence if available for use. An alternative to fluorescently label fibroblasts would be utilising quantum dots (qDots), as one study reported to successfully track MSCs *in vitro* and *vivo* with long photostability (Muller-Borer et al., 2007). First, we explored the effect of qDot-labelling on fibroblasts, to understand if qDot-labelling has any cytopathic impact on fibroblasts. A monolayer of unlabelled and labelled fibroblasts was seeded and counted daily, over the 144-hour time course. We observed no significant differences in cell number between labelled and unlabelled conditions over time (Figure 6.9 A), which suggests qDot-labelling does not cause any cytopathic effect on fibroblast cell growth.

Next, we labelled fibroblasts with qDots and assessed intracellular qDot labelling over a 96-hour time course by flow cytometry (Figure 6.9 B). 24 hour labelled qDot fibroblasts demonstrate a greater fluorescent signal, compared to unlabelled fibroblasts. Though by 72 hours and until 144 hours, the qDot signal was weakened and we saw some overlap with unlabelled fibroblasts; suggestive of a faint signal. As the fibroblasts incorporated qDots, this declining signal may be explained by the cells undergoing cell division, that potentially divides the signal in half with every division.

Nevertheless, we next incorporated these fluorescently-labelled cells into our 3D spheroid invasion assay, to determine whether the periphery of cell outgrowths is concentrated with just tumour cells, fibroblasts or a combination of both. Cell outgrowth was observed from the spheroid (DU145 control cells + fibroblasts) as early as 8 hours (Figure 6.10 A). Cells were proliferating and growing beyond the field of view at x20 microscope objective at 30 hours, with evidence of tumour cells proliferating between 16-22 hours. We observe weakly GFP-labelled tumour cells present in the cell outgrowth at 0 and 12 hours (Figure 6.10 B). Similarly, qDot-labelled fibroblast signal was present at the periphery of cell invasion at 0 hour, but the signal faded by 12 hours. As some examples, individual qDots are present within cell outgrowth, as determined by the zoomed in images; indicative of fibroblasts, albeit very faint. These results give some indication that tumour cells are present in these outgrowths, supporting cancer invasion at the leading edge. Fibroblasts are likely to be present, as some qDot positive cells were present with tumour cells at the invading front, but the signals were weak and difficult to detect over time.

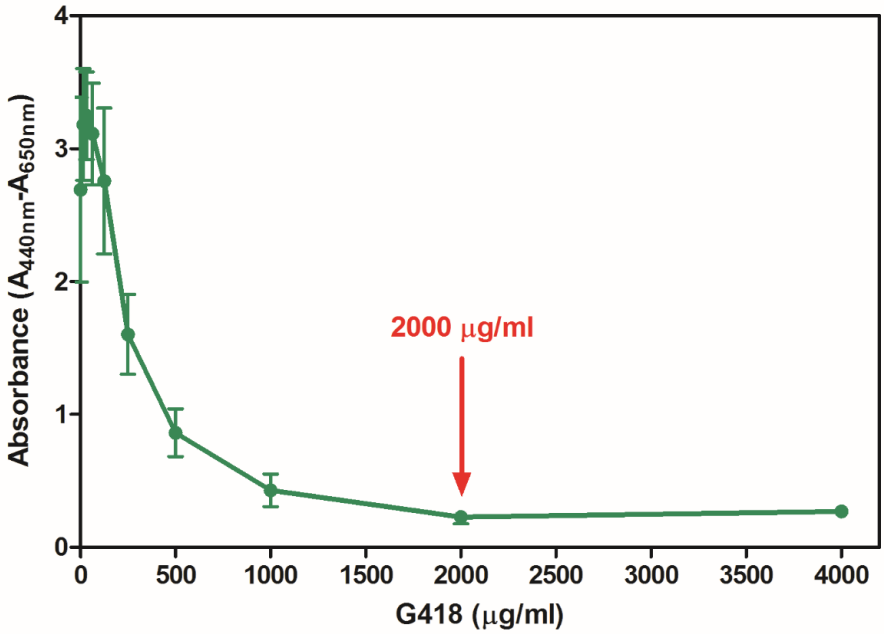

Figure 6.8: Optimisation of G418 cytotoxicity profile for DU145 cells. Cells were seeded at a density of 5,000 cells per well and incubated with a range of G418 concentrations 0-4000µg/ml. After 48 hours, cell viability was measured using the WST-1 assay. DU145 cells were stably transduced with MISSION® lentiviral transduction particles expressing GFP. Graph shows mean, based on 5 wells.

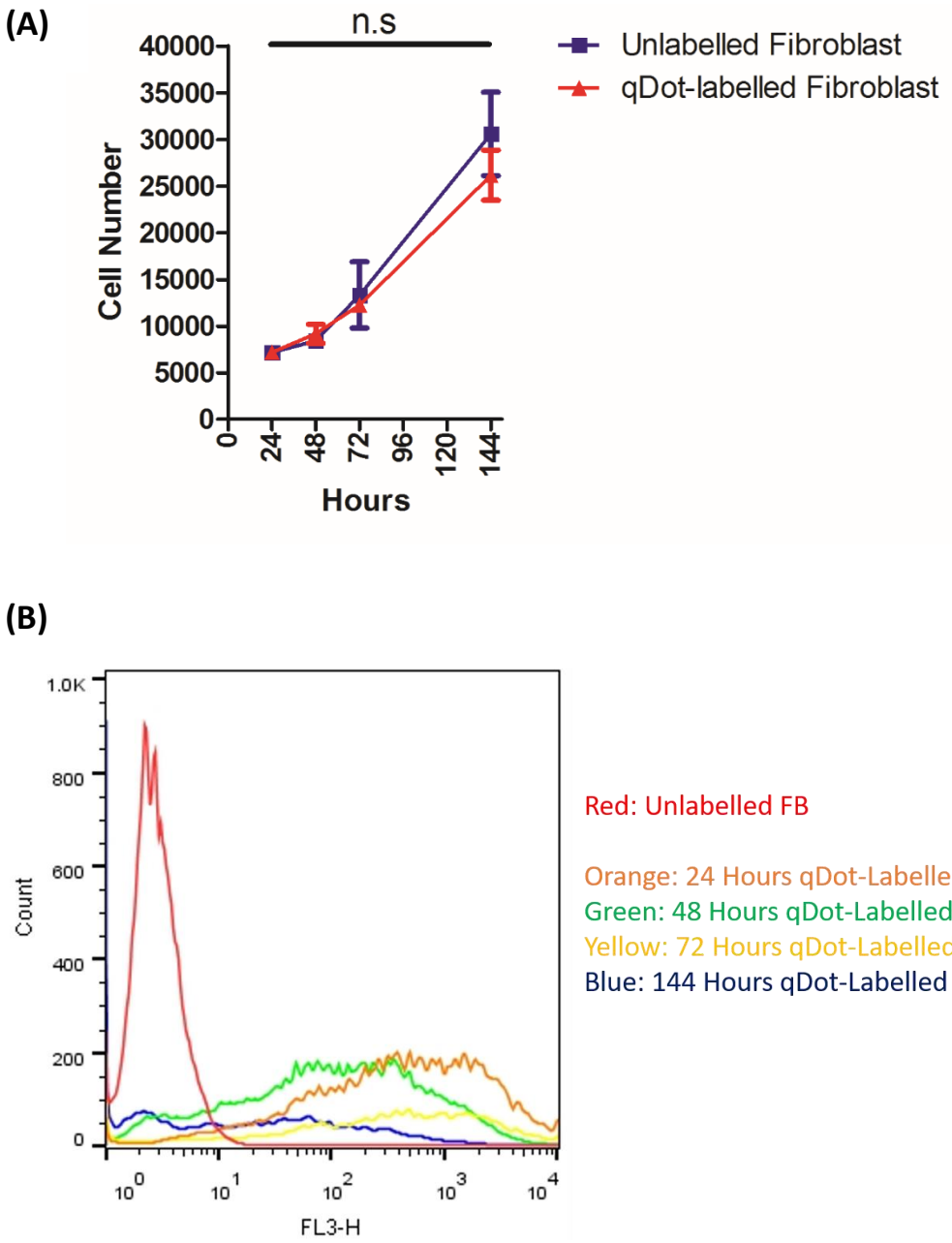

Figure 6.9: Growth curve and quantification of qDot-labelled fibroblasts over time. (A) Fibroblasts were labelled with qDots for 24 hours, prior to seeding cells at a density of 7,500 cells per well in DMEM-F12 media. The growth curve of fibroblasts was monitored daily, up to 72 hours and at 144 hours, determined by cell counts. Graph shows mean ± SEM, based on triplicate wells. n.s: non-significant. Two-way ANOVA with Tukey's post hoc test. **(B)** Flow cytometry results of qDot labelled fibroblasts at 24, 48, 72 and at 144 hours.

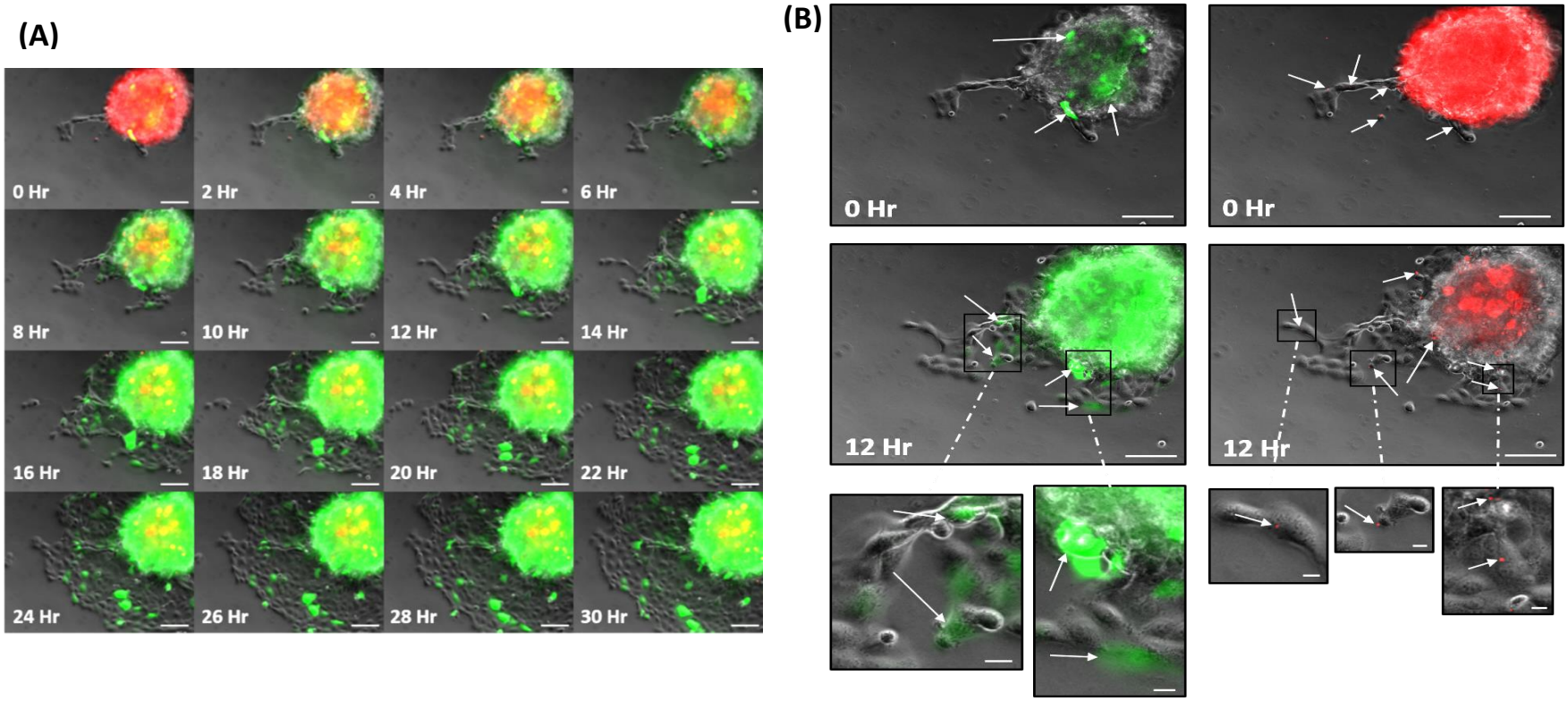

Figure 6.10: Tracking GFP-positive DU145 cells and qDot-labelled fibroblasts in the invasion assay. (A) Representative time-lapse images of GFP-positive DU145 cells (green) and qDot-labelled fibroblasts (red) images of the 3D spheroid cell outgrowths. Representative images (pictured: every 2 hours up to 30 hours) obtained hourly up to 96 hours (not shown) by the Zeiss Z1 observer. Image of spheroid cell outgrowth at 0 hour and 12-hour time points with **(B)** GFP-labelled tumour cells and qDot-labelled fibroblasts at the periphery of cellular invasion. Scale bar: 250µm. White arrows: GFP or qDot labelled cells.

6.1.5 Loss of Rab11b- or Rab35-Dependent Exosomes Attenuates MMP Levels in 3D Culture

Previous results revealed that DU145 Rab11b^{KD} or Rab35^{KD} cells significantly reduced the invasive capacity of 3D spheroids, failing to give any advantageous invasion even in the presence of fibroblast. Invasion requires a complex actin-based tumour cell migration machinery that works in tandem with the secretion of MMPs. Here, we explored the potential mechanism of action underlying these invasive differences proposed to be alterations in MMP levels, capable of degrading the ECM to support cellular invasion.

RNA was extracted from 3D spheroids at day 4. The relative levels of mRNA for MMP-1, MMP-13 and tissue inhibitor of matrix metalloproteinase-3 (TIMP-3) were compared among the different homotypic and heterotypic spheroids using Taq-Man PCR assays. Relative quantification using the comparative Ct method ($2^{-\Delta\Delta Ct}$), was used to analyse differences in gene expression of MMP-1, MMP-13 or TIMP-3 among the spheroids. MMP-1 or MMP-13 expression was measured relative to the DU145 control, Rab11b^{KD} or Rab35^{KD} cells alone. TIMP-3 expression was measured relative to DU145 control cell co-cultured with fibroblasts. The mRNA for MMP-1 and MMP-13 was significantly up-regulated by 1.7-fold ($P<0.001$) and 1.6-fold ($P<0.01$) respectively, in DU145 control cells with fibroblasts compared to control tumour cells alone (Figure 6.11 A & B). In contrast, DU145 Rab11b^{KD} or Rab35^{KD} cells, with or without fibroblasts, showed no significant differences in MMP-1 and MMP-13. Though, TIMP-3 was up-regulated by 1.5-fold in DU145 Rab11b^{KD} ($P<0.05$) and Rab35^{KD} ($P<0.05$) cells in the presence of fibroblasts respectively, compared to controls (Figure 6.11 C). Overall, at the transcript level, TIMP-3 was undetectable in the tumour cell only spheroids.

At the protein level, the pattern is similar to the mRNA data (Figure 6.12), revealing increased concentrations of both MMP-1 (4.7-fold increase) ($P<0.01$) and MMP-13 (1.6-fold increase) ($P<0.05$), in the DU145 control and fibroblast spheroid's CM, compared to control tumour cells alone. This influence is lost when using either DU145 Rab11b^{KD} or Rab35^{KD} cells (Figure 6.12 A & B). Loss of either Rab11b- or Rab35-dependent vesicles appear to shows disruptive effects on the cross-talk between tumour cells and fibroblasts. These rendered the spheroid environment lower in MMPs and elevated in TIMP-3 at the transcript level; and this may explain the differences observed in invasivity.

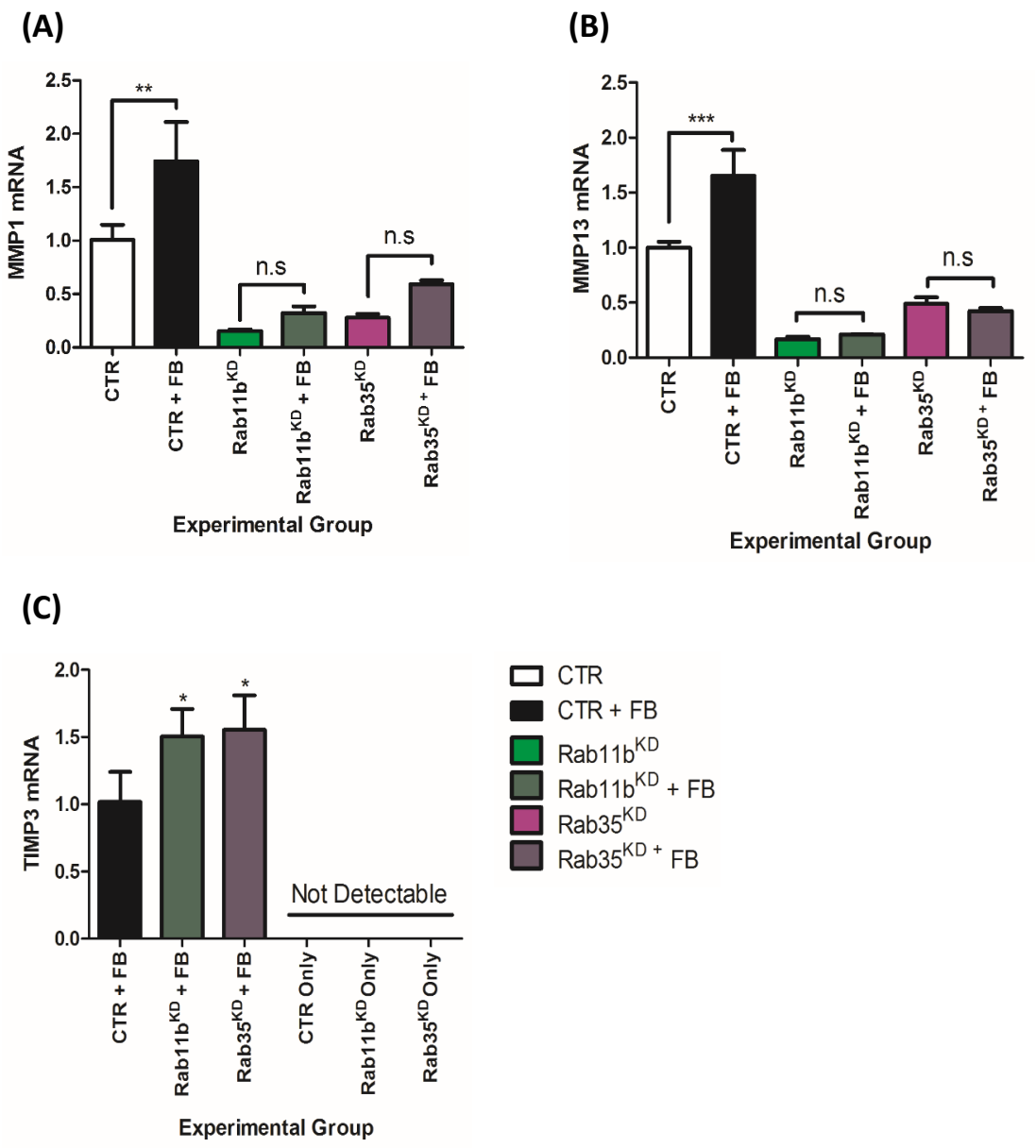

Figure 6.11: Exosome-deficient tumour spheroids have reduced transcripts for MMP-1 and MMP-13; and elevated TIMP-3. RNA was isolated from spheroids containing DU145 control, Rab11b^{KD} and Rab35^{KD} cells, with or without fibroblasts, at day 4. Quantification of mRNA expression levels for **(A)** MMP-1, **(B)** MMP-13 and **(C)** TIMP-3 in the different spheroids were measured, relative to the DU145 tumour cells alone or with fibroblasts, using qPCR. Graph shows mean ± SEM, based on triplicate wells. n.s: non-significant, *P<0.05, **P<0.01 and ***P<0.001. One-way ANOVA with Tukey's post hoc test.

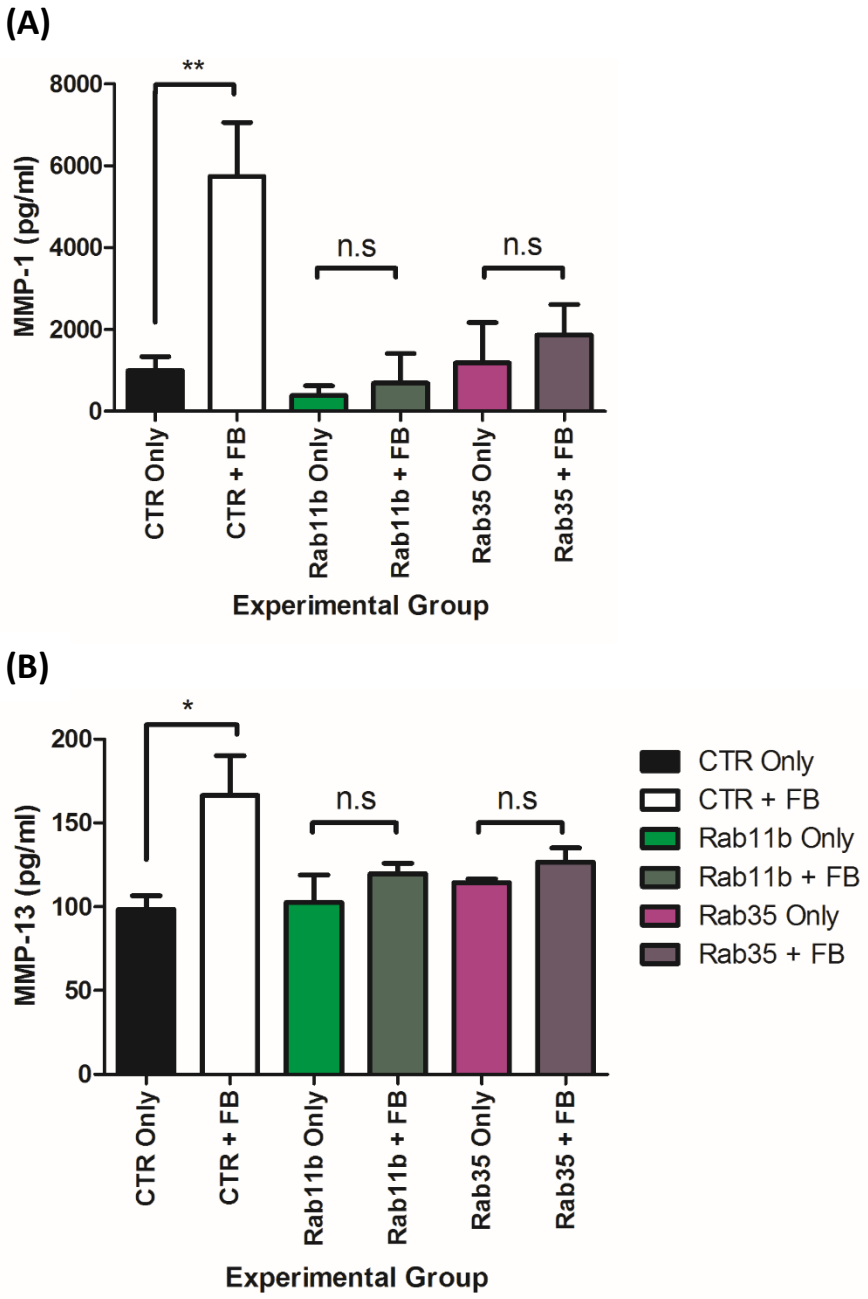

Figure 6.12: Exosome-deficient tumour cell spheroids secrete reduced levels of MMP-1 and MMP-13. Cell CM was collected from spheroids containing DU145 control, Rab11b^{KD} and Rab35^{KD} cells, with or without fibroblasts, at day 4. Quantification of protein levels for **(A)** MMP-1 and **(B)** MMP-13 in the different spheroids were measured by ELISA. Graph shows mean ± SEM, based on duplicate wells. n.s: non-significant, *P<0.05 and **P<0.01. One-way ANOVA with Tukey's post hoc test.

6.1.6 Knockdown of Rab35 Impacts Tumour Growth, but not Rab11b

Previously, our group has demonstrated that administration of DU145 control cells with fibroblasts accelerated tumour growth in mice, compared to DU145 Rab27a^{KD} cells with fibroblasts (Webber et al., 2015). Our results revealed that knockdown of Rab11b or Rab35 leaves a vesicle population that remains insufficient for driving fibroblast differentiation into myofibroblast, leading to diminished angiogenesis and attenuated behaviour in 3D *in vitro* models. Here, we explored whether we could recapitulate these *in vitro* findings into the *in vivo* setting, in terms of tumour growth.

Tumour:fibroblast xenografts consisted of DU145 (control or Rab11b^{KD} or Rab35^{KD}) cells co-cultured together with fibroblasts in a ratio of 4 tumour cells:1 fibroblast (Figure 6.13 A). These xenografts were established on the dorsal flank of CD1 athymic mice and administered by subcutaneous injection of 5 x 10^6 total cells suspended in matrigel. Once tumours became palpable, dimensions (height and width) of tumours were measured using vernier callipers every 2 to 3 days. These measurements were used to calculate tumour volume (Jensen et al., 2008, Faustino-Rocha et al., 2013), using the formula: tumour volume (mm^3) = $width^2$ x length x 0.5.

For each condition, tumours became palpable at day 7, with steady growth thereafter (Figure 6.13 B). Knockdown of Rab11b showed little difference in tumour growth rates, compared to controls, reaching a large volume of in excess of 330mm^3 by day 46, compared to 389mm^3 by the controls. In contrast, knockdown of Rab35 showed a significant attenuation of tumour growth from day 35 onwards ($P<0.001$) and at day 46, the tumour volume was less than 100mm^3. Representative images of excised tumours are shown (Figure 6.13 C), demonstrating restricted growth of the Rab35 knockdown tumour. We were surprised to see that knockdown of Rab11b did not show similar results as the Rab35 knockdown. Possibly, this may be due to other responses that we have not explored, perhaps phenotypic differences in the secretome. Though these reasons will be discussed in greater detail in the Discussion.

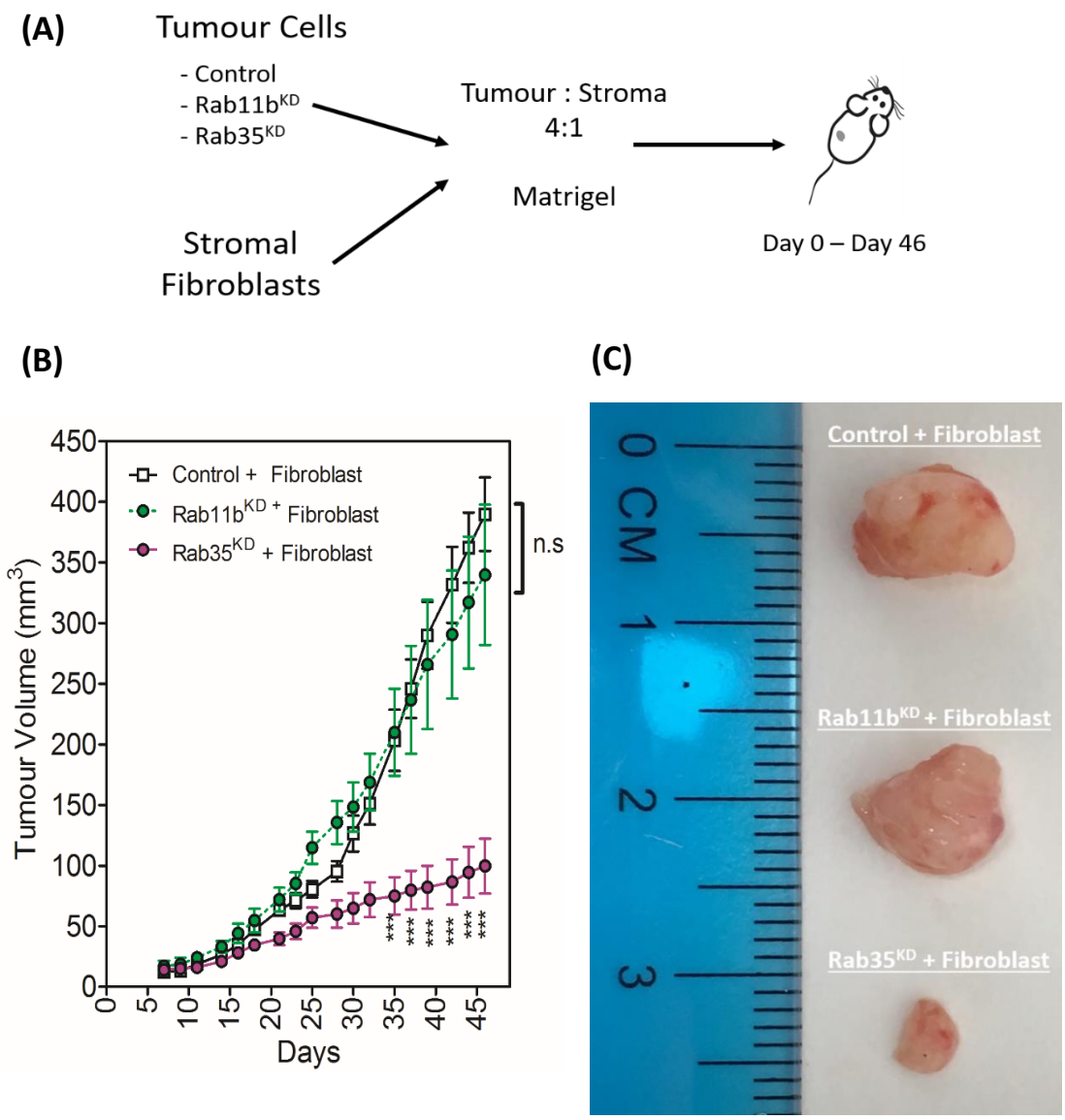

Figure 6.13: Rab35 knockdown attenuates growth *in vivo*, but not Rab11b. (A) Schematic diagram of experimental outline. A total of 5 x 10^6 cells comprising of tumour cells (DU145 control or Rab11b^{KD} or Rab35^{KD}) with fibroblasts, at a ratio of 4:1 were administered subcutaneously to the dorsal flank of CD1 athymic mice. Three groups were compared; including control tumour cells, Rab11b^{KD} or Rab35^{KD}. **(B)** When tumours were palpable, day 7 onwards, tumour growth was assessed using external callipers every 2 to 3 days and the graph shows tumour volume (mm^3) for up to 46 days. Graph shows mean ± SEM, (n=4). n.s: non-significant and ***P<0.001. Two-way ANOVA with Bonferroni post hoc test. **(C)** Tumours were excised, and photographed to represent the differences in volume at the experimental endpoint.

6.2 Discussion

In this Chapter, we investigated the implications of spheroids containing DU145 Rab11b^{KD} or Rab35^{KD} cells, co-cultured with fibroblasts on spheroid growth and invasion *in vitro* and tumour growth *in vivo*. First, spheroids generated with DU145 control, Rab11b^{KD} or Rab35^{KD} cells alone, or with fibroblasts, were cultured for 24 days. Numerous factors including spheroid generation method, culture media and cell lines can affect spheroid formation (Kelm et al., 2003, Kim, 2005). During the growth of these homotypic and heterotypic spheroids, we observed a dark dense cell core suggestive of a necrotic centre. This was commonly observed in all spheroids containing either DU145 control, Rab11b^{KD} or Rab35^{KD} cells. This feature was also observed in other 3D cell spheroids cultured *in vitro* (Folkman and Hochberg, 1973, Sherar et al., 1987, Hirschhaeuser et al., 2010). A necrotic core is recognised to be enclosed by a shell of quiescent cells and an outermost layer of live proliferating cells. Studies have described spheroids with diameters larger than 500µm, accumulating metabolic waste in the inner core which deprives cells of oxygen and nutrients, thus a necrotic centre (Anada et al., 2012, Beauchamp et al., 2015).

Analysis of these DU145 control, Rab11b^{KD} or Rab35^{KD} cells alone, or and tumour:fibroblast spheroids, revealed a reduction in size with the Poly-HEMA method, before increasing in size over time. Although Poly-HEMA coated plates can generate spheroids, it remains difficult to control a homogenous Poly-HEMA coating (Ke et al., 2004). Where uneven coating can occur, this may result in impurities or poor ethanol evaporation in Poly-HEMA, that may affect spheroid formation and growth (Atala and Lanza, 2001). There was great difficulty in using poly-HEMA generated spheroids for functional invasion assays, as spheroids became fragile and brittle. This led to companies, such as GBO, to manufacture CELLSTAR® cell-repellent surfaces plates that have a homogenously coated polymer to induce spheroid formation. Similar to Poly-HEMA, these coated polymers are proposed to prevent cell adherence, due to the negative electrostatic reduction of the polystyrene surface (Folkman and Moscona, 1978). Based on the GBO-spheroid method, an increase spheroid growth for homotypic and heterotypic spheroids was consistent with other studies (McMillan et al., 2016, Wang et al., 2016b). In contrast, the presence of tumour cells and especially fibroblasts showed an initial smaller spheroid, compared to tumour cells alone. This initial smaller spheroid may be due to cell re-organisation and cellular contraction of fibroblasts (Sodek et al., 2009, Nyga et al., 2013). However, even in the presence of exosome deficient tumour cells, this did not seem to hinder spheroid growth. Similar to other reports, there is a finite limit to the maximum size a spheroid can grow to, regardless of how frequent media is replenished or the

availability of space for spheroid growth (Folkman and Hochberg, 1973). This could be explained the spheroid's total number of cells reaches a point where their aggregate surface area is insufficient to allow adequate diffusion of catabolites. These spheroids enter a 'dormant' phase and would perhaps require vascularisation that would begin exponential growth. Furthermore, measurements of these 3D spheroids are based on 2D measurements, which is not an accurate representation of tumour growth, as we assume spheroids are perfect spheres but the surface composition may differ. Spheroids which look small, might nevertheless be complex biologically; and differences other than this may exist. Analysis of spheroid tumour growth revealed that the single parameter of size (diameter and area) was not able to show differences in experimental groups, as we initially hoped.

During tumour invasion, the stroma plays a fundamental role in secreting growth factors and matrix degrading enzymes to support tumour invasion (Hanahan and Weinberg, 2011). Therefore, we examined the invasive behaviour as a feature affected by the Rab knockdowns. Matrigel was used for *in vitro* invasion assays to mimic basement membrane matrices, which cancer cells penetrate during tumour metastasis (Albini et al., 1987, Albini, 1998). From our data, cell outgrowth from 3D spheroid into the surrounding ECM occurs readily. By observing GFP-positive tumour cells and qDot-labelled fibroblasts, there was some evidence of tumour cells at the leading invasive edge. Although, some qDot fluorescence was present at the time of invasion (12 hours), qDot fluorescent signal was lost over time. An improved approach would have been to transduce fibroblasts with lentiviral particles with a fluorescent tag (mCherry/RFP), similar to GFP-positive tumour cells. This would have sustained fluorescent signal over a longer duration, whilst addressing whether fibroblasts are present at the leading edge or within the invading mass. In other studies, fibroblasts are located at the leading edge of invasive colon and gastric cancer models (Illemann et al., 2004, Satoyoshi et al., 2015). However, this remains to be explored in detail in our model.

By using 3D spheroids in a matrigel invasion assay, DU145 control cells co-cultured with fibroblasts increased their invasivity capacity with larger outgrowths, though it remains uncertain whether this penetration occurred on top or through the matrigel. Both DU145 Rab11b^{KD} or Rab35^{KD} cells severely attenuated tumour invasion, even in the presence of fibroblasts. This suggest that Rab11b- or Rab35-dependent vesicles appear key in mediating this cross-talk in between tumour and fibroblasts, enhancing the tumour's invasive capacity.

As with stroma activation and motility, CM from fibroblasts treated with vesicles derived from DU145 Rab11b^{KD} or Rab35^{KD} cells, showed a decrease in secreted growth factors, such as VEGF-A and HGF (shown in Chapter 5), which may be involved in cancer cell invasion. The role of secreted VEGF-A and HGF by myofibroblasts, has been documented for supporting aggressive tumour cell invasion (Lewis et al., 2004, Cat et al., 2006). Overexpression of HGF and c-Met can promote cancer cell invasiveness (Ebert et al., 1994, Gao and Vande Woude, 2005). Elevation of secreted HGF and VEGF was observed in prostate cancer stromal cells and exosome-differentiated fibroblasts (Webber et al., 2015), along with uPA contributing to degradation of the basement membrane and ECM (Jeffers et al., 1996, Botta et al., 2012). It could be possible that growth factors secreted from exosome-differentiated fibroblasts may play a role in triggering a proteolytic cascade for ECM modulation, supporting tumour invasion, although we do not have direct evidence for this.

mRNA analysis from 3D spheroids, revealed highly expressed levels of MMP-1 and MMP-13 in spheroids with exosome competent tumour cells containing fibroblasts, compared to spheroid containing DU145 Rab11b^{KD} or Rab35^{KD} cells. There was only TIMP-3 mRNA present in the fibroblast containing spheroids; and knockdown of Rab11b or Rab35 had a similar effect on elevating this inhibitor of metalloproteinase function. Quantification of MMP-1 and MMP-13 at the protein level was determined by ELISA. The pattern followed that of the mRNA data, revealing heightened activity in the presence of fibroblasts; and this influence is lost using either DU145 Rab11b^{KD} or Rab35^{KD} cells. This data only reveals MMP quantity, not showing MMP activity present within this 3D-microenvironment. Therefore, performing an MMP activity assay may answer whether these MMPs are involved in promoting invasion of tumour cells.

Expression of MMP-1 and MMP-13 play a role in degrading collagen type I, II and III, which are components of the interstitial stroma (Aznavoorian et al., 1993). Consistent with a number of studies, MMP-1 overexpression has been described in a wide variety of advanced cancers (Kanamori et al., 1999, Franchi et al., 2002, Liu et al., 2012); and increased MMP activity is associated with tumour progression and aggressive invasion (Sakakibara et al., 1999, Bendardaf et al., 2007). MMP-13 has been shown to enhance pancreatic tumour cell migration and invasion *in vitro* and *vivo*; and often stained heavily in highly invasive tumour cells in pancreatic cancer tissues, compared to weakly invasive cells (Tan et al., 2010, Fan et al., 2015).

By blocking MMPs, the relative importance they demonstrate in spheroid invasion can be proposed. Blockade of MMP-13 with a selector inhibitor (Cmpd-1) has been shown to reduce the tumour growth rate of two different primary breast cancer *in vivo* (Shah et al., 2012). Similarly, blockade of MMP-1 activity with specific inhibitors and antibodies, inhibited prostate cancer cell migration and invasion *in vitro*, whilst reducing tumour growth *in vivo* (Pulukuri and Rao, 2008). In many cases, MMP activity can degrade components of the ECM (collagens, fibronectin and laminins), generating fragments that have different biological activities (Xu et al., 2001, von Nandelstadh et al., 2014). For example, type I collagen degradation is mediated by MMP-1 and their by-products aids epithelial cell migration and wound healing in culture models (Pilcher et al., 1997). Furthermore, MMP-13 can activate the precursors of MMP-9 (Knäuper et al., 1997), which can degrade basement membrane type IV collagen, allowing tumour cell invasion and spread. This positive feedback loop lead to excessive collagen by-products, elevated during cancer progression and this correlates with metastatic cancer (Kehlet et al., 2016). This may activate further MMPs, allowing a continuous breakdown of the ECM and supporting the tumour's invasive nature.

As for TIMP-3, a variety of studies have shown that TIMP-3 expression is reduced in various cancer tissues, compared to non-cancerous tissues (Wu et al., 2012). Decreased TIMP-3 expression was associated with pathological stage, nodal involvement and poor survival (Mino et al., 2007, Ninomiya et al., 2008). Furthermore, elevated TIMP-3 expression is proposed to contribute to tumour progression in head and neck squamous cell carcinomas, showing to be frequently silenced by promoter hyper-methylation during cancer progression (Worsham et al., 2006). Treatment of xenografts of human prostate or breast cancer cells *in* vivo with recombinant TIMP-3 protein, reduced tumour cell proliferation, sensitised cells to chemotherapy, reducing tumour growth and invasion (Mahller et al., 2008, Shinojima et al., 2012). Possibly, TIMP-3 expression may exert its anti-proteolytic function at the invasion front of tumour cells, to quench tumour-associated ECM degrading activity, or in the stroma itself, where soluble proteases liberate ECM-tethered factors that assist cancer invasion.

Spheroids containing both exosome competent tumour cells and fibroblasts can up-regulate matrix remodelling proteins, which may degrade the ECM and support the aggressive invasive nature of the tumour. The data in this Chapter revealed that co-culture of fibroblasts and exosome competent tumour cells, maintained an aggressive invasive capacity *in vitro*. However, loss of either DU145 Rab11b- or Rab35-derived exosomes appear detrimental in invasion, even in the presence of fibroblasts. Although we may like to believe the disease modulation is due to changes in secreted vesicles, it is important that this is not potentially

exclusive. The effects could equally be due to cell-contact dependent changes and alterations in the secretome. Nonetheless, the targets of Rabs is the best method available to target vesicles in complex 3D models or indeed *in vivo*; and it is likely these observations will be a vesicle-driven process.

Next, we attempted to recapitulate these *in vitro* findings in an *in vivo* setting, by establishing xenografts consisting of DU145 control, Rab11b^{KD} or Rab35^{KD} cells with fibroblasts. Xenografts containing DU145 control cells with fibroblasts accelerated tumour growth, compared to DU145 Rab35^{KD} cells with fibroblasts, but this difference was not similar in xenografts containing DU145 Rab11b^{KD} cells. From day 35, knockdown of Rab35 significantly reduced tumour growth, compared to which controls, suggesting functional differences between Rab11b and Rab35 were not apparent from *in vitro* experiments. Similar experiments performed previously by our group, showed differences in attenuated tumour growth in xenografts with DU145 Rab27a^{KD} cells with fibroblasts over 32 days, compared to controls (Webber et al., 2015). This may be highlighted by differences in phenotype and function between these subpopulations of vesicles.

As demonstrated previously in Chapter 4, the protein profile of remaining vesicle subpopulation and secreted cytokines, following knockdown of Rab11b and Rab35 are distinct, despite showing similar effects upon fibroblast differentiation and supporting angiogenic function. Knockdown of Rab11b was capable of triggering fibroblast differentiation, if normalised for vesicle quantity to reach a threshold for activation. In contrast, vesicles produced by knockdown of Rab35 remained deficient in differentiation, irrespective of normalisation. Perhaps this may be explained by the chronic exposure of vesicle-defective tumour cells *in vivo*, between knockdown of Rab11b or Rab35. Previously, we have shown that TRAIL expression on the vesicle pellet was >2 fold increased in DU145 Rab35^{KD} remaining vesicles and <2 fold decreased in DU145 Rab11b^{KD} remaining vesicles. Although the ability of TRAIL to trigger apoptosis in certain cell lines is well-established, its physiological role is not fully defined. Though, in mice, lower expression or genetic ablation of TRAIL supports the role for this ligand in the suppression of tumour growth and metastasis *in vivo* (Takeda et al., 2001). Similarly, there appears to be an increased susceptibility to tumour initiation and metastasis in TRAIL-deficient mice (Cretney et al., 2002). Recently, comparison of gene-expression profiles in a panel of >300 human breast cancer samples revealed down-regulation of TRAIL correlates with breast cancer metastasis to the brain (Bos et al., 2009). Therefore, it could be possible that the distinct protein profiles in remaining vesicles, following knockdown of Rab11b or Rab35 in tumour cells, may have different

implications on tumour growth, which is broader that simply the effect on stromal modulation.

Furthermore, in similar *in vivo* studies, knockdown of Rab27a attenuated exosome secretion, but also impacted the cell secretome, such as the secretion of MMP-9, PGF and PDGF which have implications on modulating the tumour microenvironment (Bobrie et al., 2012, Peinado et al., 2012). In our protein profiling data (Chapter 4), as examples, we see that LIF expression was >2 fold increased in the DU145 Rab35^{KD} cell secretome, compared to a <2 fold decrease in the DU145 Rab11b^{KD} cell secretome. It is reported that elevated LIF expression induces cell cycle arrest and apoptosis, along with inhibition of melanoma cell migration (Humbert et al., 2015). It could be possible that decreased LIF expression may not induce apoptosis and migration as extensively in the Rab11b^{KD} xenograft, compared to the Rab35^{KD}; although we do not have any direct evidence for this.

As demonstrated in Chapter 5, normalisation of vesicle quantity to protein following knockdown of Rab11b or Rab35, failed to trigger a potent fibroblast differentiation response. We did observe that DU145 Rab11b^{KD} cell-derived vesicles still triggered a moderately convincing response of fibroblast differentiating into α-SMA positive myofibroblasts, compared to DU145 Rab35^{KD} cell-derived vesicles. It could be possible these fibroblasts have been 'educated' *in vivo* under the direction of the total secretome following knockdown of Rab11b, to become myofibroblasts similar to wild-type cells. Though, we highlight that Rab35-dependent vesicles appear to be important for stromal differentiation and this results in restricted tumour growth *in vivo*. Therefore, changes in the vesicle (decreased TRAIL expression) or soluble (decreased LIF expression) secretome; and the capacity to drive fibroblast differentiation following Rab11b knockdown, may all contribute to tumour growth *in vivo*, compared to the Rab35 knockdown.

In this Chapter, I have shown that silencing Rab11b or Rab35 has major effects on tumour invasion *in vitro*. This is supported by attenuated levels of matrix degrading enzymes in this 3D-microenvironment. This is recapitulated *in vivo* with knockdown of Rab35, however, this is not as clear with Rab11b. This may be explained by differences in the remaining vesicle subpopulations or cell secretome, following knockdown of Rab11b or Rab35, which may play independent roles in tumour growth and progression.

CHAPTER 7:

GENERAL DISCUSSION

7.1 General Discussion

7.1.1 Summarising Discussion

In this study, we aimed to assess the possible roles of CD9, Rab5a, Rab11b, Rab35, VAMP7 and VPS25 in exosome secretion. ESCRT proteins are involved in MVE formation in yeast and mammalian cells. Silencing VPS25 (part of ESCRT-II) reduced exosome secretion by 20%. However, as there are reports of ESCRT-II are not required for viral budding (Langelier et al., 2006) or degradation of EGFR (Bowers et al., 2006), this suggests that ESCRT-independent pathways are potentially present. Yet, we highlight VPS25 appears important for maintaining cell viability and proliferation, with signs of toxicity upon VPS25^{KD}. To assess vesicle secretion by cells undergoing major toxicity is difficult. Dead cells are unable to produce a complex range of particulates, vesicles, molecular proteins of the cells compared to viable cells.

We chose to examine CD9, because it is very abundant on DU145-derived exosomes, isolated by size exclusion chromatography (Welton et al., 2015), sucrose gradients and cushion methods (Webber et al., 2014). It was reported that silencing CD9 reduced the secretion of EVs in Nalm-6 pre-B cells (Mazurov et al., 2013); and in mouse-derived bone marrow DCs (Chairoungdua et al., 2010). Though, we report minimal impact in quantity of secreted vesicles following CD9^{KD}, there are differences in enrichment of exosome-associated proteins. Little changes in levels of ESCRT-proteins suggests CD9 vesicles are maintained in a manner independent of ESCRT, but are perhaps dependent on LAMP or HSP. The importance of CD9 in other cell types may play roles in exosome secretion, yet it is not a major influence on exosome secretion in DU145 cells.

Few studies have attempted to address the requirement for SNAREs in vesicle secretion. We examined silencing VAMP7 reported a modest decrease in vesicle secretion, yet only a modest decrease in LAMP proteins. One study reported that VAMP7 is not required for exosome secretion in MDCK cells (Proux-Gillardeaux et al., 2007), but inhibits lysosome secretion. In contrast, VAMP7 was found to be involved in exosome secretion by K562 cells (Fader et al., 2009). Currently, 36 SNARE proteins have been described in human cells (Jahn and Scheller, 2006), but only one SNARE protein has been assessed in this study. Other studies may suggest different cell types, may have different SNARE complexes involved in fusion of MVEs with the plasma membrane. Possibly, SNARE complexes may mediate fusion of specific MVE within a single cell type; and silencing VAMP7 may affect a specific vesicle subpopulations. The quantification of several exosome-associated proteins (ESCRT and HSPs) appeared to be unaffected, compared to controls, which may provide some insight into the

latter possibility. It should be stressed, we cannot convincingly conclude the role of VAMP7 analysed here in vesicle secretion, as further studies such as molecular profiling data and functional data, will be required.

Rabs constitute the largest family of small Ras-like GTPases, with over 70 types identified now in humans (Hutagalung and Novick, 2011). By knocking down Rab5a, an increase in vesicle number was observed. Contrasting studies have shown silencing Rab5a inhibited exosome secretion (Ostrowski et al., 2010), or increased secretory granules per cell (Azouz et al 2014). Different Rab5 isoforms may play different roles, such as trafficking early endosomes or trafficking to lysosomes for degradation in different cell types (Chen et al., 2009). It remains possible that Rab5a may redirect endosomes to undergo exocytosis to release vesicles, instead of directing to lysosomes (Tan et al., 2016). As Rab5a is involved in endocytosing molecules, autocrine vesicle uptake from the cell may be abrogated; and may explain increased vesicle accumulation in the extracellular space. Nonetheless, it's important to consider other Rab5 isoforms and their roles in exosome biogenesis and secretion, but also the interplay between either autophagy or endocytosis may explain this increase in vesicle secretion.

By silencing Rab11b or Rab35, little signs of toxicity were shown. Alterations in the late endosome was present, as either knockdown revealed an accumulation of CD63, CD81 or LAMP1 in peri-nuclear structures. Similarly, these observations were reported in other cell types because of attenuated Rab11b (Grimsey et al., 2016), Rab27a (Ostrowski et al., 2010, Webber et al., 2015) and Rab35 (Hsu et al., 2010). These observations were consistent with the diminished capacity to expel these proteins out of the cell in association with vesicles. A 20% decrease in vesicle secretion was measured, following Rab11b or Rab35 knockdown by NTA. This was also shown with a decrease in exosomal-associated proteins by plate-based assays and Western blot. Despite a strong knockdown at the RNA level (95%), the impact on exosomes is rather minor. It suggests that other pathways deliver MVEs to the plasma membrane, in which Rab11b or Rab35 are redundant; and supports the notion that other co-existing MVEs are present and differentially trafficked.

It was suggested that Rab11b or Rab35 regulate the same vesicle pathway, as silencing either protein resulted in a vesicle population that was approximately 80% of control cells. It was first reported that Rab11 was involved in trafficking MVEs to the plasma membrane (Savina et al., 2002), but it remains unknown which type of MVE was trafficked. In one study both Rab11 and Rab35 mediated slow endocytic recycling through endosomes to the plasma

membrane (Stenmark, 2009). Similarly, Rab35 have been shown to promote the recruitment of other related Rab proteins to recycling endosomes in yeast models (Rahajeng et al., 2012); and in a neuroendocrine tumour cell line (Kobayashi et al., 2014). Additional roles for Rab35 has been reported to localise at the newly formed early endosomes to traffic the transferrin receptor (Kouranti et al., 2006), or the mannose-6-phosphate receptor (Cauvin et al., 2016). However, in oligodendrocytes, Rab35 has been proposed to be involved in acting on the late endosome (Hsu et al., 2010). Interestingly, work in *C. elegans* showed that the combined knockdown of both Rab11 and Rab35 leads to a dramatic enhancement of intracellular accumulation of endosomal cargo (Sato et al., 2008). We have evidence from the protein profiling array to propose both that Rab11b and Rab35 regulating distinct exosome-secretion pathways in the remaining (80%) vesicle population; with decreased CXCL6 ($Rab11b^{KD}$) and increased CXCL6 ($Rab35^{KD}$) as an example. However, the specific endosomal compartments that Rab11b and Rab35 regulate are poorly understood; although this thesis provides evidence that they possess independent parallel roles in endosomal trafficking rather than acting in sequential stages.

Attenuating Rab proteins has been demonstrated to impact on the soluble secretome (Bobrie et al., 2012). Our protein profiling data agrees with this notion, in relation to Rab11b and Rab35. As one example, LIF and IL-6 were significantly elevated in the Rab35-knockdown secretome, but this was not a feature of the vesicles. This suggests that these factors are present as soluble factors, rather than association with vesicles. Profiles of the secretome highlight examples of dissimilarities and show that knockdown of Rab11b or Rab35 impart distinct effects on the general secretome, which are not vesicle-exclusive effect.

Previously, it was demonstrated that tumour exosomes can drive fibroblast differentiation into myofibroblast (Webber et al., 2010). This distinct myofibroblastic phenotype arising from tumour exosome treatment, differs to cancer-associated stromal cells treated with rhTGF-β1, as they promote angiogenesis *in vitro* and tumour growth *in vivo* (Webber et al., 2015). Here, we report that the general secretome appeared to lack the capacity to drive fibroblast differentiation, despite containing other factors as well as the presence of vesicles. Though, this issue may be due to a lack of seeded cell numbers, hence, the number of vesicles available from the total secretome is minimal. However, fibroblast differentiation resided in the vesicle concentrates, implicating this is a vesicle-driven process. Following vesicle concentration from Rab11b or Rab35 knockdown, there was a diminished capacity to drive differentiation. This vesicle-mediated differentiation mechanism is dependent on the levels of vesicle-tethered TGF-β1 (Webber et al., 2010). This could be explained by the loss of as

little as 20% of the vesicle subpopulation to disrupt the threshold required for differentiation. Similar studies have also not achieved the required threshold in vesicles, with changes in lymphocyte mRNA expression (Muller et al., 2016) or invasion of trophoblasts (Salomon et al., 2013).

Alternatively, a possible explanation for this failure to drive fibroblast differentiation is that the vesicle phenotype following knockdown of Rab11b or Rab35 is altered, which renders the remaining vesicle population insufficient in this functional activity. We report that by treating fibroblasts with equal vesicle quantities in control, Rab11b^{KD} and Rab35^{KD}; the Rab11b^{KD} were still capable of driving sufficient differentiation. This was only capable if vesicles were added to reach the correct threshold for activation. In contrast, the vesicles secreted from Rab35^{KD} cells appeared to be deficient in their ability to differentiation, irrespective of normalisation. It could be possible that these Rab35-dependent vesicles may contain specific mRNA/miRNA (Valadi et al., 2007), proteins or other molecules, along with TGF-β1 delivery, that may drive fibroblast differentiation. Additional investigation would be required to understand the molecular features of Rab11b (functional) and Rab35 (dysfunctional). The profiling performed so far is not of sufficient breadth and complexity to provide us with these answers and a more extensive analysis would be required. This data highlights the distinct vesicle profiles remaining in cells following knockdown of either Rab11b or Rab35, revealing Rab35-dependent vesicles are required for fibroblast differentiation into myofibroblasts.

In the absence of fibroblast differentiation, stromal cells that arise demonstrate poor tumour-supporting function, such as angiogenesis. The direct effect of cancer exosomes on endothelial cells promoting angiogenesis (Sheldon et al., 2010), or indirectly through differentiated myofibroblasts to support angiogenesis has been reported (Webber et al., 2015). We showed a loss of Rab11b- or Rab35-dependent vesicles can strongly attenuate the secretion of pro-angiogenic growth factors, HGF and VEGF; slowing endothelial cell migration and inhibiting vessel formation. These regulators also appear to be relevant in context of a 3D-microenvironment of a tumour:fibroblast co-culture model, that appear to drive an aggressive matrix invasive behaviour. We provided some evidence that the presence of tumour cells and fibroblasts are present within the leading edge, yet the signal for fibroblasts was weak and difficult to detect over time. This invasive behaviour was attenuated when Rab11b or Rab35 were knocked down, as this may have interfered with tumour-stroma communication. However, we cannot state this effect is exclusively due to vesicle loss, as the

knockdowns could influence the soluble secretome, which may impact other aspects of cell behaviour, such as adhesion or motility.

This aggressive invasive behaviour was attenuated in the absence of Rab11b or Rab35, or even in the presence of fibroblasts. We reported a reduction in levels of MMPs within the 3D-microenvironment, containing the knockdown of Rab11b or Rab35. MMPs are reported to play roles in promoting tumour growth (Franchi et al., 2002, Shah et al., 2012), by enabling penetration through the ECM (Pilcher et al., 1997), supporting invasion (Hsu et al., 2006, Bendardaf et al., 2007). However, it remains difficult to determine whether enhanced MMP secretion is truly relevant to this aggressive invasion that is observed. Methods would include inhibition of MMP activity or detecting levels of MMP activity within the 3D-microenvironment. It could be possible MMPs may be present on the vesicles, playing this invasive function of tumour cells, as demonstrated in melanoma derived exosomes (Hakulinen et al., 2008). Nevertheless, this data reports that Rab11b and Rab35 have an influence on the invasivity of heterotypic spheroids and MMP levels present in the 3D-microenvironment; and together with the previous data, this emphasises the importance for activation of the tumour-supportive fibroblast functions.

Many of the *in vitro* experiments in this study demonstrated that knocking down of either Rab11b or Rab35 gives rise to functionally similar effects shown in a multitude of short-term based assays. Here, we reported that injecting these manipulated tumour cells with fibroblasts showed significant differences. Knockdown of Rab11b had no significant impact on tumour growth *in vivo*, with tumour volume similar to controls. Alternatively, knockdown of Rab35 significantly attenuated tumour growth after 46 days. This may be explained by differences in the secretome following knockdown of Rab11b or Rab35. The chronic exposure to vesicle-defective tumour cells *in vivo* revealed functional differences that were not clear from *in vitro* experiments. Furthermore, we show differences in secretion of growth factors from fibroblasts treated with vesicles, following knockdown of Rab11b (increased FGF-2) or Rab35 (decreased uPA). From previous data, we showed differences in the levels of CXCL6 following knockdown with decreased CXCL6 ($Rab11b^{KD}$) and increased CXCL6 ($Rab35^{KD}$) as an example. These secreted cytokines may play roles in modulating the immune response or enhancing tumour cell proliferation *in vivo*. In similar models, blockade of Rab27a attenuated exosome secretion and impacted the secretion of growth factors (PIGF-2 or PDGF) or MMP-9, reducing tumour growth and metastasis *in vivo* (Bobrie et al., 2012, Peinado et al., 2012, Webber et al., 2015). Nevertheless, the collective functional data

demonstrates the differences in phenotype between vesicle subpopulations and the influence they have in driving tumour growth.

In this Thesis, the data identifies a minor role for Rab11b and Rab35 in regulating the overall secretion of vesicles from prostate cancer cells. Interfering with these pathways attenuates vesicle secretion by 20%, impacting vesicle-mediated communication between tumour and stromal cells; restricting stromal differentiation, angiogenic and invasive behaviours. Here, we showed that Rab11b and Rab35 GTPases regulate distinct pathways, resulting in different vesicle molecular phenotypes. Attenuating the Rab35-dependent vesicle subpopulation that remains functionally important for stromal differentiation, results in reduced tumour growth *in vivo*, as shown in Figure 7.1. Molecular targeting of this specific vesicle subpopulation may provide to be a novel avenue likely to attenuate the tumour promoting microenvironment to ultimately slow disease progression.

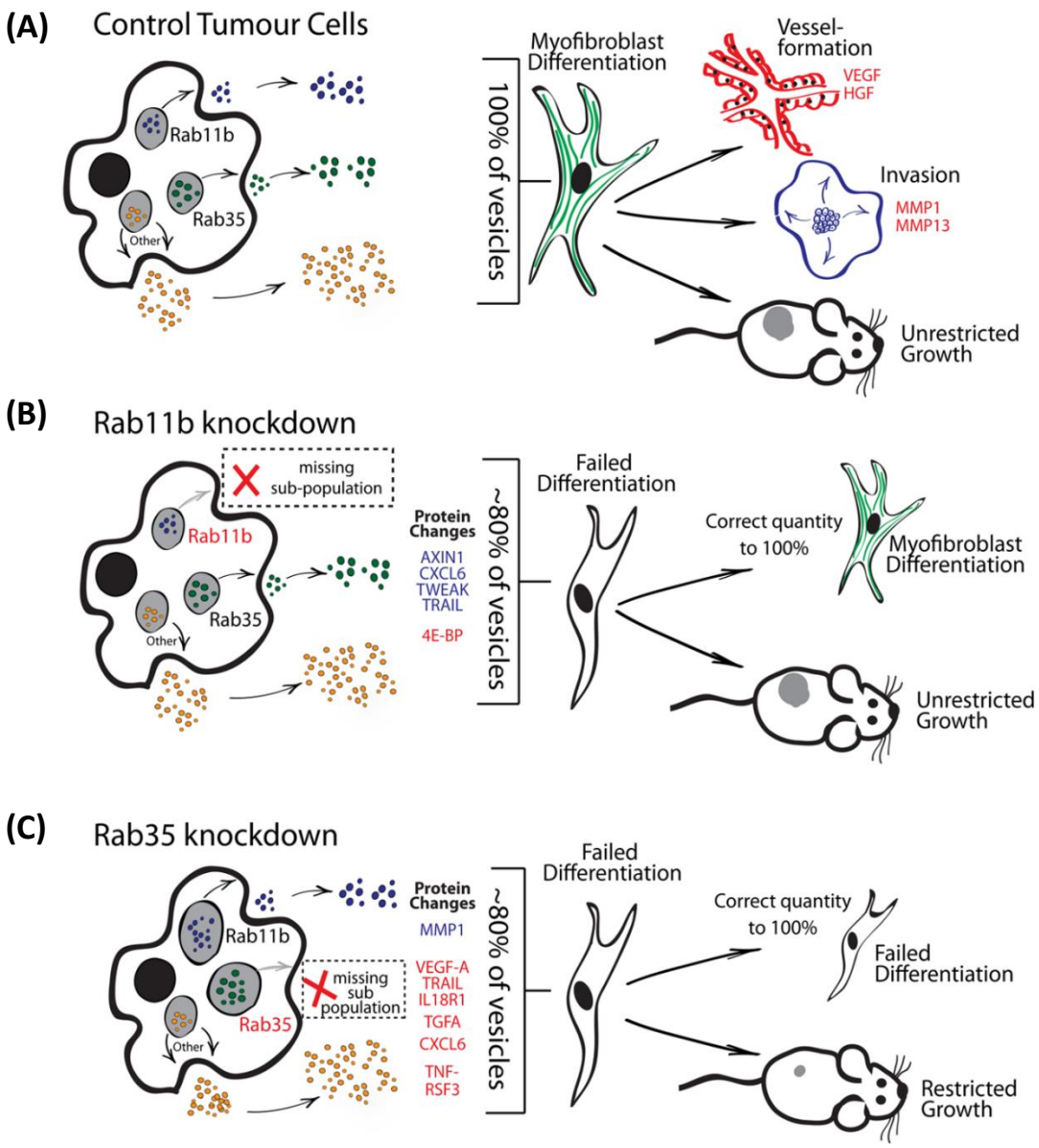

Figure 7.1. Schematic summary of Rab11b- or Rab35-dependent vesicle effects on the stroma and *in vivo*. (A) Wild-type tumour cells secrete a heterogeneously subpopulation of exosomes, which drives fibroblast differentiation into myofibroblast with a subsequent supportive pro-angiogenic and invasive phenotype. This results in unrestricted growth in xenografts *in vivo*. **(B)** Knockdown of Rab11b resulted in a 20% loss in total vesicles, with decreased (Blue) and increased levels (Red) in secreted protein; though this is not critical, as the remaining population retains the ability to support differentiation and tumour growth. **(C)** Likewise, knockdown of Rab35 resulted in a 20% loss in total vesicles and the remaining vesicles exhibit a distinct protein profile. With these vesicles, however, differentiation does not occur and restrict tumour growth was shown *in vivo*.

7.1.2 Future Directions

Within this study, specific exosome subpopulations have been demonstrated to be strong drivers of fibroblast differentiation, that can aid tumour growth and progression. Understanding the molecular phenotype of these Rab35-dependent exosomes and their interaction with other cell types within the stroma, may provide additional avenues to slow tumour growth and progression.

Exploring the Importance of CD9, Rab5a and VAMP7

We have not explored the full importance of CD9, Rab5a and VAMP7 in other roles involved in endocytic trafficking. In this study, we have indicated that Rab5a may have a role for elevating the EV content of the total secretome, that could occur through accelerated exosome secretion or by regulating the capacity of endocytic uptake of exosomes. The role of Rab5a has been predominantly involved in mediating the early endocytic pathway (Gorvel et al., 1991), or an autophagy-mediated dependent pathway (Tan et al., 2016). As Rab5a is involved in endocytosing molecules, autocrine vesicle uptake from the cell may be abrogated; and may explain increased vesicle accumulation in the extracellular space. One area of investigation would be to explore if different endocytosis pathways are dependent on the Rab5a protein; does blockade of Rab5a lead to inhibition of specific endocytosis pathways leading to the accumulation of vesicles in the extracellular space? Would the presence of additional vesicles within the extracellular space lead to a more aggressive tumour-supporting phenotype?

Few studies have addressed the requirement for SNAREs in exosome secretion. VAMP7 was indicated to have a role for attenuating EV secretion (Fader et al., 2009); as shown in this Thesis. It could be possible different SNARE complexes could mediate fusion of specific subpopulations of MVEs within a single cell type, potentially impacting a specific vesicle subpopulations. The data suggests knockdown of VAMP7 or CD9 does not impact ESCRT-related proteins. Instead, CD9 might be involved in cargo loading on MVEs, as there was no significant differences in vesicle number, but changes in the levels of exosomal-associated proteins. One area of investigation would be to explore the molecular profile of the vesicles following knockdown of CD9, Rab5a and VAMP7, that will give us a greater comprehensive understanding of proteins present on the surface. Furthermore, it would be important to understand whether these proteins can redirect endosomal trafficking or mediate cargo loading onto MVEs.

The in-depth Mechanism of Exosome-Induced Myofibroblast Differentiation

The mechanism behind the generation of myofibroblasts by cancer exosomes remains poorly understood. Here, we highlight the role of Rab35-dependent vesicles on triggering differentiation and it could be possible these vesicles may incorporate distinct miRNA and mRNA (Valadi et al., 2007) into recipient cells, that vary from Rab11b-dependent vesicles. Studies have focused on the role of exosomal miRNA in their regulatory role on gene expression (Kosaka et al., 2010). As one example, tumour-associated myofibroblasts express significantly higher levels of miRNA-21, compared to ovarian tumour cells (Au Yeung et al., 2016). Co-culture experiments highlight transfer of miRNA-21 to neighbouring tumour cells suppressing apoptosis. Though, there are limitations to some of the current functional studies associated with exosomal miRNA. As mentioned previously, there are multiple methods to isolate vesicles which may vary in the exosomal content, including proteins and miRNA (Kosaka et al., 2010, Hu et al., 2012). Though, it leads us to question the role of exosomal miRNA, to investigate if Rab35-dependent vesicles contain miRNA differing from Rab11b-dependent vesicles that would exert a different functional capacity, such as fibroblast differentiation. Though, some studies have implicated exosomes do not exert any functions via miRNA, and this is all due to cellular miRNA, it remains to be questioned and investigated in greater detail.

Targeting Rab35-Dependent Vesicles as a Therapeutic Approach

Since the data emphasises the role of Rab35-dependent vesicles for driving fibroblast to myofibroblast differentiation, leading to diminished angiogenesis and attenuated invasive behaviours in 3D *in vitro* models. Silencing Rab35-dependent vesicles significantly reduced tumour growth rates *in vivo* and targeting these vesicles may act as a therapeutic approach to slow tumour growth and progression.

In breast cancer, the expression of human epidermal growth factor receptor 2 (HER2) protein can stimulate tumour growth and progression, where this intracellular signalling is proposed to be exemplified with exosomes (Marleau et al., 2012). Herceptin® (HER2-blocking antibody) is often used as a therapeutic antibody to treat breast cancer and exosomes can interfere with its activity. There has been the development of the extracorporeal haemofiltration of exosomes from the whole circulatory system, using an affinity plasmapheresis platform, known as Aethlon ADAPT™ (adaptive dialysis-like affinity technology system), which separates particles based on size and phenotype (Marleau et al., 2012). This device consists of an outer compartment containing immobilised affinity agents (proteins of interest), which the compartment is integrated with a standard renal dialysis

machine. As blood passes through this system, particles smaller than 200nm will pass through that will be able to specifically bind to exosomes expressing proteins of interest; in our case Rab35. Currently, this machine is being used to eliminate Hepatitis C viruses from the circulatory system in some infected patients. Though, the safety and efficacy of this ADAPT™ machine for exosomal removal remains to be clinically tested, it may introduce a new therapeutic avenue to remove vesicle subpopulations.

There has been approaches to develop inhibitors to block exosome secretion to attenuate different disease states. It was demonstrated that a ceramide-dependent mechanism is present to secrete exosomes in mouse oligodendroglial cells (Trajkovic et al., 2008). This led to the development of the GW4869 drug, a neutral sphingomyelinase (sphingomyelinase hydrolyses sphingomyelin into phosphocholine and ceramide) inhibitor, first used to inhibit exosome secretion in human embryonic kidney cells (Kosaka et al., 2010); and in mouse cardiac endothelial cells (Wang et al., 2014). However, it has been reported that administering GW4869 in primary cell line induces cell death, which provides an unreliable analysis of exosomes (Colombo et al., 2014); and demonstrated to be cytotoxic even when administered at low doses to myeloma cells (Vuckovic et al., 2017). Alternative approaches have been investigated in exploring the role of V-ATPase (large multi-subunit proton pump) on exosomes. They have roles in acidifying the endosomal lumen by localising the concentration of protons, powered by ATP hydrolysis. A study reported that V-ATPase has a direct interaction with VAMP protein, appearing to play a role in fusion neurotransmitter release (El Far and Seagar, 2011). V-ATPase inhibitors, balfilomycin A1 and concanamycin A, were proposed to inhibit the secretion of Rab27b-dependent vesicles in breast cancer cells (Rasschaert et al., 2015).

Here, we would propose developing an inhibitor would be a novel approach to prevent the Rab35-dependent vesicle subpopulation, that has the capacity to activate the stroma and promote tumour growth *in vivo*. Future investigation would utilise a high-throughput approach to screen for inhibitors, to target their protein-protein interactions *in silico* and translate these findings *in vitro* and *vivo*. This would open a novel avenue to target a Rab35-dependent vesicle subpopulation that is key in driving tumour growth and progression, although a limited number of pharmacological approaches have been investigated and this would open for further investigation.

Concluding Remark

For the first time, we show that Rab35-dependent tumour vesicles is key for communication between cancer and stromal cells; and is essential for generating a tumour microenvironment favourable for disease progression. This emphasises along with the current literature that the presence of exosome heterogeneity is present and targeting a specific subpopulation may provide a novel valuable therapeutic approach for attenuating tumour growth and progression.

References

ABOUNADER, R. & LATERRA, J. 2005. Scatter factor/hepatocyte growth factor in brain tumor growth and angiogenesis. *Neuro Oncol,* 7**,** 436 - 451.

ABRAMI, L., BRANDI, L., MOAYERI, M., BROWN, M. J., KRANTZ, B. A., LEPPLA, S. H. & VAN DER GOOT, F. G. 2013. Hijacking multivesicular bodies enables long-term and exosome-mediated long-distance action of anthrax toxin. *Cell Rep,* 5**,** 986-96.

ABUSAMRA, A. J., ZHONG, Z., ZHENG, X., LI, M., ICHIM, T. E., CHIN, J. L. & MIN, W. P. 2005. Tumor exosomes expressing Fas ligand mediate CD8+ T-cell apoptosis. *Blood Cells Mol Dis,* 35**,** 169-73.

ADAMS, R. H. & ALITALO, K. 2007. Molecular regulation of angiogenesis and lymphangiogenesis. *Nat Rev Mol Cell Biol,* 8**,** 464-78.

ALBINI, A. 1998. Tumor and endothelial cell invasion of basement membranes. The matrigel chemoinvasion assay as a tool for dissecting molecular mechanisms. *Pathol Oncol Res,* 4**,** 230 - 241.

ALBINI, A., IWAMOTO, Y., KLEINMAN, H., MARTIN, G., AARONSON, S., KOZLOWSKI, J. & MCEWAN, R. 1987. A rapid in *vitro assay* for quantitating the invasive potential of tumor cells. *Cancer Res,* 47**,** 3239 - 3245.

ALIMIRAH, F., CHEN, J., BASRAWALA, Z., XIN, H. & CHOUBEY, D. 2006. DU-145 and PC-3 human prostate cancer cell lines express androgen receptor: implications for the androgen receptor functions and regulation. *FEBS Lett,* 580**,** 2294-300.

ANADA, T., FUKUDA, J., SAI, Y. & SUZUKI, O. 2012. An oxygen-permeable spheroid culture system for the prevention of central hypoxia and necrosis of spheroids. *Biomaterials,* 33**,** 8430-41.

ANDERSON, H. & REYNOLDS, J. 1973. Pyrophosphate stimulation of calcium uptake into cultured embryonic bones. Fine structure of matrix vesicles and their role in calcification. *Dev Biol,* 34**,** 211 - 227.

ANDERSON, L. & SEILHAMER, J. 1997. A comparison of selected mRNA and protein abundances in human liver. *Electrophoresis,* 18**,** 533 - 537.

ANDRÉ, F., SCHARTZ, N., CHAPUT, N., FLAMENT, C., RAPOSO, G., AMIGORENA, S., ANGEVIN, E. & ZITVOGEL, L. 2002. Tumor-derived exosomes: a new source of tumor rejection antigens. *Vaccine,* 20**,** A28 - 31.

ANDREOLA, G., RIVOLTINI, L., CASTELLI, C., HUBER, V., PEREGO, P., DEHO, P., SQUARCINA, P., ACCORNERO, P., LOZUPONE, F., LUGINI, L., STRINGARO, A., MOLINARI, A., ARANCIA, G., GENTILE, M., PARMIANI, G. & FAIS, S. 2002. Induction of lymphocyte apoptosis by tumor cell secretion of FasL-bearing microvesicles. *Journal Exp Med,* 195**,** 1303-1316.

ATALA, A. & LANZA, R. 2001. *Methods of Tissue Engineering*, Academic Press.

AU YEUNG, C. L., CO, N. N., TSURUGA, T., YEUNG, T. L., KWAN, S. Y., LEUNG, C. S., LI, Y., LU, E. S., KWAN, K., WONG, K. K., SCHMANDT, R., LU, K. H. & MOK, S. C. 2016. Exosomal transfer of stroma-derived miR21 confers paclitaxel resistance in ovarian cancer cells through targeting APAF1. *Nat Commun,* 7**,** 11150.

AVGUSTINOVA, A., IRAVANI, M., ROBERTSON, D., FEARNS, A., GAO, Q., KLINGBEIL, P., HANBY, A. M., SPEIRS, V., SAHAI, E., CALVO, F. & ISACKE, C. M. 2016. Tumour cell-derived Wnt7a recruits and activates fibroblasts to promote tumour aggressiveness. *Nat Commun,* 7**,** 10305.

AXCRONA, K., AALTOMAA, S., DA SILVA, C. M., OZEN, H., DAMBER, J. E., TANKO, L. B., COLLI, E. & KLARSKOV, P. 2012. Androgen deprivation therapy for volume reduction, lower urinary tract symptom relief and quality of life improvement in patients with prostate cancer: degarelix vs goserelin plus bicalutamide. *BJU Int,* 110**,** 1721-8.

AYALA, A. & RO, J. 2007. Prostatic intraepithelial neoplasia: recent advances. *Arch Pathol Lab Med,* 131**,** 1257 - 1266.

AZNAVOORIAN, S., MURPHY, A., STETLER-STEVENSON, W. & LIOTTA, L. 1993. Molecular aspects of tumor cell invasion and metastasis. *Cancer,* 71**,** 1368 - 1383.

AZOUZ, N. P., ZUR, N., EFERGAN, A., OHBAYASHI, N., FUKUDA, M., AMIHAI, D., HAMMEL, I., ROTHENBERG, M. E. & SAGI-EISENBERG, R. 2014. Rab5 is a novel regulator of mast cell secretory granules: impact on size, cargo, and exocytosis. *J Immunol,* 192**,** 4043-53.

BABST, M., KATZMANN, D., ESTEPA-SABAL, E., MEERLOO, T. & EMR, S. 2002a. Escrt-III: an endosome-associated heterooligomeric protein complex required for mvb sorting. *Dev Cell,* 3**,** 271 - 282.

BABST, M., KATZMANN, D., SNYDER, W., WENDLAND, B. & EMR, S. 2002b. Endosome-associated complex, ESCRT-II, recruits transport machinery for protein sorting at the multivesicular body. *Dev Cell,* 3**,** 283 - 289.

BABST, M., WENDLAND, B., ESTEPA, E. & EMR, S. 1998. The Vps4p AAA ATPase regulates membrane association of a Vps protein complex required for normal endosome function. *EMBO J,* 17**,** 2982 - 2993.

BACHE, K. G., BRECH, A., MEHLUM, A. & STENMARK, H. 2003. Hrs regulates multivesicular body formation via ESCRT recruitment to endosomes. *Cell Biol,* 162**,** 435-442.

BAGLIO, S. R., LAGERWEIJ, T., PEREZ LANZON, M., XUAN HO, D., LEVEILLE, N., MELO, S. A., CLETON-JANSEN, A. M., JORDANOVA, E. S., RONCUZZI, L., GRECO, M., VAN EIJNDHOVEN, M. A., GRISENDI, G., DOMINICI, M., BONAFEDE, R., LOUGHEED, S., DE GRUIJL, T. D., ZINI, N., CERVO, S., STEFFAN, A., CANZONIERI, V., MARTSON, A., MAASALU, K., KOKS, S., WURDINGER, T., BALDINI, N. & PEGTEL, D. M. 2017. Blocking tumor-educated MSC paracrine activity halts osteosarcoma progression. *Clin Cancer Res,* 23**,** 3721 - 3733.

BAHARVAND, H., HASHEMI, S. M., KAZEMI ASHTIANI, S. & FARROKHI, A. 2006. Differentiation of human embryonic stem cells into hepatocytes in 2D and 3D culture systems in vitro. *Int J Dev Biol,* 50**,** 645-52.

BAIETTI, M. F., ZHANG, Z., MORTIER, E., MELCHIOR, A., DEGEEST, G., GEERAERTS, A., IVARSSON, Y., DEPOORTERE, F., COOMANS, C., VERMEIREN, E., ZIMMERMANN, P. & DAVID, G. 2012. Syndecan-syntenin-ALIX regulates the biogenesis of exosomes. *Nat Cell Biol,* 14**,** 677-85.

BAJOU, K., LEWALLE, J. M., MARTINEZ, C. R., SORIA, C., LU, H., NOEL, A. & FOIDART, J. M. 2002. Human breast adenocarcinoma cell lines promote angiogenesis by providing cells with uPA-PAI-1 and by enhancing their expression. *Int J Cancer,* 100**,** 501-6.

BAKER, B. M. & CHEN, C. S. 2012. Deconstructing the third dimension: how 3D culture microenvironments alter cellular cues. *J Cell Sci,* 125**,** 3015-24.

BAKER, M., ROBINSON, S. D., LECHERTIER, T., BARBER, P. R., TAVORA, B., D'AMICO, G., JONES, D. T., VOJNOVIC, B. & HODIVALA-DILKE, K. 2011. Use of the mouse aortic ring assay to study angiogenesis. *Nat Protoc,* 7**,** 89-104.

BEAUCHAMP, P., MORITZ, W., KELM, J. M., ULLRICH, N. D., AGARKOVA, I., ANSON, B. D., SUTER, T. M. & ZUPPINGER, C. 2015. Development and characterization of a scaffold-free 3D spheroid model of induced pluripotent stem cell-derived human cardiomyocytes. *Tiss Eng Part C Methods,* 21**,** 852-61.

BECKETT, K., MONIER, S., PALMER, L., ALEXANDRE, C., GREEN, H., BONNEIL, E., RAPOSO, G., THIBAULT, P., LE BORGNE, R. & VINCENT, J. P. 2013. *Drosophila* S2 cells secrete wingless on exosome-like vesicles but the wingless gradient forms independently of exosomes. *Traffic,* 14**,** 82-96.

BELLACEN, K. & LEWIS, E. C. 2009. Aortic ring assay. *J Vis Exp,* 33**,** 1564.

BEN-SHLOMO, Y., EVANS, S., IBRAHIM, F., PATEL, B., ANSON, K., CHINEGWUNDOH, F., CORBISHLEY, C., DORLING, D., THOMAS, B., GILLATT, D., KIRBY, R., MUIR, G., NARGUND, V., POPERT, R., METCALFE, C., PERSAD, R. & GROUP, P. S. 2008. The risk of prostate cancer amongst black men in the United Kingdom: the PROCESS cohort study. *Eur Urol,* 53**,** 99-105.

BENDARDAF, R., BUHMEIDA, A., RISTAMAKI, R., SYRJANEN, K. & PYRHONEN, S. 2007. MMP-1 (collagenase-1) expression in primary colorectal cancer and its metastases. *Scand J Gastroenterol,* 42**,** 1473-8.

BENMERAH, A. & LAMAZE, C. 2007. Clathrin-coated pits: vive la difference? *Traffic,* 8**,** 970-82.

BENYA, P. & SHAFFER, J. 1982. Dedifferentiated chondrocytes reexpress the differentiated collagen phenotype when cultured in agarose gels. *Cell,* 30**,** 215 - 224.

BERNATCHEZ, P., SOKER, S. & SIROIS, M. 1999. Vascular endothelial growth factor effect on endothelial cell proliferation, migration, and platelet-activating factor synthesis is Flk-1-dependent. *J Biol Chem,* 274**,** 31047 - 31054.

BETTENDORF, O., SCHMIDT, H., STAEBLER, A., GROBHOLZ, R., HEINECKE, A., BOECKER, W., HERTLE, L. & SEMJONOW, A. 2008. Chromosomal imbalances, loss of heterozygosity, and immunohistochemical expression of TP53, RB1, and PTEN in intraductal cancer, intraepithelial neoplasia, and invasive adenocarcinoma of the prostate. *Genes Chromosomes Cancer,* 47**,** 565-72.

BOBRIE, A., KRUMEICH, S., REYAL, F., RECCHI, C., MOITA, L. F., SEABRA, M. C., OSTROWSKI, M. & THERY, C. 2012. Rab27a supports exosome-dependent and -independent mechanisms that modify the tumor microenvironment and can promote tumor progression. *Cancer Res,* 72**,** 4920-30.

BOCCACCIO, C., ANDÒ, M., TAMAGNONE, L., BARDELLI, A., MICHIELI, P., BATTISTINI, C. & COMOGLIO, P. 1998. Induction of epithelial tubules by growth factor HGF depends on the STAT pathway. *Nature,* 391**,** 285 - 288.

BOIRE, A., COVIC, L., AGARWAL, A., JACQUES, S., SHERIFI, S. & KULIOPULOS, A. 2005. PAR1 is a matrix metalloprotease-1 receptor that promotes invasion and tumorigenesis of breast cancer cells. *Cell,* 120**,** 303-13.

BORGES, F. T., MELO, S. A., OZDEMIR, B. C., KATO, N., REVUELTA, I., MILLER, C. A., GATTONE, V. H., 2ND, LEBLEU, V. S. & KALLURI, R. 2013. TGF-β1-containing exosomes from injured epithelial cells activate fibroblasts to initiate tissue regenerative responses and fibrosis. *J Am Soc Nephrol,* 24**,** 385-92.

BOS, P. D., ZHANG, X. H., NADAL, C., SHU, W., GOMIS, R. R., NGUYEN, D. X., MINN, A. J., VAN DE VIJVER, M. J., GERALD, W. L., FOEKENS, J. A. & MASSAGUE, J. 2009. Genes that mediate breast cancer metastasis to the brain. *Nature,* 459**,** 1005-9.

BOTTA, A., DELTEIL, F., METTOUCHI, A., VIEIRA, A., ESTRACH, S., NEGRONI, L., STEFANI, C., LEMICHEZ, E., MENEGUZZI, G. & GAGNOUX-PALACIOS, L. 2012. Confluence switch signaling regulates ECM composition and the plasmin proteolytic cascade in keratinocytes. *J Cell Sci,* 125**,** 4241-52.

BOWERS, K., PIPER, S. C., EDELING, M. A., GRAY, S. R., OWEN, D. J., LEHNER, P. J. & LUZIO, J. P. 2006. Degradation of endocytosed epidermal growth factor and virally ubiquitinated major histocompatibility complex class I is independent of mammalian ESCRTII. *J Biol Chem,* 281**,** 5094-105.

BRENNECKE, J., STARK, A., RUSSELL, R. B. & COHEN, S. M. 2005. Principles of microRNA-target recognition. *PLoS Biol,* 3**,** e85.

BRETTON, P., EVANS, W., BORDEN, J. & CASTELLANOS, R. 1994. The use of prostate specific antigen density to improve the sensitivity of prostate specific antigen in detecting prostate carcinoma. *Cancer,* 74**,** 2991 - 2995.

BUNKER, C., PATRICK, A., MAHARAJ, G., KEENAN, H., RAMNARINE, S., BELLE, A., RICHARD, J. & DHIR, R. 2002. Prostate cancer risk is three-fold higher among men, aged 50-64, of African descent compared with men of Asian-Indian descent in Trinidad and Tobago. *Ethn Dis,* 12**,** S3-30-3.

BUSCHOW, S. I., NOLTE-'T HOEN, E. N., VAN NIEL, G., POLS, M. S., TEN BROEKE, T., LAUWEN, M., OSSENDORP, F., MELIEF, C. J., RAPOSO, G., WUBBOLTS, R., WAUBEN, M. H. & STOORVOGEL, W. 2009. MHC II in dendritic cells is targeted to lysosomes or T cell-induced exosomes via distinct multivesicular body pathways. *Traffic,* 10**,** 1528-42.

BUSSOLINO, F., DI RENZO, M., ZICHE, M., BOCCHIETTO, E., OLIVERO, M., NALDINI, L., GAUDINO, G., TAMAGNONE, L., COFFER, A. & COMOGLIO, P. 1992. Hepatocyte growth factor is a potent angiogenic factor which stimulates endothelial cell motility and growth. *J Cell Biol,* 119**,** 629 - 641.

CABALLERO, M., GRAU, J., BLANCH, J., DOMINGO-DOMENECH, J., AUGE, J., JIMENEZ, W. & BERNAL-SPREKELSEN, M. 2007. Serum vascular endothelial growth factor as a predictive factor in metronomic (weekly) Paclitaxel treatment for advanced head and neck cancer. *Arch Otolaryngol Head Neck Surg,* 133**,** 1143 - 1148.

CABY, M. P., LANKAR, D., VINCENDEAU-SCHERRER, C., RAPOSO, G. & BONNEROT, C. 2005. Exosomal-like vesicles are present in human blood plasma. *Int Immunol,* 17**,** 879-87.

CAI, W., ROOK, S., JIANG, Z., TAKAHARA, N. & AIELLO, L. 2000. Mechanisms of hepatocyte growth factor-induced retinal endothelial cell migration and growth. *Invest Ophthalmol Vis Sci,* 41**,** 1885 - 1893.

CALON, A., LONARDO, E., BERENGUER-LLERGO, A., ESPINET, E., HERNANDO-MOMBLONA, X., IGLESIAS, M., SEVILLANO, M., PALOMO-PONCE, S., TAURIELLO, D. V., BYROM, D., CORTINA, C., MORRAL, C., BARCELO, C., TOSI, S., RIERA, A., ATTOLINI, C. S., ROSSELL, D., SANCHO, E. & BATLLE, E. 2015. Stromal gene expression defines poor-prognosis subtypes in colorectal cancer. *Nat Genet,* 47**,** 320-9.

CANNON, G. & GETZENBERG, R. 2008. Biomarkers for benign prostatic hyperplasia progression. *Curr Urol Rep,* 9**,** 279 - 283.

CANO, P., GODOY, A., ESCAMILLA, R., DHIR, R. & ONATE, S. A. 2007. Stromal-epithelial cell interactions and androgen receptor-coregulator recruitment is altered in the tissue microenvironment of prostate cancer. *Cancer Res,* 67**,** 511-9.

CANTIN, R., DIOU, J., BELANGER, D., TREMBLAY, A. M. & GILBERT, C. 2008. Discrimination between exosomes and HIV-1: purification of both vesicles from cell-free supernatants. *J Immunol Methods,* 338**,** 21-30.

CAO, H., EPPINGA, R. D., RAZIDLO, G. L., KRUEGER, E. W., CHEN, J., QIANG, L. & MCNIVEN, M. A. 2015. Stromal fibroblasts facilitate cancer cell invasion by a novel invadopodia-independent matrix degradation process. *Oncogene,* 35**,** 1099 - 1110.

CARLTON, J. G., AGROMAYOR, M. & MARTIN-SERRANO, J. 2008. Differential requirements for Alix and ESCRT-III in cytokinesis and HIV-1 release. *Proc Natl Acad Sci USA,* 105**,** 10541-6.

CARMELIET, P., FERREIRA, V., BREIER, G., POLLEFEYT, S., KIECKENS, L., GERTSENSTEIN, M., FAHRIG, M., VANDENHOECK, A., HARPAL, K., EBERHARDT, C., DECLERCQ, C., PAWLING, J., MOONS, L., COLLEN, D., RISAU, W. & A., N. 1996. Abnormal blood vessel development and lethality in embryos lacking a single VEGF allele. *Nature,* 380**,** 435 - 439.

CARMELIET, P. & JAIN, R. 2000. Angiogenesis in cancer and other diseases. *Nature,* 407**,** 249 - 257.

CARTER, B., BEATY, T., STEINBERG, G., CHILDS, B. & WALSH, P. 1992. Mendelian inheritance of familial prostate cancer. *Proc Natl Acad Sci USA,* 89**,** 3367 - 3371.

CAT, B., STUHLMANN, D., STEINBRENNER, H., ALILI, L., HOLTKÖTTER, O., SIES, H. & BRENNEISEN, P. 2006. Enhancement of tumor invasion depends on transdifferentiation of skin fibroblasts mediated by reactive oxygen species. *J Cell Sci,* 15**,** 4691 - 4703.

CATALONA, W., SMITH, D., RATLIFF, T., DODDS, K., COPLEN, D., YUAN, J., PETROS, J. & ANDRIOLE, G. 1991. Measurement of prostate-specific antigen in serum as a screening test for prostate cancer. *N Engl J Med,* 324**,** 1156 - 1161.

CAUVIN, C., ROSENDALE, M., GUPTA-ROSSI, N., ROCANCOURT, M., LARRAUFIE, P., SALOMON, R., PERRAIS, D. & ECHARD, A. 2016. Rab35 GTPase triggers switch-like recruitment of the lowe syndrome lipid phosphatase OCRL on newborn endosomes. *Curr Biol,* 26**,** 120-8.

CHAINEAU, M., DANGLOT, L. & GALLI, T. 2009. Multiple roles of the vesicular-SNARE TI-VAMP in post-Golgi and endosomal trafficking. *FEBS Lett,* 583**,** 3817-26.

CHAIROUNGDUA, A., SMITH, D. L., POCHARD, P., HULL, M. & CAPLAN, M. J. 2010. Exosome release of β-catenin: a novel mechanism that antagonizes Wnt signaling. *J Cell Biol,* 190**,** 1079-91.

CHEN, N. & ZHOU, Q. 2016. The evolving Gleason grading system. *Chin J Cancer Res,* 28**,** 58-64.

CHEN, P. I., KONG, C., SU, X. & STAHL, P. D. 2009. Rab5 isoforms differentially regulate the trafficking and degradation of epidermal growth factor receptors. *J Biol Chem,* 284**,** 30328-38.

CHEN, W. X., LIU, X. M., LV, M. M., CHEN, L., ZHAO, J. H., ZHONG, S. L., JI, M. H., HU, Q., LUO, Z., WU, J. Z. & TANG, J. H. 2014. Exosomes from drug-resistant breast cancer cells transmit chemoresistance by a horizontal transfer of microRNAs. *PLoS One,* 9**,** e95240.

CHINEGWUNDOH, F., ENVER, M., LEE, A., NARGUND, V., OLIVER, T. & BEN-SHLOMO, Y. 2006. Risk and presenting features of prostate cancer amongst African-Caribbean, South Asian and European men in North-east London. *BJU Int,* 98**,** 1216-20.

CHO, J. A., YEO, D. J., SON, H. Y., KIM, H. W., JUNG, D. S., KO, J. K., KOH, J. S., KIM, Y. N. & KIM, C. W. 2005. Exosomes: a new delivery system for tumor antigens in cancer immunotherapy. *Int J Cancer,* 114**,** 613-22.

CHOWDHURY, R., WEBBER, J., GURNEY, M., MASON, M., TABI, Z. & CLAYTON, A. 2015. Cancer exosomes trigger mesenchymal stem cell differentiation into pro-angiogenic and pro-invasive myofibroblasts. *Oncotarget,* 20**,** 715 - 731.

CHRONOPOULOS, A., ROBINSON, B., SARPER, M., CORTES, E., AUERNHEIMER, V., LACHOWSKI, D., ATTWOOD, S., GARCIA, R., GHASSEMI, S., FABRY, B. & DEL RIO HERNANDEZ, A. 2016. ATRA mechanically reprograms pancreatic stellate cells to suppress matrix remodelling and inhibit cancer cell invasion. *Nat Commun,* 7**,** 12630.

CHRZANOWSKA-WODNICKA, M. & BURRIDGE, K. 1996. Rho-stimulated contractility drives the formation of stress fibers and focal adhesions. *J Cell Biol,* 133**,** 1403 - 1415.

CHU, D. I., DE NUNZIO, C., GERBER, L., THOMAS, J. A., 2ND, CALLOWAY, E. E., ALBISINNI, S., SENOCAK, C., MCKEEVER, M. G., MOREIRA, D. M., TUBARO, A., MOUL, J. W., FREEDLAND, S. J. & BANEZ, L. L. 2011. Predictive value of digital rectal examination for prostate cancer detection is modified by obesity. *Prostate Cancer Prostatic Dis,* 14**,** 346-53.

CLARK, A. K., TAUBENBERGER, A. V., TAYLOR, R. A., NIRANJAN, B., CHEA, Z. Y., ZOTENKO, E., SIEH, S., PEDERSEN, J. S., NORDEN, S., FRYDENBERG, M., GRUMMET, J. P., POOK, D. W., AUSTRALIAN PROSTATE CANCER, B., STIRZAKER, C., CLARK, S. J., LAWRENCE, M. G., ELLEM, S. J., HUTMACHER, D. W. & RISBRIDGER, G. P. 2013. A bioengineered

microenvironment to quantitatively measure the tumorigenic properties of cancer-associated fibroblasts in human prostate cancer. *Biomaterials,* 34**,** 4777-85.

CLARK, R. A. F. 1990. Fibronectin matrix deposition and fibronectin receptor expression in healing and normal skin. *J Invest Dermatol,* 94**,** s128-s134.

CLAYTON, A., AL-TAEI, S., WEBBER, J., MASON, M. D. & TABI, Z. 2011. Cancer exosomes express CD39 and CD73, which suppress T cells through adenosine production. *J Immunol,* 187**,** 676-83.

CLAYTON, A., COURT, J., NAVABI, H., ADAMS, M., MASON, M., HOBOT, J., NEWMAN, G. & JASANI, B. 2001. Analysis of antigen presenting cell derived exosomes, based on immuno-magnetic isolation and flow cytometry. *J Immunol Methods,* 247**,** 163 - 174.

CLAYTON, A., MITCHELL, J. P., COURT, J., LINNANE, S., MASON, M. D. & TABI, Z. 2008. Human tumor-derived exosomes down-modulate NKG2D expression. *Immunol,* 180**,** 7249-7258.

CLAYTON, A., MITCHELL, J. P., COURT, J., MASON, M. D. & TABI, Z. 2007. Human tumor-derived exosomes selectively impair lymphocyte responses to interleukin-2. *Cancer Res,* 67**,** 7458-66.

CLAYTON, A. & TABI, Z. 2005. Exosomes and the MICA-NKG2D system in cancer. *Blood Cells Mol Dis,* 34**,** 206-13.

COLOMBO, M., MOITA, C., VAN NIEL, G., KOWAL, J., VIGNERON, J., BENAROCH, P., MANEL, N., MOITA, L., THÉRY, C. & RAPOSO, G. 2013. Analysis of ESCRT functions in exosome biogenesis, composition and secretion highlights the heterogeneity of extracellular vesicles. *J Cell Sci,* 126**,** 5553 - 5565.

COLOMBO, M., RAPOSO, G. & THERY, C. 2014. Biogenesis, secretion, and intercellular interactions of exosomes and other extracellular vesicles. *Annu Rev Cell Dev Biol,* 30**,** 255-89.

CONDE-VANCELLS, J., RODRIGUEZ-SUAREZ, E., EMBADE, N., GIL, D., MATTHIESEN, R., VALLE, M., ELORTZA, F., LU, S., MATO, J. & FALCON-PEREZ, J. 2008. Characterization and comprehensive proteome profiling of exosomes secreted by hepatocytes. *J Proteome Res,* 7**,** 5157 - 5166.

COUSSENS, L. & WERB, Z. 2002. Inflammation and cancer. *Nature,* 420**,** 860 - 867.

CRETNEY, E., TAKEDA, K., YAGITA, H., GLACCUM, M., PESCHON, J. J. & SMYTH, M. J. 2002. Increased susceptibility to tumor initiation and metastasis in TNF-related apoptosis-inducing ligand-deficient mice. *Immunol,* 168**,** 1356-1361.

CRUK. 2015. *Prostate cancer statistics* [Online]. Available: http://www.cancerresearchuk.org/health-professional/cancer-statistics/statistics-by-cancer-type/prostate-cancer#heading-One [Accessed 04 March 2017].

DARBY, I., SKALLI, O. & GABBIANI, G. 1990. α-smooth muscle actin is transiently expressed by myofibroblasts during experimental wound healing. *Lab Invest,* 63**,** 21 - 29.

DARBY, I. A., LAVERDET, B., BONTE, F. & DESMOULIERE, A. 2014. Fibroblasts and myofibroblasts in wound healing. *Clin Cosmet Investig Dermatol,* 7**,** 301-11.

DE BONO, J., OUDARD, S., OZGUROGLU, M., HANSEN, S., MACHIELS, J., KOCAK, I., GRAVIS, G., BODROGI, I., MACKENZIE, M., SHEN, L., ROESSNER, M., GUPTA, S., SARTOR, A. & INVESTIGATORS., T. 2010. Prednisone plus cabazitaxel or mitoxantrone for metastatic castration-resistant prostate cancer progressing after docetaxel treatment: a randomised open-label trial. *Lancet,* 376**,** 1147 - 1154.

DE SOUSA ABREU, R., PENALVA, L. O., MARCOTTE, E. M. & VOGEL, C. 2009. Global signatures of protein and mRNA expression levels. *Mol Biosyst,* 5**,** 1512-26.

DE WEVER, O., WESTBROEK, W., VERLOES, A., BLOEMEN, N., BRACKE, M., GESPACH, C., BRUYNEEL, E. & MAREEL, M. 2004. Critical role of N-cadherin in myofibroblast

invasion and migration *in vitro* stimulated by colon-cancer-cell-derived TGF-β or wounding. *J Cell Sci,* 117**,** 4691 - 4703.

DELA PAZ, N. G. & D'AMORE, P. A. 2009. Arterial versus venous endothelial cells. *Cell Tissue Res,* 335**,** 5-16.

DEMIR, A., CECEN, K., KARADAG, M., KOCAASLAN, R. & TURKERI, L. 2014. The course of metastatic prostate cancer under treatment. *SpringerPlus,* 3**,** 1 - 5.

DESAI, V. D., HSIA, H. C. & SCHWARZBAUER, J. E. 2014. Reversible modulation of myofibroblast differentiation in adipose-derived mesenchymal stem cells. *PLoS One,* 9**,** e86865.

DESMOULIÈRE, A., CHAPONNIER, C. & GABBIANI, G. 2005. Tissue repair, contraction, and the myofibroblast. *Wound Rep Regen,* 13**,** 7 - 12.

DESMOULIÈRE, A., GEINOZ, A., GABBIANI, F. & GABBIANI, G. 1993. Transforming growth factor-β1 induces α-smooth muscle actin expression in granulation tissue myofibroblasts and in quiescent and growing cultured fibroblasts. *J Cell Biol,* 122**,** 103 - 111.

DESNOS, C., SCHONN, J. S., HUET, S., TRAN, V. S., EL-AMRAOUI, A., RAPOSO, G., FANGET, I., CHAPUIS, C., MENASCHE, G., DE SAINT BASILE, G., PETIT, C., CRIBIER, S., HENRY, J. P. & DARCHEN, F. 2003. Rab27A and its effector MyRIP link secretory granules to F-actin and control their motion towards release sites. *J Cell Biol,* 163**,** 559-70.

DING, S., CHEN, G., ZHANG, W., XING, C., XU, X., XIE, H., LU, A., CHEN, K., GUO, H., REN, Z., ZHENG, S. & ZHOU, L. 2015. MRC-5 fibroblast-conditioned medium influences multiple pathways regulating invasion, migration, proliferation, and apoptosis in hepatocellular carcinoma. *J Transl Med,* 13**,** 237.

DOHERTY, G. J. & MCMAHON, H. T. 2009. Mechanisms of endocytosis. *Annu Rev Biochem,* 78**,** 857-902.

DOUBLIER, S., BELISARIO, D., POLIMENI, M., ANNARATONE, L., RIGANTI, C., ALLIA, E., GHIGO, D., BOSIA, A. & SAPINO, A. 2012. HIF-1 activation induces doxorubicin resistance in MCF7 3-D spheroids via P-glycoprotein expression: a potential model of the chemo-resistance of invasive micropapillary carcinoma of the breast. *BMC Cancer,* 12**,** 1 - 15.

DRAGOVIC, R. A., GARDINER, C., BROOKS, A. S., TANNETTA, D. S., FERGUSON, D. J., HOLE, P., CARR, B., REDMAN, C. W., HARRIS, A. L., DOBSON, P. J., HARRISON, P. & SARGENT, I. L. 2011. Sizing and phenotyping of cellular vesicles using Nanoparticle Tracking Analysis. *Nanomedicine,* 7**,** 780-8.

DUAN, H. F., WU, C. T., LU, Y., WANG, H., LIU, H. J., ZHANG, Q. W., JIA, X. X., LU, Z. Z. & WANG, L. S. 2004. Sphingosine kinase activation regulates hepatocyte growth factor induced migration of endothelial cells. *Exp Cell Res,* 298**,** 593-601.

DUNN, I., HEESE, O. & BLACK, P. 2000. Growth factors in glioma angiogenesis: FGFs, PDGF, EGF, and TGFs. *J Neurooncol,* 50**,** 121 - 137.

DVORAK, H. 1986. Tumors: wounds that do not heal. Similarities between tumor stroma generation and wound healing. *N Engl J Med,* 315**,** 1650 - 1659.

EBERT, M., YOKOYAMA, M., FRIESS, H., BÜCHLER, M. & KORC, M. 1994. Coexpression of the c-met proto-oncogene and hepatocyte growth factor in human pancreatic cancer. *Cancer Res,* 54**,** 5775 - 5778.

EISENBERGER, M., BLUMENSTEIN, B., CRAWFORD, E., MILLER, G., MCLEOD, D., LOEHRER, P., WILDING, G., SEARS, K., CULKIN, D., THOMPSON, I. J., BUESCHEN, A. & LOWE, B. 1998. Bilateral orchiectomy with or without flutamide for metastatic prostate cancer. *N Engl J Med,* 339**,** 1036 - 1042.

EL FAR, O. & SEAGAR, M. 2011. A role for V-ATPase subunits in synaptic vesicle fusion? *J Neurochem,* 117**,** 603-12.

ESCOLA, J. M., KLEIJMEER, M. J., STOORVOGEL, W., GRIFFITH, J. M., YOSHIE, O. & GEUZE, H. J. 1998. Selective enrichment of tetraspan proteins on the internal vesicles of multivesicular endosomes and on exosomes secreted by human B-lymphocytes. *J Biol Chem,* 273**,** 20121-20127.

ESKELINEN, E. L. 2006. Roles of LAMP-1 and LAMP-2 in lysosome biogenesis and autophagy. *Mol Aspects Med,* 27**,** 495-502.

FADER, C. M., SANCHEZ, D. G., MESTRE, M. B. & COLOMBO, M. I. 2009. TI-VAMP/VAMP7 and VAMP3/cellubrevin: two v-SNARE proteins involved in specific steps of the autophagy/multivesicular body pathways. *Biochim Biophys Acta,* 1793**,** 1901-16.

FALKE, L. L., GHOLIZADEH, S., GOLDSCHMEDING, R., KOK, R. J. & NGUYEN, T. Q. 2015. Diverse origins of the myofibroblast-implications for kidney fibrosis. *Nat Rev Nephrol,* 11**,** 233-44.

FAN, Y., GAN, Y., SHEN, Y., CAI, X., SONG, Y., ZHAO, F., YAO, M., GU, J. & TU, H. 2015. Leptin signaling enhances cell invasion and promotes the metastasis of human pancreatic cancer via increasing MMP-13 production. *Oncotarget,* 6**,** 16120 - 16134.

FARMER, R. 2008. Prostate cancer: epidemiology and risk factors. *Trends in Urology & Men's Health,* 13**,** 32 - 34.

FAURE, J., LACHENAL, G., COURT, M., HIRRLINGER, J., CHATELLARD-CAUSSE, C., BLOT, B., GRANGE, J., SCHOEHN, G., GOLDBERG, Y., BOYER, V., KIRCHHOFF, F., RAPOSO, G., GARIN, J. & SADOUL, R. 2006. Exosomes are released by cultured cortical neurones. *Mol Cell Neurosci,* 31**,** 642-8.

FAUSTINO-ROCHA, A., OLIVEIRA, P. A., PINHO-OLIVEIRA, J., TEIXEIRA-GUEDES, C., SOARES-MAIA, R., DA COSTA, R. G., COLACO, B., PIRES, M. J., COLACO, J., FERREIRA, R. & GINJA, M. 2013. Estimation of rat mammary tumor volume using caliper and ultrasonography measurements. *Lab Anim (NY),* 42**,** 217-24.

FERRARA, N. 1993. Vascular endothelial growth factor. *Trends Cardiovasc Med,* 3**,** 244 - 250.

FILIPE, V., HAWE, A. & JISKOOT, W. 2010. Critical evaluation of Nanoparticle Tracking Analysis (NTA) by NanoSight for the measurement of nanoparticles and protein aggregates. *Pharm Res,* 27**,** 796-810.

FISHER, R. D., CHUNG, H. Y., ZHAI, Q., ROBINSON, H., SUNDQUIST, W. I. & HILL, C. P. 2007. Structural and biochemical studies of ALIX/AIP1 and its role in retrovirus budding. *Cell,* 128**,** 841-52.

FIVEASH, J., HANKS, G., ROACH, M., WANG, S., VIGNEAULT, E., MCLAUGHLIN, P. & SANDLER, H. 2000. 3D conformal radiation therapy (3DCRT) for high grade prostate cancer: a multi-institutional review. *Int J Radiat Oncol Biol Phys,* 47**,** 335 - 342.

FOLKMAN, J. 1971. Tumor angiogenesis: therapeutic implications. *N Engl J Med,* 285**,** 1182 - 1186.

FOLKMAN, J. & HOCHBERG, M. 1973. Self-regulation of growth in three dimensions. *J Exp Med,* 138**,** 745 - 753.

FOLKMAN, J. & MOSCONA, A. 1978. Role of cell shape in growth control. *Nature,* 273**,** 345 - 349.

FRANCHI, A., SANTUCCI, M., MASINI, E., SARDI, I., PAGLIERANI, M. & GALLO, O. 2002. Expression of matrix metalloproteinase 1, matrix metalloproteinase 2, and matrix metalloproteinase 9 in carcinoma of the head and neck. *Cancer,* 95**,** 1902-10.

FRUHBEIS, C., FROHLICH, D., KUO, W. P., AMPHORNRAT, J., THILEMANN, S., SAAB, A. S., KIRCHHOFF, F., MOBIUS, W., GOEBBELS, S., NAVE, K. A., SCHNEIDER, A., SIMONS, M., KLUGMANN, M., TROTTER, J. & KRAMER-ALBERS, E. M. 2013. Neurotransmitter-triggered transfer of exosomes mediates oligodendrocyte-neuron communication. *PLoS Biol,* 11**,** e1001604.

FUTTER, C., PEARSE, A., HEWLETT, L. & HOPKINS, C. 1996. Multivesicular endosomes containing internalized EGF-EGF receptor complexes mature and then fuse directly with lysosomes. *J Cell Biol,* 132**,** 1011 - 1023.

GABBIANI, G. 2003. The myofibroblast in wound healing and fibrocontractive diseases. *J Pathol,* 200**,** 500-3.

GAO, C. & VANDE WOUDE, G. 2005. HGF/SF-Met signaling in tumor progression. *Cell Res,* 15**,** 49 - 51.

GAO, Y., HUANG, Y., ZHANG, R., YANG, Y., ZHANG, Q., HOU, M. & WANG, Y. 2014. Benign prostatic hyperplasia: prostatic arterial embolization versus transurethral resection of the prostate-a prospective, randomized, and controlled clinical trial. *Radiology,* 270**,** 920 - 928.

GARDINER, C., SHAW, M., HOLE, P., SMITH, J., TANNETTA, D., REDMAN, C. W. & SARGENT, I. L. 2014. Measurement of refractive index by nanoparticle tracking analysis reveals heterogeneity in extracellular vesicles. *J Extracell Vesicles,* 3**,** 25361.

GASTPAR, R., GEHRMANN, M., BAUSERO, M., ASEA, A., GROSS, C., SCHROEDER, J. & MULTHOFF, G. 2005. Heat shock protein 70 surface-positive tumor exosomes stimulate migratory and cytolytic activity of natural killer cells. *Cancer Res,* 65**,** 5238 - 5247.

GÉMINARD, C., DE GASSART, A., BLANC, L. & VIDAL, M. 2004. Degradation of AP2 during reticulocyte maturation enhances binding of hsc70 and Alix to a common site on TFR for sorting into exosomes. *Traffic,* 5**,** 181 - 193.

GESIERICH, S., BEREZOVSKIY, I., RYSCHICH, E. & ZOLLER, M. 2006. Systemic induction of the angiogenesis switch by the tetraspanin D6.1A/CO-029. *Cancer Res,* 66**,** 7083-94.

GHOSSOUB, R., LEMBO, F., RUBIO, A., GAILLARD, C. B., BOUCHET, J., VITALE, N., SLAVIK, J., MACHALA, M. & ZIMMERMANN, P. 2014. Syntenin-ALIX exosome biogenesis and budding into multivesicular bodies are controlled by ARF6 and PLD2. *Nat Commun,* 5**,** 3477.

GIANNONI, E., BIANCHINI, F., MASIERI, L., SERNI, S., TORRE, E., CALORINI, L. & CHIARUGI, P. 2010. Reciprocal activation of prostate cancer cells and cancer-associated fibroblasts stimulates epithelial-mesenchymal transition and cancer stemness. *Cancer Res,* 70**,** 6945-56.

GILL, S., THOMAS, J., FOX, C., KRON, T., ROLFO, A., LEAHY, M., CHANDER, S., WILLIAMS, S., TAI, K., DUCHESNE, G. & FOROUDI, F. 2011. Acute toxicity in prostate cancer patients treated with and without image-guided radiotherapy. *Radiat Oncol,* 6**,** 1 - 7.

GODUGU, C., PATEL, A. R., DESAI, U., ANDEY, T., SAMS, A. & SINGH, M. 2013. AlgiMatrix based 3D cell culture system as an *in-vitro* tumor model for anticancer studies. *PLoS One,* 8**,** e53708.

GORVEL, J., CHAVRIER, P., ZERIAL, M. & GRUENBERG, J. 1991. Rab5 controls early endosome fusion in vitro. *Cell,* 64**,** 915 - 925.

GOULD, G. & LIPPINCOTT-SCHWARTZ, J. 2009. New roles for endosomes: from vesicular carriers to multi-purpose platforms. *Nat Rev Mol Cell Biol,* 10**,** 287 - 292.

GRIMSEY, N. J., CORONEL, L. J., CORDOVA, I. C. & TREJO, J. 2016. Recycling and endosomal sorting of protease-activated receptor-1 is distinctly regulated by Rab11A and Rab11B proteins. *J Biol Chem,* 291**,** 2223-36.

GROSSFELD, G., HAYWARD, S., TLSTY, T. & CUNHA, G. 1998. The role of stroma in prostatic carcinogenesis. *Endocr Relat Cancer,* 5**,** 253 - 270.

GRUENBERG, J. 2001. The endocytic pathway: a mosaic of domains. *Nat Rev Mol Cell Biol,* 2**,** 721 - 730.

GRUGAN, K., MILLER, C., YAO, Y., MICHAYLIRA, C., OHASHI, S., KLEIN-SZANTO, A., DIEHL, J., HERLYN, M., HAN, M., NAKAGAWA, H. & RUSTGI, A. 2010. Fibroblast-secreted

hepatocyte growth factor plays a functional role in esophageal squamous cell carcinoma invasion. *Proc Natl Acad Sci USA,* 107**,** 11026 - 11031.

GU, J., QIAN, H., SHEN, L., ZHANG, X., ZHU, W., HUANG, L., YAN, Y., MAO, F., ZHAO, C., SHI, Y. & XU, W. 2012. Gastric cancer exosomes trigger differentiation of umbilical cord derived mesenchymal stem cells to carcinoma-associated fibroblasts through TGF-beta/Smad pathway. *PLoS One,* 7**,** e52465.

GUO, X., OSHIMA, H., KITMURA, T., TAKETO, M. M. & OSHIMA, M. 2008. Stromal fibroblasts activated by tumor cells promote angiogenesis in mouse gastric cancer. *J Biol Chem,* 283**,** 19864-71.

HAGIWARA, M., KOKUBU, E., SUGIURA, S., KOMATSU, T., TADA, H., ISODA, R., TANIGAWA, N., KATO, Y., ISHIDA, N., KOBAYASHI, K., NAKASHIMA, M., ISHIHARA, K. & MATSUSHITA, K. 2014. Vinculin and Rab5 complex is required for uptake of *Staphylococcus aureus* and interleukin-6 expression. *PLoS One,* 9**,** e87373.

HAKULINEN, J., SANKKILA, L., SUGIYAMA, N., LEHTI, K. & KESKI-OJA, J. 2008. Secretion of active membrane type 1 matrix metalloproteinase (MMP-14) into extracellular space in microvesicular exosomes. *J Cell Biochem,* 105**,** 1211-8.

HANAHAN, D. & WEINBERG, R. A. 2011. Hallmarks of cancer: the next generation. *Cell,* 144**,** 646-74.

HANSON, P. I. & CASHIKAR, A. 2012. Multivesicular body morphogenesis. *Annu Rev Cell Dev Biol,* 28**,** 337-62.

HARDING, C., HEUSER, J. & STAHL, P. 1983. Receptor-mediated endocytosis of transferrin and recycling of the transferrin receptor in rat reticulocytes. *J Cell Biol,* 97**,** 329 - 339.

HARVEY, C. J., PILCHER, J., RICHENBERG, J., PATEL, U. & FRAUSCHER, F. 2012. Applications of transrectal ultrasound in prostate cancer. *Br J Radiol,* 85 Spec No 1**,** S3-17.

HAYWARD, S., ROSEN, M. & CUNHA, G. 1997. Stromal-epithelial interactions in the normal and neoplastic prostate. *Br J Urol,* 79**,** 18 - 26.

HAYWARD, S., WANG, Y., CAO, M., HOM, Y., ZHANG, B., GROSSFELD, G., SUDILOVSKY, D. & CUNHA, G. 2001. Malignant transformation in a nontumorigenic human prostatic epithelial cell line. *Cancer Res,* 61**,** 8135 - 8142.

HEIJNEN, H., SCHIEL, A., FIJNHEER, R., GEUZE, H. & SIXMA, J. 1999. Activated platelets release two types of membrane vesicles: microvesicles by surface shedding and exosomes derived from exocytosis of multivesicular bodies and α-granules. *Blood,* 94**,** 3791 - 3799.

HERZ, H. M., CHEN, Z., SCHERR, H., LACKEY, M., BOLDUC, C. & BERGMANN, A. 2006. vps25 mosaics display non-autonomous cell survival and overgrowth, and autonomous apoptosis. *Development,* 133**,** 1871-80.

HINZ, B., CELETTA, G., TOMASEK, J., GABBIANI, G. & CHAPONNIER, C. 2001. α-smooth muscle actin expression upregulates fibroblast contractile activity. *Mol Biol Cell,* 12**,** 2730 - 2741.

HINZ, B., PHAN, S. H., THANNICKAL, V. J., PRUNOTTO, M., DESMOULIERE, A., VARGA, J., DE WEVER, O., MAREEL, M. & GABBIANI, G. 2012. Recent developments in myofibroblast biology: paradigms for connective tissue remodeling. *Am J Pathol,* 180**,** 1340-55.

HIRSCHHAEUSER, F., MENNE, H., DITTFELD, C., WEST, J., MUELLER-KLIESER, W. & KUNZ-SCHUGHART, L. A. 2010. Multicellular tumor spheroids: an underestimated tool is catching up again. *J Biotechnol,* 148**,** 3-15.

HOEBEN, A., LANDUYT, B., HIGHLEY, M. S., WILDIERS, H., VAN OOSTEROM, A. T. & DE BRUIJN, E. A. 2004. Vascular endothelial growth factor and angiogenesis. *Pharmacol Rev,* 56**,** 549-80.

HOFFMAN, R., GILLILAND, F., ELEY, J., HARLAN, L., STEPHENSON, R., STANFORD, J., ALBERTSON, P., HAMILTON, A., HUNT, W. & POTOSKY, A. 2001. Racial and ethnic differences in advanced-stage prostate cancer: the Prostate Cancer Outcomes Study. *J Natl Cancer Inst,* 93**,** 388 - 395.

HONG, B. S., CHO, J. H., KIM, H., CHOI, E. J., RHO, S., KIM, J., KIM, J. H., CHOI, D. S., KIM, Y. K., HWANG, D. & GHO, Y. S. 2009. Colorectal cancer cell-derived microvesicles are enriched in cell cycle-related mRNAs that promote proliferation of endothelial cells. *BMC Genomics,* 10**,** 556.

HOOGENDAM, A., BUNTINX, F. & DE VET, H. 1999. The diagnostic value of digital rectal examination in primary care screening for prostate cancer: a meta-analysis. *Fam Pract,* 16**,** 621 - 626.

HOSAKA, K., YANG, Y., SEKI, T., FISCHER, C., DUBEY, O., FREDLUND, E., HARTMAN, J., RELIGA, P., MORIKAWA, H., ISHII, Y., SASAHARA, M., LARSSON, O., COSSU, G., CAO, R., LIM, S. & CAO, Y. 2016. Pericyte-fibroblast transition promotes tumor growth and metastasis. *Proc Natl Acad Sci U S A,* 113**,** E5618 - 5627.

HOSSEINI-BEHESHTI, E., PHAM, S., ADOMAT, H., LI, N. & TOMLINSON, G. E. 2012. Exosomes as biomarker enriched microvesicles: characterization of exosomal proteins derived from a panel of prostate cell lines with distinct AR phenotypes. *Mol Cell Proteomics,* 11**,** 863 - 865.

HOTTE, S. & SAAD, F. 2010. Current management of castrate-resistant prostate cancer. *Curr Oncol,* 17**,** S72 - S79.

HSU, C., MOROHASHI, Y., YOSHIMURA, S., MANRIQUE-HOYOS, N., JUNG, S., LAUTERBACH, M. A., BAKHTI, M., GRONBORG, M., MOBIUS, W., RHEE, J., BARR, F. A. & SIMONS, M. 2010. Regulation of exosome secretion by Rab35 and its GTPase-activating proteins TBC1D10A-C. *J Cell Biol,* 189**,** 223-32.

HSU, C. P., SHEN, G. H. & KO, J. L. 2006. Matrix metalloproteinase-13 expression is associated with bone marrow microinvolvement and prognosis in non-small cell lung cancer. *Lung Cancer,* 52**,** 349-57.

HU, G., DRESCHER, K. M. & CHEN, X. M. 2012. Exosomal miRNAs: biological properties and therapeutic potential. *Front Genet,* 3**,** 56.

HUANG, L., XU, A. M., LIU, S., LIU, W. & LI, T. J. 2014. Cancer-associated fibroblasts in digestive tumors. *World J Gastroenterol,* 20**,** 17804-18.

HUANG, Z. & FENG, Y. 2016. Exosomes derived from hypoxic colorectal cancer cells promotes angiogenesis through Wnt4 induced β-catenin signaling in endothelial cells. *Oncol Res*.

HUMBERT, L., GHOZLAN, M., CANAFF, L., TIAN, J. & LEBRUN, J. J. 2015. The leukemia inhibitory factor (LIF) and p21 mediate the TGFβ tumor suppressive effects in human cutaneous melanoma. *BMC Cancer,* 15**,** 200.

HUMPHREY, P. A. 2004. Gleason grading and prognostic factors in carcinoma of the prostate. *Mod Pathol,* 17**,** 292-306.

HURLEY, J. H. & ODORIZZI, G. 2012. Get on the exosome bus with ALIX. *Nat Cell Biol,* 14**,** 654-5.

HUTAGALUNG, A. H. & NOVICK, P. J. 2011. Role of Rab GTPases in membrane traffic and cell physiology. *Physiol Rev,* 91**,** 119-49.

IAVELLO, A., FRECH, V. S., GAI, C., DEREGIBUS, M. C., QUESENBERRY, P. J. & CAMUSSI, G. 2016. Role of Alix in miRNA packaging during extracellular vesicle biogenesis. *Int J Mol Med,* 37**,** 958-66.

ILLEMANN, M., HANSEN, U., NIELSEN, H. J., ANDREASEN, P. A., HØYER-HANSEN, G., LUND, L. R., DANØ, K. & NIELSEN, B. S. 2004. Leading-edge myofibroblasts in human colon cancer express plasminogen activator inhibitor-1. *Am J Clin Pathol,* 122**,** 256-265.

ISAACS, J. & COFFEY, D. 1981. Adaptation versus selection as the mechanism responsible for the relapse of prostatic cancer to androgen ablation therapy as studied in the Dunning R-3327-H adenocarcinoma. *Cancer Res,* 41**,** 5070 - 5075.

IVAN, M., BOND, J., PRAT, M., COMOGLIO, P. & WYNFORD-THOMAS, D. 1997. Activated ras and ret oncogenes induce over-expression of c-met (hepatocyte growth factor receptor) in human thyroid epithelial cells. *Oncogene,* 14**,** 2417 - 2423.

JAEGER, T., WEIDNER, N., CHEW, K., MOORE, D., KERSCHMANN, R., WALDMAN, F. & CARROLL, P. 1995. Tumor angiogenesis correlates with lymph node metastases in invasive bladder cancer. *J Urol,* 154**,** 69 - 71.

JAHN, R. & SCHELLER, R. H. 2006. SNAREs--engines for membrane fusion. *Nat Rev Mol Cell Biol,* 7**,** 631-43.

JAIN, R. 2003. Molecular regulation of vessel maturation. *Nat Med,* 9**,** 685 - 693.

JEFFERS, M., RONG, S. & VANDE WOUDE, G. 1996. Enhanced tumorigenicity and invasion-metastasis by hepatocyte growth factor/scatter factor-met signalling in human cells concomitant with induction of the urokinase proteolysis network. *Mol Cell Biol,* 16**,** 1115 - 1125.

JENSEN, M. M., JORGENSEN, J. T., BINDERUP, T. & KJAER, A. 2008. Tumor volume in subcutaneous mouse xenografts measured by microCT is more accurate and reproducible than determined by 18F-FDG-microPET or external caliper. *BMC Med Imaging,* 8**,** 16.

JEPPESEN, D. K., NAWROCKI, A., JENSEN, S. G., THORSEN, K., WHITEHEAD, B., HOWARD, K. A., DYRSKJOT, L., ORNTOFT, T. F., LARSEN, M. R. & OSTENFELD, M. S. 2014. Quantitative proteomics of fractionated membrane and lumen exosome proteins from isogenic metastatic and nonmetastatic bladder cancer cells reveal differential expression of EMT factors. *Proteomics,* 14**,** 699-712.

JOHNSTONE, R., ADAM, M., HAMMOND, J., ORR, L. & TURBIDE, C. 1987. Vesicle formation during reticulocyte maturation. Association of plasma membrane activities with released vesicles (exosomes). *J Biol Chem,* 262**,** 9412 - 9420.

JOYCE, J. A. & POLLARD, J. W. 2009. Microenvironmental regulation of metastasis. *Nat Rev Cancer,* 9**,** 239-52.

KALLURI, R. & ZEISBERG, M. 2006. Fibroblasts in cancer. *Nat Rev Cancer,* 6**,** 392-401.

KALRA, H., SIMPSON, R., JI, H., AIKAWA, E., ALTEVOGT, P., ASKENASE, P., BOND, V., BORRÀS, F., BREAKEFIELD, X., BUDNIK, V., BUZAS, E., CAMUSSI, G., CLAYTON, A., COCUCCI, E., FALCON-PEREZ, J., GABRIELSSON, S., GHO, Y., GUPTA, D., HARSHA, H., HENDRIX, A., HILL, A., INAL, J., JENSTER, G., KRÄMER-ALBERS, E., LIM, S., LLORENTE, A., LÖTVALL, J., MARCILLA, A., MINCHEVA-NILSSON, L., NAZARENKO, I., NIEUWLAND, R., NOLTE-'T HOEN, E., PANDEY, A., PATEL, T., PIPER, M., PLUCHINO, S., PRASAD, T., RAJENDRAN, L., RAPOSO, G., RECORD, M., REID, G., SÁNCHEZ-MADRID, F., SCHIFFELERS, R., SILJANDER, P., STENSBALLE, A., STOORVOGEL, W., TAYLOR, D., THERY, C., VALADI, H., VAN BALKOM, B., VÁZQUEZ, J., VIDAL, M., WAUBEN, M., YÁÑEZ-MÓ, M., ZOELLER, M. & MATHIVANAN, S. 2012. Vesiclepedia: a compendium for extracellular vesicles with continuous community annotation. *PLoS Biol,* 10**,** e1001450.

KAMOUN, W. S., CHAE, S. S., LACORRE, D. A., TYRRELL, J. A., MITRE, M., GILLISSEN, M. A., FUKUMURA, D., JAIN, R. K. & MUNN, L. L. 2010. Simultaneous measurement of RBC velocity, flux, hematocrit and shear rate in vascular networks. *Nat Methods,* 7**,** 655-60.

KANAMORI, Y., MATSUSHIMA, M., MINAGUCHI, T., KOBAYASHI, K., SAGAE, S., KUDO, R., TERAKAWA, N. & NAKAMURA, Y. 1999. Correlation between expression of the matrix metalloproteinase-1 gene in ovarian cancers and an insertion/deletion polymorphism in its promoter region. *Cancer Res,* 59**,** 4225 - 4227.

KARAGIANNIS, G. S., BERK, A., DIMITROMANOLAKIS, A. & DIAMANDIS, E. P. 2013. Enrichment map profiling of the cancer invasion front suggests regulation of colorectal cancer progression by the bone morphogenetic protein antagonist, gremlin-1. *Mol Oncol,* 7**,** 826-39.

KARAN, D., THRASHER, J. B. & LUBAROFF, D. 2008. Prostate cancer: genes, environment, immunity and the use of immunotherapy. *Prostate Cancer Prostatic Dis,* 11**,** 230-6.

KATZMANN, D. J., ODORIZZI, G. & EMR, S. D. 2002. Receptor downregulation and multivesicular-body sorting. *Nat Rev Mol Cell Biol,* 3**,** 893-905.

KE, N., ALBERS, A., CLAASSEN, G., YU, D., CHATTERTON, J., HU, X., MEYHACK, B., WONG-STAAL, F. & LI, Q. 2004. One-week 96-well soft agar growth assay for cancer target validation. *Biotechniques,* 36**,** 826 - 828.

KEHLET, S. N., SANZ-PAMPLONA, R., BRIX, S., LEEMING, D. J., KARSDAL, M. A. & MORENO, V. 2016. Excessive collagen turnover products are released during colorectal cancer progression and elevated in serum from metastatic colorectal cancer patients. *Sci Rep,* 6**,** 30599.

KELM, J. M., TIMMINS, N. E., BROWN, C. J., FUSSENEGGER, M. & NIELSEN, L. K. 2003. Method for generation of homogeneous multicellular tumor spheroids applicable to a wide variety of cell types. *Biotechnol Bioeng,* 83**,** 173-80.

KICINSKI, M., VANGRONSVELD, J. & NAWROT, T. S. 2011. An epidemiological reappraisal of the familial aggregation of prostate cancer: a meta-analysis. *PLoS One,* 6**,** e27130.

KIM, D. K., LEE, J., KIM, S. R., CHOI, D. S., YOON, Y. J., KIM, J. H., GO, G., NHUNG, D., HONG, K., JANG, S. C., KIM, S. H., PARK, K. S., KIM, O. Y., PARK, H. T., SEO, J. H., AIKAWA, E., BAJ-KRZYWORZEKA, M., VAN BALKOM, B. W., BELTING, M., BLANC, L., BOND, V., BONGIOVANNI, A., BORRAS, F. E., BUEE, L., BUZAS, E. I., CHENG, L., CLAYTON, A., COCUCCI, E., DELA CRUZ, C. S., DESIDERIO, D. M., DI VIZIO, D., EKSTROM, K., FALCON-PEREZ, J. M., GARDINER, C., GIEBEL, B., GREENING, D. W., GROSS, J. C., GUPTA, D., HENDRIX, A., HILL, A. F., HILL, M. M., NOLTE-'T HOEN, E., HWANG, D. W., INAL, J., JAGANNADHAM, M. V., JAYACHANDRAN, M., JEE, Y. K., JORGENSEN, M., KIM, K. P., KIM, Y. K., KISLINGER, T., LASSER, C., LEE, D. S., LEE, H., VAN LEEUWEN, J., LENER, T., LIU, M. L., LOTVALL, J., MARCILLA, A., MATHIVANAN, S., MOLLER, A., MORHAYIM, J., MULLIER, F., NAZARENKO, I., NIEUWLAND, R., NUNES, D. N., PANG, K., PARK, J., PATEL, T., POCSFALVI, G., DEL PORTILLO, H., PUTZ, U., RAMIREZ, M. I., RODRIGUES, M. L., ROH, T. Y., ROYO, F., SAHOO, S., SCHIFFELERS, R., SHARMA, S., SILJANDER, P., SIMPSON, R. J., SOEKMADJI, C., STAHL, P., STENSBALLE, A., STEPIEN, E., TAHARA, H., TRUMMER, A., VALADI, H., VELLA, L. J., WAI, S. N., WITWER, K., YANEZ-MO, M., YOUN, H., ZEIDLER, R. & GHO, Y. S. 2015. EVpedia: a community web portal for extracellular vesicles research. *Bioinformatics,* 31**,** 933-9.

KIM, J. B. 2005. Three-dimensional tissue culture models in cancer biology. *Semin Cancer Biol,* 15**,** 365-77.

KIMLIN, L. C., CASAGRANDE, G. & VIRADOR, V. M. 2013. *In vitro* three-dimensional (3D) models in cancer research: an update. *Mol Carcinog,* 52**,** 167-82.

KNÄUPER, V., SMITH, B., LÓPEZ-OTIN, C. & MURPHY, G. 1997. Activation of progelatinase B (proMMP-9) by active collagenase-3 (MMP-13). *Eur J Biochem,* 248**,** 369 - 373.

KOBAYASHI, H., ETOH, K., OHBAYASHI, N. & FUKUDA, M. 2014. Rab35 promotes the recruitment of Rab8, Rab13 and Rab36 to recycling endosomes through MICAL-L1 during neurite outgrowth. *Biol Open,* 3**,** 803-14.

KOBAYASHI, T., VISCHER, U., ROSNOBLET, C., LEBRAND, C., LINDSAY, M., PARTON, R., KRUITHOF, E. & GRUENBERG, J. 2000. The tetraspanin CD63/lamp3 cycles between endocytic and secretory compartments in human endothelial cells. *Mol Biol Cell,* 11**,** 1829-1843.

KOLES, K., NUNNARI, J., KORKUT, C., BARRIA, R., BREWER, C., LI, Y., LESZYK, J., ZHANG, B. & BUDNIK, V. 2012. Mechanism of evenness interrupted (Evi)-exosome release at synaptic boutons. *J Biol Chem,* 287**,** 16820-34.

KOMINSKY, S. L., DOUCET, M., THORPE, M. & WEBER, K. L. 2008. MMP-13 is over-expressed in renal cell carcinoma bone metastasis and is induced by TGF-β1. *Clin Exp Metastasis,* 25**,** 865-70.

KOSAKA, N., IGUCHI, H., YOSHIOKA, Y., TAKESHITA, F., MATSUKI, Y. & OCHIYA, T. 2010. Secretory mechanisms and intercellular transfer of microRNAs in living cells. *J Biol Chem,* 285**,** 17442-52.

KOURANTI, I., SACHSE, M., AROUCHE, N., GOUD, B. & ECHARD, A. 2006. Rab35 regulates an endocytic recycling pathway essential for the terminal steps of cytokinesis. *Curr Biol,* 16**,** 1719-25.

KOUSSOUNADIS, A., LANGDON, S. P., UM, I. H., HARRISON, D. J. & SMITH, V. A. 2015. Relationship between differentially expressed mRNA and mRNA-protein correlations in a xenograft model system. *Sci Rep,* 5**,** 10775.

KOVACS, M. & SCHALLY, A. V. 2001. Comparison of mechanisms of action of luteinizing hormone-releasing hormone (LHRH) antagonist cetrorelix and LHRH agonist triptorelin on the gene expression of pituitary LHRH receptors in rats. *Proc Natl Acad Sci USA,* 98**,** 12197-202.

KOWAL, J., ARRAS, G., COLOMBO, M., JOUVE, M., MORATH, J., PRIMDAL-BENGTSON, B., DINGLI, F., LOEW, D., TKACH, M. & THÉRY, C. 2016. Proteomic comparison defines novel markers to characterize heterogeneous populations of extracellular vesicle subtypes. *Proc Natl Acad Sci USA,* 113**,** E968 - 977.

KUPELIAN, P. A., POTTERS, L., KHUNTIA, D., CIEZKI, J. P., REDDY, C. A., REUTHER, A. M., CARLSON, T. P. & KLEIN, E. A. 2004. Radical prostatectomy, external beam radiotherapy <72 Gy, external beam radiotherapy ≥72 Gy, permanent seed implantation, or combined seeds/external beam radiotherapy for stage T1–T2 prostate cancer. *Int J Radiation Onco Biol Phys,* 58**,** 25-33.

KURAHASHI, N., IWASAKI, M., SASAZUKI, S., OTANI, T., INOUE, M., TSUGANE, S. & JAPAN PUBLIC HEALTH CENTER-BASED PROSPECTIVE STUDY, G. 2007. Soy product and isoflavone consumption in relation to prostate cancer in Japanese men. *Cancer Epidemiol Biomarkers Prev,* 16**,** 538-45.

LABRIE, F., LUU-THE, V., LIN, S., LABRIE, C., SIMARD, J., BRETON, R. & BÉLANGER, A. 1997. The key role of 17 β-hydroxysteroid dehydrogenases in sex steroid biology. *Steroids,* 62**,** 148 - 158.

LAMALICE, L., LE BOEUF, F. & HUOT, J. 2007. Endothelial cell migration during angiogenesis. *Circ Res,* 100**,** 782-94.

LAMPARSKI, H., METHA-DAMANI, A., YAO, J., PATEL, S., HSU, D., RUEGG, C. & LE PECQ, J. 2002. Production and characterization of clinical grade exosomes derived from dendritic cells. *J Immunol Methods,* 270**,** 211 - 226.

LANGELIER, C., VON SCHWEDLER, U. K., FISHER, R. D., DE DOMENICO, I., WHITE, P. L., HILL, C. P., KAPLAN, J., WARD, D. & SUNDQUIST, W. I. 2006. Human ESCRT-II complex and its role in human immunodeficiency virus type 1 release. *J Virol,* 80**,** 9465-80.

LANGLEY, S. E. & LAING, R. W. 2004. Iodine seed prostate brachytherapy: an alternative first-line choice for early prostate cancer. *Prostate Cancer Prostatic Dis,* 7**,** 201-7.

LAULAGNIER, K., MOTTA, C., HAMDI, S., ROY, S., FAUVELLE, F., PAGEAUX, J., KOBAYASHI, T., SALLES, J., PERRET, B., BONNEROT, C. & RECORD, M. 2004. Mast cell- and dendritic cell-derived exosomes display a specific lipid composition and an unusual membrane organization. *Biochem J,* 380**,** 161 - 171.

LAZARO-IBANEZ, E., SANZ-GARCIA, A., VISAKORPI, T., ESCOBEDO-LUCEA, C., SILJANDER, P., AYUSO-SACIDO, A. & YLIPERTTULA, M. 2014. Different gDNA content in the

subpopulations of prostate cancer extracellular vesicles: apoptotic bodies, microvesicles, and exosomes. *Prostate,* 74**,** 1379-90.

LEE, Y., AHN, C., HAN, J., CHOI, H., KIM, J., YIM, J., LEE, J., PROVOST, P., RÅDMARK, O., KIM, S. & KIM, V. 2003. The nuclear RNase III Drosha initiates microRNA processing. *Nature,* 425**,** 415 - 419.

LEEMAN, M., MCKAY, J. & MURRAY, G. 2002. Matrix metalloproteinase 13 activity is associated with poor prognosis in colorectal cancer. *J Clin Pathol,* 55**,** 758 - 762.

LEON, A., BURIANI, A., DAL TOSO, R., FABRIS, M., ROMANELLO, S., ALOE, L. & LEVI-MONTALCINI, R. 1994. Mast cells synthesize, store, and release nerve growth factor. *Proc Natl Acad Sci USA,* 91**,** 3739 - 3743.

LEVCHENKO, A., MEHTA, B. M., NIU, X., KANG, G., VILLAFANIA, L., WAY, D., POLYCARPE, D., SADELAIN, M. & LARSON, S. M. 2005. Intercellular transfer of P-glycoprotein mediates acquired multidrug resistance in tumor cells. *Proc Natl Acad Sci USA,* 102**,** 1933-8.

LEWIS, M. P., LYGOE, K. A., NYSTROM, M. L., ANDERSON, W. P., SPEIGHT, P. M., MARSHALL, J. F. & THOMAS, G. J. 2004. Tumour-derived TGF-β1 modulates myofibroblast differentiation and promotes HGF/SF-dependent invasion of squamous carcinoma cells. *Br J Cancer,* 90**,** 822-32.

LI, J., JIA, Z., KONG, J., ZHANG, F., FANG, S., LI, X., LI, W., YANG, X., LUO, Y., LIN, B. & LIU, T. 2016. Carcinoma-associated fibroblasts lead the invasion of salivary gland adenoid cystic carcinoma cells by creating an invasive track. *PLoS One,* 11**,** e0150247.

LIANG, C. C., PARK, A. Y. & GUAN, J. L. 2007. *In vitro* scratch assay: a convenient and inexpensive method for analysis of cell migration *in vitro*. *Nat Protoc,* 2**,** 329-33.

LINDSAY, A., JOLLIVET, F., HORGAN, C., KHAN, A., RAPOSO, G., MCCAFFREY, M. & GOUD, B. 2013. Identification and characterization of multiple novel Rab-myosin Va interactions. *Mol Biol Cell,* 24**,** 3420 - 3434.

LIU, H., KATO, Y., ERZINGER, S., KIRIAKOVA, G., QIAN, Y., PALMIERI, D., STEEG, P. & JE., P. 2012. The role of MMP-1 in breast cancer growth and metastasis to the brain in a xenograft model. *BMC Cancer,* 12**,** doi: 10.1186/1471-2407-12-583.

LIU, T., MENDES, D. E. & BERKMAN, C. E. 2014. Functional prostate-specific membrane antigen is enriched in exosomes from prostate cancer cells. *Int J Oncol,* 44**,** 918-22.

LOGOZZI, M., DE MILITO, A., LUGINI, L., BORGHI, M., CALABRO, L., SPADA, M., PERDICCHIO, M., MARINO, M. L., FEDERICI, C., IESSI, E., BRAMBILLA, D., VENTURI, G., LOZUPONE, F., SANTINAMI, M., HUBER, V., MAIO, M., RIVOLTINI, L. & FAIS, S. 2009. High levels of exosomes expressing CD63 and caveolin-1 in plasma of melanoma patients. *PLoS One,* 4**,** e5219.

LOPES, P. M., SEPULVEDA, L., RAMOS, R. & SOUSA, P. 2015. The role of transrectal ultrasound in the diagnosis of prostate cancer: new contributions. *Radiol Bras,* 48**,** 7-11.

LORENTZ, A., BAUMANN, A., VITTE, J. & BLANK, U. 2012. The SNARE Machinery in Mast Cell Secretion. *Front Immunol,* 3**,** 143.

LOTVALL, J., HILL, A. F., HOCHBERG, F., BUZAS, E. I., DI VIZIO, D., GARDINER, C., GHO, Y. S., KUROCHKIN, I. V., MATHIVANAN, S., QUESENBERRY, P., SAHOO, S., TAHARA, H., WAUBEN, M. H., WITWER, K. W. & THERY, C. 2014. Minimal experimental requirements for definition of extracellular vesicles and their functions: a position statement from the International Society for Extracellular Vesicles. *J Extracell Vesicles,* 3**,** 26913.

LU, P., TAKAI, K., WEAVER, V. M. & WERB, Z. 2011. Extracellular matrix degradation and remodeling in development and disease. *Cold Spring Harb Perspect Biol,* 3.

LU, Q., HOPE, L. W., BRASCH, M., REINHARD, C. & COHEN, S. N. 2003. TSG101 interaction with HRS mediates endosomal trafficking and receptor down-regulation. *Proc Natl Acad Sci USA,* 100**,** 7626-31.

LUKSIC, I., SUTON, P., MANOJLOVIC, S., VIRAG, M., PETROVECKI, M. & MACAN, D. 2015. Significance of myofibroblast appearance in squamous cell carcinoma of the oral cavity on the occurrence of occult regional metastases, distant metastases, and survival. *Int J Oral Maxillofac Surg,* 44**,** 1075-80.

LV, L. H., WAN, Y. L., LIN, Y., ZHANG, W., YANG, M., LI, G. L., LIN, H. M., SHANG, C. Z., CHEN, Y. J. & MIN, J. 2012. Anticancer drugs cause release of exosomes with heat shock proteins from human hepatocellular carcinoma cells that elicit effective natural killer cell antitumor responses *in vitro*. *J Biol Chem,* 287**,** 15874-85.

MADERSBACHER, S., ALCARAZ, A., EMBERTON, M., HAMMERER, P., PONHOLZER, A., SCHRODER, F. H. & TUBARO, A. 2011. The influence of family history on prostate cancer risk: implications for clinical management. *BJU Int,* 107**,** 716-21.

MAHLLER, Y. Y., VAIKUNTH, S. S., RIPBERGER, M. C., BAIRD, W. H., SAEKI, Y., CANCELAS, J. A., CROMBLEHOLME, T. M. & CRIPE, T. P. 2008. Tissue inhibitor of metalloproteinase-3 via oncolytic herpesvirus inhibits tumor growth and vascular progenitors. *Cancer Res,* 68**,** 1170-9.

MAIER, T., GUELL, M. & SERRANO, L. 2009. Correlation of mRNA and protein in complex biological samples. *FEBS Lett,* 583**,** 3966-73.

MALKOWICZ, S. 2001. The role of diethylstilbestrol in the treatment of prostate cancer. *Urology,* 58**,** 108 - 113.

MALVERN INSTRUMENTS. 2017. *Nanoparticle Tracking Analysis* [Online]. Available: http://www.malvern.com/en/products/technology/nanoparticle-tracking-analysis/ [Accessed 20 April 2017 2017].

MARLEAU, A. M., CHEN, C. S., JOYCE, J. A. & TULLIS, R. H. 2012. Exosome removal as a therapeutic adjuvant in cancer. *J Transl Med,* 10**,** 134.

MARONI, P., BENDINELLI, P., RESNATI, M., MATTEUCCI, E., MILAN, E. & DESIDERIO, M. A. 2016. The autophagic process occurs in human bone metastasis and implicates molecular mechanisms differently affected by Rab5a in the early and late Stages. *Int J Mol Sci,* 17**,** 443.

MATHIVANAN, S. & SIMPSON, R. J. 2009. ExoCarta: A compendium of exosomal proteins and RNA. *Proteomics,* 9**,** 4997-5000.

MAYER, M. P. & BUKAU, B. 2005. Hsp70 chaperones: cellular functions and molecular mechanism. *Cell Mol Life Sci,* 62**,** 670-84.

MAZUROV, D., BARBASHOVA, L. & FILATOV, A. 2013. Tetraspanin protein CD9 interacts with metalloprotease CD10 and enhances its release via exosomes. *FEBS J,* 280**,** 1200-13.

MCDONALD, D. & BALUK, P. 2002. Significance of blood vessel leakiness in cancer. *Cancer Res,* 62**,** 5381 - 5385.

MCMILLAN, K. S., MCCLUSKEY, A. G., SORENSEN, A., BOYD, M. & ZAGNONI, M. 2016. Emulsion technologies for multicellular tumour spheroid radiation assays. *Analyst,* 141**,** 100-10.

MCNEIL, P., MUTHUKRISHNAN, L., WARDER, E. & D'AMORE, P. 1989. Growth factors are released by mechanically wounded endothelial cells. *J Cell Biol,* 109**,** 811 - 822.

MEIRINGER, C. T., AUFFARTH, K., HOU, H. & UNGERMANN, C. 2008. Depalmitoylation of Ykt6 prevents its entry into the multivesicular body pathway. *Traffic,* 9**,** 1510-21.

MENG, X. M., NIKOLIC-PATERSON, D. J. & LAN, H. Y. 2016. TGF-beta: the master regulator of fibrosis. *Nat Rev Nephrol,* 12**,** 325-38.

MIDGLEY, A. C., ROGERS, M., HALLETT, M. B., CLAYTON, A., BOWEN, T., PHILLIPS, A. O. & STEADMAN, R. 2013. Transforming growth factor-β1 (TGF-β1)-stimulated fibroblast

to myofibroblast differentiation is mediated by hyaluronan (HA)-facilitated epidermal growth factor receptor (EGFR) and CD44 co-localization in lipid rafts. *J Biol Chem,* 288**,** 14824-38.

MINO, N., TAKENAKA, K., SONOBE, M., MIYAHARA, R., YANAGIHARA, K., OTAKE, Y., WADA, H. & TANAKA, F. 2007. Expression of tissue inhibitor of metalloproteinase-3 (TIMP-3) and its prognostic significance in resected non-small cell lung cancer. *J Surg Oncol,* 95**,** 250-7.

MISHRA, P. J., MISHRA, P. J., HUMENIUK, R., MEDINA, D. J., ALEXE, G., MESIROV, J. P., GANESAN, S., GLOD, J. W. & BANERJEE, D. 2008. Carcinoma-associated fibroblast-like differentiation of human mesenchymal stem cells. *Cancer Res,* 68**,** 4331-9.

MITCHELL, J. P., COURT, J., MASON, M. D., TABI, Z. & CLAYTON, A. 2008. Increased exosome production from tumour cell cultures using the Integra CELLine Culture System. *J Immunol Methods,* 335**,** 98-105.

MIYAKE, H., SAKAI, I., HARADA, K., MURAMAKI, M. & FUJISAWA, M. 2012. Significance of docetaxel-based chemotherapy as treatment for metastatic castration-resistant prostate cancer in Japanese men over 75 years old. *Int Urol Nephrol,* 44**,** 1697-703.

MÖBIUS, W., VAN DONSELAAR, E., OHNO-IWASHITA, Y., SHIMADA, Y., HEIJNEN, H., SLOT, J. & GEUZE, H. 2003. Recycling compartments and the internal vesicles of multivesicular bodies harbor most of the cholesterol found in the endocytic pathway. *Traffic,* 4**,** 222 - 231.

MOFFAT, J., GRUENEBERG, D. A., YANG, X., KIM, S. Y., KLOEPFER, A. M., HINKLE, G., PIQANI, B., EISENHAURE, T. M., LUO, B., GRENIER, J. K., CARPENTER, A. E., FOO, S. Y., STEWART, S. A., STOCKWELL, B. R., HACOHEN, N., HAHN, W. C., LANDER, E. S., SABATINI, D. M. & ROOT, D. E. 2006. A lentiviral RNAi library for human and mouse genes applied to an arrayed viral high-content screen. *Cell,* 124**,** 1283-98.

MOHILE, S. G., LACY, M., RODIN, M., BYLOW, K., DALE, W., MEAGER, M. R. & STADLER, W. M. 2010. Cognitive effects of androgen deprivation therapy in an older cohort of men with prostate cancer. *Crit Rev Oncol Hematol,* 75**,** 152-9.

MOORMAN, A. M., VINK, R., HEIJMANS, H. J., VAN DER PALEN, J. & KOUWENHOVEN, E. A. 2012. The prognostic value of tumour-stroma ratio in triple-negative breast cancer. *Eur J Surg Oncol,* 38**,** 307-13.

MORITA, E., SANDRIN, V., CHUNG, H., MORHAM, S., GYGI, S., RODESCH, C. & SUNDQUIST, W. 2007. Human ESCRT and ALIX proteins interact with proteins of the midbody and function in cytokinesis. *EMBO J,* 26**,** 4215 - 4227.

MULLER-BORER, B. J., COLLINS, M. C., GUNST, P. R., CASCIO, W. E. & KYPSON, A. P. 2007. Quantum dot labeling of mesenchymal stem cells. *J Nanobiotechnology,* 5**,** 9.

MULLER, L., MITSUHASHI, M., SIMMS, P., GOODING, W. E. & WHITESIDE, T. L. 2016. Tumor-derived exosomes regulate expression of immune function-related genes in human T cell subsets. *Sci Rep,* 6**,** 20254.

MURPHY, D. A., MAKONNEN, S., LASSOUED, W., FELDMAN, M. D., CARTER, C. & LEE, W. M. 2006. Inhibition of tumor endothelial ERK activation, angiogenesis, and tumor growth by sorafenib (BAY43-9006). *Am J Pathol,* 169**,** 1875-85.

NAGY, J. 2003. VEGF-A164/165 and PlGF roles in angiogenesis and arteriogenesis. *Trends in Cardiovas Med,* 13**,** 169-175.

NAGY, J. A., CHANG, S. H., SHIH, S. C., DVORAK, A. M. & DVORAK, H. F. 2010. Heterogeneity of the tumor vasculature. *Semin Thromb Hemost,* 36**,** 321-31.

NAZARENKO, I., RANA, S., BAUMANN, A., MCALEAR, J., HELLWIG, A., TRENDELENBURG, M., LOCHNIT, G., PREISSNER, K. T. & ZOLLER, M. 2010. Cell surface tetraspanin Tspan8 contributes to molecular pathways of exosome-induced endothelial cell activation. *Cancer Res,* 70**,** 1668-78.

NELSON, C. M. & BISSELL, M. J. 2005. Modeling dynamic reciprocity: engineering three-dimensional culture models of breast architecture, function, and neoplastic transformation. *Semin Cancer Biol,* 15**,** 342-52.

NICKERS, P., KUNKLER, I. & SCALLIET, P. 1997. Modern brachytherapy: current state and future prospects. *Eur J Cancer,* 33**,** 1747 - 1751.

NICKERSON, D., WEST, M., HENRY, R. & ODORIZZI, G. 2010. Regulators of Vps4 ATPase activity at endosomes differentially influence the size and rate of formation of intralumenal vesicles. *Mol Biol Cell,* 21**,** 1023 - 1032.

NINOMIYA, I., KAWAKAMI, K., FUSHIDA, S., FUJIMURA, T., FUNAKI, H., TAKAMURA, H., KITAGAWA, H., NAKAGAWARA, H., TAJIMA, H., KAYAHARA, M. & T., O. 2008. Quantitative detection of TIMP-3 promoter hypermethylation and its prognostic significance in esophageal squamous cell carcinoma. *Oncol Rep,* 20**,** 1489 - 1495.

NOMA, K., SMALLEY, K. S., LIONI, M., NAOMOTO, Y., TANAKA, N., EL-DEIRY, W., KING, A. J., NAKAGAWA, H. & HERLYN, M. 2008. The essential role of fibroblasts in esophageal squamous cell carcinoma-induced angiogenesis. *Gastroenterology,* 134**,** 1981-93.

NYGA, A., LOIZIDOU, M., EMBERTON, M. & CHEEMA, U. 2013. A novel tissue engineered three-dimensional *in vitro* colorectal cancer model. *Acta Biomater,* 9**,** 7917-26.

ODEDINA, F. T., AKINREMI, T. O., CHINEGWUNDOH, F., ROBERTS, R., YU, D., REAMS, R. R., FREEDMAN, M. L., RIVERS, B., GREEN, B. L. & KUMAR, N. 2009. Prostate cancer disparities in Black men of African descent: a comparative literature review of prostate cancer burden among Black men in the United States, Caribbean, United Kingdom, and West Africa. *Infect Agent Cancer,* 4**,** S2.

OHLUND, D., ELYADA, E. & TUVESON, D. 2014. Fibroblast heterogeneity in the cancer wound. *J Exp Med,* 211**,** 1503-23.

OLUMI, A., GROSSFELD, G., HAYWARD, S., CARROLL, P., TLSTY, T. & CUNHA, G. 1999. Carcinoma-associated fibroblasts direct tumor progression of initiated human prostatic epithelium. *Cancer Res,* 59**,** 5002 - 5011.

ORIMO, A., GUPTA, P. B., SGROI, D. C., ARENZANA-SEISDEDOS, F., DELAUNAY, T., NAEEM, R., CAREY, V. J., RICHARDSON, A. L. & WEINBERG, R. A. 2005. Stromal fibroblasts present in invasive human breast carcinomas promote tumor growth and angiogenesis through elevated SDF-1/CXCL12 secretion. *Cell,* 121**,** 335-48.

OSTENFELD, M. S., JEPPESEN, D. K., LAURBERG, J. R., BOYSEN, A. T., BRAMSEN, J. B., PRIMDAL-BENGTSON, B., HENDRIX, A., LAMY, P., DAGNAES-HANSEN, F., RASMUSSEN, M. H., BUI, K. H., FRISTRUP, N., CHRISTENSEN, E. I., NORDENTOFT, I., MORTH, J. P., JENSEN, J. B., PEDERSEN, J. S., BECK, M., THEODORESCU, D., BORRE, M., HOWARD, K. A., DYRSKJOT, L. & ORNTOFT, T. F. 2014. Cellular disposal of miR23b by RAB27-dependent exosome release is linked to acquisition of metastatic properties. *Cancer Res,* 74**,** 5758-71.

OSTROWSKI, M., CARMO, N. B., KRUMEICH, S., FANGET, I., RAPOSO, G., SAVINA, A., MOITA, C. F., SCHAUER, K., HUME, A. N., FREITAS, R. P., GOUD, B., BENAROCH, P., HACOHEN, N., FUKUDA, M., DESNOS, C., SEABRA, M. C., DARCHEN, F., AMIGORENA, S., MOITA, L. F. & THERY, C. 2010. Rab27a and Rab27b control different steps of the exosome secretion pathway. *Nat Cell Biol,* 12**,** 19-30.

PAN, B., TENG, K., WU, C., ADAM, M. & JOHNSTONE, R. 1985. Electron microscopic evidence for externalization of the transferrin receptor in vesicular form in sheep reticulocytes. *J Cell Biol,* 101**,** 942 - 948.

PANG, W., SU, J., WANG, Y., FENG, H., DAI, X., YUAN, Y., CHEN, X. & YAO, W. 2015. Pancreatic cancer-secreted miR-155 implicates in the conversion from normal fibroblasts to cancer-associated fibroblasts. *Cancer Sci,* 106**,** 1362-9.

PARANGI, S., O'REILLY, M., CHRISTOFORI, G., HOLMGREN, L., GROSFELD, J., FOLKMAN, J. & HANAHAN, D. 1996. Antiangiogenic therapy of transgenic mice impairs *de novo* tumor growth. *Proc Natl Acad Sci USA,* 93**,** 2002 - 2007.

PASCAL, L. E., TRUE, L. D., CAMPBELL, D. S., DEUTSCH, E. W., RISK, M., COLEMAN, I. M., EICHNER, L. J., NELSON, P. S. & LIU, A. Y. 2008. Correlation of mRNA and protein levels: cell type-specific gene expression of cluster designation antigens in the prostate. *BMC Genomics,* 9**,** 246.

PEINADO, H., ALECKOVIC, M., LAVOTSHKIN, S., MATEI, I., COSTA-SILVA, B., MORENO-BUENO, G., HERGUETA-REDONDO, M., WILLIAMS, C., GARCIA-SANTOS, G., GHAJAR, C., NITADORI-HOSHINO, A., HOFFMAN, C., BADAL, K., GARCIA, B. A., CALLAHAN, M. K., YUAN, J., MARTINS, V. R., SKOG, J., KAPLAN, R. N., BRADY, M. S., WOLCHOK, J. D., CHAPMAN, P. B., KANG, Y., BROMBERG, J. & LYDEN, D. 2012. Melanoma exosomes educate bone marrow progenitor cells toward a pro-metastatic phenotype through MET. *Nat Med,* 18**,** 883-91.

PENA, C., CESPEDES, M. V., LINDH, M. B., KIFLEMARIAM, S., MEZHEYEUSKI, A., EDQVIST, P. H., HAGGLOF, C., BIRGISSON, H., BOJMAR, L., JIRSTROM, K., SANDSTROM, P., OLSSON, E., VEERLA, S., GALLARDO, A., SJOBLOM, T., CHANG, A. C., REDDEL, R. R., MANGUES, R., AUGSTEN, M. & OSTMAN, A. 2013. STC1 expression by cancer-associated fibroblasts drives metastasis of colorectal cancer. *Cancer Res,* 73**,** 1287-97.

PEREIRA-LEAL, J. & SEABRA, M. 2001. Evolution of the Rab family of small GTP-binding proteins. *J Mol Biol,* 313**,** 889 - 901.

PEREZ-HERNANDEZ, D., GUTIERREZ-VAZQUEZ, C., JORGE, I., LOPEZ-MARTIN, S., URSA, A., SANCHEZ-MADRID, F., VAZQUEZ, J. & YANEZ-MO, M. 2013. The intracellular interactome of tetraspanin-enriched microdomains reveals their function as sorting machineries toward exosomes. *J Biol Chem,* 288**,** 11649-61.

PFEFFER, S. 2001. Rab GTPases: specifying and deciphering organelle identity and function. *Trends Cell Biol,* 11**,** 487 - 491.

PICCIN, A., MURPHY, W. G. & SMITH, O. P. 2007. Circulating microparticles: pathophysiology and clinical implications. *Blood Rev,* 21**,** 157-71.

PIERORAZIO, P. M., GUZZO, T. J., HAN, M., BIVALACQUA, T. J., EPSTEIN, J. I., SCHAEFFER, E. M., SCHOENBERG, M., WALSH, P. C. & PARTIN, A. W. 2010. Long-term survival after radical prostatectomy for men with high Gleason sum in pathologic specimen. *Urology,* 76**,** 715-21.

PILCHER, B., DUMIN, J., SUDBECK, B., KRANE, S., WELGUS, H. & PARKS, W. 1997. The activity of collagenase-1 is required for keratinocyte migration on a type I collagen matrix. *J Cell Biol,* 137**,** 1445 - 1457.

PIN, A. L., HOULE, F., FOURNIER, P., GUILLONNEAU, M., PAQUET, E. R., SIMARD, M. J., ROYAL, I. & HUOT, J. 2012. Annexin-1-mediated endothelial cell migration and angiogenesis are regulated by vascular endothelial growth factor (VEGF)-induced inhibition of miR-196a expression. *J Biol Chem,* 287**,** 30541-51.

POTEMPA, S. & RIDLEY, A. 1998. Activation of both MAP kinase and phosphatidylinositide 3-kinase by Ras is required for hepatocyte growth factor/scatter factor-induced adherens junction disassembly. *Mol Biol Cell,* 9**,** 2185 - 2200.

PROUX-GILLARDEAUX, V., RAPOSO, G., IRINOPOULOU, T. & GALLI, T. 2007. Expression of the Longin domain of TI-VAMP impairs lysosomal secretion and epithelial cell migration. *Biol Cell,* 99**,** 261-71.

PULUKURI, S. & RAO, J. 2008. Matrix metalloproteinase-1 promotes prostate tumor growth and metastasis. *Int J Oncol,* 32**,** 757 - 765.

PUNGLIA, R., D'AMICO, A., CATALONA, W., ROEHL, K. & KUNTZ, K. 2003. Effect of verification bias on screening for prostate cancer by measurement of prostate-specific antigen. *N Engl J Med,* 349**,** 335 - 342.

PURI, N. & ROCHE, P. A. 2008. Mast cells possess distinct secretory granule subsets whose exocytosis is regulated by different SNARE isoforms. *Proc Natl Acad Sci U S A,* 105**,** 2580-5.

QUILLIN, M. & MATTHEWS, B. 2000. Accurate calculation of the density of proteins. *Acta Crystallogr D Biol Crystallogr,* 56**,** 791 - 794.

QUON, J. S., MOOSAVI, B., KHANNA, M., FLOOD, T. A., LIM, C. S. & SCHIEDA, N. 2015. False positive and false negative diagnoses of prostate cancer at multi-parametric prostate MRI in active surveillance. *Insights Imaging,* 6**,** 449-63.

RADISKY, D. C., KENNY, P. A. & BISSELL, M. J. 2007. Fibrosis and cancer: do myofibroblasts come also from epithelial cells via EMT? *J Cell Biochem,* 101**,** 830-9.

RAHAJENG, J., GIRIDHARAN, S. S., CAI, B., NASLAVSKY, N. & CAPLAN, S. 2012. MICAL-L1 is a tubular endosomal membrane hub that connects Rab35 and Arf6 with Rab8a. *Traffic,* 13**,** 82-93.

RAO, S. K., HUYNH, C., PROUX-GILLARDEAUX, V., GALLI, T. & ANDREWS, N. W. 2004. Identification of SNAREs involved in synaptotagmin VII-regulated lysosomal exocytosis. *J Biol Chem,* 279**,** 20471-9.

RAPOSO, G., MARKS, M. S. & CUTLER, D. F. 2007. Lysosome-related organelles: driving post-Golgi compartments into specialisation. *Curr Opin Cell Biol,* 19**,** 394-401.

RAPOSO, G., NIJMAN, H., STOORVOGEL, W., LIEJENDEKKER, R., HARDING, C., MELIEF, C. & GEUZE, H. 1996. B lymphocytes secrete antigen-presenting vesicles. *J Exp Med,* 183**,** 1161 - 1172.

RASSCHAERT, G., HENDRIX, A. & DE WEVER, O. 2015. Modulation of exosome release by cancer cells: a screening of potential inhibitors. *Abstract book : 9th Leiden International Medical Student Conference***,** 87.

RAYMOND, C., HOWALD-STEVENSON, I., VATER, C. & STEVENS, T. 1992. Morphological classification of the yeast vacuolar protein sorting mutants: evidence for a prevacuolar compartment in class E vps mutants. *Mol Biol Cell,* 3**,** 1389 - 1402.

RECINE, F. & STERNBERG, C. N. 2015. Hormonal therapy and chemotherapy in hormone-naive and castration resistant prostate cancer. *Transl Androl Urol,* 4**,** 355-64.

RIEDER, S., BANTA, L., KÖHRER, K., MCCAFFERY, J. & EMR, S. 1996. Multilamellar endosome-like compartment accumulates in the yeast vps28 vacuolar protein sorting mutant. *Mol Biol Cell,* 7**,** 985 - 999.

ROYO, F., MORENO, L., MLECZKO, J., PALOMO, L., GONZALEZ, E., CABRERA, D., COGOLLUDO, A., VIZCAINO, F. P., VAN-LIEMPD, S. & FALCON-PEREZ, J. M. 2017. Hepatocyte-secreted extracellular vesicles modify blood metabolome and endothelial function by an arginase-dependent mechanism. *Sci Rep,* 7**,** 42798.

RUBINO, M., MIACZYNSKA, M., LIPPÉ, R. & ZERIAL, M. 2000. Selective membrane recruitment of EEA1 suggests a role in directional transport of clathrin-coated vesicles to early endosomes. *J Biol Chem,* 275**,** 3745 - 3748.

RUIZ-MARTINEZ, M., NAVARRO, A., MARRADES, R., VIÑOLAS, N., SANTASUSAGNA, S., MUÑOZ, C., RAMÍREZ, J., MOLINS, L. & MONZO, M. 2016. YKT6 expression, exosome release, and survival in non-small cell lung cancer. *Oncotarget,* 7**,** 51515 - 51524.

RUSTEN, T. E., VACCARI, T. & STENMARK, H. 2012. Shaping development with ESCRTs. *Nat Cell Biol,* 14**,** 38-45.

RYAN, G., CLIFF, W., GABBIANI, G., IRLÉ, C., MONTANDON, D., STATKOV, P. & MAJNO, G. 1974. Myofibroblasts in human granulation tissue. *Hum Pathol,* 5**,** 55 - 67.

RYAN, G., CLIFF, W., GABBIANI, G., IRLE, C., STATKOV, P. & MAJNO, G. 1973. Myofibroblasts in an avascular fibrous tissue. *Lab Invest,* 29**,** 197 - 206.

RYBIN, V., ULLRICH, O., RUBINO, M., ALEXANDROV, K., SIMON, I., SEABRA, M., GOODY, R. & ZERIAL, M. 1996. GTPase activity of Rab5 acts as a timer for endocytic membrane fusion. *Nature,* 383**,** 266 - 269.

SACHSE, M., STROUS, G. & KLUMPERMAN, J. 2004. ATPase-deficient hVPS4 impairs formation of internal endosomal vesicles and stabilizes bilayered clathrin coats on endosomal vacuoles. *J Cell Sci,* 117**,** 1699 - 1708.

SACHSE, M., URBE, S., OORSCHOT, V., STROUS, G. J. & KLUMPERMAN, J. 2002. Bilayered clathrin coats on endosomal vacuoles are involved in protein sorting toward lysosomes. *Mol Biol Cell,* 13**,** 1313-28.

SAFAEI, R., LARSON, B. J., CHENG, T. C., GIBSON, M. A., OTANI, S., NAERDEMANN, W. & HOWELL, S. B. 2005. Abnormal lysosomal trafficking and enhanced exosomal export of cisplatin in drug-resistant human ovarian carcinoma cells. *Mol Cancer Ther,* 4**,** 1595-604.

SAKAKIBARA, M., KOIZUMI, S., SAIKAWA, Y., WADA, H., ICHIHARA, T., SATO, H., HORITA, S., MUGISHIMA, H., KANEKO, Y. & KOIKE, K. 1999. Membrane-type matrix metalloproteinase-1 expression and activation of gelatinase A as prognostic markers in advanced pediatric neuroblastoma. *Cancer,* 85**,** 231 - 239.

SAKR, W. 1999. Prostatic intraepithelial neoplasia: A marker for high-risk groups and a potential target for chemoprevention. *Eur Urol,* 35**,** 474 - 478.

SALAUN, C., GOULD, G. W. & CHAMBERLAIN, L. H. 2005. Lipid raft association of SNARE proteins regulates exocytosis in PC12 cells. *J Biol Chem,* 280**,** 19449-53.

SALEEM, S. N. & ABDEL-MAGEED, A. B. 2015. Tumor-derived exosomes in oncogenic reprogramming and cancer progression. *Cell Mol Life Sci,* 72**,** 1-10.

SALOMON, C., KOBAYASHI, M., ASHMAN, K., SOBREVIA, L., MITCHELL, M. D. & RICE, G. E. 2013. Hypoxia-induced changes in the bioactivity of cytotrophoblast-derived exosomes. *PLoS One,* 8**,** e79636.

SANG, Q. 1998. Complex role of matrix metalloproteinases in angiogenesis. *Cell Res,* 8**,** 171 - 177.

SARODE, N., MIRACLE, B., PENG, X., RYAN, O. & REYNOLDS, T. B. 2011. Vacuolar protein sorting genes regulate mat formation in Saccharomyces cerevisiae by Flo11p-dependent and -independent mechanisms. *Eukaryot Cell,* 10**,** 1516-26.

SATO, M., SATO, K., LIOU, W., PANT, S., HARADA, A. & GRANT, B. 2008. Regulation of endocytic recycling by C. elegans Rab35 and its regulator RME-4, a coated-pit protein. *EMBO J,* 27**,** 1183 - 1196.

SATOYOSHI, R., KURIYAMA, S., AIBA, N., YASHIRO, M. & TANAKA, M. 2015. Asporin activates coordinated invasion of scirrhous gastric cancer and cancer-associated fibroblasts. *Oncogene,* 34**,** 650-60.

SAVINA, A., FADER, C. M., DAMIANI, M. T. & COLOMBO, M. I. 2005. Rab11 promotes docking and fusion of multivesicular bodies in a calcium-dependent manner. *Traffic,* 6**,** 131-43.

SAVINA, A., FURLAN, M., VIDAL, M. & COLOMBO, M. I. 2003. Exosome release is regulated by a calcium-dependent mechanism in K562 cells. *J Biol Chem,* 278**,** 20083-90.

SAVINA, A., VIDAL, M. & COLOMBO, M. 2002. The exosome pathway in K562 cells is regulated by Rab11. *J Cell Sci,* 115**,** 2505 - 2515.

SAYLOR, P. J. & SMITH, M. R. 2009. Metabolic complications of androgen deprivation therapy for prostate cancer. *J Urol,* 181**,** 1998-2006.

SCHAFER, M. & WERNER, S. 2008. Cancer as an overhealing wound: an old hypothesis revisited. *Nat Rev Mol Cell Biol,* 9**,** 628-38.

SCHER, H. I., HALABI, S., TANNOCK, I., MORRIS, M., STERNBERG, C. N., CARDUCCI, M. A., EISENBERGER, M. A., HIGANO, C., BUBLEY, G. J., DREICER, R., PETRYLAK, D., KANTOFF, P., BASCH, E., KELLY, W. K., FIGG, W. D., SMALL, E. J., BEER, T. M., WILDING, G., MARTIN, A., HUSSAIN, M. & PROSTATE CANCER CLINICAL TRIALS WORKING, G. 2008. Design and end points of clinical trials for patients with progressive prostate cancer and castrate levels of testosterone: recommendations of the Prostate Cancer Clinical Trials Working Group. *J Clin Oncol,* 26**,** 1148-59.

SCHMITT, B., WILT, T., SCHELLHAMMER, P., DEMASI, V., SARTOR, O., CRAWFORD, E. & BENNETT, C. 2001. Combined androgen blockade with nonsteroidal antiandrogens for advanced prostate cancer: a systematic review. *Urology,* 57**,** 727 - 732.

SCHWANHAUSSER, B., BUSSE, D., LI, N., DITTMAR, G., SCHUCHHARDT, J., WOLF, J., CHEN, W. & SELBACH, M. 2011. Global quantification of mammalian gene expression control. *Nature,* 473**,** 337-42.

SCIENTIFIC LABORATORY SUPPLIES. 2017. *(I90010) - Wheaton CELLine Classic Bioreactor CL350 - Analab (an SLS Company)* [Online]. Available: http://www.analab.co.uk/product/I90010 [Accessed [Accessed 26 March 2017]].

SELLEY, S., DONOVAN, J., FAULKNER, A., COAST, J. & GILLATT, D. 1997. Diagnosis, management and screening of early localised prostate cancer. *Health Technol Assess,* 1**,** 1 - 96.

SERPA NETO, A., TOBIAS-MACHADO, M., KALIKS, R., WROCLAWSKI, M. L., POMPEO, A. C. & DEL GIGLIO, A. 2011. Ten years of docetaxel-based therapies in prostate adenocarcinoma: a systematic review and meta-analysis of 2244 patients in 12 randomized clinical trials. *Clin Genitourin Cancer,* 9**,** 115-23.

SERRETTA, V., CATANESE, A., DARICELLO, G., LIOTTA, R., ALLEGRO, R., MARTORANA, A., ARAGONA, F. & MELLONI, D. 2008. PSA reduction (after antibiotics) permits to avoid or postpone prostate biopsy in selected patients. *Prostate Cancer Prostatic Dis,* 11**,** 148-52.

SHAH, M., HUANG, D., BLICK, T., CONNOR, A., REITER, L. A., HARDINK, J. R., LYNCH, C. C., WALTHAM, M. & THOMPSON, E. W. 2012. An MMP13-selective inhibitor delays primary tumor growth and the onset of tumor-associated osteolytic lesions in experimental models of breast cancer. *PLoS One,* 7**,** e29615.

SHAO, J., SHENG, G. G., MIFFLIN, R. C., POWELL, D. W. & SHENG, H. 2006. Roles of myofibroblasts in prostaglandin E2-stimulated intestinal epithelial proliferation and angiogenesis. *Cancer Res,* 66**,** 846-55.

SHAW, T. J. & MARTIN, P. 2009. Wound repair at a glance. *J Cell Sci,* 122**,** 3209-13.

SHELDON, H., HEIKAMP, E., TURLEY, H., DRAGOVIC, R., THOMAS, P., OON, C. E., LEEK, R., EDELMANN, M., KESSLER, B., SAINSON, R. C., SARGENT, I., LI, J. L. & HARRIS, A. L. 2010. New mechanism for Notch signaling to endothelium at a distance by Delta-like 4 incorporation into exosomes. *Blood,* 116**,** 2385-94.

SHERAR, M., NOSS, M. & FOSTER, F. 1987. Ultrasound backscatter microscopy images the internal structure of living tumour spheroids. *Nature,* 330**,** 493 - 495.

SHI, K., QUEIROZ, K. C., STAP, J., RICHEL, D. J. & SPEK, C. A. 2013. Protease-activated receptor-2 induces migration of pancreatic cancer cells in an extracellular ATP-dependent manner. *J Thromb Haemost,* 11**,** 1892-902.

SHIN, M., BEANE, T. J., QUILLIEN, A., MALE, I., ZHU, L. J. & LAWSON, N. D. 2016. Vegfa signals through ERK to promote angiogenesis, but not artery differentiation. *Development,* 143**,** 3796-3805.

SHINOJIMA, T., YU, Q., HUANG, S. K., LI, M., MIZUNO, R., LIU, E. T., HOON, D. S. & LESSARD, L. 2012. Heterogeneous epigenetic regulation of TIMP3 in prostate cancer. *Epigenetics,* 7**,** 1279-89.

SIGMA. 2016. *MISSION® shRNA* [Online]. Available: http://www.sigmaaldrich.com/life-science/functional-genomics-and-rnai/shrna/learning-center/getting-started.html [Accessed 16 November 2016 2016].

SIME, P., XING, Z., GRAHAM, F., CSAKY, K. & GAULDIE, J. 1997. Adenovector-mediated gene transfer of active transforming growth factor-β1 induces prolonged severe fibrosis in rat lung. *J Clin Invest,* 100**,** 768 - 776.

SINGER, O. & VERMA, I. 2008. Applications of lentiviral vectors for shRNA delivery and transgenesis. *Curr Gene Ther,* 8**,** 483 - 488.

SKOG, J., WURDINGER, T., VAN RIJN, S., MEIJER, D. H., GAINCHE, L., SENA-ESTEVES, M., CURRY, W. T., JR., CARTER, B. S., KRICHEVSKY, A. M. & BREAKEFIELD, X. O. 2008. Glioblastoma microvesicles transport RNA and proteins that promote tumour growth and provide diagnostic biomarkers. *Nat Cell Biol,* 10**,** 1470-6.

SMITH, Z. J., LEE, C., ROJALIN, T., CARNEY, R. P., HAZARI, S., KNUDSON, A., LAM, K., SAARI, H., IBANEZ, E. L., VIITALA, T., LAAKSONEN, T., YLIPERTTULA, M. & WACHSMANN-HOGIU, S. 2015. Single exosome study reveals subpopulations distributed among cell lines with variability related to membrane content. *J Extracell Vesicles,* 4**,** 28533.

SODEK, K. L., RINGUETTE, M. J. & BROWN, T. J. 2009. Compact spheroid formation by ovarian cancer cells is associated with contractile behavior and an invasive phenotype. *Int J Cancer,* 124**,** 2060-70.

SOKOLOVA, V., LUDWIG, A. K., HORNUNG, S., ROTAN, O., HORN, P. A., EPPLE, M. & GIEBEL, B. 2011. Characterisation of exosomes derived from human cells by nanoparticle tracking analysis and scanning electron microscopy. *Colloids Surf B Biointerfaces,* 87**,** 146-50.

SRINIVASAN, R., ZABUAWALA, T., HUANG, H., ZHANG, J., GULATI, P., FERNANDEZ, S., KARLO, J. C., LANDRETH, G. E., LEONE, G. & OSTROWSKI, M. C. 2009. Erk1 and Erk2 regulate endothelial cell proliferation and migration during mouse embryonic angiogenesis. *PLoS One,* 4**,** e8283.

SRIVASTAVA, P. 2002. Interaction of heat shock proteins with peptides and antigen presenting cells: chaperoning of the innate and adaptive immune responses. *Annu Rev Immunol,* 20**,** 395-425.

STADNYK, A. 1994. Cytokine production by epithelial cells. *FASEB J,* 8**,** 1041 - 1047.

STATON, C. A., BROWN, N. J., RODGERS, G. R., CORKE, K. P., TAZZYMAN, S., UNDERWOOD, J. C. & LEWIS, C. E. 2004. Alphastatin, a 24-amino acid fragment of human fibrinogen, is a potent new inhibitor of activated endothelial cells *in vitro* and *in vivo*. *Blood,* 103**,** 601-6.

STEIN, M., GOODIN, S., DOYLE-LINDRUD, S., SILBERBERG, J., KANE, M., METZGER, D., EDDY, S., SHIH, W. & DIPAOLA, R. 2012. Transdermal estradiol in castrate and chemotherapy resistant prostate cancer. *Med Sci Monit,* 18**,** CR260 - 264.

STENMARK, H. 2009. Rab GTPases as coordinators of vesicle traffic. *Nat Rev Mol Cell Biol,* 10**,** 513-25.

STEWART, S. A. 2003. Lentivirus-delivered stable gene silencing by RNAi in primary cells. *Rna,* 9**,** 493-501.

STONE, K., MICKEY, D., WUNDERLI, H., MICKEY, G. & PAULSON, D. 1978. Isolation of a human prostate carcinoma cell line (DU 145). *Int J Cancer,* 21**,** 274 - 281.

STOORVOGEL, W., KLEIJMEER, M., GEUZE, H. & RAPOSO, G. 2002. The biogenesis and functions of exosomes. *Traffic,* 3**,** 321 - 330.

STOORVOGEL, W., STROUS, G., GEUZE, H., OORSCHOT, V. & SCHWARTZ, A. 1991. Late endosomes derive from early endosomes by maturation. *Cell,* 65**,** 417 - 427.

STUFFERS, S., SEM WEGNER, C., STENMARK, H. & BRECH, A. 2009. Multivesicular endosome biogenesis in the absence of ESCRTs. *Traffic,* 10**,** 925-37.

SU, X., LODHI, I. J., SALTIEL, A. R. & STAHL, P. D. 2006. Insulin-stimulated Interaction between insulin receptor substrate 1 and p85α and activation of protein kinase B/Akt require Rab5. *J Biol Chem,* 281**,** 27982-90.

SUNKARA, V., WOO, H. K. & CHO, Y. K. 2016. Emerging techniques in the isolation and characterization of extracellular vesicles and their roles in cancer diagnostics and prognostics. *Analyst,* 141**,** 371-81.

TAKAHASHI, T., SHIRASAWA, T., MIYAKE, K., YAHAGI, Y., MARUYAMA, N., KASAHARA, N., KAWAMURA, T., MATSUMURA, O., MITARAI, T. & SAKAI, O. 1995. Protein tyrosine kinases expressed in glomeruli and cultured glomerular cells: Flt-1 and VEGF expression in renal mesangial cells. *Biochem Biophys Res Commun,* 209**,** 218 - 226.

TAKAHASHI, Y., HORI, Y., YAMAMOTO, T., URASHIMA, T., OHARA, Y. & TANAKA, H. 2015. Three-dimensional (3D) spheroid cultures improve the metabolic gene expression profiles of HepaRG cells. *Bioscience Reports*.

TAKEDA, K., HAYAKAWA, Y., SMYTH, M., KAYAGAKI, N., YAMAGUCHI, N., KAKUTA, S., IWAKURA, Y., YAGITA, H. & OKUMURA, K. 2001. Involvement of tumor necrosis factor-related apoptosis-inducing ligand in surveillance of tumor metastasis by liver natural killer cells. *Nat Med,* 7**,** 94 - 100.

TAMAI, K., TANAKA, N., NAKANO, T., KAKAZU, E., KONDO, Y., INOUE, J., SHIINA, M., FUKUSHIMA, K., HOSHINO, T., SANO, K., UENO, Y., SHIMOSEGAWA, T. & SUGAMURA, K. 2010. Exosome secretion of dendritic cells is regulated by Hrs, an ESCRT-0 protein. *Biochem Biophys Res Commun,* 399**,** 384-90.

TAN, J. Y., JIA, L. Q., SHI, W. H., HE, Q., ZHU, L. & YU, B. 2016. Rab5a mediated autophagy regulates the phenotype and behavior of vascular smooth muscle cells. *Mol Med Rep,* 14**,** 4445-4453.

TAN, X., ZHOU, L., WANG, W., WANG, B., EGAMI, H., BABA, H. & DAI, X. 2010. Genomic analysis of invasion-metastasis-related factors in pancreatic cancer cells. *Exp Ther Med,* 1**,** 211-216.

TANNOCK, I., OSOBA, D., STOCKLER, M., ERNST, D., NEVILLE, A., MOORE, M., ARMITAGE, G., WILSON, J., VENNER, P., COPPIN, C. & MURPHY, K. 1996. Chemotherapy with mitoxantrone plus prednisone or prednisone alone for symptomatic hormone-resistant prostate cancer: a Canadian randomized trial with palliative end points. *J Clin Oncol,* 14**,** 1756 - 1764.

TAURO, B. J., GREENING, D. W., MATHIAS, R. A., JI, H., MATHIVANAN, S., SCOTT, A. M. & SIMPSON, R. J. 2012. Comparison of ultracentrifugation, density gradient separation, and immunoaffinity capture methods for isolating human colon cancer cell line LIM1863-derived exosomes. *Methods,* 56**,** 293-304.

TEH, B., MAI, W., UHL, B., AUGSPURGER, M., GRANT, W. R., LU, H., WOO, S., CARPENTER, L., CHIU, J. & BUTLER, E. 2001. Intensity-modulated radiation therapy (IMRT) for prostate cancer with the use of a rectal balloon for prostate immobilization: acute toxicity and dose-volume analysis. *Int J Radiat Oncol Biol Phys,* 49**,** 705 - 712.

TEIS, D., SAKSENA, S. & EMR, S. D. 2008. Ordered assembly of the ESCRT-III complex on endosomes is required to sequester cargo during MVB formation. *Dev Cell,* 15**,** 578-89.

TEIS, D., SAKSENA, S., JUDSON, B. L. & EMR, S. D. 2010. ESCRT-II coordinates the assembly of ESCRT-III filaments for cargo sorting and multivesicular body vesicle formation. *EMBO J,* 29**,** 871-83.

TEO, H., VEPRINTSEV, D. B. & WILLIAMS, R. L. 2004. Structural insights into endosomal sorting complex required for transport (ESCRT-I) recognition of ubiquitinated proteins. *J Biol Chem,* 279**,** 28689-96.

THANNICKAL, V. J., LEE, D. Y., WHITE, E. S., CUI, Z., LARIOS, J. M., CHACON, R., HOROWITZ, J. C., DAY, R. M. & THOMAS, P. E. 2003. Myofibroblast differentiation by transforming

growth factor-β1 is dependent on cell adhesion and integrin signaling via focal adhesion kinase. *J Biol Chem,* 278**,** 12384-9.

THEOS, A. C., TRUSCHEL, S. T., TENZA, D., HURBAIN, I., HARPER, D. C., BERSON, J. F., THOMAS, P. C., RAPOSO, G. & MARKS, M. S. 2006. A lumenal domain-dependent pathway for sorting to intralumenal vesicles of multivesicular endosomes involved in organelle morphogenesis. *Dev Cell,* 10**,** 343-54.

THÉRY, C., AMIGORENA, S., RAPOSO, G. & CLAYTON, A. 2006. Isolation and characterization of exosomes from cell culture supernatants and biological fluids. *Curr Protoc Cell Biol,* Chapter 3.

THÉRY, C., BOUSSAC, M., VERON, P., RICCIARDI-CASTAGNOLI, P., RAPOSO, G., GARIN, J. & AMIGORENA, S. 2001. Proteomic analysis of dendritic cell-derived exosomes: a secreted subcellular compartment distinct from apoptotic vesicles. *Immunol,* 166**,** 7309-7318.

THÉRY, C., OSTROWSKI, M. & SEGURA, E. 2009. Membrane vesicles as conveyors of immune responses. *Nat Rev Immunol,* 9**,** 581-93.

THÉRY, C., REGNAULT, A., GARIN, J., WOLFERS, J., ZITVOGEL, L., RICCIARDI-CASTAGNOLI, P., RAPOSO, G. & AMIGORENA, S. 1999. Molecular characterization of dendritic cell-derived exosomes. Selective accumulation of the heat shock protein hsc73. *J Cell Biol,* 147**,** 599 - 610.

THOMMEN, R., HUMAR, R., MISEVIC, G., PEPPER, M., HAHN, A., JOHN, M. & BATTEGAY, E. 1997. PDGF-BB increases endothelial migration on cord movements during angiogenesis *in vitro*. *J Cell Biochem,* 64**,** 403 - 413.

THOMPSON, C. A., PURUSHOTHAMAN, A., RAMANI, V. C., VLODAVSKY, I. & SANDERSON, R. D. 2013. Heparanase regulates secretion, composition, and function of tumor cell-derived exosomes. *J Biol Chem,* 288**,** 10093-9.

THOMPSON, I., PAULER, D., GOODMAN, P., TANGEN, C., LUCIA, M., PARNES, H., MINASIAN, L., FORD, L., LIPPMAN, S., CRAWFORD, E., CROWLEY, J. & COLTMAN, C. J. 2004. Prevalence of prostate cancer among men with a prostate-specific antigen level < or =4.0 ng per milliliter. *N Engl J Med,* 350**,** 2239 - 2246.

TIAN, Q., STEPANIANTS, S. B., MAO, M., WENG, L., FEETHAM, M. C., DOYLE, M. J., YI, E. C., DAI, H., THORSSON, V., ENG, J., GOODLETT, D., BERGER, J. P., GUNTER, B., LINSELEY, P. S., STOUGHTON, R. B., AEBERSOLD, R., COLLINS, S. J., HANLON, W. A. & HOOD, L. E. 2004. Integrated genomic and proteomic analyses of gene expression in Mammalian cells. *Mol Cell Proteomics,* 3**,** 960-9.

TOMAS, D., SPAJIC, B., MILOSEVIC, M., DEMIROVIC, A., MARUSIC, Z. & KRUSLIN, B. 2010. Intensity of stromal changes predicts biochemical recurrence-free survival in prostatic carcinoma. *Scand J Urol Nephrol,* 44**,** 284-90.

TOMASEK, J. J., GABBIANI, G., HINZ, B., CHAPONNIER, C. & BROWN, R. A. 2002. Myofibroblasts and mechano-regulation of connective tissue remodelling. *Nat Rev Mol Cell Biol,* 3**,** 349-63.

TRAJKOVIC, K., HSU, C., CHIANTIA, S., RAJENDRAN, L., WENZEL, D., WIELAND, F., SCHWILLE, P., BRUGGER, B. & SIMONS, M. 2008. Ceramide triggers budding of exosome vesicles into multivesicular endosomes. *Science,* 319**,** 1244-7.

TRAMS, E., LAUTER, C., SALEM, N. J. & HEINE, U. 1981. Exfoliation of membrane ecto-enzymes in the form of micro-vesicles. *Biochim Biophys Acta,* 645**,** 63 - 70.

TROJAN, L., THOMAS, D., KNOLL, T., GROBHOLZ, R., ALKEN, P. & MICHEL, M. S. 2004. Expression of pro-angiogenic growth factors VEGF, EGF and bFGF and their topographical relation to neovascularisation in prostate cancer. *Urol Res,* 32**,** 97-103.

TUXHORN, J., AYALA, G. & ROWLEY, D. 2002a. Reactive stroma in prostate cancer progression. *J Urol,* 166**,** 2472 - 2483.

TUXHORN, J., AYALA, G., SMITH, M., SMITH, V., DANG, T. & ROWLEY, D. 2002b. Reactive stroma in human prostate cancer: induction of myofibroblast phenotype and extracellular matrix remodeling. *Clin Cancer Res,* 8**,** 2912 - 2923.

UHLEN, M., OKSVOLD, P., FAGERBERG, L., LUNDBERG, E., JONASSON, K., FORSBERG, M., ZWAHLEN, M., KAMPF, C., WESTER, K., HOBER, S., WERNERUS, H., BJORLING, L. & PONTEN, F. 2010. Towards a knowledge-based Human Protein Atlas. *Nat Biotechnol,* 28**,** 1248-50.

UMEZU, T., OHYASHIKI, K., KURODA, M. & OHYASHIKI, J. H. 2013. Leukemia cell to endothelial cell communication via exosomal miRNAs. *Oncogene,* 32**,** 2747-55.

URBE, S., SACHSE, M., ROW, P. E., PREISINGER, C., BARR, F. A., STROUS, G., KLUMPERMAN, J. & CLAGUE, M. J. 2003. The UIM domain of Hrs couples receptor sorting to vesicle formation. *J Cell Sci,* 116**,** 4169-79.

USATYUK, P. V., FU, P., MOHAN, V., EPSHTEIN, Y., JACOBSON, J. R., GOMEZ-CAMBRONERO, J., WARY, K. K., BINDOKAS, V., DUDEK, S. M., SALGIA, R., GARCIA, J. G. & NATARAJAN, V. 2014. Role of c-Met/phosphatidylinositol 3-kinase (PI3k)/Akt signaling in hepatocyte growth factor (HGF)-mediated lamellipodia formation, reactive oxygen species (ROS) generation, and motility of lung endothelial cells. *J Biol Chem,* 289**,** 13476-91.

VALADI, H., EKSTROM, K., BOSSIOS, A., SJOSTRAND, M., LEE, J. J. & LOTVALL, J. O. 2007. Exosome-mediated transfer of mRNAs and microRNAs is a novel mechanism of genetic exchange between cells. *Nat Cell Biol,* 9**,** 654-9.

VALENTI, M., AZZARELLO, G., BALDUCCI, E., SARTORE, S., SANDRI, M., MANCONI, R., SICARI, U., BARI, M. & VINANTE, O. 2001. Conditioned medium from MCF-7 cell line induces myofibroblast differentiation, decreased cell proliferation, and increased apoptosis in cultured normal fibroblasts but not in fibroblasts from malignant breast tissue. *Histochem J,* 31**,** 499 - 509.

VAN CRUIJSEN, H., GIACCONE, G. & HOEKMAN, K. 2005. Epidermal growth factor receptor and angiogenesis: Opportunities for combined anticancer strategies. *Int J Cancer,* 117**,** 883-8.

VAN DEN HAUTE, C., EGGERMONT, K., NUTTIN, B., DEBYSER, Z. & BAEKELANDT, V. 2003. Lentiviral vector-mediated delivery of short hairpin RNA results in persistent knockdown of gene expression in mouse brain. *Hum Gene Ther,* 14**,** 1799 - 1807.

VAN DEUN, J., MESTDAGH, P., SORMUNEN, R., COCQUYT, V., VERMAELEN, K., VANDESOMPELE, J., BRACKE, M., DE WEVER, O. & HENDRIX, A. 2014. The impact of disparate isolation methods for extracellular vesicles on downstream RNA profiling. *J Extracell Vesicles,* 3.

VAN NIEL, G., CHARRIN, S., SIMOES, S., ROMAO, M., ROCHIN, L., SAFTIG, P., MARKS, M. S., RUBINSTEIN, E. & RAPOSO, G. 2011. The tetraspanin CD63 regulates ESCRT-independent and -dependent endosomal sorting during melanogenesis. *Dev Cell,* 21**,** 708-21.

VAN NIEL, G., MALLEGOL, J., BEVILACQUA, C., CANDALH, C., BRUGIÈRE, S., TOMASKOVIC-CROOK, E., HEATH, J., CERF-BENSUSSAN, N. & HEYMAN, M. 2003. Intestinal epithelial exosomes carry MHC class II/peptides able to inform the immune system in mice. *Gut,* 52**,** 1690 - 1697.

VELAZQUEZ, O., SNYDER, R., LIU, Z., FAIRMAN, R. & HERLYN, M. 2002. Fibroblast-dependent differentiation of human microvascular endothelial cells into capillary-like 3-dimensional networks. *FASEB J,* 16**,** 1316 - 1318.

VINCI, M., GOWAN, S., BOXALL, F., PATTERSON, L., ZIMMERMANN, M., COURT, W., LOMAS, C., MENDIOLA, M., HARDISSON, D. & ECCLES, S. A. 2012. Advances in establishment and analysis of three-dimensional tumor spheroid-based functional assays for target validation and drug evaluation. *BMC Biol,* 10**,** 29.

VOGEL, C. & MARCOTTE, E. M. 2012. Insights into the regulation of protein abundance from proteomic and transcriptomic analyses. *Nat Rev Genet,* 13**,** 227-32.

VON NANDELSTADH, P., GUCCIARDO, E., LOHI, J., LI, R., SUGIYAMA, N., CARPEN, O. & LEHTI, K. 2014. Actin-associated protein palladin promotes tumor cell invasion by linking extracellular matrix degradation to cell cytoskeleton. *Mol Cell Biol,* 25**,** 2556 - 2570.

VUCKOVIC, S., VANDYKE, K., RICKARDS, D. A., MCCAULEY WINTER, P., BROWN, S. H., MITCHELL, T. W., LIU, J., LU, J., ASKENASE, P. W., YURIEV, E., CAPUANO, B., RAMSLAND, P. A., HILL, G. R., ZANNETTINO, A. C. & HUTCHINSON, A. T. 2017. The cationic small molecule GW4869 is cytotoxic to high phosphatidylserine-expressing myeloma cells. *Br J Haematol,* 177**,** 423 - 440.

VYALOV, S., GABBIANI, G. & KAPANCI, Y. 1993. Rat alveolar myofibroblasts acquire α-smooth muscle actin expression during bleomycin-induced pulmonary fibrosis. *Am J Pathol,* 143**,** 1754 - 1765.

WANG, J., DE VEIRMAN, K., FAICT, S., FRASSANITO, M. A., RIBATTI, D., VACCA, A. & MENU, E. 2016a. Multiple myeloma exosomes establish a favourable bone marrow microenvironment with enhanced angiogenesis and immunosuppression. *J Pathol,* 239**,** 162-73.

WANG, J., ZHANG, X., LI, X., ZHANG, Y., HOU, T., WEI, L., QU, L., SHI, L., LIU, Y., ZOU, L. & LIANG, X. 2016b. Anti-gastric cancer activity in three-dimensional tumor spheroids of bufadienolides. *Sci Rep,* 6**,** 24772.

WANG, X., HUANG, W., LIU, G., CAI, W., MILLARD, R. W., WANG, Y., CHANG, J., PENG, T. & FAN, G. C. 2014. Cardiomyocytes mediate anti-angiogenesis in type 2 diabetic rats through the exosomal transfer of miR-320 into endothelial cells. *J Mol Cell Cardiol,* 74**,** 139-50.

WEBBER, J. & CLAYTON, A. 2013. How pure are your vesicles? *J Extracell Vesicles,* 2.

WEBBER, J., JENKINS, R. H., MERAN, S., PHILLIPS, A. & STEADMAN, R. 2009. Modulation of TGFβ1-dependent myofibroblast differentiation by hyaluronan. *Am J Pathol,* 175**,** 148-60.

WEBBER, J., STEADMAN, R., MASON, M. D., TABI, Z. & CLAYTON, A. 2010. Cancer exosomes trigger fibroblast to myofibroblast differentiation. *Cancer Res,* 70**,** 9621-30.

WEBBER, J., STONE, T., KATILIUS, E., SMITH, B., GORDON, B., MASON, M., TABI, Z., BREWIS, I. & CLAYTON, A. 2014. Proteomics analysis of cancer exosomes using a novel modified aptamer-based array (SOMAscan™) platform. *Mol Cell Proteomics,* 13**,** 1050 - 106.

WEBBER, J. P., SPARY, L. K., SANDERS, A. J., CHOWDHURY, R., JIANG, W. G., STEADMAN, R., WYMANT, J., JONES, A. T., KYNASTON, H., MASON, M. D., TABI, Z. & CLAYTON, A. 2015. Differentiation of tumour-promoting stromal myofibroblasts by cancer exosomes. *Oncogene,* 34**,** 290-302.

WEBBER, M., WAGHRAY, A. & BELLO, D. 1995. Prostate-specific antigen, serine protease, facilitates human prostate cancer cell invasion. *Clin Cancer Res,* 1**,** 1089 - 1094.

WEIDNER, N., CARROLL, P., FLAX, J., BLUMENFELD, W. & FOLKMAN, J. 1993. Tumor angiogenesis correlates with metastasis in invasive prostate carcinoma. *Am J Pathol,* 143**,** 401-9.

WEIGEL, K. J., JAKIMENKO, A., CONTI, B. A., CHAPMAN, S. E., KALINEY, W. J., LEEVY, W. M., CHAMPION, M. M. & SCHAFER, Z. T. 2014. CAF-secreted IGFBPs regulate breast cancer cell anoikis. *Mol Cancer Res,* 12**,** 855-66.

WEISWALD, L. B., BELLET, D. & DANGLES-MARIE, V. 2015. Spherical cancer models in tumor biology. *Neoplasia,* 17**,** 1-15.

WELTON, J., KHANNA, S., GILES, P., BRENNAN, P., BREWIS, I., STAFFURTH, J., MASON, M. & CLAYTON, A. 2010. Proteomics analysis of bladder cancer exosomes. *Mol Cell Proteomics,* 9**,** 1324 - 1338.

WELTON, J. L., WEBBER, J. P., BOTOS, L. A., JONES, M. & CLAYTON, A. 2015. Ready-made chromatography columns for extracellular vesicle isolation from plasma. *J Extracell Vesicles,* 4**,** 27269.

WERNIMONT, A. K. & WEISSENHORN, W. 2004. Crystal structure of subunit VPS25 of the endosomal trafficking complex ESCRT-II. *BMC Struct Biol,* 4**,** 10.

WHITE, I., BAILEY, L., AGHAKHANI, M., MOSS, S. & FUTTER, C. 2006. EGF stimulates annexin 1-dependent inward vesiculation in a multivesicular endosome subpopulation. *EMBO J,* 25**,** 1 - 12.

WILLMS, E., JOHANSSON, H. J., MAGER, I., LEE, Y., BLOMBERG, K. E., SADIK, M., ALAARG, A., SMITH, C. I., LEHTIO, J., EL ANDALOUSSI, S., WOOD, M. J. & VADER, P. 2016. Cells release subpopulations of exosomes with distinct molecular and biological properties. *Sci Rep,* 6**,** 22519.

WILSON, A. A., KWOK, L. W., PORTER, E. L., PAYNE, J. G., MCELROY, G. S., OHLE, S. J., GREENHILL, S. R., BLAHNA, M. T., YAMAMOTO, K., JEAN, J. C., MIZGERD, J. P. & KOTTON, D. N. 2013. Lentiviral delivery of RNAi for in vivo lineage-specific modulation of gene expression in mouse lung macrophages. *Mol Ther,* 21**,** 825-33.

WIPFF, P. J., RIFKIN, D. B., MEISTER, J. J. & HINZ, B. 2007. Myofibroblast contraction activates latent TGF-β1 from the extracellular matrix. *J Cell Biol,* 179**,** 1311-23.

WOLFERS, J., LOZIER, A., RAPOSO, G., REGNAULT, A., THÉRY, C., MASURIER, C., FLAMENT, C., POUZIEUX, S., FAURE, F., TURSZ, T., ANGEVIN, E., AMIGORENA, S. & ZITVOGEL, L. 2001. Tumor-derived exosomes are a source of shared tumor rejection antigens for CTL cross-priming. *Nat Med,* 7**,** 297 - 303.

WOLLERT, T., WUNDER, C., LIPPINCOTT-SCHWARTZ, J. & HURLEY, J. H. 2009. Membrane scission by the ESCRT-III complex. *Nature,* 458**,** 172-7.

WORSHAM, M., CHEN, K., MEDURI, V., NYGREN, A., ERRAMI, A., SCHOUTEN, J. & BENNINGER, M. 2006. Epigenetic events of disease progression in head and neck squamous cell carcinoma. *Arch Otolaryngol Head Neck Surg,* 132**,** 668 - 677.

WU, D. W., TSAI, L. H., CHEN, P. M., LEE, M. C., WANG, L., CHEN, C. Y., CHENG, Y. W. & LEE, H. 2012. Loss of TIMP-3 promotes tumor invasion via elevated IL-6 production and predicts poor survival and relapse in HPV-infected non-small cell lung cancer. *Am J Pathol,* 181**,** 1796-806.

WU, Y., GODOY, A., AZZOUNI, F., WILTON, J. H., IP, C. & MOHLER, J. L. 2013. Prostate cancer cells differ in testosterone accumulation, dihydrotestosterone conversion, and androgen receptor signaling response to steroid 5α-reductase inhibitors. *Prostate,* 73**,** 1470-82.

WYSOCZYNSKI, M. & RATAJCZAK, M. Z. 2009. Lung cancer secreted microvesicles: underappreciated modulators of microenvironment in expanding tumors. *Int J Cancer,* 125**,** 1595-603.

XIANG, X., POLIAKOV, A., LIU, C., LIU, Y., DENG, Z. B., WANG, J., CHENG, Z., SHAH, S. V., WANG, G. J., ZHANG, L., GRIZZLE, W. E., MOBLEY, J. & ZHANG, H. G. 2009. Induction of myeloid-derived suppressor cells by tumor exosomes. *Int J Cancer,* 124**,** 2621-33.

XIAO, G. H., JEFFERS, M., BELLACOSA, A., MITSUUCHI, Y., VANDE WOUDE, G. F. & TESTA, J. R. 2001. Anti-apoptotic signaling by hepatocyte growth factor/Met via the phosphatidylinositol 3-kinase/Akt and mitogen-activated protein kinase pathways. *Proc Natl Acad Sci USA,* 98**,** 247-52.

XIAO, W., ZHANG, Q., JIANG, F., PINS, M., KOZLOWSKI, J. & WANG, Z. 2003. Suppression of prostate tumor growth by U19, a novel testosterone-regulated apoptosis inducer. *Cancer Res,* 63**,** 4698 - 4704.

XIE, C., RITCHIE, R. P., HUANG, H., ZHANG, J. & CHEN, Y. E. 2011. Smooth muscle cell differentiation *in vitro*: models and underlying molecular mechanisms. *Arterioscler Thromb Vasc Biol,* 31**,** 1485-94.

XIN, X., YANG, S., INGLE, G., ZLOT, C., RANGELL, L., KOWALSKI, J., SCHWALL, R., FERRARA, N. & GERRITSEN, S. M. 2001. Hepatocyte growth factor enhances vascular endothelial growth factor-induced angiogenesis *in vitro* and in vivo. *Am J Pathol,* 158**,** 1111 - 1120.

XU, J., RODRIGUEZ, D., PETITCLERC, E., KIM, J. J., HANGAI, M., MOON, Y. S., DAVIS, G. E. & BROOKS, P. C. 2001. Proteolytic exposure of a cryptic site within collagen type IV is required for angiogenesis and tumor growth *in vivo*. *J Cell Biol,* 154**,** 1069-79.

XU, L. & DENG, X. 2006. Suppression of cancer cell migration and invasion by protein phosphatase 2A through dephosphorylation of mu- and m-calpains. *J Biol Chem,* 281**,** 35567-75.

YAMASHITA, M., OGAWA, T., ZHANG, X., HANAMURA, N., KASHIKURA, Y., TAKAMURA, M., YONEDA, M. & SHIRAISHI, T. 2012. Role of stromal myofibroblasts in invasive breast cancer: stromal expression of α-smooth muscle actin correlates with worse clinical outcome. *Breast Cancer,* 19**,** 170-6.

YANG, C. & ROBBINS, P. D. 2011. The roles of tumor-derived exosomes in cancer pathogenesis. *Clin Dev Immunol,* 2011**,** 842849.

YAO, Q., QU, X., YANG, Q., WEI, M. & KONG, B. 2009. CLIC4 mediates TGF-β1-induced fibroblast-to-myofibroblast transdifferentiation in ovarian cancer. *Oncol Rep,* 22**,** 541 - 548.

YOUNG, S., BANSAL, P., VELLA, E., FINELLI, A., LEVITT, C. & LOBLAW, A. 2015. Systematic review of clinical features of suspected prostate cancer in primary care. *Can Fam Physician,* 61**,** e26 - 35.

YU, S., LIU, C., SU, K., WANG, J., LIU, Y., ZHANG, L., LI, C., CONG, Y., KIMBERLY, R., GRIZZLE, W. E., FALKSON, C. & ZHANG, H. G. 2007. Tumor exosomes inhibit differentiation of bone marrow dendritic cells. *The Journal of Immunology,* 178**,** 6867-6875.

YU, X., HARRIS, S. L. & LEVINE, A. J. 2006. The regulation of exosome secretion: a novel function of the p53 protein. *Cancer Res,* 66**,** 4795-801.

YU, Y., XIAO, C. H., TAN, L. D., WANG, Q. S., LI, X. Q. & FENG, Y. M. 2014. Cancer-associated fibroblasts induce epithelial-mesenchymal transition of breast cancer cells through paracrine TGF-β signalling. *Br J Cancer,* 110**,** 724-32.

YUANA, Y., KONING, R. I., KUIL, M. E., RENSEN, P. C., KOSTER, A. J., BERTINA, R. M. & OSANTO, S. 2013. Cryo-electron microscopy of extracellular vesicles in fresh plasma. *J Extracell Vesicles,* 2.

ZEIGERER, A., GILLERON, J., BOGORAD, R. L., MARSICO, G., NONAKA, H., SEIFERT, S., EPSTEIN-BARASH, H., KUCHIMANCHI, S., PENG, C. G., RUDA, V. M., DEL CONTE-ZERIAL, P., HENGSTLER, J. G., KALAIDZIDIS, Y., KOTELIANSKY, V. & ZERIAL, M. 2012. Rab5 is necessary for the biogenesis of the endolysosomal system *in vivo*. *Nature,* 485**,** 465-70.

ZEISBERG, E. M., POTENTA, S., XIE, L., ZEISBERG, M. & KALLURI, R. 2007. Discovery of endothelial to mesenchymal transition as a source for carcinoma-associated fibroblasts. *Cancer Res,* 67**,** 10123-8.

ZELEFSKY, M., FUKS, Z., HUNT, M., YAMADA, Y., MARION, C., LING, C., AMOLS, H., VENKATRAMAN, E. & LEIBEL, S. 2002. High-dose intensity modulated radiation therapy for prostate cancer: early toxicity and biochemical outcome in 772 patients. *Int J Radiat Oncol Biol Phys,* 53**,** 1111 - 1116.

ZHANG, D., OUYANG, J., WANG, N., ZHANG, Y., BIE, J. & ZHANG, Y. 2010. Promotion of PDGF-induced endothelial cell migration by phosphorylated VASP depends on PKA anchoring via AKAP. *Mol Cell Biochem,* 335**,** 1-11.

ZHANG, Y. W., SU, Y., VOLPERT, O. V. & VANDE WOUDE, G. F. 2003. Hepatocyte growth factor/scatter factor mediates angiogenesis through positive VEGF and negative thrombospondin 1 regulation. *Proc Natl Acad Sci U S A,* 100**,** 12718-23.

ZHAO, X. P., WANG, M., SONG, Y., SONG, K., YAN, T. L., WANG, L., LIU, K. & SHANG, Z. J. 2015. Membrane microvesicles as mediators for melanoma-fibroblasts communication: roles of the VCAM-1/VLA-4 axis and the ERK1/2 signal pathway. *Cancer Lett,* 360**,** 125-33.

ZITVOGEL, L., REGNAULT, A., LOZIER, A., WOLFERS, J., FLAMENT, C., TENZA, D., RICCIARDI-CASTAGNOLI, P., RAPOSO, G. & AMIGORENA, S. 1998. Eradication of established murine tumors using a novel cell-free vaccine: dendritic cell-derived exosomes. *Nat Med,* 4**,** 594 - 600.

ZOLLER, M. 2009. Tetraspanins: push and pull in suppressing and promoting metastasis. *Nat Rev Cancer,* 9**,** 40-55.